
A functional role for brain-derived neurotrophic factor
from circulating blood platelets and potential
neuroprotective applications

Andrew Want



2022

School of Optometry and Vision Sciences
Cardiff University

This dissertation is submitted for the degree of

Doctor of Philosophy

Acknowledgements

I would like to thank my lead supervisor, Prof. James Morgan, for helping to make this project possible. Thank you for your guidance from the initial ideas, your endless optimism despite the challenges that have been faced throughout and your continuing encouragement for the future. I would also like to thank my co-supervisor Prof. Yves-Alain Barde for his generous support throughout. I am incredibly grateful for the knowledge, advice and stories you have shared with me and it has been a privilege to work with you.

I am also grateful to the Welsh Clinical Academic Track (WCAT) programme and Fight for Sight and supporting this project, and to Fujifilm WAKO for providing their advice and materials for the ELISA.

I must also extend a huge thank you to all of the wonderful people that I have been fortunate enough to have worked with over the last few years and who have given their time and help to me throughout. Thank you to Gloria Cimaglia for the mutual support at every stage of the journey through our PhDs. Between covid lockdowns and lab closures, it has been an eventful few years. You have been an amazing friend and colleague through it all and I know you have an incredible future ahead of you. Thank you to Ryan Bevan and Eirini Kokkali for teaching me how to perform the essential techniques from the very beginning and for all of your continued help, support and problem solving over the years that followed. Thank you to Erin Wosnitzka and Sarah Ateaque, not only for teaching me skills in the lab and putting up with all of my questions about BDNF, but for helping me to find a new path in my future career. Thank you to Sara Jörgensen, Cris Llinares Benadero and Ian Fox for all of the laughs, coffees and emotional support, especially over the last few months getting the thesis completed. I would also like to thank Xinsheng Nan and Hayley Dingsdale for their extraordinary work developing the genetic mouse model, without which none of this would have been possible. Thank you also to all of the staff in the Cardiff University animal facilities for their exceptional care of the animals that were central to this project. As well as the training, advice and collaborations with experiments, your understanding and insights were never taken for granted.

Finally, I must thank my parents and sister for their unwavering love and support, not only over the past three years, but throughout my time in clinical medicine, and for giving me the confidence to go on to the next steps.

“Complications arose, ensued, were overcome.”

Summary

Brain-derived neurotrophic factor (BDNF) is well known as a major effector of synaptic plasticity and for its role as a neuroprotectant. It has been extensively investigated as a possible treatment for neurodegenerative conditions such as glaucoma, a condition characterised by the progressive loss of retinal ganglion cells. Unfortunately, the physical properties of BDNF and a reduced effect over time due to interactions with its target receptor have prevented it from being translated into a clinical treatment. This thesis explores whether some of these challenges can be avoided by accessing an endogenous source of BDNF.

In humans and other primates, blood platelets contain high concentrations of BDNF due to the expression of the *BDNF* gene in megakaryocytes. By contrast mice, typically used to investigate the impact of CNS lesions, have no demonstrable levels of BDNF in platelets and megakaryocytes. The potential contributions of platelet BDNF were explored in the context of glaucoma models, by comparing wild type mice to a novel, humanised mouse model engineered to express the *Bdnf* gene under the control of a megakaryocyte-specific promoter.

A robust neuroprotective effect was seen on the retinal ganglion cells in both an *ex vivo* retinal explant and *in vivo* optic nerve crush models of retinal ganglion cell damage in the mice engineered to contain BDNF in platelets, demonstrated by preservation of dendrite complexity. Proof of concept experiments were then completed to try and enhance BDNF release from platelets to demonstrate how this concept could be translated into clinical practice.

These findings shed light on how peripheral BDNF interacts with CNS structures. This not only suggests new strategies of BDNF delivery in neurodegenerative conditions, but indicates that platelet BDNF is likely to be a significant neuroprotective factor in primates.

Table of Contents

List of Figures	ix
List of Tables	xii
List of abbreviations	xiii
Chapter 1. Introduction	16
1.1. The Eye	16
1.1.1. Anterior Eye Structures	2
1.1.2. Retina	4
1.1.3. Retinal Ganglion Cells	7
1.2. Glaucoma	11
1.2.1. Disease Entity	11
1.2.2. Pathophysiology	11
1.2.3. Approach to management of glaucoma	12
1.2.4. Neuroprotection in glaucoma	12
1.3. Brain-derived Neurotrophic Factor	16
1.3.1. Neurotrophic factor family and discovery	16
1.3.2. Neurotrophin receptors	18
1.3.3. BDNF Structure and properties	21
1.3.4. BDNF Transcription and regulation	21
1.3.5. BDNF Signalling	22
1.3.6. Cellular effects of BDNF	26
1.4. Physiology of BDNF	27
1.4.1. BDNF in development	27
1.4.2. BDNF in retinal development	28
1.4.3. BDNF in the mature retina	29
1.4.4. Peripheral BDNF	31
1.4.5. Platelets	32
1.5. BDNF associated pathologies	40
1.5.1. BDNF associated CNS pathologies	40
1.5.2. BDNF in glaucoma	40
1.5.3. Strategies for BDNF glaucoma treatments	43
1.6. Rosa26-LSL-Bdnf-myc-IG/Pf4iCre Mouse	45
1.7. Glaucoma models	47
1.7.1. Non-hypertensive models	47
1.7.2. Hypertensive models	48
1.7.3. Models selected	52
1.8. Summary	53
Chapter 2. Methods and Materials	54
2.1. Animals	54
2.1.1. Animal husbandry	54
2.1.2. Rosa26-LSL-Bdnf-myc-IG/Pf4iCre Mouse	54
2.1.3. C57BL/6J Mice	57
2.1.4. Genotyping - DNA Extraction	57
2.1.5. Genotyping - PCR Reaction	58
2.2. Tissue harvest and dissection	59

2.2.1.	Enucleation and dissection	59
2.3	Retina immunohistochemistry.....	60
2.3.1.	Cryosection preparation	60
2.3.2.	Retinal flat mount preparation	60
2.3.3.	Immunohistochemistry protocol	61
2.4.	Retina DiOlistics	61
2.4.1	Choice of technique	61
2.4.2.	Bullet preparation.....	62
2.4.3.	DiOlistics Gene gun shooting and retina preparation.....	63
2.5.	Confocal Microscopy	64
2.6.	RGC Locations.....	66
2.7.	Imaris Image Analysis and Neuronal Reconstruction.....	67
2.8.	Sholl analysis	67
2.9.	RGC count.....	70
2.10.	Blood collection and sample preparation.....	72
2.10.1.	Blood sampling.....	72
2.10.2.	Serum sample preparation	72
2.10.3.	Plasma sample preparation	72
2.10.4.	Washed platelet sample preparation	73
2.11.	BDNF ELISA (Enzyme-linked Immunosorbent Assay)	73
2.12.	Exercise tracking.....	75
2.13.	Statistical Analysis	77
Chapter 3.	<i>Baseline characteristics</i>	78
3.1	Introduction	79
3.2	Physical characteristics.....	79
3.3	Retinal features.....	79
3.3.1.	Introduction	79
3.3.2.	Experimental setup	79
3.3.3.	Results.....	80
3.3.4.	Discussion.....	81
3.4.	Serum BDNF concentration	82
3.4.1.	Introduction	82
3.4.2.	Experimental setup	83
3.4.3.	Results.....	84
3.4.4.	Discussion.....	86
3.5.	Summary.....	87
Chapter 4.	<i>Development of Models and Techniques</i>	88
4.1.	Short introduction	88
4.2.	Retinal Explants.....	88
4.2.1.	Introduction	88
4.2.2.	Experimental setup	88
4.2.3.	Results.....	90
4.2.4.	Discussion.....	92
4.3.	Optic Nerve Crush.....	92

4.3.1.	Introduction	92
4.3.2.	Experimental setup	93
4.3.3.	Results	94
4.3.4.	Discussion.....	94
4.4.	Microbead model	96
4.4.1.	Introduction	96
4.4.2.	Experimental setup	101
4.4.3.	Results.....	103
4.4.4.	Discussion.....	108
4.5.	Summary.....	109
Chapter 5.	<i>Investigating the Effect of Platelet BDNF on Retinal Ganglion Cells Using a Retinal Explant Model</i>	111
5.1.	Short Introduction	111
5.2.	Experimental setup.....	111
5.3.	Results.....	111
5.3.1.	Analysis of RGC Dendrite Morphology – Comparison of Genotypes	111
5.3.2.	Analysis of RGC Dendrite Morphology – Comparison with media supplementation	115
5.3.3.	Analysis of global RGC loss by measurement of cell count	118
5.4.	Discussion.....	121
Chapter 6.	<i>Investigating the Effect Platelet BDNF on Retinal Ganglion Cells Using an Optic Nerve Crush Model</i>	122
6.1.	Short Introduction	122
6.2.	Experimental setup.....	123
6.3.	Results.....	123
6.3.1.	Analysis of RGC dendrite morphology 7 days following ONC	123
6.3.2.	Analysis of RGC count 7 days following ONC	124
6.3.3.	Analysis of RGC Dendrite Morphology 3 days following ONC.....	128
6.4.	Discussion.....	130
Chapter 7.	<i>Stimulation of BDNF release from platelets</i>	131
7.1	Short introduction	131
7.2.	Exercise tracking – serum BDNF following 7 days of exercise, WT mice	133
7.2.1.	Introduction	133
7.2.2.	Experimental set up	135
7.2.3.	Results.....	135
7.2.4.	Discussion.....	137
7.3.	Exercise tracking – serum BDNF following 7 days of exercise, B Cre+ mice	138
7.3.1.	Introduction	138
7.3.2.	Experimental setup	138
7.3.3.	Results.....	138
7.3.4.	Discussion.....	140
7.4.	Exercise tracking – plasma BDNF following 3 days of exercise, B Cre+ mice.....	141
7.4.1.	Introduction	141
7.4.2.	Experimental set up	141
7.4.3.	Results.....	142
7.4.4.	Discussion.....	144

7.5. Stimulation of BDNF release by ultrasound	146
7.5.1. Introduction	146
7.5.2. Experimental setup	150
7.5.3. Results	151
7.5.4. Discussion	152
Chapter 8. General Discussion	154
8.1. Main Findings	154
8.2. Platelet BDNF in different species	155
8.3. BDNF access to the nervous system	158
8.4. Clinical applications	158
8.5. Conclusion and outlook	159
References	161
Appendix	190
Appendix 1	191
A1.1. Reagents	191
A1.2. Antibodies	192
A1.3. Solutions	192
A1.4. Other Consumables	193
A1.5. Equipment	194
A1.6. Medications	194
Appendix 2 – Exercise Tracker	196
A2.1. Construction Materials	196
A2.2. Circuit Diagram	197
A2.3. Exercise tracker Python Script	198
A2.4. Exercise Tracker R Script	199
Appendix 3 – Additional RStudio Scripts	203
A3.1. RGC Sholl Collation	203
A3.2. RGC Field Area Collation	205
A3.3. RGC Cell Count Heatmap	206
Appendix 4 - PCR Records	208
Appendix 5 – Exercise Tracking data	211
A5.1. Exercise tracking data – serum BDNF following 7 days of exercise, WT mice	212
A5.2. Exercise tracking data – serum BDNF following 7 days of exercise in B Cre+ mice	220
A5.3. Exercise tracking data – plasma BDNF following 3 days of exercise, B Cre+ mice	228

List of Figures

Figure 1.1: Anterior eye anatomical structures	3
Figure 1.2: Structure of the retina	4
Figure 1.3: Arborization levels of ON, OFF and ON/OFF RGC subtypes	8
Figure 1.4: Illustration of the differences in arborisation level of RGC subtypes	8
Figure 1.5. Subtypes of RGCs based on morphology	9
Figure 1.6: Interactions of neurotrophins and the Trk and p75 ^{NTR} receptors	18
Figure 1.7: Production of BDNF	20
Figure 1.8: BDNF formation and receptors	23
Figure 1.9: BDNF RNA Expression in RGC clusters	28
Figure 1.10: Formation of platelets	31
Figure 1.11: Platelet activation	32
Figure 1.12: Changes in platelet shape that occur following activation	34
Figure 1.13: Illustration of BDNF measurement in plasma and serum preparations	36
Figure 1.14: Expression of BDNF in mouse, rat and human megakaryocytes	37
Figure 1.15: Whole blood cell counts of the Rosa26-LSL-Bdnf-myc-IG/Pf4iCre mouse comparing Cre-negative and Cre-positive animals	44
Figure 1.16: Microbeads blocking aqueous outflow by obstructing the trabecular meshwork	49
Figure 2.1. Generation of a mouse model expressing a myc tagged BDNF in platelets	53
Figure 2.2: Example PCR results for genotyping the Rosa26-Bdnf-myc/Pf4iCre Mouse	56
Figure 2.3: Preparation of 'bullets' for DiOlistic labelling	61
Figure 2.4: Overview of DiOlistic labelling method	60
Figure 2.5: Confocal imaging of DiOlistically labelled retinas	61
Figure 2.6: Excitation and emission ranges for Dil and DiO	62
Figure 2.7: Neuronal reconstruction using Imaris Filament Tracer module	63
Figure 2.8: Example of a Sholl analysis of a single mouse retina ganglion cell plotting number of intersections against distance from soma	65
Figure 2.9: RGC counting method using RBPMS labelling	67
Figure 2.10: Base of modified RB3R cages for exercise tracking experiments	72
Figure 2.11: Exercise tracking equipment	73

Figure 3.1: RGC count of B Cre ⁺ mice and WT controls based on RBPMS labelling	76
Figure 3.2: Immunolabelling of retina cryosections showing TrkB (red) in B Cre ⁺ mice and WT controls	77
Figure 3.3: Depletion of serum BDNF to validate ELISA specificity	80
Figure 3.4: BDNF levels in the serum of homozygous (B ^{+/+} Cre ⁺), heterozygous (B ^{+/-} Cre ⁺) and Cre ⁻	80
Figure 3.5: ELISA results showing further investigation of serum BDNF concentration in C57BL/6J mice	81
Figure 4.1: Overview of retinal explant method	84
Figure 4.2: Sholl analysis comparing retinal explants over time	86
Figure 4.3: Overview of optic nerve crush procedure	89
Figure 4.4: Analysis of RGCs 7 days after optic nerve crush injury	90
Figure 4.5: Overview of magnetic microbead model	98
Figure 4.6: Examples of magnetic microbead injection attempts and alternative strategies attempted to improve the results	100
Figure 4.7: Preparation of glass needles and injection equipment	101
Figure 4.8: Collated Sholl analysis of mice achieving IOP ≥ 16 mmHg across different microbead trials	102
Figure 4.9: Summary of Sholl analysis results from WT mouse RGCs for each of the three experimental models	105
Figure 5.1: Preservation of RGC dendrite complexity in B Cre ⁺ mouse retinas was seen in both homozygous and heterozygous genotypes. Analysis by time point.	108
Figure 5.2: Preservation of RGC dendrite complexity in B Cre ⁺ mouse retinas was seen in both homozygous and heterozygous genotypes. Analysis by genotype.	108
Figure 5.2: Preservation of RGC dendrite complexity in B Cre ⁺ mouse retinas and with supplementation of BDNF and ZEB85	111
Figure 5.3: Sholl analysis of separated ON and OFF-centre RGCs	112
Figure 5.4: RGC cell loss in retinas explanted from B Cre ⁺ mice compared with wild type retinas cultures in either control media, or supplemented with BDNF or ZEB85	114

Figure 6.1: Analysis of RGCs 7 days after optic nerve crush injury	119
Figure 6.2: Cell count of RBPMS+ cells was reduced in B Cre+ and WT retinas after ONC	120
Figure 6.3: Heatmaps showing the mean cell count at different retinal locations	121
Figure 6.4: Analysis of RGCs 3 days after optic nerve crush injury	123
Figure 7.1: Customised exercise tracking equipment	129
Figure 7.2: Serum BDNF concentration after 7 days of voluntary exercise compared to controls in WT mice	131
Figure 7.3: Further analysis of exercise tracking experiment 1	132
Figure 7.4: Exercise tracking data from individual cages	133
Figure 7.5: Serum BDNF concentration after 7 days of voluntary exercise compared to controls in B Cre+ mice	136
Figure 7.6: Further data analysis of exercise tracking experiment 2	137
Figure 7.7: Exercise tracking data from individual cages	138
Figure 7.8: Alterations made to IR sensor mounting	140
Figure 7.9: Plasma BDNF concentration after 3 days of voluntary exercise compared to controls	142
Figure 7.10: Further analysis of exercise tracking experiment 3	143
Figure 7.11: Exercise tracking data from individual cages	144
Figure 7.12: Illustration of stable and inertial acoustic cavitation	148
Figure 7.13: Platelet aggregation induced by 1.8 W/cm ² of ultrasound at different frequencies	150
Figure 7.14: Experimental setup for ultrasound stimulated BDNF release from platelets	152
Figure 7.15: Exposure of rat platelets to ultrasound	153
Figure 8.1: Serum BDNF concentrations reported in different species	156

List of Tables

Table 2.1: Primers for BDNF/Rosa26 PCR reaction	55
Table 2.2: Primers for iCre/Jarid1 PCR reaction	55
Table 2.3: Recombinant BDNF Standards for ELISA	70
Table 2.4: Power calculations determining recommended RGC sample size based on estimated effect size	74
Table 4.1: Summary of magnetic microbead models in rats	94
Table 4.2: Summary of magnetic microbead models in mice	95
Table 8.1: Serum BDNF concentrations reported in different species	157

List of abbreviations

%	percentage
°C	degrees Celsius
µg	microgram(s)
µl	microlitre(s)
µM	micromolar
µm	micrometre(s)
AC	anterior chamber
ACD	acid-citrate-dextrose
ALT	argon laser trabeculoplasty
ANOVA	analysis of variance
AUC	area under curve
BBB	blood-brain barrier
BDNF	brain-derived neurotrophic factor
<i>BDNF</i>	brain-derived neurotrophic factor (human gene)
<i>Bdnf</i>	brain-derived neurotrophic factor (rodent gene)
bp	base pair
BRB	blood-retinal barrier
BSA	bovine serum albumin
CCT	central corneal thickness
cm	centimetre
CNS	central nervous system
ddH ₂ O	distilled and dionised water
DiI	1,1'-Diocadecyl-3,3',3'-Tetramethylindocarbocyanine perchlorate
DiO	3,3'-Diocadecyloxacarbocyanine perchlorate
DMSO	dimethyl sulfoxide
DNA	deoxyribonucleic acid
EDTA	ethylenediaminetetraacetic acid
eGFP/GFP	enhanced green fluorescent protein
ELISA	enzyme-linked immunosorbent assay
EM	electron microscope
ER	endoplasmic reticulum
EtBr	ethidium bromide

FBS	foetal bovine serum
g	gram(s)
G	gauge
GAPDH	glyceraldehyde 3-phosphate dehydrogenase
GCL	ganglion cell layer
GFP	(enhanced) green fluorescent protein
HBSS	Hank's balanced salt solution
Het/HET	heterozygous
Hom/HOM	homozygous
HRP	horseradish peroxidase
IgG	immunoglobulin G
IOP	intraocular pressure
INL	inner nuclear layer
IPL	inner plexiform layer
IR	infrared
IRES	internal ribosome entry site
LC	lamina cribrosa
LDCVs	large dense core vesicles
LSL	lox-STOP-lox
M	molar
mAb	monoclonal antibody
mBDNF	mature brain-derived neurotrophic factor
mg	milligram(s)
min	minutes(s)
MK	megakaryocyte
mm	millimetre(s)
mmHg	millimetres of mercury
mRNA	messenger ribonucleic acid
ms	millisecond(s)
ns	not significant
ng	nanogram(s)
NGF	nerve growth factor
NLS	nuclear localisation sequence

nm	nanometre(s)
nM	nanomolar
NT3	neurotrophin-3
NT4	neurotrophin-4
NTG	normal tension glaucoma
NTRK2	neurotrophin receptor tyrosine kinase 2 (human TrkB gene)
OCT	optical cutting temperature compound
OHT	ocular hypertension
ON	optic nerve
ONL	outer nuclear layer
OPL	outer plexiform layer
p	probability value
P2A	2a self-cleaving peptide
p75 ^{NTR}	p75 neurotrophin receptor
PBS	phosphate buffered saline
PCR	polymerase chain reaction
PF4	platelet factor 4
PFA	paraformaldehyde
pg	picogram(d)
PNS	peripheral nervous system
POAG	primary open angle glaucoma
pro-BDNF	pro-brain-derived neurotrophic factor
Pur	puromycin resistance cassette
rBDNF	recombinant brain-derived neurotrophic factor
RBPMs	ribonucleic acid-binding protein with multiple splicing
RGC	retinal ganglion cell
RIPA	radioimmunoprecipitation assay
RNA	ribonucleic acid
RPE	retinal pigment epithelium
RPM	revolutions per minute
RT	room temperature
RTK	receptor tyrosine kinase
s	seconds
SC	superior colliculus
SEM	standard error of the mean
SNP	single nucleotide polymorphisms

TAE	tris-aminomethane base, acetic acid and ethylenediaminetetraacetic acid
TBS	tris-buffered saline
TBS-T	tris-buffered saline with 0.1% Tween ® 20
TGN	trans-Golgi network
TM	trabecular meshwork
Tris	tris-aminomethane
Trk(A/B/C)	tropomyosin receptor kinase (A/B/C)
<i>TrkB</i>	tropomyosin receptor kinase B (rodent gene)
V	volts
wt/WT	wild type
YAG	yttrium aluminium garnet

Chapter 1. Introduction

1.1. The Eye

There are many different forms of eyes found in nature but they all serve the same purpose, to collect light and convert this into a neuronal impulse. While the size and dimensions of the eye may change between different species, the overall ocular structures are similar across mammals (Baden et al., 2020).

The eye is formed from outgrowths of the embryonic diencephalon and is a part of the central nervous system (CNS). Many of the anterior structures of the eye such as the eyelids, the lens and the cornea epithelium are derived from the surface ectoderm, whereas the retina, optic nerve, iris and ciliary body epithelium are formed from the neuroectoderm. Waves of migrating mesenchyme form the majority of the remaining structures such as the sclera. By a combination of the refractive power of the cornea and the lens, light is focused onto the retina. Within the retina, this light stimulus is processed and converted into a neurological impulse that can be transmitted via the optic nerve to the brain. A knowledge of these structures and the interactions between them is necessary to understand the normal processes of the eye, the features of disease and the mechanisms underlying the experimental models used in ophthalmic research.

1.1.1. Anterior Eye Structures

Cornea

The cornea is a transparent layer that provides most of the refractive power of the eye in humans. The majority of the thickness of the cornea is the corneal stroma, a layer of predominantly Type I collagen, with some smaller amounts of type V and VI. The regular orientation of the fibres confers the transparency, with the corneal curvature creating the refractive power. The cornea terminates peripherally at the limbus, where the epithelium, stroma and endothelium transition into the conjunctiva, sclera and trabecular meshwork respectively.

Aqueous humour

Aqueous humour is a clear fluid produced by the epithelial cells of the ciliary body. The purpose of the aqueous is to transport vital metabolites to the avascular lens and cornea, and to remove waste products produced by the anterior chamber structures. It comprises 99% water, with predominantly electrolytes, low-molecular weight compounds and some protein (Kong et al., 2002). Notably high levels of ascorbic acid may provide some protection against harmful solar radiation (Koskela et al., 1989), and detectable levels of various growth factors and chemokines suggest aqueous may also have a role in the immune response (Flynn et al., 2008). The rate of aqueous humour production is around 2-3 μ l/min in humans (Brubaker, 1991) and 0.18 μ L/min in mice (Aihara et al., 2003). However, this rate is variable with fluctuations seen at different times of day and can be influenced by different medications, an effect utilised by several topical drops in the reduction of eye pressure, central to the management of glaucoma.

Trabecular meshwork

The trabecular meshwork (TM) consists of a complex lattice of connective tissue beams and forms a circumferential band at the angle between the cornea and the iris. The TM has three subdivisions: the innermost uveal meshwork with thicker cord-like bands of tissue (trabeculae), the corneoscleral meshwork with flattened trabeculae, and the cribriform meshwork beneath the wall of the Schlemm's canal. In humans, the fenestrations between the trabeculae are approximately 25-27 μ m in the uveal meshwork and 2-15 μ m in the corneoscleral meshwork (Abu-Hassan et al., 2014). Aqueous humour passes from the anterior chamber of the eye, through the pores of the trabecular meshwork and into the Schlemm's

canal. As it passes through, TM cells filter and phagocytose debris in the aqueous humour produced from tissues within the eye (Johnson et al., 1989).

This pathway through the TM is known as the conventional aqueous outflow pathway. After reaching the Schlemm's canal, the aqueous passes into collector channels, a deep scleral plexus, intrascleral venous plexus, episcleral veins and finally into the anterior ciliary veins. Conventional aqueous outflow is primarily a pressure driven and accounts for approximately 90% of aqueous outflow (although this is variable). With the unconventional, or uveoscleral pathway, which accounts for the remaining 10% of the outflow, aqueous humour passes between the intracellular spaces of the ciliary muscle cells and into the suprachoroidal space.

Ciliary body

The ciliary body forms part of the uveal tract and has several important roles in the eye. It is the source of aqueous humour, formed by transport of water and electrolytes from capillaries in the ciliary processes and eventually secreted by the ciliary body epithelium. It also provides the blood and nerve supply to the anterior segment, and contains the muscles that produce accommodation of the lens.

Lens

The lens is formed from the surface ectoderm and comprises mainly of specialised cells, modified to form fibres. They are highly organized, arranged and maintained in a way that produces a transparent structure that provides additional refractive power to the eye. Under the influence of the ciliary body, the lens can change shape to adjust the refractive power of the eye, allowing light from varying distances to be focused on the retina.

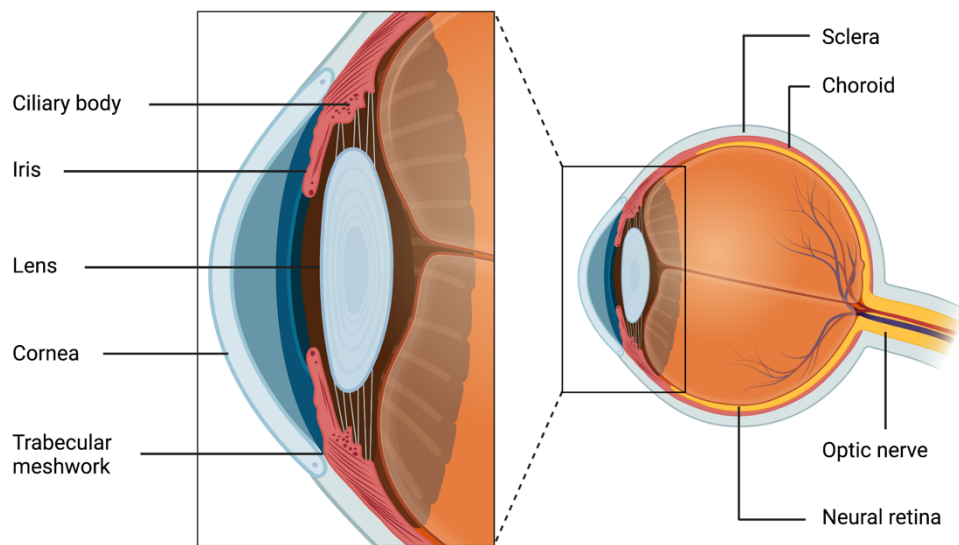


Figure 1.1: Anterior eye anatomical structures.
Created using Biorender.com.

1.1.2. Retina

Retina Structure

Light, focused by the cornea and the lens, passes through the layers to stimulate the photoreceptors in the outer retina. The resulting signal is then passed in the opposite direction from outer to inner retina before being sent to the brain via the axons of the retinal ganglion cells (RGCs). While this inverted arrangement may at first seem slightly counter-intuitive, it has the advantage of ensuring that photoreceptors are close to the dense vascular bed in the choroid, without obscuring the path of the travelling light. The retina has the highest energy demand of any tissue in the body and the high blood flow through the choroid helps to meet this demand (Wong-Riley, 2010). The choroid supplies the outer retina up to the ONL, whereas the inner retina is supplied by the retinal vessels. The different cell types in the retina originate from retinal progenitor cells (Cepko, 2014), with the exception of astrocytes and microglia that migrate in afterwards.

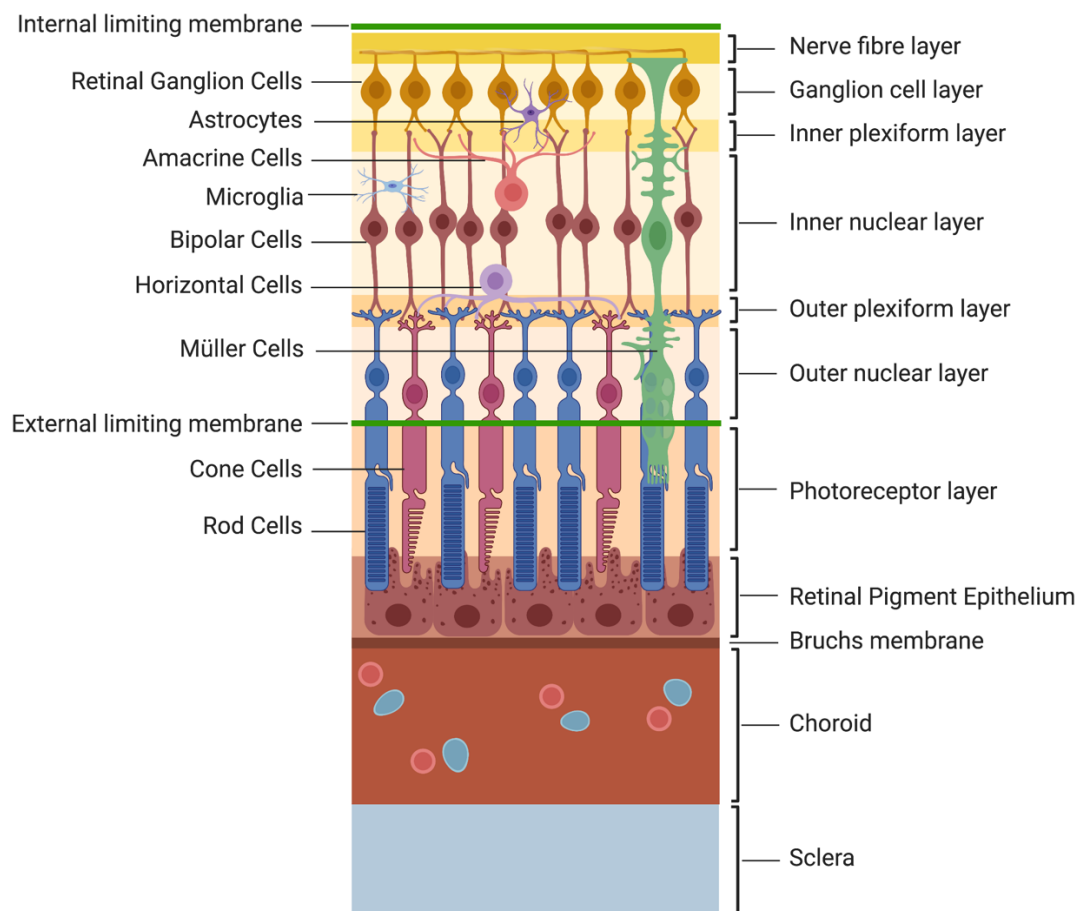


Figure 1.2: Structure of the retina.
Created using Biorender.com.

Retinal Pigment Epithelium

The retinal pigment epithelium (RPE) absorbs light and participates in the maintenance and turnover of the photoreceptor outer segments. The RPE forms the outer component of the blood retinal barrier, regulating transport between the choroid and the retina (the inner component is formed by retinal capillaries)(Díaz-Coránguez et al., 2017).

Photoreceptors

Photoreceptor cells are the first stage in the conversion of light stimuli reaching the retina into neural impulses. There are two types of photoreceptors in mammalian eyes: rods and cones. In humans there are approximately 115 million rods and 6.5 million cones. The mouse retina contains approximately 6.4 million rods and 180,000 cones (Jeon et al., 1998). Rods predominantly occupy the peripheral retina, and the input from them is processed for the detection of contrast, brightness and motion and, whereas cones support the detection of

colour vision and fine resolution and are found with the highest density towards the macula, with the fovea being occupied exclusively by cones. All photoreceptors hyperpolarise in response to light. Photon absorption by the photopigment causes isomerisation of the chromophore, retinal, from 11-cis to all-trans. This causes hyperpolarisation of the photoreceptor and reduces neurotransmitter release. Conversely in dark conditions, the photoreceptors become depolarised and release glutamate. Glutamate then acts on both horizontal and bipolar cells.

Horizontal cells

As their name suggests, horizontal cells have extensive horizontal projections of their cell processes. They have an important role in retinal processing and release inhibitory neurotransmitters to modulate and integrate inputs from multiple photoreceptors.

Glial cells

Glial cells within the retina provide neuronal support and homeostasis, and include three types; Müller cells, microglia and astrocytes. Müller cells are the principle glial cells within the retina. Their cell bodies lie in the inner nuclear layer and extend large projections that can span the retina from the inner and outer limiting membranes. They form architectural support structures, as well as protecting against glutamate toxicity. Müller cells are known to phagocytose cellular debris; however, the primary phagocytosing cells are the microglia. Microglia can be activated and phagocytose retinal neurons. This can be seen in trauma and pathological conditions, and as part of neuronal elimination in retinal development (Anderson et al., 2019).

Bipolar cells

There are two classes of bipolar cells for the cone pathway, ON and OFF. The synaptic junction of OFF bipolar cells is sign conserving, whereas the junction of the ON bipolar cells is sign inverting. This is achieved by differences in the receptors present in the different classes, and results in opposite effects when glutamate is released from the photoreceptors. The ON bipolar receptor is mGluR6 and its activation leads to the closing of the channels causing hyperpolarisation. OFF bipolar receptors are mGluR1 and 2. Their activation leads to the opening of channels causing depolarisation. The ON and OFF bipolar cells will synapse with corresponding ON and OFF RGCs. In most primates, rods connect directly through ON bipolar cells for rods. Rod ON and OFF channels are instead created by interactions of amacrine cells creating signalling circuits between the bipolar cells and RGCs and bipolar cells from the cone pathways.

Amacrine cells

Amacrine cells operate predominantly in the IPL but their cell bodies may be found in the ganglion cell layer (GCL). Displaced amacrine cells in the GCL account for approximately 60% of the total neurons in this layer, with the rest being RGCs (Jeon et al., 1998). Amacrine cells are the most diverse cell class, but broadly speaking, their role is to modulate the signals reaching RGCs by mediating lateral interactions between bipolar cells and RGC dendrites. They are varied in terms of size, morphology, function and neurotransmitters. GABA and glycine account for the vast majority of cells, but there are small populations that contain acetylcholine and dopamine among others (Kolb, 1997).

Retinal Ganglion Cells

RGCs transmit the signals produced within the retina to the brain. Their cell bodies form the GCL, and their axons the nerve fibre layer (NFL). Together with their dendrites, they are characteristically lost in glaucoma and as such, are a major focus of this thesis. They are therefore described in greater detail in the following section.

1.1.3. Retinal Ganglion Cells***Structure and Function***

RGCs act as the output neuron of the retina, the primary function being to transmit the signals initiated in the retina to the brain. There are approximately 1.2 million RGCs in the human retina, with the highest density at the fovea, tapering off towards the periphery. In a typical mouse retina, there are approximately 45,000 RGCs, (Jeon et al., 1998), with an average density of 3300 cells/mm². Peak RGC density in the mouse is approximately 8000 cells/mm² just temporal to the disc, and lowest density in the most dorsal part of the retina at around 2000 cells/mm² (Drager and Olsen, 1981).

The cell bodies of the RGCs are found within the ganglion cell layer of the retina. They have a broad, laminar dendritic tree that arborises in the inner plexiform layer (IPL) where synapses are formed with bipolar cells and amacrine cells. RGCs are stimulated by the release of glutamate from the end terminals of depolarised bipolar cells, which results in the depolarisation of the RGC soma. Synaptic contact is on the actual shaft of the dendrite in RGCs, as unlike neurons in the brain, their dendrites do not have spines. The RGC dendrites receive all synaptic inputs into the cell.

The axons of RGCs extend towards the optic disc, forming the retinal nerve fibre layer. These axons then travel through the lamina cribrosa and collectively form the optic nerve. RGC axons only become myelinated once they have passed through the lamina cribrosa. When the two optic nerves meet, a proportion of the axons will cross to the contralateral side at the optic chiasm. The proportion of axons that cross at the optic chiasm is extremely variable depending on species. Animals that have developed a wider field of binocular vision with forward facing eyes, such as carnivores and primates have a more equal division of axons between the contralateral and ipsilateral sides of the chiasm, with approximately 48% of axons remaining on the ipsilateral side in humans. Due to the more lateral position of the mouse eye, the binocular field only accounts for the central 30-40° of the total receptive field (Scholl et al., 2013). Only 2-3% of mouse RGC axons project ipsilaterally at the chiasm, with the rest crossing over to the contralateral side (Chalupa, Leo and Williams, Robert, 2008). Of note, a greater proportion of axons cross to the contralateral side in albinism, a feature seen in both mice and humans (Creel and Wiikop, 1974; Guillery et al., 1975; Rebsam et al., 2012).

Following the chiasm, the RGCs will project to areas of the brain for visual processing. In primates, this is primarily to the lateral geniculate nucleus (LGN), with approximately 10% of RGCs projecting to the superior colliculus (SC) (Perry and Cowey, 1984). This is very different in mice, in which 85-90% of RGCs project to the SC (Ellis et al., 2016).

Subtypes

There are at least 40 different subtypes of RGC (Sanes and Masland, 2015), and arguably more depending on the method used to try to categorise them. One of the simplest ways RGCs can be characterised is as either ON, OFF or ON/OFF. The characterisation of ON and OFF cells is not only functional, related to the synapses with the corresponding bipolar cells, but can be seen in the morphology of the dendritic tree. The ON cells arborise more superficially in sublamina b in the IPL, with OFF cells arborising in the deeper sublayer a. ON/OFF cells are bistratified, with a plane of dendrite branches in each layer (Figure 1.2). Wässle et al., 1983 used reduced silver staining of RGCs in the cat retina to show the distinct spatial segregation of the ON and OFF dendritic fields, and furthermore, they were able to show that the two layers form their own independent, regular lattices (Figure 1.3). The ON-centre RGCs have a higher energy requirement and, as such, are more sensitive to degeneration (Sanes and Masland, 2015).

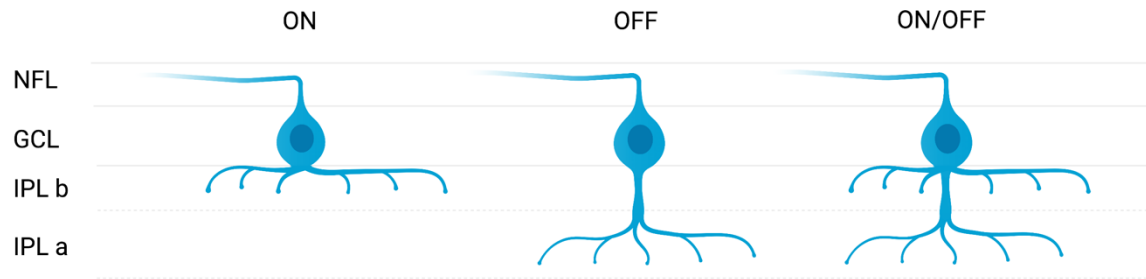


Figure 1.3: Arborization levels of ON, OFF and ON/OFF RGC subtypes.

Created using Biorender.com.

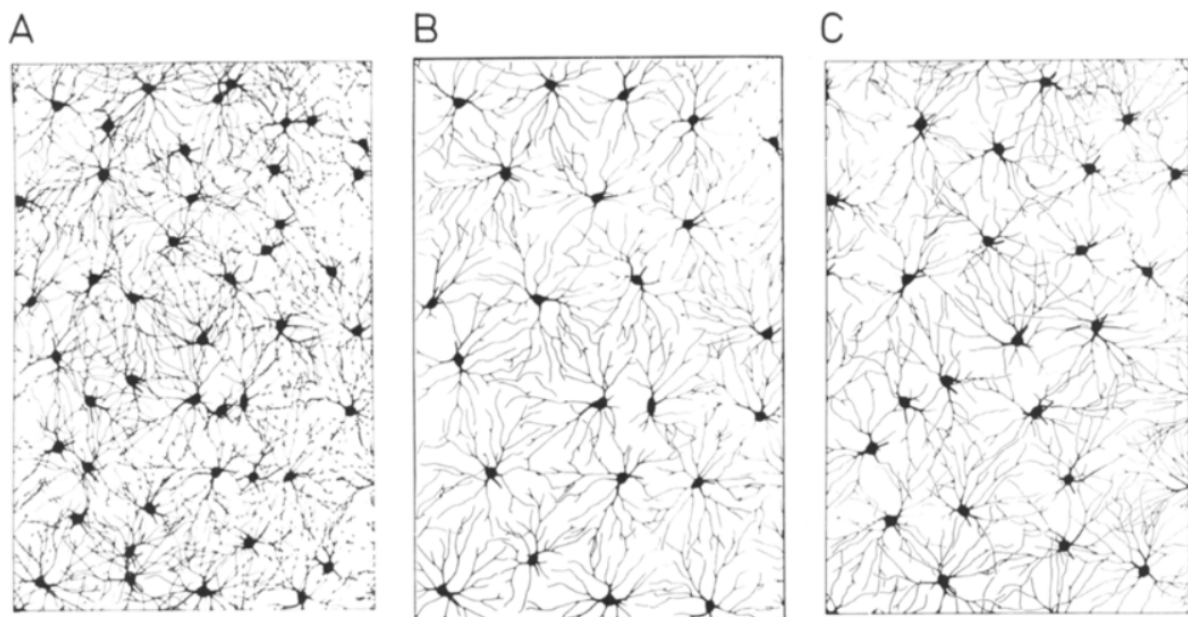


Figure 1.4: Illustration of the differences in arborisation level of RGC subtypes.

ON cells arborise in IPL b, OFF cells in IPL a and ON/OFF cells in both. Dendritic territories of alpha-cells. **(A)** all cells, **(B)** ON cells only, **(C)** OFF cells only, showing the independent lattices of ON and OFF levels of the IPL. (Wässle et al., 1983).

Beyond this initial ON and OFF distinction, RGCs also have a huge variety of different patterns seen in the structure of the dendritic branches. This variation was seen in the early RGC studies performed by Golgi, with new subtypes being noted as the methods of staining and visualising the RGCs improved. Sun et al., 2002 completed a detailed survey of mouse RGCs with a comprehensive morphological classification (Figure 1.4).

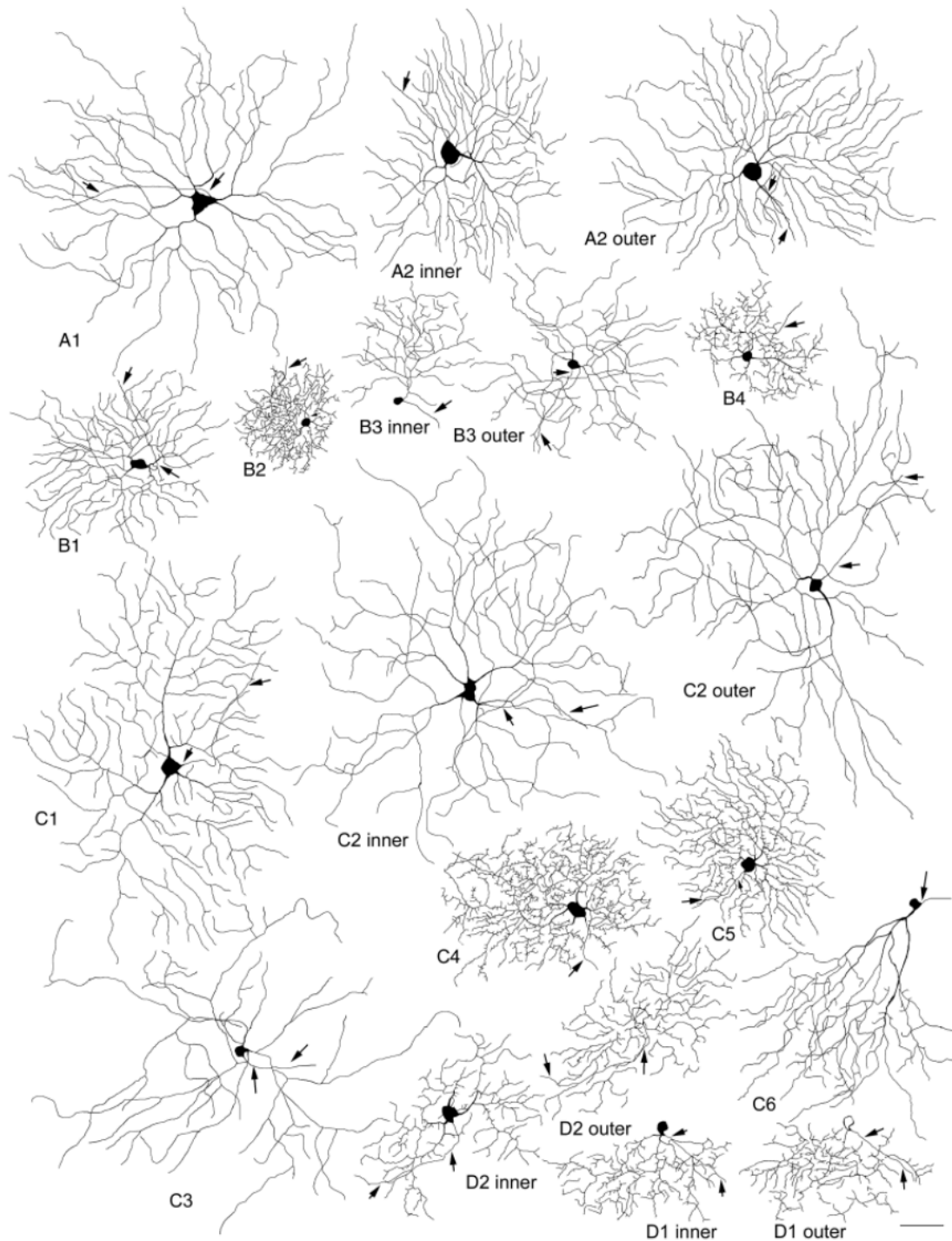


Figure 1.5. Subtypes of mouse RGCs based on morphology.

Four groups and fourteen subtypes were classified. Cells were classified as type A – large soma and large dendritic field, B – small to medium-sized soma and small to medium-sized dendritic field, C – small to medium-sized soma with medium to large-sized dendritic field, D – unequivocally bistratified cells. Groups were then further divided into subtypes based on density and pattern of dendritic branches. Scale bar = 50 μ m, arrow indicates the axon. Taken from Sun et al, (2002).

The introduction of single-cell transcriptional profiling has given further insight into the variation seen between individual RGCs, and an alternative method to try and categorise them. Using

this technique Rheaume et al., (2018) proposed 40 subtypes of mouse RGC based on clusters of gene expression. The roles of the different subtypes and the intricacies of their interactions are not yet fully understood.

1.2. Glaucoma

1.2.1. Disease Entity

Glaucoma is a group of conditions characterised by progressive degeneration of the optic nerve leading to visual field loss and irreversible blindness (Quigley, 2011). It is the leading cause of irreversible blindness worldwide, with approximately 80 million people thought to be affected and projections of up to 111.8 million by 2040 (Tham et al., 2014). It is most commonly associated with an elevated intraocular pressure (IOP) but there is a subset of patients that show glaucomatous damage with IOP within the normal range (11-21 mmHg), referred to as normal tension glaucoma (NTG). Glaucoma most commonly refers to primary open angle glaucoma (POAG), a chronic condition typically seen in older patients that requires lifelong monitoring and management. Other forms of glaucoma include angle closure glaucoma, caused by a narrowing and closure of the angle between the cornea and iris that obstructs aqueous outflow through the trabecular meshwork, secondary glaucoma, for example TM obstruction caused by neovascularisation in diabetes, and congenital glaucoma.

1.2.2. Pathophysiology

Degeneration of RGCs is central to the pathophysiology of all forms of glaucoma. Loss of these cells leads to loss of the visual field as well as the characteristic clinical features of NFL thinning and increased optic disc/cup ratio (Quigley, 2011). It has also been established that RGCs undergo significant structural changes before cell death. There is a period of atrophy characterised by pruning of RGC dendrites, reduction in the dendrite area and loss of soma volume with a reduction in axonal diameter (Morgan, 2012). The loss of dendritic complexity compromises the synaptic contacts between the RGC and bipolar cells, reducing the efficiency with which RGCs can translate signals from the peripheral retina and the reliability of the RGC response to a light stimulus. This has been demonstrated in primate studies that showed reduced contrast sensitivity and firing frequency in RGCs from glaucomatous eyes (Weber and Harman, 2005). RGCs may be particularly susceptible to damage due to their unmyelinated axons, high energy demand and large, complex dendritic arbours (Inman and Harun-Or-Rashid, 2017).

RGC death in glaucoma is due to apoptosis, a programmed cell death that can be triggered by a variety of stimuli. However, while the link between elevated IOP (both chronically and acute) and RGC loss is well established, the underlying mechanisms of the progressive degeneration of RGCs that leads to apoptosis are not fully understood. Several mechanisms have been proposed including, but not limited to, mitochondrial dysfunction, oxidative stress, raised glutamate and deprivation of neurotrophic factors (discussed below). The search to understand these processes continues to guide the development of neuroprotective strategies and new ideas for glaucoma management.

1.2.3. Approach to management of glaucoma

The current approach to managing glaucoma relies on careful monitoring, and reduction of IOP to limit the progression of the disease, the benefits of which were confirmed in the Early Manifest Glaucoma Trial . In this landmark study, Argon laser trabeculoplasty (ALT) and, if needed, topical antihypertensives (Betaxolol) were used to reduce IOP by 25%. Overall, the study estimated that for each 1mmHg of IOP reduction, there was a 10% decrease in the risk of glaucoma progression. The benefits of IOP reduction are also seen in normal tension glaucoma, even though the presenting IOP is considered within the normal range (Heijl et al., 2002; Anderson and Normal Tension Glaucoma Study, 2003).

Current glaucoma treatments using topical drops, laser or surgical procedures are all aimed at reducing the IOP as this is the only modifiable risk factor that has been identified. However, there is still a large cohort of patients who continue to deteriorate and lose their sight despite having their IOP reduced. Combined with an ageing population and the pressures on healthcare services, there is a desperate need for alternative forms of treatment. In order to truly move the management of glaucoma forward, new approaches must be found, approaches that are not focused on IOP but target the disease from entirely new directions.

1.2.4. Neuroprotection in glaucoma

Neuroprotection refers to the prevention of neuronal cell death by interventions that inhibit the processes and pathways that lead to neuronal dysfunction and death. This is seen physiologically by the action of several neurotrophic factors, a family of bioactive molecules that support, growth, differentiation, proliferation and survival of neurons in both the developing and mature nervous system. Considering that glaucoma is characterised by loss

of RGCs, direct neuroprotection of these cells has been of great interest. There are several ways to try and achieve this goal. One method has been to investigate in greater detail the mechanism that lead to RGC loss, in an effort to find points in the relevant pathways that could be targeted.

While there are many different events that can cause a cell to trigger the apoptotic pathway, the process often converges with the actions of either pro- or anti-apoptotic proteins. B-cell lymphoma protein 2 (BCL-2) is anti-apoptotic, whereas BCL-2 associated protein X (BAX) is pro-apoptotic. The activity and interaction of BCL-2 and BAX are further modulated, and inhibited or activation via the action of other related proteins, in particular Bcl-2 homology 3 only (BH3-only) proteins (Maes et al., 2017). Stresses on the cell can push the balance of this system in a pro-apoptotic direction, with BAX activation leading to pore formation in mitochondrial membranes, and subsequent release of cytochrome c. This is generally considered to be “a point of no return in the cell death process” (Chang et al., 2002).

There are additional pathways that can lead to RGC death. For example, RGCs express N-methyl-D-aspartate (NMDA) receptors, over activation of which by glutamate can lead to cell death. Activation of NMDA leads to influx of calcium, which in turn leads to leakage of cytochrome c from mitochondria, formation of free radicals and nitric oxide and cell death by apoptosis. *Bax*-deficiency was not able to protect against NMDA receptor-mediated excitotoxicity, suggesting that this was a separate mechanism from the classical BAX-dependent apoptotic pathway (Dargusch et al., 2008).

Another strategy to prevent neurodegeneration has been to try understand the stresses on neurons that lead to apoptosis being triggered. Mitochondrial dysfunction can lead to oxidative stress and free radical production. This has been implicated in a variety of neurodegenerative conditions, including glaucoma, and occurs prior to detectable neuronal degeneration (Williams et al., 2017:3). Supporting mitochondrial function may therefore be able to be a viable way to preserve neuronal function.

Intensive efforts have been made to try and understand in greater detail the mechanisms that lead to RGC loss, and ways to interact with these systems in order to prevent cell death. Over the years, different concepts have received significant attention but have so far failed to deliver on early promises. Nevertheless, despite the ongoing struggles, there are approaches that do show potential.

BAX inhibition

Knockout of the *Bax* gene in mouse models was able to successfully block the initiation of apoptosis, enabling RGCs to survive following serious insults (Howell et al., 2007). However, although these cells may be alive, they are not functioning in a normal, healthy way. Deletion of BAX traps them in a state of limbo between life and death, now often referred to as “zombie cells” (Maes et al., 2017). It is clear that effective neuroprotective treatments need to not only prevent cell death, but ensure the retention of cells in their normal functioning state.

NMDA inhibition

RGCs express N-methyl-D-aspartate (NMDA) receptors, over activation of which by glutamate can lead to cell death. Activation of NMDA leads to influx of calcium, which in turn leads to leakage of cytochrome c from mitochondria, formation of free radicals and nitric oxide and cell death by apoptosis. Glutamate-induced excitotoxicity has been implicated in glaucoma and so inhibiting NMDA receptors has been extensively investigated. There have been challenges finding an agent that could be potent enough to prevent RGC loss while not interfering with the normal physiological functions of glutamate. One example is memantine, a selective, non-competitive NMDA receptor blocker that showed promising results in animal studies and even reached a phase 3 clinical trial using an oral treatment (Weinreb et al., 2018). Unfortunately, no significant preservation of visual function was found in that trial. Combined with suggestions that the beneficial effects may also have a limited duration (Hare et al., 2004), these disappointing results have meant that NMDA antagonists have largely fallen out of favour. Nevertheless, there are newer versions being developed and it is hoped these may be more successful (Fang et al., 2010; Sánchez-Vidaña et al., 2019).

Caspase inhibitors

Efforts were also made to identify the downstream pathways of NMDA receptor mediated cell death to try and find new targets for neuroprotection. In doing so, several caspases were identified to have key roles. Caspases are cysteine proteases that can be classed as either extrinsic (receptor mediated) or intrinsic (stress induced). Caspase 3 is among the most thoroughly studied and considered a key protease in excitotoxic cell neuronal death. Levels in RGCs peak at around 5-6 days after optic nerve injury (Sánchez-Migallón et al., 2016; Fernandes et al., 2012), highlighting its role in RGC degeneration. Inhibition of caspases can show some protective effects with Schuetttauf et al., 2011 demonstrating that NMDA-induced death can be partially prevented by intraocular injection of inhibitors of caspases 3, 6, 8 and 9. However, so far inhibiting caspase activity has only produced moderate protection for RGCs. Caspase activity has been implicated in a range of neurological, inflammatory and metabolic diseases with some caspase inhibitors having reached phase 2 trials. Unfortunately, clinical and pre-clinical studies have consistently been faced with poor efficacy and adverse

effects including considerable organ toxicity in some animal models (reviewed in (Dhani et al., 2021)). The complex web of caspase functions and interactions under both normal and pathological conditions is far from understood, and it is clear that a substantial amount of further research is needed before this will become a viable clinical treatment.

NMNAT2

Alternative strategies have focused on different targets and pathways within the neuron. NMNAT2 is an enzyme that synthesises NAD⁺, which was found to be essential for axon maintenance in neurons. Mice lacking in NMNAT2 have severely truncated RGCs, with axons failing to reach the optic chiasm. This appeared to be due to a failure in development rather than a later degeneration of formed axons (Gilley et al., 2013). Liu et al., 2021 sought to determine if NMNAT2 could have a neuroprotective effect in RGCs in a model of optic neuritis. Here, they used a mouse experimental autoimmune encephalomyelitis (EAE) model that replicates optic neuritis and significant RGC soma and axon loss. An RGC-specific promoter was then used to drive expression of a long half-life NMNAT2 mutant in mouse RGCs in vivo. Unfortunately, no neuroprotective effect was seen using this treatment.

Nicotinamide

The mitochondrial abnormalities in RGCs occur prior to neurodegeneration in glaucoma, in both humans and animal models and is another potential target for new treatments (Tribble et al., 2019) (Williams et al., 2017). Nicotinamide (NAM) is a precursor of Nicotinamide adenine dinucleotide (NAD), an essential metabolite for neuronal survival that is known to be reduced in neurodegenerative conditions. NAM supplementation prevents metabolic disruption, has a buffering effect against metabolic stress and increases the size and motility of mitochondria (Tribble et al., 2021). The combination of these effects has a profound neuroprotective effect on RGCs in experimental glaucoma models. The results of animal models have been extremely encouraging and clinical trials are now in progress with glaucoma patients (De Moraes et al., 2022). The ongoing story of NAM as a supplementary treatment in glaucoma is certainly an area to watch with interest.

Neurotrophic factors

Retinal neurons and glial cells express receptors for different trophic factors, activation of which may enhance RGC survival. Furthermore, disruption of axonal transport has been demonstrated in glaucoma models, suggesting that the interruption of the retrograde supply of trophic factors may play a role in the pathophysiology (Pease et al., 2000; Quigley et al., 2000). This raises the possibility of supplementing trophic factors in order to preserve RGCs. There are several varieties of growth and trophic factors relevant to RGCs, but brain-derived

neurotrophic factor (BDNF) appears to be of particular importance for RGC function and survival (discussed in detail below). This has been documented since some of the earliest experiments using BDNF (Johnson et al., 1986), making it a strong candidate for a possible therapeutic. These findings are in line with other studies that have demonstrated beneficial effects from BDNF in other parts of the central and peripheral nervous system (Sendtner et al., 1992; Yan et al., 1992; Nagahara and Tuszynski, 2011) suggesting there is potential in further exploring the role of BDNF in glaucoma.

Despite the neuroprotective effects being known for over 40 years, there are still no clinical treatments available based on BDNF. Admittedly, this may be somewhat of a red flag when considering undertaking a research project in this area. However, in this time a much greater understanding of the associated pathways and mechanisms has been gained with novel strategies being implemented to try and overcome the associated difficulties. Despite the challenges involved, the profound effects of BDNF are undeniable, and it remains one of the strongest candidates for a neuroprotective treatment.

1.3. Brain-derived Neurotrophic Factor

1.3.1. Neurotrophic factor family and discovery

The neurotrophins are a group of dimeric proteins that share similar structural features and have important roles in the development of the peripheral and central nervous system. They later emerged, BDNF in particular, as major effectors of synaptic plasticity, both functional and structural (Zagrebelsky and Korte, 2014). The discovery of the neurotrophins started with NGF (see below), stemming from work in 1909 demonstrating that removal of a limb from a developing chick embryo led to the loss of sensory and motor neurons that would have innervated the limb (Shorey, 1909). Bueker, 1948 later demonstrated that transplantation of mouse sarcoma tumour cells onto developing chick embryos stimulated growth of sensory and sympathetic neurons towards the transplanted tumour. They hypothesised that there was an agent released from the transplanted sarcoma cells that could trigger neuronal growth. In 1960, this agent was successfully isolated from the mouse submandibular gland (Cohen, 1960) and formally described and named as nerve growth factor (NGF). The *in vivo* relevance of NGF was demonstrated by developing an anti-serum and using this to block growth, leading to the loss of sympathetic neurons in murine models (Cohen, 1960; Levi-Montalcini and Booker, 1960).

Based on the collective work investigating NGF, Hamburger et al., 1981 proposed that the main function of NGF was to prevent the normally occurring cell death that is seen as part of normal development, and that it acts in a targeted manner. A key principle that emerged from this work was that specific types of neurons required specific factors during their development. The critical role of NGF in the peripheral nervous system (PNS) prompted other researchers to search for similar agents that targeted other types of neurons, including those in the CNS.

While seeking this CNS equivalent to NGF, Barde et al., 1982 isolated a substance from pig brain that was able to promote the survival of sensory neurons unresponsive to NGF. It was subsequently named Brain-Derived Neurotrophic Factor (BDNF). Further work showed that BDNF promotes survival of several types of neurons, and of particular interest, placode-derived nodose ganglion neurons, also known not to be supported by NGF (Lindsay et al., 1985). Conversely, BDNF could not support the survival of NGF-dependent neurons, for example sympathetic neurons. Investigations into the structure of BDNF revealed similarities in the sequences of the BDNF and NGF. Considering the similarities in their function, this prompted the question as to whether they could be part of a wider neurotrophin family, with other related members to be discovered. By using polymerase chain reaction (PCR) targeted to the shared sequences and homology cloning, two additional members of this family were discovered and named Neurotrophin-3 (NT3) and Neurotrophin-4 (NT4) (Hohn et al., 1990; Jones and Reichardt, 1990; Kaisho et al., 1990; Maisonpierre et al., 1990; Rosenthal et al., 1990; Hallböök et al., 1991).

Studies of NT3 confirmed a prominent role in the survival of specific populations of PNS neurons, in particular those involved in proprioception and hearing. It is essential for survival of large myelinated axons in the dorsal root ganglion and spiral ganglion, leading to interest in developing treatments for deafness based on NT3 (Leake et al., 2020). There is also evidence that within the CNS, NT3 may have a role in synaptic plasticity and dendrite development. However, there are fewer data on this action compared to BDNF.

NT4 was found to bind to the same receptor as BDNF (TrkB). Less is known about its function but the common receptor suggests there is some overlap with BDNF. Deletion of the NT4 gene is not fatal and produces only a moderate phenotype in mouse models (Liu et al., 1995). This is in contrast to loss of the other three neurotrophins, all of which result in death within a few weeks after birth. This has led to speculation that NT4 may have been a more recent addition to the family in the course of evolution.

All four mature neurotrophins have 50% homology in primer sequences with similar isoelectric points (9 - 10) and molecular weights ranging from 13.2-15.9 kD (Mowla et al., 2001). Six cysteine residues are conserved in the same relative position across the neurotrophins which leads to the three intra-chain disulphide bridges and a cysteine knot structure (McDonald et al., 1991). The function and affinity for different receptors arises from the peptide loop regions. In their native state, both the precursor and mature neurotrophins exist as non-covalent homodimers (Kolbeck et al., 1994).

All neurotrophin genes are translated as a pre-pro-protein precursor. These precursors contain a signal peptide that directs the neurotrophin to the correct secretory pathway. This is followed by a pro-sequence that shows moderate conservation between the neurotrophins, specifically the conservation of features such as a glycosylation site at the same position, suggesting a critical role for N-linked glycosylation in the trafficking and maturation of neurotrophins (Mowla et al., 2001). The purpose of the pro-sequence is thought to be to allow the correct folding of the mature neurotrophin sequence (Suter et al., 1991). The pro-neurotrophin is cleaved by proteases at furin-like cleavage sites to leave the final mature neurotrophin. However, uncleaved, pro-neurotrophins also have actions of their own and in particular can interact with the p75 neurotrophin receptor to cause apoptosis (discussed below).

1.4.2. Neurotrophin receptors

Neurotrophins exert their action by binding to two different classes of receptors, the tropomyosin receptor kinase (Trk) receptors, and the p75 neurotrophin receptor (p75^{NTR}) (Figure 1.7). Trk and p75^{NTR} receptors both form homodimers but can also form heterodimers at high concentrations (Meeker and Williams, 2014).

Trk receptors

TrkA, TrkB and TrkC receptors are transmembrane glycoproteins, approximately 140 kD, that share significant sequence homology (40-45%) (Ultsch et al., 1999). They are single-pass transmembrane receptors, heavily N-glycosylated and comprising a signal sequence followed by leucine-rich repeats flanked by cysteine-rich sequences, followed by immunoglobulin-like domains. Each neurotrophin preferentially binds to a different receptor, with NGF binding to TrkA, BDNF and NT4 binding to TrkB and NT3 binding to TrkC. NT3 also binds to and

activates TrkA and TrkB, however it has recently been shown that NT3 selectively activates TrkC when the receptor is co-expressed with TrkB (Ateaque et al., 2022). The *in vivo* relevance of these biochemical observations are not entirely clear (Figure 1.6).

The neurotrophin interacts with the Trk receptor via the extracellular, immunoglobulin-like domain. Binding activates receptor dimerization and autophosphorylation of the tyrosine in the kinase domain. Kinase phosphorylation then enables recruitment of the intracellular adapter proteins, leading to the activation of cascades regulating gene transcription.

p75^{NTR} receptor

The p75^{NTR} was the first member of the tumour necrosis factor receptor superfamily to be identified. It was initially characterised as a receptor for NGF, but upon realisation that it could also bind BDNF, the receptor was renamed p75 neurotrophin receptor based on its molecular weight (MW = 75kD). It binds all of the neurotrophins with nanomolar affinity ($K_D = 10^{-9}$ M) (Rodríguez-Tébar and Barde, 1988; Rodríguez-Tébar et al., 1991), with a higher affinity for the pro-neurotrophins ($K_D = 10^{-11}$ M) (Lee et al., 2001). The effects of p75^{NTR} can be quite variable depending on the context and associations of the receptor, activating either pro-survival pathways, long-term depression, growth cone retraction, reduction in dendrite complexity and density or cell death by apoptosis. Due to these pleiotropic characteristics, Malik et al., 2021 described the p75^{NTR} as the “molecular nexus of cell death, survival and differentiation”. As well as the mature and pro forms of the neurotrophins, p75^{NTR} can bind several other ligands including amyloid- β , prion protein peptides and proteins of viral envelopes.

In contrast to the Trk receptors, p75^{NTR} has no intrinsic enzymatic activity. Instead, it achieves its effects via co-receptors and recruitment of cytoplasmic interactors. Around 30 of these interactors have so far been identified (Malik et al., 2021), helping to illustrate the diversity and complexity of the effects that p75^{NTR} can illicit. Additionally, p75^{NTR} expression varies greatly during development. All pro-neurotrophins mediate cell death when p75^{NTR} is associated with Sortilin (Jansen et al., 2007). p75^{NTR} can also interact with all three Trk receptors, modulating their binding specificity and affinity (Esposito et al., 2001). In the absence of Trk, p75^{NTR} is still capable of inducing apoptosis, even without a ligand. TrkA and TrkC can also cause cell death in a similar manner but TrkB does not appear to act in this way. The apoptotic action of p75^{NTR} has an important function in the normal maturation of the nervous system, but considering that is upregulated in some pathological conditions, for example after axotomy, it may also be a potential target for therapeutic treatments in the future.

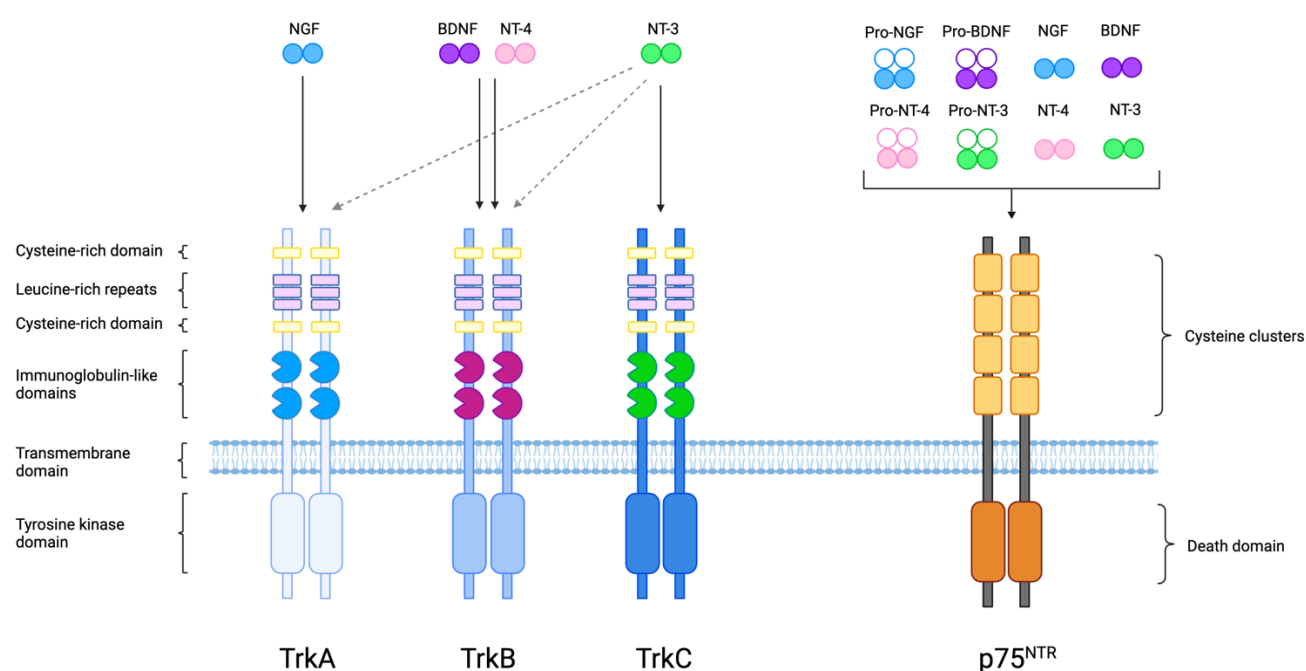


Figure 1.6: Interactions of neurotrophins and the Trk and p75^{NTR} receptors.

Each Trk receptor is comprised of an extracellular, a transmembrane and an intracellular domain. The extracellular domain consists of two cysteine-rich domains, a series of leucine-rich repeats and two immunoglobulin-like domains. The mature neurotrophins bind to the immunoglobulin-like domain closer to the transmembrane domain and trigger autophosphorylation in the intracellular tyrosine kinase domain. The p75^{NTR} receptor extracellular domain is largely comprised of cysteine clusters, and can interact with mature and pro-forms of all neurotrophins. Edited from Sánchez-Sánchez and Arévalo, 2017.

While all neurotrophins influence several cellular functions in the developing CNS including proliferation, differentiation, axon growth, and dendrite and synapse formation (Almasieh et al., 2012), the BDNF/TrkB pathway appears to have a particularly potent role in neuroprotection and has therefore received significant interest. *In vitro* experiments on multiple subtypes of neurons have consistently shown that BDNF can have a protective effect. However, research into BDNF has also revealed several challenges related to its use which have so far prevented BDNF being translated into a viable treatment. Many of these difficulties stem from the fundamental properties of the molecule (such as its high net charge and tendency to adhere to glass and plastic), and the pathways BDNF can activate. One example being the profound and prolonged downregulation of its receptor TrkB when BDNF is used at saturating concentrations (see below). It has only been recently realised that re-activation of TrkB in human neurons is possible provided sub-saturating concentrations of BDNF are used to activate TrkB (Ateaque et al., 2022).

1.3.3. BDNF Structure and properties

BDNF has a similar structure to the other members of the neurotrophin family, consisting of a non-covalently linked homodimer with a signal peptide following the initiation codon and pro-region containing an N-linked glycosylation site. Mature BDNF has a relatively small protein molecular mass (13kDa, forming a 26.5kDa homodimer) and a high net charge (pI of 9.6) (Leibrock et al., 1989). These properties mean that BDNF diffuses very poorly in tissues and across membranes such as the blood-brain barrier (BBB) (Pardridge, W et al., 1994; Poduslo and Curran, 1996). Rapid systemic clearance means BDNF also has a short half-life in humans, circulating for less than 30 minutes for serum measurements and 60 minutes for plasma (Gilder et al., 2014; Kishino et al., 2001).

1.3.4. BDNF Transcription and regulation

The *Bdnf* gene comprises nine exons that span 52.3 kb of chromosome 2qE3 in mice and 11p14.1 in humans (West et al., 2014). In neurons, BDNF promoters respond to synaptically driven neuronal activity in a calcium-dependent manner (Tao et al., 1998). BDNF has been shown to increase in the CNS experimentally in induced seizures as well as other conditions that stimulate neuronal activity (Timmusk et al., 1995). BDNF is expressed as a function of demand, and as a result, the genomic organisation is far more complex than other neurotrophins. It comprises of at least 9 different promoters, a number of splice variants and an antisense mRNA. Stimulus-selective activation of distinct sets of transcription factors bound to each of these promoters means that BDNF expression is influenced by a wide range of different stimuli (reviewed in West et al., 2014).

By disrupting the ability of cAMP response element-binding protein (CREB) to bind to *Bdnf* promoter IV in a mouse model, Hong et al., 2008 evaluated the functional significance of activity-dependent *Bdnf* transcription. They showed that it is required for developing appropriate inhibition in the cortex, but does not affect the survival of GABAergic neurons. CREB is a cellular transcription factor, the activity of which can increase or decrease gene transcription. Activation of CREB has been linked to neuronal plasticity (Caracciolo et al., 2018), and it is involved in the BDNF/TrkB pathway (Figure 1.8).

As well as the different promoters, *Bdnf* transcripts have two alternative poly A sites, creating two populations of mRNA (Timmusk et al., 1993) that are localised to different areas of the

neuron. One with a short 3' untranslated region (UTR) is restricted to the soma, whereas the other with a long 3' UTR is also targeted to dendrites (An et al., 2008; Gorski et al., 2003).

1.3.5. BDNF Signalling

The *BDNF* gene encodes a precursor protein (pre-proBDNF), that is cleaved into the smaller 32-kDa proBDNF in the endoplasmic reticulum. ProBDNF consists of a prodomain and mature BDNF. Moving via the golgi apparatus, pro-BDNF is folded and packaged into dense-core vesicles before being trafficked through the cell. Within the Golgi network and secretory vesicles, proBDNF is differentially sorted for use in secretory pathways. Furin or proconvertases cleave proBDNF into mature BDNF and the prodomain (Mowla et al., 1999) (Figure 1.7). ProBDNF, BDNF and the isolated prodomain can all be secreted from neurons and are involved in their own respective pathways (Figure 1.8). ProBDNF can also be cleaved extracellularly after being secreted from the cell by plasmin or selective matrix metalloproteinases (MMP3, MMP7 and MMP9) and will also produce mature BDNF and the isolated prodomain.

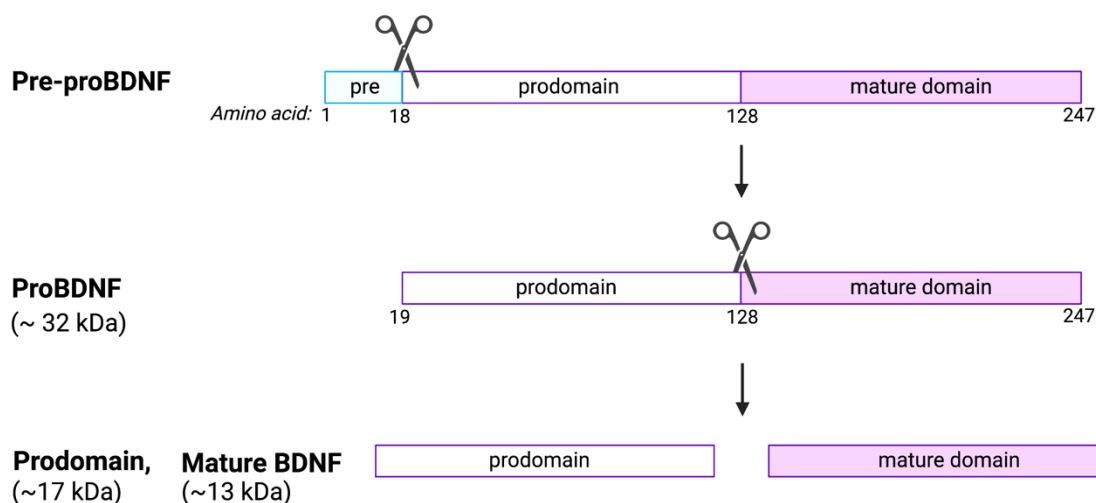


Figure 1.7: Production of BDNF, including pre-proBDNF, proBDNF and cleavage to produce mature BDNF and prodomain.

Edited from Dieni et al., 2012.

BDNF and its related structures can elicit a variety of cellular functions depending on the expression of their receptors. BDNF has the highest affinity for the tyrosine kinase B (TRKB) receptor, also known as NTRK2 after the gene encoding the receptor. It is this pathway that is responsible for promoting neuronal survival, differentiation and plasticity, as well as support

and modulation of dendrites and synapse formation. As described above, TrkB has an extracellular domain with many sites of glycosylation and an intracellular domain characterised by tyrosine kinase activity. When BDNF binds to the TrkB receptor, TrkB dimerises and autophosphorylates, activating tyrosine kinases that initiate signalling cascades. Several small G proteins including Ras as well as MAP kinase, PI3-kinase and phospholipase-C- γ (PLC-) pathways are upregulated (Bathina and Das, 2015). Ultimately, this will lead to protein translation and gene expression resulting in neuronal survival, differentiation and synapse plasticity (Figure 1.8).

TrkB receptors can be located on both the pre- and post- synaptic cell surfaces. Neighbouring cells (e.g. astrocytes) can also respond to secreted BDNF via a variant of the TrkB receptor, known as truncated TrkB, in their cell surface that lacks the tyrosine kinase domain. Activation of this receptor can regulate astrocytic morphology and also astrocytic activation in disease states (Rose et al., 2003). Truncated TrkB is seen most abundantly in glial cells but is can also be seen alongside full length TrkB in neurons. As well as having its own signalling function (Baxter et al., 1997), truncated TrkB can inhibit full length TrkB moving to the cell surface, reducing its availability. In non-neuronal cells it can rapidly bind and internalise BDNF preventing it diffusing to adjacent tissues (Mysona et al., 2017).

The expression of the TrkB receptor is notably dynamic. Neuronal activity increases the localisation of TrkB to the cell surface to allow binding with BDNF. Conversely, following the binding of BDNF, TrkB expression is downregulated with prolonged exposure to BDNF leading to complete loss of Ras signalling and disappearance of TrkB-binding sites (Carter et al., 1995). It is only the full-length TrkB receptor that sees this downregulation, with the truncated form of the receptor seemingly unaffected (Sommerfeld et al., 2000). Similarly, the downregulation following ligand binding is not seen with NGF/TrkA. By creating chimeric combinations of the TrkA and TrkB receptors, Sommerfeld et al. demonstrated that it is the intracellular, cytoplasmic domain of the TrkB receptor that is responsible for this effect. Downregulation is rapid, within one to two hours of exposure of the cells to BDNF, suggesting that the BDNF acts at the protein level rather than reducing transcription of TrkB mRNA.

This variation and feedback has a critical role in embryological development, with cessation of TrkB expression governing the essential dendritic retraction and functional maturation needed in neuronal development (Schechter et al., 2012). In mature neurons, the implications of this process can have significant consequences. For example, BDNF has been shown to rise in status epilepticus (SE) (Rudge et al., 1998). This was initially thought to have a protective role against seizure-mediated excitotoxicity. However, it has since been shown

that, in response to the elevated BDNF, TrkB is downregulated with p75^{NTR} being upregulated. This leads to neuronal injury and suggests that BDNF and/or pro-BDNF have more of an apoptotic function in SE. In this situation, administering function-blocking antibodies against BDNF in rat models of SE prevented both the downregulation of TrkB and the subsequent neuronal degeneration (Unsain et al., 2009). While TrkB is associated with cell survival, p75^{NTR} can stimulate survival or long-term depression, growth cone retraction, reduction in dendrite complexity and density or cell death by apoptosis. The isolated prodomain can also bind to the SORCS2 part of the complex directly to induce growth cone retraction. The sorting and cleaving of proBDNF is therefore an important mechanism that can regulate and balance the pro-survival effects of BDNF/TrkB activation with the pro-apoptotic effects of the proBDNF/p75^{NTR} activation.

Understanding the factors influencing TrkB availability and keeping this system in favour of its pro-survival effects has been a significant challenge in trying to develop a clinical treatment based on BDNF. It is often difficult to separate the effects of BDNF p75 activation from induced neuronal degeneration on experimental models (such as axon crush or transection) *in vivo*, with unsuccessful BDNF treatments often seeing survival equivalent to those in controls (discussed in section 1.5.3.), but there is evidence of BDNF/proBDNF reducing cell survival *in vitro* (Bamji et al., 1998; Teng, 2005; Jansen et al., 2007), and the evidence from SE studies illustrate the importance of this effect in the human CNS.

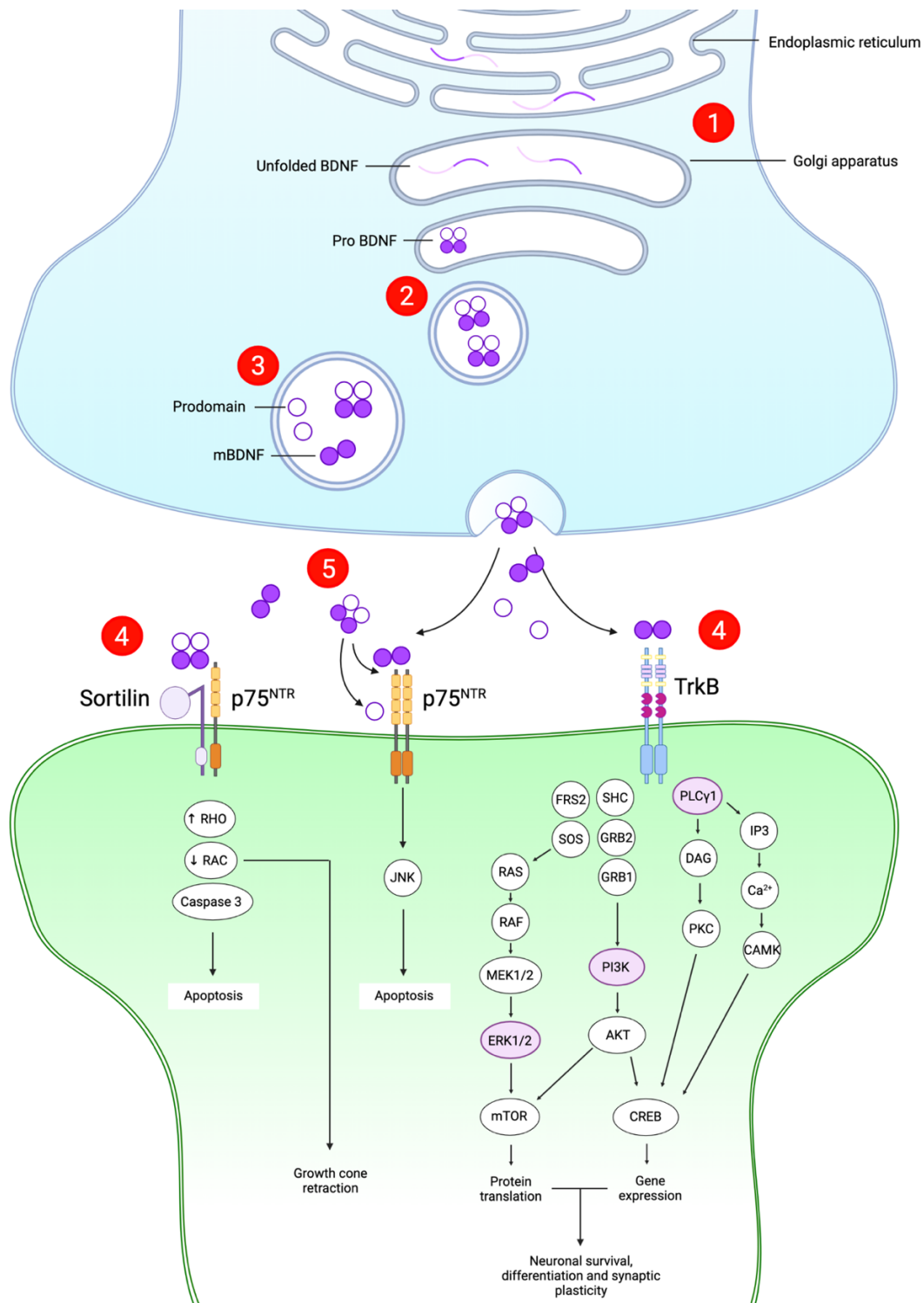


Figure 1.8: BDNF formation and receptors.

1. Unfolded proBDNF synthesised in endoplasmic reticulum, consisting of prodomain and mature BDNF. 2. ProBDNF is folded in Golgi apparatus and packaged into dense-core vesicles to be transported through the cell. 3. Intracellular processing where proBDNF is cleaved by furin or proconvertases in the trans-Golgi network or secretory vesicles respectively to release mBDNF and the prodomain. 4. mBDNF can bind to p75^{NTR} and TRKB receptors. ProBDNF can bind to a complex of p75^{NTR} and Sortilin. 5. Extracellular processing of proBDNF by MMPs or plasmin. Edited from Anastasia and Hempstead, 2013. Created using Biorender.com.

1.3.6. Cellular effects of BDNF

The pathways initiated by activation of TrkB result in several different effects, many of which are extremely important for the cell connectome, including but not limited to:

Synaptogenesis

BDNF/TrkB signalling is responsible for the formation and modulation of new synapses. This is achieved by increasing the arborisation of axons and dendrites, inducing axonal and dendrite bouton formation and stabilising existing synapses (Wang et al., 2022).

Dendritogenesis

Activation of PIK3 via TrkB leads to increased trafficking of postsynaptic density-95 (PSD-95) to dendrites and synaptic puncta (Yoshii and Constantine-Paton, 2007). Through Rac and Rho signalling, PSD-95 stimulates actin remodelling of the cytoskeleton causing growth of dendrites and spines (Penzes et al., 2001).

Synapse stability

Alpha-amino-3-hydroxy-5-methyl-4-isoxazolepropionic acid (AMPA) receptors are formed by the association of GluR1-GluR4 subunits and are responsible for most fast excitatory responses in the CNS (Gomes et al., 2003). They respond to glutamate and play an important role in synaptic plasticity, determined by the number, composition and location. Activation of TrkB by BDNF upregulates the expression of the AMPA receptor subunits and induces the delivery of AMPA receptors to the synapse (Jourdi and Kabbaj, 2013). This suggests that BDNF not only initiates the formation of new synapses, but has an important role in long term synaptic support.

Maintenance of neuronal excitation

Gamma-aminobutyric acid (GABA) is the primary inhibitory neurotransmitter. BDNF is able to cause post-synaptic suppression of GABAergic signalling by protein kinase C (PKC) following TrkB activation (Henneberger et al., 2002). PKC phosphorylates the GABAA receptor, limiting its activity and preventing the inhibitory GABA action and maintaining elevated levels of neuronal excitation.

1.4. Physiology of BDNF

1.4.1. BDNF in development

The role of BDNF in development was first demonstrated using *in vitro* studies and quail embryos *in vivo*, where administration of additional BDNF prevented the naturally occurring cell death of certain neuronal populations seen as part of normal development (Davies et al., 1986; Hofer and Barde, 1988). Building on these findings, the essential role of BDNF in development was then shown through the generation of mice with homozygous deletion of *Bdnf* (*Bdnf*^{-/-}). Most *Bdnf*^{-/-} mice die during the second postnatal week, and rarely survive beyond three weeks, primarily because of defects of the peripheral sensory ganglia (Ernfors et al., 1994; Jones et al., 1994). Excessive degeneration of the vestibular ganglia is seen, with the remaining vestibular axons failing to connect to the vestibular sensory epithelia and instead terminating in the adjacent connective tissue (Ernfors et al., 1994). As a result, these mice show severe deficiencies in balance and coordination and the affected animals are unable to compete with the other heterozygous or unaffected animals in the litter to feed. Even when care is taken to ensure the pups can feed, the lifespan is still limited to a maximum of 3-4 weeks due to additional deficits. Defects are seen in the nodose/petrosal ganglion (NPG), a population of cells responsible for relaying sensory information to the CNS to regulate heart rate, respiration and blood pressure. During development, these cells rely on BDNF synthesised by the carotid body and arterial baroreceptors. A loss of 58% of NPG neurons was reported (Erickson et al., 1996), with similar findings documented in other papers (Brady et al., 1999).

In contrast to the PNS changes seen, the CNS is grossly normal in *Bdnf*^{-/-} mice, however investigations were restricted by the limited lifespan of the *Bdnf*^{-/-} mouse. To address this problem, Rauskolb et al., 2010 developed a mouse model with conditional BDNF knockout in the CNS, while retaining normal expression in the periphery (achieved by inserting Cre recombinase into the *tau* locus, a gene expressed in postmitotic neurons). The behaviour of these animals was markedly altered, exhibiting a clasping phenomenon, long periods of inactivity and impaired light/dark exploration behaviour. They also demonstrated reduced postnatal growth in the striatum, as well as decreased dendritic complexity and spine density, however the CNS was otherwise, grossly normal. This has demonstrated that while BDNF is a key mediator of synaptic plasticity in both the developing and mature CNS, it is not essential for CNS neuronal survival (in the absence of lesion such as axotomy).

1.4.2. BDNF in retinal development

BDNF is expressed in specific locations at different stages in development of the vertebrate eye. This has been demonstrated in multiple species and described in the mouse eye in detail by Bennett et al., 1999. A mouse strain with a reporter gene lacZ, encoding the enzyme β -galactosidase, was used targeting the BDNF locus. The expression of BDNF was then inferred from the distribution of β -gal on enzyme histochemistry illustrating changes at different stages in embryological development. Expression could be seen in both the neuroretina and the anterior segment structures. BDNF is first seen in the primordial lens epithelium at approximately E10.5. As the eye develops, BDNF expression can also be seen in the majority of eye structures including the cornea, ciliary body, iris, pigment epithelium and the neuroretina. At birth, the retina has progressed to a mature two-layered structure, with BDNF expression limited to the RGCs and distinct cells along the inner margin of the ONL. In the mouse, the retina undergoes further changes in the early postnatal period before reaching the configuration of the mature adult with distinct RGC, IPL, INL, OPL and ONL layers. However, BDNF expression did not appear to change significantly from the distribution seen at birth, with expression remaining in the RGCs and sporadic cells within the INL.

Studies in hamsters have shown that expression of BDNF in the SC during development correlates with the innervation of RGCs (Frost et al., 2001). BDNF levels were initially very low, but rise in the SC (measured in dissected SC, not divided by cell types) from E14-P4 as RGCs form side branches. BDNF expression then remains high until P15 when arborization nears completion (Bhide and Frost, 1991; Frost et al., 2001). Levels rise in the retina at P12-P18 when RGC axon arbores in the SC mature. BDNF expression is then activity dependent during the normal period of RGC death and synapse formation in the maturing retina (Karlsson and Hallböös, 1998).

Numerous studies have indicated that BDNF prevents the death of RGCs, in cultured cells, retinal explants and in nerve crush studies. However, it appears that during the development of the retina other factors are involved. The administration of exogenous BDNF into the SC has been reported to reduce the rate of normal developmental RGC death in rodents (Ma et al., 1998) but did not prevent the programmed death of RGCs during the phase of target innervation in chick embryos *in ovo* (Drum et al., 1996). In spite of notable levels of BDNF in the developing neuroretina, the RGC population is not reduced in *Bdnf*^{-/-} mice (Cellerino et al., 1997). Furthermore, no overt differences were observed in the GCL, or any of the other

retinal layers when assessed at P13. The cross-sectional area of the optic nerve was reduced by 28%, as was the diameter of individual axons, but there was no apparent shrinkage of neurons in the GCL, indicating that RGCs were not noticeably atrophic in spite of the smaller axonal diameter. These observations suggest that BDNF is one of several factors promoting RGC survival in development, and that other neurotrophic pathways are able to compensate if one of these factors is removed.

The retrograde transport of BDNF from SC to the retina is seen in development and continues through to adulthood, whereas anterograde transport appears to be more prominent during the visual system development. During development, BDNF differentially affects RGCs depending on the location and source of the BDNF. Based on a series of *Xenopus* experiments, intraocular injections of BDNF decrease RGC dendrite complexity but had no effect on axon projections, whereas tectal-derived BDNF increased the arborization of both axons in the optic tectum and dendrites in the retina (Cohen-Cory and Fraser, 1995; Lom and Cohen-Cory, 1999; Lom et al., 2002). These findings suggest there is still much to be learned about the dynamics of axonal transport of BDNF in RGCs, and the interplay of retrograde and anterograde transport under different circumstances and at different stages

1.4.3. BDNF in the mature retina

The most prominent distribution of BDNF in the mature neuroretina is consistently found in RGCs, with differential expression of BDNF between subtypes. Rheaume et al., 2018 used single-cell RNA-seq to analyse 6225 RGCs, detecting around 5000 genes per cell, and classified them using a clustering algorithm into 40 subtypes according to gene expression. While all clusters showed some BDNF RNA expression, there were certain clusters that showed notably higher expression than others. The highest levels of BDNF RNA were found in what the authors designate clusters 16 and 19, followed by 26 and 36 (Figure 1.10). How these clusters may relate to function of other RGC characteristics is not yet known.

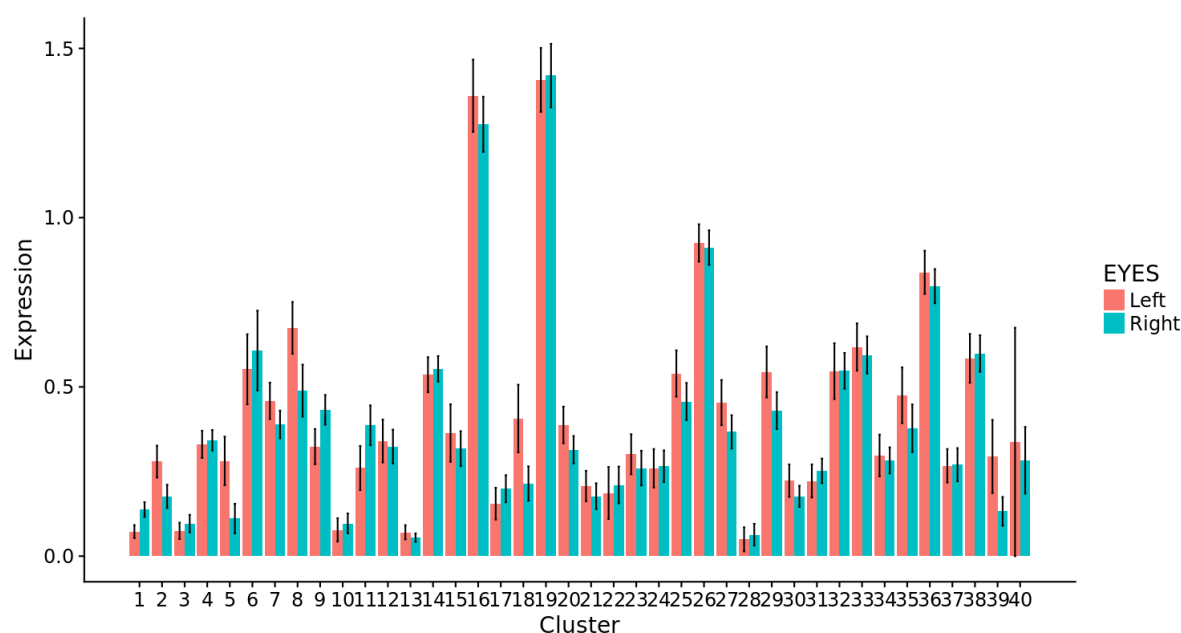


Figure 1.9: BDNF RNA Expression in RGC clusters.

Taken from Rheume et al., 2018.

Work with immunostaining has been able to demonstrate that there are sporadic BDNF positive cells in the INL, likely to be amacrine cells, with further investigation revealing that BDNF expression is found in specific subsets of amacrine cells (Fujieda and Sasaki, 2008). Under normal lighting conditions, approximately 50% of the cholinergic amacrine cells in the INL and approximately 70% of the displaced amacrine cells in the GCL of the rat retina were BDNF positive. As many as 75% of all BDNF positive cells in the INL were shown to be cholinergic amacrine cells. This is an interesting finding since cholinergic amacrine cells only account for 3-4% of all amacrine cells within the INL. Dopaminergic amacrine cells can be further divided into subtypes 1 and 2, with 40-50% of type 1 cells also being BDNF positive, and type 2 being negative. Fujieda and Sasaki, 2008 also reported that rats raised in light/light cycles as opposed to light/dark cycles led to increased BDNF expression in both RGCs and cholinergic amacrine cells.

Similar to BDNF, TrkB protein and mRNA are expressed in RGCs and glia in the inner retina (Perez and Caminos, 1995). $P75^{NTR}$ is expressed in developing RGCs but not in adults. It is however expressed in adult Müller cells and there is evidence that its activation is linked with RGC death. Pharmacological blockade of $p75^{NTR}$ in Müller glia enhanced the survival of axotomized RGCs (Lebrun-Julien et al., 2009), while ligand activation of $p75^{NTR}$ increased RGC loss (Bai et al., 2010). Therefore, while the $p75^{NTR}$ pathway is not seen in adult RGCs themselves, it has an important influence on RGC survival in both acute and chronic optic nerve injuries, and an important consideration for potential neurotrophin based treatments.

1.4.4. Peripheral BDNF

Though it retains the name *brain-derived* neurotrophic factor, it is well established that BDNF is also expressed by many cells and tissues outside the brain, including lung, spleen, muscle, vascular smooth muscle, monocytes, lymphocytes and eosinophils. BDNF mediates the activation and survival of endothelial cells, suggesting a role in angiogenesis, and may play a role in several types of cancers (Meng et al., 2018). Furthermore, BDNF is readily measurable in the blood of humans and other primates. Circulating BDNF exists in two pools: BDNF bound within platelets, and the BDNF that is free in plasma. This free BDNF also primarily originates from platelets (see below) although it has been suggested that other sources may provide small contributions.

Brain

There has been debate as to whether the brain contributes to BDNF plasma concentrations. Neurons produce BDNF in an activity-dependent manner, but questions remain as to whether this could reach the peripheral circulation. There are reports that BDNF may cross the BBB with bidirectional movement. However, the evidence conflicts with other studies that fail to show movement, and which cite the lack of a BDNF transporter and the cationic charge of the protein as explanatory factors. Krabbe et al., 2007 measured the differences in plasma BDNF from jugular arterial and venous samples in humans and reported a difference of approximately 500pg/mL at rest. This was further investigated by other researchers including Rasmussen et al., 2009, who reported that jugular venous plasma BDNF concentration was nearly five times higher than arterial at rest (442 pg/mL v 95 pg/mL). After 4 hours of rowing exercise the difference increased to 1172 pg/mL v 270 pg/mL. The interpretation of these findings by the authors was that “almost three quarters of the BDNF present in the venous circulation originated from brain structures” and that “brain tissue is the major contributor to the circulating BDNF”. The statement is surprising since that the authors had not compared arterial versus venous samples from other parts of the body. Considering the amount of BDNF contained in platelets, only a small amount of platelet activation within the cerebrovascular tissue would be required to produce this result. Additionally, the lack of detectable BDNF in the serum of animals such as mice and pigs that contain BDNF in the CNS at levels comparable to humans (Chacón-Fernández et al., 2016; Radka et al., 1996), argues against the view that the brain is a significant source of the BDNF as measured in peripheral blood.

Skeletal muscle

Skeletal muscle produces BDNF in response to activity. This was confirmed by Matthews et al., 2009 using contracting muscle cells *in vitro*, and following periods of exercise *in vivo* in

humans. But despite this production of BDNF, it did not appear to be released into circulation. Skeletal muscle overproduction of BDNF in rats also failed to increase circulating levels of BDNF. An assumption from this work was that skeletal muscle was unlikely to be a source of the additional BDNF seen with acute exercise. However, more recently there have been findings that support a role of skeletal muscle BDNF as a key factor mediating increased glucose metabolism in response to exercise (Fulgenzi et al., 2020). Mice lacking TrkB in pancreatic beta cells showed impaired glucose tolerance and insulin secretion, and this same phenotype was seen with skeletal muscle-specific BDNF knockout. Therefore, while there may be other elements involved in the response to exercise, this suggests a metabolic regulatory function of skeletal muscle BDNF. Serum BDNF has been described as “undetectable” in mice, suggesting BDNF may be present at concentrations below the detection limit of standard methods (see Chapter 3).

Vascular endothelial cells

Vascular endothelial cells have attracted significant interest regarding their role in the production of peripheral BDNF. They have been shown to rapidly secrete BDNF in response to sheer stress (Prigent-Tessier et al., 2013) and a decrease in PO₂, both factors that occur during exercise. Conversely, the endothelial production of BDNF production in hypertension. Phosphorylation of endothelial cell TrkB increases the activity of endothelial nitric oxide synthase, in turn causing the rapid, dose-dependent production of nitric oxide (Meuchel et al., 2011). Therefore, circulating BDNF can increase the production of endothelial TrkB, providing a mechanism by which endothelial cells may provide direct neurotrophic support to active neural tissues. However, the contribution of endothelial cells to circulating BDNF appears to be minimal, and these mechanisms may have a more local effect.

1.4.5. Platelets

Platelets are small anuclear blood cells produced from megakaryocytes. Like all other blood cells, megakaryocytes develop from haemopoietic stem cells (Figure 1.10), which are located in the bone marrow in adults. Before releasing platelets into the circulation, megakaryocytes have a unique process of development. They undergo multiple DNA replications without cell division, in a process known as endomitosis. There can be two to six endomitosis cycles resulting in a polyploid megakaryocyte with multiple chromosome copies. This process creates a functional gene amplification, increasing protein synthesis and enlarging the cell. The megakaryocyte then undergoes a maturation stage where the cytoplasm fills with platelet specific proteins, organelles, and the formation of granules and other ultrastructural features.

Long cytoplasmic extensions then project from the megakaryocytes with platelet-sized swellings. These extensions are often termed “proplatelets” and are thought to be the site from which platelets are released, although other mechanisms have been suggested (Machlus and Italiano, 2019). Although the megakaryocytes originate from bone marrow, they can migrate to the blood stream, meaning platelet production can also occur in other locations such as blood and the lungs. The primary role of platelets is in haemostasis, preventing blood loss in response to vessel damage, but they are actively involved in many other physiological pathways.

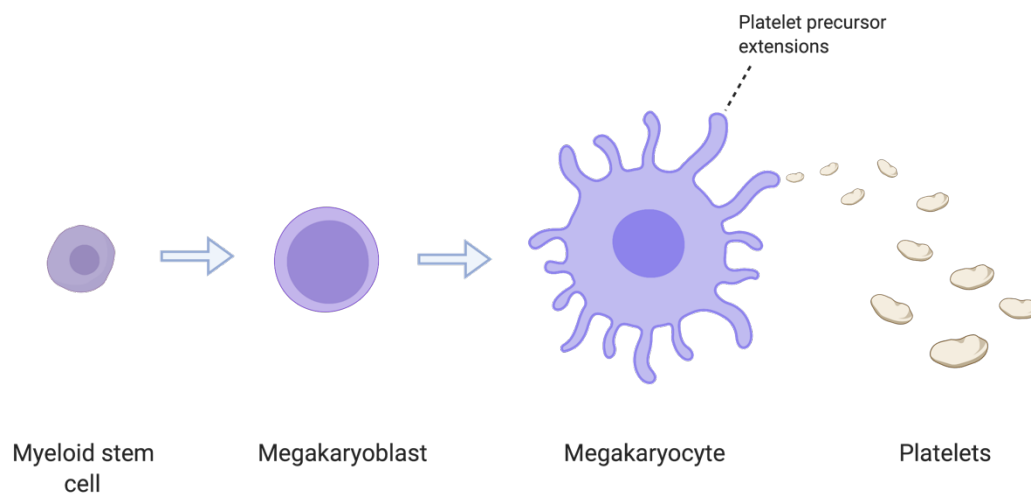


Figure 1.10: Formation of platelets.

Myeloid stem cells in the bone marrow differentiate into megakaryoblasts, which in turn develop into megakaryocytes. Platelets are then released from megakaryocytes into circulation. Created using Biorender.com.

Once released into circulation, platelets have a lifespan of approximately 8-10 days. The majority of platelets will exist in a resting state, pending activation by specific stimuli. Although platelets can be activated through several receptor-mediated pathways (Figure 1.11), they are primarily activated in response to injury to the blood vessel wall. At the site of injury, von Willebrand Factor (vWF) binds to the exposed subendothelial collagen. Under shear conditions, platelets will be captured when GP1b-IX-V receptors in the plasma membrane bind to the exposed vWF as the platelets flow past. GP1b-IX-V is one of several receptors that are highly mobile in the plasma membrane, allowing it to absorb some of the kinetic energy of the moving platelet when binding to slow it down. Under lower shear conditions, platelets bind to subendothelial collagen, initially by GPIa/IIa receptors. These receptors activate phospholipase C-mediated cascades, resulting in a rise in intracellular calcium leading to platelet activation (Sangkuhl et al., 2011). Stimulation as a result of adhesion causes

spreading and activation of GPIIb/IIIa, enabling binding of soluble fibrinogen and granule secretion. The contents of these granules activate and recruit other platelets to the area, leading to platelet aggregation.

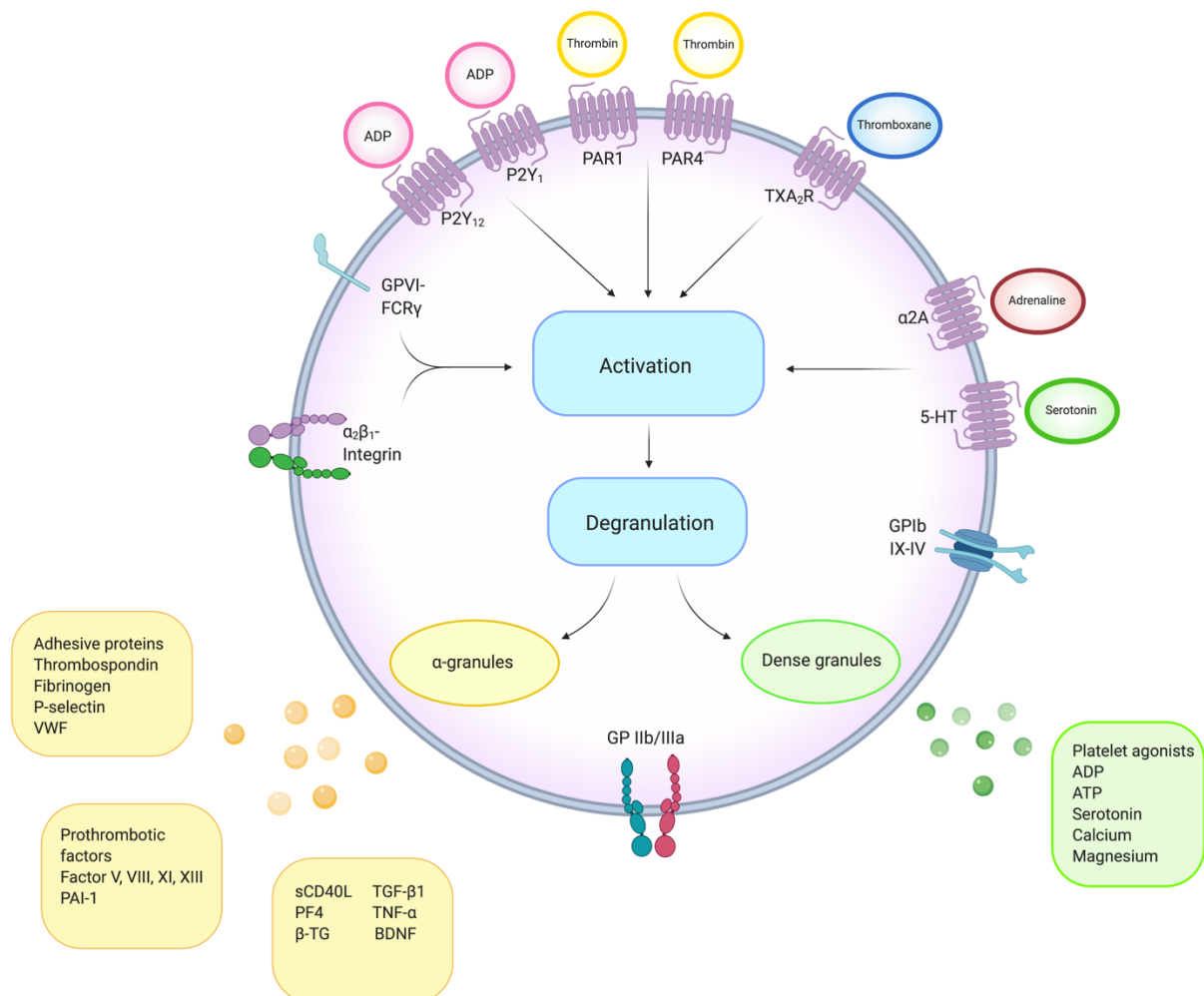


Figure 1.11: Platelet activation. Platelets can be activated by different agonists through several receptor-mediated pathways (thrombin, TXA₂, collagen, adrenaline, serotonin). Stimulation of associated G proteins ultimately activates GP IIb/IIIa receptors promoting the interaction of adjacent platelets within the clot. When the platelet is stimulated a transient influx of calcium occurs followed by extrusion of platelet storage granule contents. Edited from Serra-Millàs, 2016. Created using Biorender.com.

Platelets contain three main types of granules: alpha granules, dense granules and lysosomes (Serra-Millàs, 2016; Thomas, 2019). These are all derived from the Golgi apparatus in the megakaryocytes, but maturation continues in circulating platelets (Heijnen et al., 1998).

Alpha granules

Alpha granules are the most abundant platelet organelles with usually 40-80 granules distributed throughout the cell. They are oval in shape and approximately 200-500nm in

diameter (King and Reed, 2002). Alpha granules contain a large number of proteins with a wide variety of roles and functions that are released when the platelet is activated. For example, as well as haemostasis, they are involved in the initiation and extension of the inflammatory response (May et al., 2008). Alpha granules contain adhesive glycoproteins such as P-selectin, fibrinogen and vWF, coagulation factors, mitogenic factors, angiogenic proteins such as CD63, and various chemokines including platelet factor 4 (PF4) (Figure 1.11). PF4 is a small cytokine that promotes coagulation and is often used experimentally as a marker for platelet activation. BDNF is primarily found within this type of granule (Tamura et al., 2011), as well as other growth factors including TGF-beta, platelet-derived growth factor (PDGF) and Vascular endothelial growth factor (VEGF) (Smith, 2022). Platelet alpha granules also contain chemokines that are directly microbicidal and released in response to pathogens as part of the host antimicrobial defence (Clawson et al., 1975; Tang et al., 2002; McMorran et al., 2009). The composition of alpha-granules within platelets vary, with evidence that granules containing different components are released in response to specific stimuli (Coppinger et al., 2007; Italiano et al., 2008).

Dense granules

Dense granules are smaller and less frequent than alpha granules, with around 3-8 per platelet and a diameter of 150nm (White, 2008). They are formed through a different pathway with a less varied contents, mainly composed of cations, polyphosphates and adenine nucleotides needed for haemostasis. In particular ADP and serotonin are important secondary agonists for amplifying the platelet response.

Lysosomes

Lysosomes comprise the third type of granule, which contain a number of different degradative enzymes. These are spherical, membrane-bound organelles, approximately 200-250nm in diameter with 0-3 per platelet. The function of platelet lysosomes is poorly understood, but it is thought to involve degradation of proteins and other components within the cytoplasm. However, lysosomal contents can also be secreted during platelet activation and may therefore have an extracellular function in haemostasis as well (Ciferri et al., 2000).

Upon activation, platelets undergo a series of structural changes (Figure 1.13). In the resting state, platelets have a discoid shape with multiple folds in the plasma membrane. Once activated, the platelet sends out filopodia, spreading out around the cell. Lamellipodial sheets then fill out between the filopodia as the platelet spreads to cover a larger area, and the folds in the plasma membrane disappear as the cell becomes fully spread. These changes in shape are driven by changes in the platelet cytoskeleton following activation (Hartwig, 1992). Large

amounts of P-selectin released from alpha granules mobilise to the cell surface. Via its ligand, P-selectin glycoprotein ligand-1 (PSGL-1), P-selectin cross-links platelets and leucocytes causing aggregation and clot formation (Yun et al., 2016).

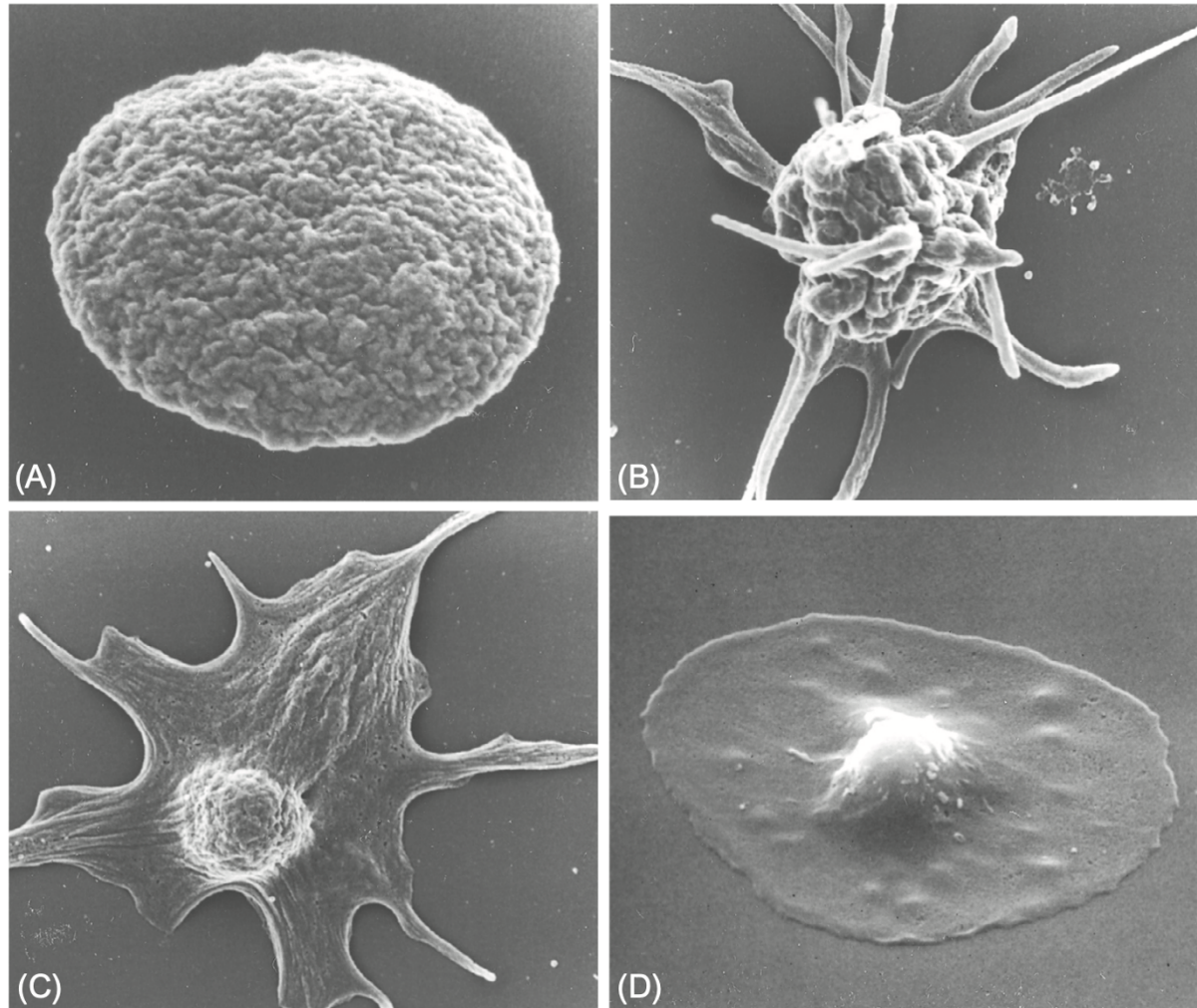


Figure 1.12: Changes in platelet shape that occur following activation.

Scanning electron micrographs of platelets at various stage of activation. **(A)** A resting discoid platelet showing delicate folds in the plasma membrane which may contribute to the increase in plasma membrane required upon spreading (magnification 30,000). **(B)** An activated platelet showing the extension of filopodia that occurs during early spreading and activation (magnification 13,000). **(C)** An activated spreading platelet showing the formation of lamellipodial sheets that fill out between the filopodia. The folds in the cell body are gradually disappearing as the platelet spreads (magnification 11,000). **(D)** A fully spread platelet imaged by conventional SEM (magnification 9000). Taken from Thomas, 2019.

These features are common to all platelets, but platelets exhibit a significant amount of variation in volume, density and reactivity (Baaten et al., 2017). Contributing factors to this heterogeneity include variability between megakaryocytes, platelet aging and unequal exposure to bioactive substances within their life time. Additionally, the expression of mRNA varies greatly within platelets. Platelets lack a nucleus and DNA, but there is evidence that

platelet RNA is inherited from the original megakaryocytes in a selective fashion (Rowley et al., 2012). Furthermore, platelets are able to release and sequester small molecules from plasma, which can include mRNA (Best et al., 2017). The rapid onset of the platelet activation pathways and the action of the mediators involved suggest that platelets are able to independently sustain translation and transcriptional gene regulation (Gremmel et al., 2016). Indeed, platelets are also capable of splicing mRNAs. This is particularly relevant for interleukin-1 beta that is translated into an active protein as part of the process of platelet activation.

Platelets and their precursor megakaryocytes, contain approximately ninety percent of blood-borne BDNF (Fujimura, Hironobu et al., 2002). They play an important role in storing mature BDNF, which they release it to target tissues following platelet activation. Fujimura et al., 2002 showed that the BDNF concentration of serum was in good agreement with the BDNF concentration of washed platelets, suggesting that platelets are the origin of almost all the BDNF in serum. Serum preparation involves complete platelet activation and contains approximately 100-200 times more BDNF than plasma in humans (Robert D. Rosenfeld et al., 1995). As previously stated, circulating BDNF is either bound within platelets, or free in plasma. It is the smaller, unbound portion of BDNF that is active within the system and able to bind to TrkB or p75 receptors. Thus, the difference in BDNF between serum and plasma may represent the amount of BDNF stored in the platelet reservoir, that can be released in response to physiological demands. Only the BDNF within alpha-granules is released on platelet activation (Tamura et al., 2011). The choice of either serum or plasma in experiments measuring peripheral BDNF, and the understanding of what these different measurements will represent, is therefore extremely important (Figure 1.13).

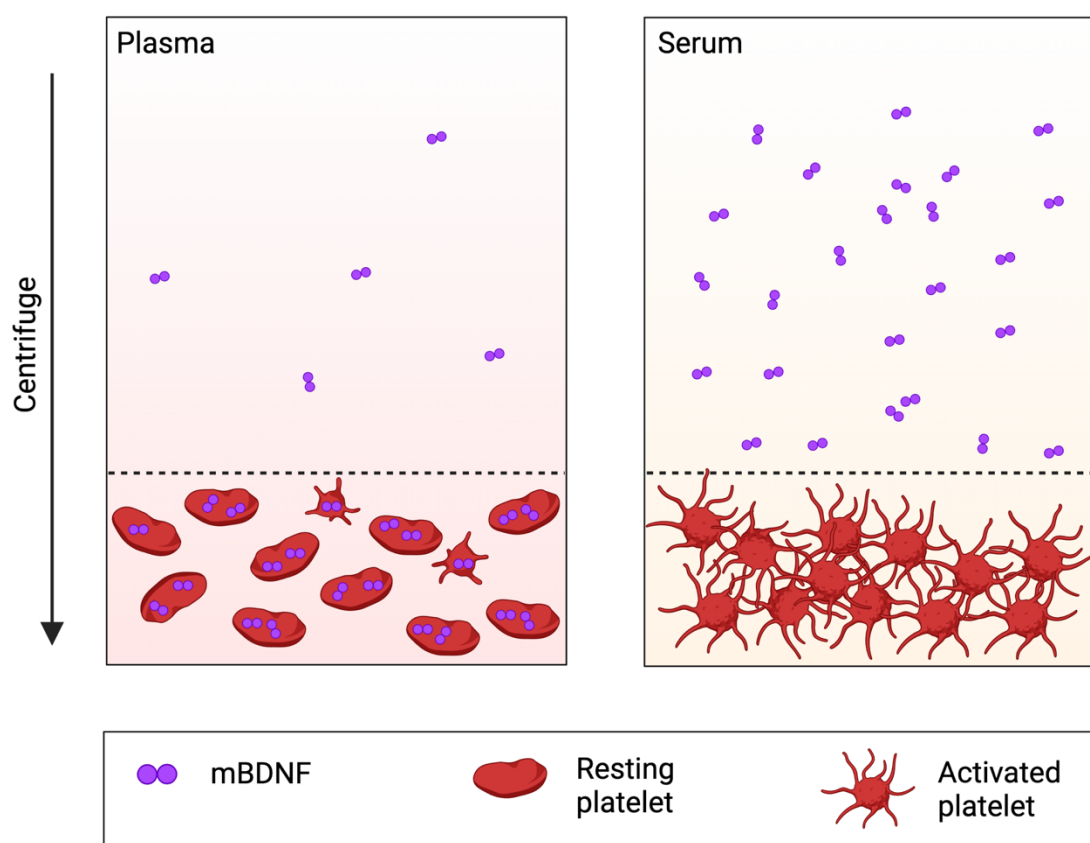


Figure 1.13: Illustration of BDNF measurement in plasma and serum preparations.

Plasma preparation uses an anticoagulant when blood is collected, preventing platelet activation and release of BDNF. Centrifuging sample pellets red blood cells to the bottom of the tube, allowing the top fraction (plasma) to be collected. Plasma concentration represents non-platelet sources of BDNF and a very small portion of the platelet store that is released under normal physiological conditions. Serum preparation does not use any additional reagents for collection, but allows the blood to fully coagulate. This involves full platelet activation and maximum mBDNF release. Centrifuging sample pellets red blood cells to the bottom of the tube, allowing the top fraction (serum) to be collected. Serum concentration represents sum of platelet and non-platelet sources of mBDNF.

Based on work by Chacón-Fernández et al., 2016, the BDNF within platelets originates from megakaryocytes. BDNF is expressed in the megakaryocytes of rats and human, with the pattern of mRNA transcripts seen in the megakaryocytes notably similar to that seen in neurons. Expression of BDNF and colocalization with PF4 (indicating storage in alpha granules) was confirmed with immunocytochemistry, which also showed BDNF in proplatelets, suggesting that platelets contain BDNF by the time they separate from the megakaryocytes (Figure 1.14). BDNF was undetectable in the megakaryocytes and serum of mice, in line with previous reports (Radka et al., 1996).

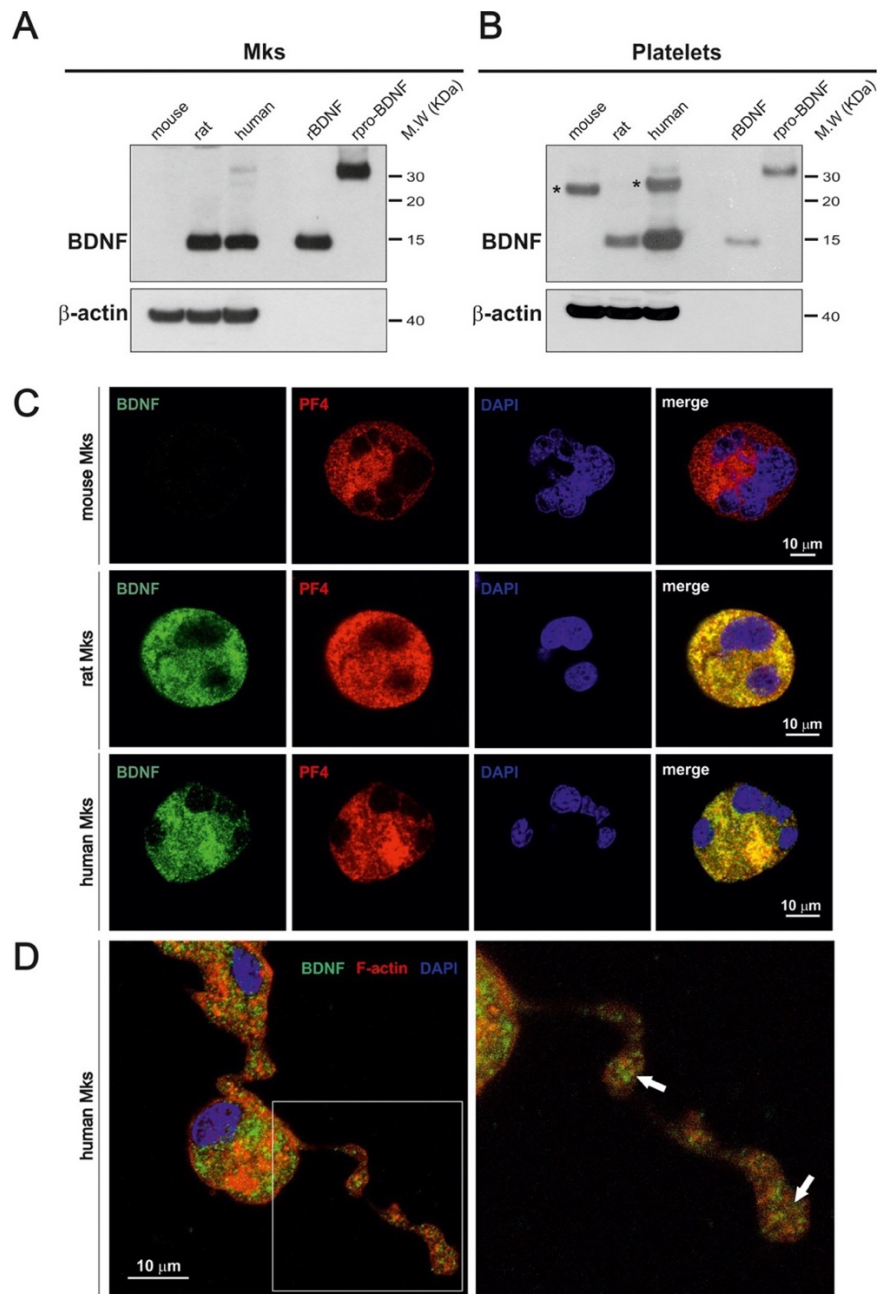


Figure 1.14: Expression of BDNF in mouse, rat and human megakaryocytes. Absence of BDNF in mouse megakaryocytes is noted, as well as the colocalization with PF4 in humans and rats. Western blot lysates of cultured Megakaryocytes (Mks) **(A)** and blood platelets **(B)** are shown. Recombinant BDNF and pro-BDNF were used as molecular mass markers and antibodies to β -actin as loading controls. Asterisks (top right panels) point to a band unrelated to BDNF likely corresponding to immunoglobulin light chains in the mouse sample. **(C)** Antibodies to BDNF (green) and PF4 (red). Blue, DAPI staining. **(D)** immunofluorescence staining of F-actin (red) and BDNF (green) in proplatelet-forming cultured human Mks. Arrows indicate BDNF accumulation in proplatelet buds. Taken from Chacón-Fernández et al., 2016.

1.5. BDNF associated pathologies

1.5.1. BDNF associated CNS pathologies

BDNF is widely expressed in the CNS, prominent in parts of the brain such as the hippocampus and frontal cortex, suggesting a role in the regulation of emotion and memory. Further evidenced by individuals carrying the Val66Met (rs6265) *BDNF* polymorphism being associated with reduced hippocampal volumes and mild deficits in learning and memory (Bueller et al., 2006; Egan et al., 2003). There is also evidence that BDNF may be involved in the pathophysiology of several neurological and psychological disorders. BDNF levels decline in the striatum and cerebral cortex in Huntington's disease (Zuccato et al., 2005) and in the substantia nigra in Parkinson's disease (Mogi et al., 1999). Serum BDNF has been found to be reduced in depressive disorders (Shimizu et al., 2003), schizophrenia (Toyooka et al., 2002) and Alzheimer's disease (Laske et al., 2007) and has been considered as a possible biomarker to aid in diagnosis and prognosis. In fact, the TrkB receptor appears to be the target of all antidepressants (reviewed in Ateaque and Barde, 2021). Conversely BDNF is increased peripherally following exercise (See Chapter 7 for full discussion). Physical exercise is well established as having benefits for the nervous system and mood, and it is thought that this may be in part mediated by BDNF activity.

1.5.2. BDNF in glaucoma

In relation to glaucoma, patients with primary open angle glaucoma (POAG) and normal tension glaucoma (NTG) have been reported to have reduced serum BDNF concentrations compared to controls. This finding has been documented in several different populations (Igarashi et al., 2020; Ghaffariyeh et al., 2011; Oddone et al., 2017; Shpak et al., 2018), with the difference most significant at the early stages of the disease. There have also been reports that lowering IOP with trabeculectomy can lead to an increase in serum BDNF 3 months after the procedure (Uzel et al., 2018). However, it should be noted that no mechanism was proposed to explain this finding, and it is unclear how this surgical intervention would be able to influence serum levels. Nevertheless, BDNF has again been proposed as a possible biomarker to aid with screening (although the mechanism behind the apparent association has not been explained). There have been reports that BDNF concentrations are also reduced in aqueous humour (Shpak et al., 2018) however, the documented values are quite variable, with additional variation seen when different ELISA methods are used (Igarashi et al., 2021).

Consequently, the relationship between glaucoma and aqueous concentration remains uncertain. At this stage it may be most accurate to simply say that aqueous BDNF levels vary widely, and that they are often at the lower sensitivity limit of for common BDNF ELISA methods.

Within the retina, animal models have shown there are local effects in response to RGC injury. Acute injury models such as optic nerve crush (ONC) have demonstrated changes in expression of BDNF and the TrkB receptor. There is some variation between studies but the overall trend is of an early increase in BDNF in the days following the crush injury, followed by a rapid loss of RGCs that is accompanied by reduced expression of BDNF and TrkB (Gao et al., 1997). This suggests that the BDNF/TrkB pathway may be part of a response mechanism to retinal injury.

Chronic ocular hypertensive models have also revealed changes in retinal BDNF. The optic nerve head is susceptible to stress caused by increases in IOP in both humans and animal models, and is thought to be a focal point of injury to RGC axons as they pass through the lamina cribrosa. Disruption of axonal transport due to elevated IOP has been demonstrated in glaucoma models, inhibiting the movement of BDNF from the superior colliculus to the RGCs (Pease et al., 2000; Quigley et al., 2000). In these studies, focal accumulation of BDNF was reported at the optic nerve and it was hypothesised that interruption of transport at this point would deprive the retina of BDNF and lead to cell death. This concept was supported by confirmation of BDNF retrograde transport in cultured rat RGCs, where fluorescently tagged BDNF was tracked via live-cell imaging. Evidence of disrupted axons and transport was also reported in genetic mouse models of glaucoma with elevated IOP (DBA/2J mouse model, see section 1.7.2 for discussion of model) (Dengler-Crish et al., 2014; Howell et al., 2007) and in the post mortem examination of the eyes from human glaucoma patients (Knox, 2007; Quigley et al., 1981). Additionally, the intentional disruption of the axon by optic nerve injury or lidocaine led to a rapid reduction of RGC function and eventual cell death (Chou et al., 2013). Despite this fairly convincing narrative, the processes that lead to cell death may be more complicated. The focus on axonal transport alone fails to clearly demonstrate its functional significance and does not take account of local sources of BDNF and other neurotrophic factors. BDNF can be expressed by RGCs, Müller cells and amacrine cells (García et al., 2003; Seki et al., 2005; Vecino et al., 2002), demonstrating that axonal transport is not the only supply for the retina. Critically, ablation of the SC in adult rats failed to cause a significant loss in RGCs (Yang et al., 2013), and destruction of the dLGN in cats did not lead to any loss of RGCs until around 6 months later (Pearson and Thompson, 1993). This seems at odds the notion that target-derived BDNF/neurotrophins are essential for RGC survival if the destruction

of said retinorecipient targets has minimal effect. It should be noted however that mature RGCs can project to several different areas (Ellis et al., 2016) and so destruction of a single location may not have entirely disrupted the target-derived supply. Deprivation of BDNF and/or other neurotrophic factors appears to play an important role in the loss of RGCs, but whether this is due to a decrease in target-derived sources, local sources or a combination of both remains to be determined.

The potential benefits of administering exogenous BDNF as a treatment for glaucoma have been considered since some of the earliest *in vitro* studies on BDNF established the neuroprotective effects on rat RGCs (Johnson et al., 1986). Administering BDNF with intravitreal injections and injections directly into the SC increased RGC survival in rat disease models (Mey and Thanos, 1993a; Ma et al., 1998; Igarashi et al., 2016), and Chen and Weber, 2001 found improved survival of RGCs in cats following optic nerve crush injuring, showing that the neuroprotective effects are seen in larger vertebrates as well. Binley et al., 2016 showed that mouse retinal explants supplemented with BDNF over 3 days had a significant reduction in RGC dendritic atrophy, and furthermore, they showed that delayed BDNF supplementation (3 days in BDNF free media followed by 3 days in BDNF supplemented media) also had a neuroprotective effect. This is particularly relevant to the clinical presentation of glaucoma where the disease process will already be progressing before a treatment is introduced.

The results from these studies are extremely encouraging and sparked a plethora of projects seeking to translate this into a viable, clinical treatment. However, the therapeutic application of BDNF has been constrained by its physical properties. The high net charge (pI ~9.6), a propensity to readily adhere to surfaces such as glass and plastic, and poor diffusion make a poor drug candidate, (Croll et al., 1998; Merkouris et al., 2018) and when in circulation, it is rapidly filtered by the kidney due to its 26.5 kD molecular weight. Furthermore, even when BDNF has reached its target, prolonged exposure causes downregulation of TrkB and loss of neuroprotective effects (Frank et al., 1996; Sommerfeld et al., 2000b). Collectively, these contributing factors have made the successful delivery of exogenous BDNF challenging. A number of strategies have been explored to overcome these technical difficulties and, while some have shown promising results in experimental models (Merkouris et al., 2018; Palasz et al., 2020), none have been sufficient to support effective clinic translation.

1.5.3. Strategies for BDNF glaucoma treatments

Intravitreal injection

Regular intravitreal injections have become common practice in ophthalmology for treating retinal conditions such as wet age-related macular degeneration, and are a natural choice to consider. This can be challenging in animal models as small rodent eyes do not tolerate repeat injections well, especially when they have already been disrupted by the increase in pressure. The poor diffusion of BDNF also means that the intravitreal injection must be performed correctly in order to ensure it is reaching the retina. Nevertheless, injections at weekly intervals in a rat ocular hypertensive model (episcleral vein cauterization) increased the survival of RGCs by around 10% at 33 days (Ko et al., 2001). But the effect of BDNF did not increase significantly with repeat injections, with the protection seemingly only lasting for around 2 weeks. This is likely in part due to the downregulation of TrkB, but may also have been due to a tendency of neurotrophins to enhance necrotic cell death after an excitotoxic insult (Koh et al., 1995). Several researchers have arrived at a similar endpoint, with BDNF losing its protective effect after around 2 weeks and the closing remarks of Ko et al., 2001 being echoed in many other papers: *"In summary, BDNF provides partial neuroprotection to RGC... However, it did not permanently rescue RGC from death."*

Topical drops

Topical treatments have been trialled as a much less invasive option than intravitreal injections. In the trials using the DBA/2J mouse both methods were able to rescue visual responses (Domenici et al., 2014). This suggested that topical BDNF was able to reach the retina, however this approach is still being validated. There is also the caveat that other inflammatory processes may be at work anteriorly in the DBA/2J mouse (see below) and the effect may not be solely due to BDNF action at the retina.

TrkB agonists

The challenging physical properties of BDNF, and the potential of activating the p75^{NTR} apoptotic pathway could potentially be avoided by developing an alternative agonist to TrkB that has a more targeted action with more suitable pharmacological properties. Bai et al., 2010 managed to delay RGC death and preservation of retina structure in acute and chronic retinal injury models *in vivo*. More recently, Zebra Biologics successfully developed several potent TrkB agonist antibodies and characterised one that was particularly successful, ZEB85 (Merkouris et al., 2018). Using TrkB reporter cell lines and neurons derived from human embryonic stem cells, ZEB85 was shown to have comparable potency to BDNF in TrkB

activation, canonical signal transduction and mRNA transcriptional regulation. Additionally, they showed that the TrkB agonists could preserve RGC dendrite complexity in a retinal explant model. The development of these agonist antibodies is an area worth following, although, it remains to be seen whether sustained exposure would downregulate TrkB in the same way as BDNF, limiting the long-term protective effects.

Gene therapies

Another alternative strategy has been to introduce a gene in the retina that will lead to sustained expression of BDNF in RGCs (Martin et al., 2003; Ren et al., 2012) or in Müller cells (Di Polo et al., 1998). This provides long-term delivery without the need for such frequent injections. While these studies have been able to initially find a protective effect, the same problems are seen with injection of recombinant BDNF. Prolonged exposure leads to downregulation of TrkB, and accumulation of unprocessed pro-BDNF binds to p75^{NTR} receptors. Ultimately, this leads to the familiar loss of the protective effect from the BDNF treatment with time. In order to address these issues, Osborne et al., 2018 developed a novel gene therapy construct containing a coding sequence for both TrkB and mBDNF by a viral-2A peptide linker. Administration of this treatment by intravitreal injection leads to transfection of the inner retina (predominantly RGCs with some amacrine/Müller glial cells) and expression of both proteins. This avoids the production of pro-BDNF, the hypothesis being that since mBDNF binds preferentially to TrkB, the p75^{NTR} pathway would be largely avoided. Expressing TrkB with the mBDNF would also solve the problem of downregulation, allowing for a sustained neuroprotective effect long-term. They were able to show a 3-fold increase of TrkB and mBDNF compared to controls, with sustained expression of both proteins. Although the outcomes have been positive, there are some important considerations that must be made. Coding for mBDNF alone omits the pre-pro-BDNF and pro-BDNF stages of endogenous mBDNF. The generation of pro-BDNF is needed for the formation of disulphide bonds that are essential for the correct folding of mBDNF and this means that while the sequence of the resulting protein would be the same, the quaternary structure may be quite different. The results from the study suggest that this form of mBDNF is able to activate TrkB but there may be other consequences to the change in structure.

As a wider consideration with these gene therapy approaches, sustained high dose delivery of BDNF may not be the optimal solution, even if the downregulation of TrkB is addressed. BDNF is normally found in very low concentrations in the CNS (Barde et al., 1982), with limited exposure. It is unclear what the effects would be of such high sustained BDNF concentrations,

especially when considering a condition such as glaucoma that would likely need ongoing treatment for at least 20-30 years.

Releasing endogenous BDNF

An alternative approach may be to explore endogenous, non-neuronal, sources of BDNF which would overcome issues of bioavailability and avoid the need for repeated administration. Platelets are a promising candidate for this physiological method of BDNF delivery because of their large store of BDNF. This reservoir is attractive as it is ready-made system that produces, stores, transports and delivers BDNF on demand throughout the body. The importance of this store has been highlighted by the surprising and hitherto incompletely understood correlations between low serum concentrations of BDNF and conditions such as depression (Shimizu et al., 2003), Huntington's disease (Ciammola et al., 2007) and Alzheimer's disease (Laske et al., 2007). These observations raise the question as to whether the enhanced release of BDNF from platelet stores could be beneficial in the treatment of neurodegenerative conditions. Unfortunately, the factors that control the storage and release of BDNF from platelets are not well understood and serum concentrations can show considerable variation under normal conditions (Naegelin et al., 2018). It is also unclear why BDNF levels in platelets or serum should reflect levels in the brain and what the underlying mechanisms of any association may be, thus highlighting the need for further investigation.

1.6. Rosa26-LSL-Bdnf-myc-IG/Pf4iCre Mouse

To further the study of platelet BDNF, a transgenic mouse model was developed expressing BDNF in megakaryocytes and platelets. This was achieved using a megakaryocyte-specific promoter excising a stop cassette from a ubiquitously expressed BDNF construct (Dingsdale et al., 2021). This mouse has been shown to be fertile with no overt behavioural or physical abnormalities, and has already been used to study the movement of BDNF between foetal and maternal circulation (Dingsdale et al., 2021). The development of the *Rosa26-LSL-Bdnf-myc-IG/Pf4iCre* mouse creates a unique opportunity study the contribution of platelet BDNF by comparing these animals to wild type mice as a control. The platelet BDNF component can be essentially isolated in a way that is not possible when studying rats or humans.

The transgenic mouse model was described in detail in Dingsdale et al. (2021) including confirmation of BDNF expression in megakaryocytes, and analysis of the other blood cells. Whole blood cell counts including red blood cells and leukocytes, were similar between Cre-

positive and Cre-negative mice, as were the composition of the major subtypes of leukocytes (Figure 1.15 A, B). There was no significant difference in platelet counts (Figure 1.15 C), and the reported counts were also comparable to those reported in C57BL6 mice in other studies (Fukuda et al., 2017). The construct used in this transgenic mouse contains a GFP marker, which was used to confirm expression in platelets. Fluorescence activated cell sorting (FACS) analysis was performed on platelets (identified by CD41) demonstrated that they could be sorted based on genotype using the GFP signal (Figure 1.15 D). This was not the case for any other cell types of the same blood lineage. The lack of GFP expression in these other cell types suggests that the inserted construct (and therefore BDNF) has not been expressed in other blood cells. The additional FACS analysis of other cell types were not included in the Dingsdale et al. 2021. The data were generated at Cardiff University, School of Biosciences by Xinsheng Nan and Annett Mueller.

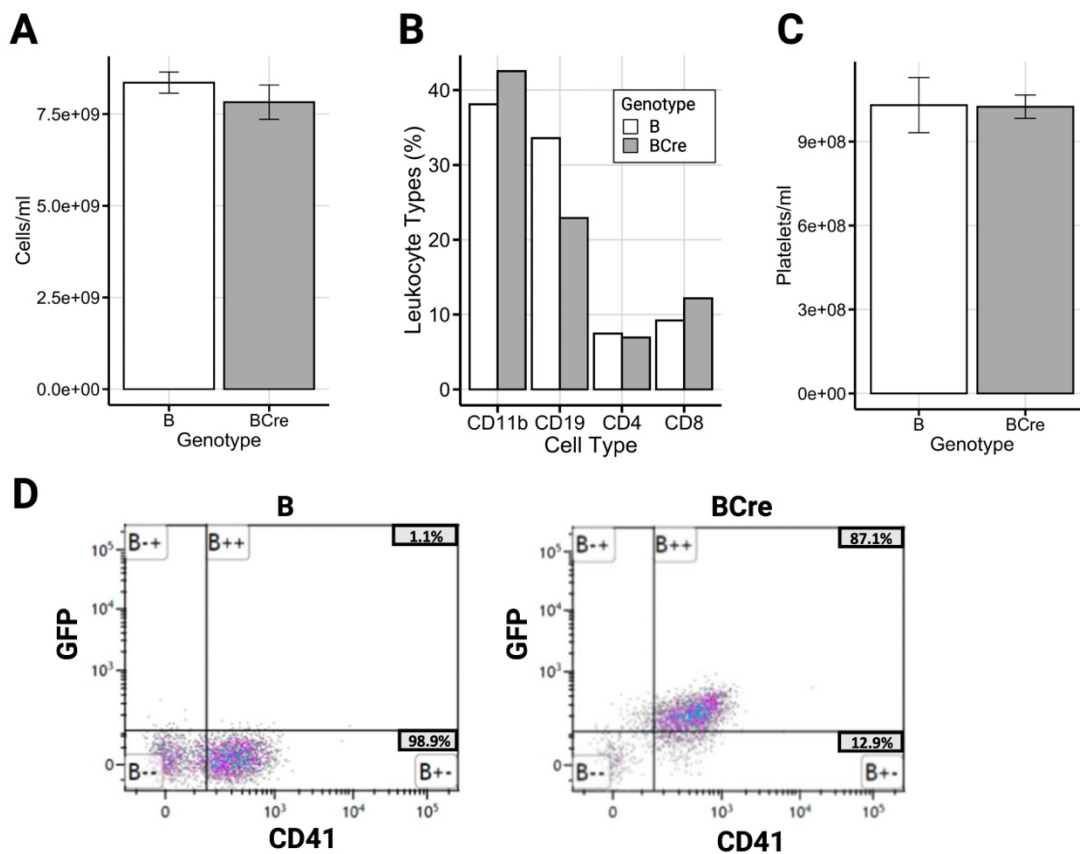


Figure 1.15: Whole blood cell counts of the *Rosa26-LSL-Bdnf-myc-IG/Pf4iCre* mouse comparing Cre negative (B) and Cre positive (BCre) animals.

(A) Whole blood cell counts (including red blood cells and leucocytes), t test: $p=0.377$; $n=4$; mean \pm SEM. (B) Composition of the major subtypes of leukocytes. (C) Platelet counts, t test $p=0.960$; $n=4$, mean \pm SEM). (D) Expression of GFP in platelets from BCre and B animals by FACS analysis. Taken from Dingsdale et al., 2021.

The primary aim of this thesis was to use the *Rosa26-LSL-Bdnf-myc-IG/Pf4iCre* mouse to explore a novel method of delivering BDNF for the protection of RGCs. Established experimental glaucoma models will be applied to the *Rosa26-LSL-Bdnf-myc-IG/Pf4iCre* mouse and compared to Cre negative, phenotypically wild type mice to determine if BDNF derived from platelets can have a neuroprotective effect on the RGCs. There are several different experimental models of glaucoma, many of which have been alluded to earlier in this chapter. Different models have different advantages and disadvantages related to costs, the difficulty of surgical procedures and the type of damage to RGCs that is induced. To investigate the effect that platelet derived BDNF may have on RGC degeneration, a selection of these models will be used.

1.7. Glaucoma models

The gaps in knowledge of the underlying pathophysiology of glaucoma means that is not currently possible to replicate the condition exactly. However, there are methods that can mimic elements of the damage seen in glaucoma. When used appropriately, with knowledge of the limitations and advantages of each technique, they have helped to gain new insights into the condition and supported the developments of new treatments. There are several well-established mouse models of glaucoma available that could be considered for the intended research project. Broadly, these can be grouped into non-hypertensive, and hypertensive models.

1.7.1. Non-hypertensive models

Genetic models

Normotensive genetic models are relatively rare, but there are some examples that have been used to try and demonstrate potential underlying mechanisms in glaucoma. For example, mice deficient in the glutamate transporters GLAST or EAAC1 developed degeneration of RGCs without changes to IOP (Harada et al., 2007). The authors proposed that this could be used as animal models of normal tension glaucoma to aid further investigation. Other knockout mouse models have been used in the study of congenital forms of glaucoma that are secondary to developmental structural abnormalities (for example knockout of cytochrome P450 family 1, subfamily B, polypeptide 1 (*CYP1B1*) or tyrosine gene (*Tyr*) can both result in

ocular drainage abnormalities resembling those in human primary congenital glaucoma (Libby et al., 2003)), but these are not standard tools in glaucoma research.

Retinal Explants

Retinas can be removed immediately after death, following optic nerve transection, and cultured in an incubator for several days. Over this time, a predictable and progressive degeneration and death of RGCs is seen (Bull et al., 2011; Murali et al., 2019). While the mechanism that leads to the degeneration of the RGCs in this model is clearly very different from clinical glaucoma, there are several advantages with this method. The procedure is relatively straightforward to perform, and degeneration is seen after only a few days allowing rapid turnover (in contrast to the need to sustain elevated eye pressure in ocular hypertensive models for several weeks). Additionally, the environment *in vitro* can be carefully controlled, with precise concentrations of active agents added to media and strict control of temperature and other conditions. While there are limitations when extrapolating findings from retinal explants, it is an exceptionally useful model for gaining early insights into the behaviour of RGCs.

Optic nerve crush

Injury to the optic nerve leads to axonal degeneration and gradual loss of RGCs by apoptosis. This can be achieved experimentally by the application of pressure to the optic nerve using calibrated forceps to crush the axons without severing them (Tang et al., 2011). This provides a standardised method of initiating RGC degeneration over time and can be used to study the mechanisms involved in neuronal deterioration and death *in vivo*. The optic nerve crush (ONC) model is once again achieving degeneration through a mechanism that differs from clinical glaucoma. However, the reliability and predictable nature of the technique have made it a central part of glaucoma research for decades, and it has been widely used in preclinical studies for a range of interventions in many different species.

1.7.2. Hypertensive models

While methods such as ONC has proven to be a valuable and reliable experimental model, other strategies are also used to induce optic neuropathy by increasing the IOP, both chronically and acutely, in an attempt to create conditions closer to the clinical picture of glaucoma.

Genetic models

The most widely used genetic animal model for glaucoma research is the DBA/2J mouse. This strain develops raised IOP due to pigment dispersion from the iris that leads to occlusion of the trabecular meshwork and development of synechiae. IOP is typically 8 mmHg at 4 months, rising to around 16 mmHg at 12 months. This increase in IOP leads to a characteristic optic neuropathy, with loss of RGCs seen at approximately 6-8 months, reaching end stage disease by 12 months (Libby et al., 2005). This model has the advantage of producing RGC damage representative of glaucoma without the need for interventional procedures. While this is beneficial, the time taken for pathology to develop does incur significant time and financial costs. Additionally, a longitudinal study of the DBA/2J mice was not able to find a correlation between IOP and axon loss, leading to a suggestion that other factors such as an inflammatory response may also be playing a role (Scholz et al., 2008). Furthermore, the onset and progression of optic neuropathy between individuals can be inconsistent, creating an element of variation even when mice are age-matched. Caution should therefore, be taken when extrapolating findings made with this model. Despite the limitations of the model, it is nevertheless a valuable tool and has been widely used.

Laser trabeculoplasty

Laser photocoagulation of the trabecular meshwork (TM) obstructs outflow of aqueous leading to elevated IOP. The model was first applied to rodents in 1998 (Ueda et al., 1998) with modifications made to the technique as experience has increased and the laser equipment has developed (Yun et al., 2014). When applied to mice, the IOP outcomes are variable, but broadly this method can induce IOPs of >30mmHg for around 4 weeks, although it may often require repeat procedures to maintain these levels (Grozdanic et al., 2003; Ji et al., 2005). This sustained elevation in IOP makes this model attractive to longer-term treatments. However, the procedure requires laser equipment and training that can be expensive. The energy absorbed from the laser is also dependent on the pigmentation of the target tissue, and must therefore be titrated depending on the strain and species of animal used. Even between individuals there is some variation in laser uptake, and the increased energy absorbed can exacerbate inflammation and lead to inconsistent changes in IOP (Johnson and Tomarev, 2010). As with the DBA/2J mouse, it can be difficult to ascertain if the changes seen are due to the elevated IOP, or an inflammatory response caused by the model.

Episcleral vein cauterization

Episcleral veins can be cauterised using handheld devices or laser, and while this does produce a significant IOP rise in rodent models, there is usually a decline at around 7 days

(Shareef et al., 1995). This may be due to an accommodating effect from the remaining episcleral veins and collateral vessels. Cauterising all episcleral vessels delays the decline in IOP until around 10 days in rats, however it causes corneal decompensation and is therefore generally unsuitable. Furthermore, repeat treatments for inducing elevated IOP are difficult, and direct retinal damage can occur (Rho et al., 2014). This method is therefore better suited for experiments that use a shorter duration of elevated IOP.

Sclerosis of Episcleral Veins

Injection of hypertonic saline into the episcleral veins causes sclerosis of the vessels that increases the resistance of aqueous outflow. This causes a chronic elevation in IOP that can be sustained for several weeks (Morrison et al., 2008). This is a very effective model however it is technically challenging. The small episcleral vessels must be delicately cannulated, a challenging task even for an experienced surgeon. It requires a very long training period and even then, the success rate is researcher dependent. Therefore, despite being arguably one of the most successful models in rodents, it is not the most accessible choice (Morgan and Tribble, 2015).

Microbead Models

Other alternative methods to elevate the IOP involve injecting microparticles into the anterior chamber that will accumulate in the TM and obstruct aqueous outflow. Only partial/segmental obstruction of the TM is needed to raise the IOP, although repeated delivery of the microparticles is often needed. These approaches have a long history of use in experimental glaucoma and can be applied to many different models and species. They have a certain degree of variability and control that allows the technique to be adapted as needed for a given study. Early experiments used ghost red blood cells, but there are now a wide range of high-quality microbeads available with different sizes and materials. Polystyrene, latex, polyurethane (PU) and polymethylmethacrylate (PMMA) are among the most common and have different material properties. For example, polystyrene and PMMA are relatively rigid, whereas PU is more flexible and may be able to penetrate deeper into the TM pores (Rho et al., 2014).

A drawback of microbead models is that the excess material can obscure the visual axis and limit the ability to accurately monitor the health and function of the retina. To minimise this effect, Samsel et al., 2011 developed a method in which magnetic microspheres are injected into the anterior chamber and then relocated towards the TM using an external magnet (Figure 1.16). While the natural flow of aqueous through the TM will slowly carry all microparticles in this direction, the magnetic model allows for far more control over the position of the beads.

Additionally, the microbeads can be dissociated from the carrier solution during injection. The magnet can also draw the microbeads away from the injection site preventing loss associated with reflux through the wound when injecting, a common problem with the microbead model.

The control and versatility that the microbead models provide has made them very popular, although they can be technically challenging to perform. Several factors, including cannulation technique, injection time, volume of beads used, and species, can all impact the outcomes and lead to some variation in results between different experimenters, (Urcola et al., 2006; Sappington et al., 2010; Samsel et al., 2011a; Cone et al., 2012; Frankfort et al., 2013; Morgan and Tribble, 2015).

The choice of methods and materials will depend on the degree and duration of IOP changes required and the species being used. Microbead models are particularly useful in rodents due to the small anterior chamber, and the possibility of combining the technique with different genetic models (Morgan and Tribble, 2015).

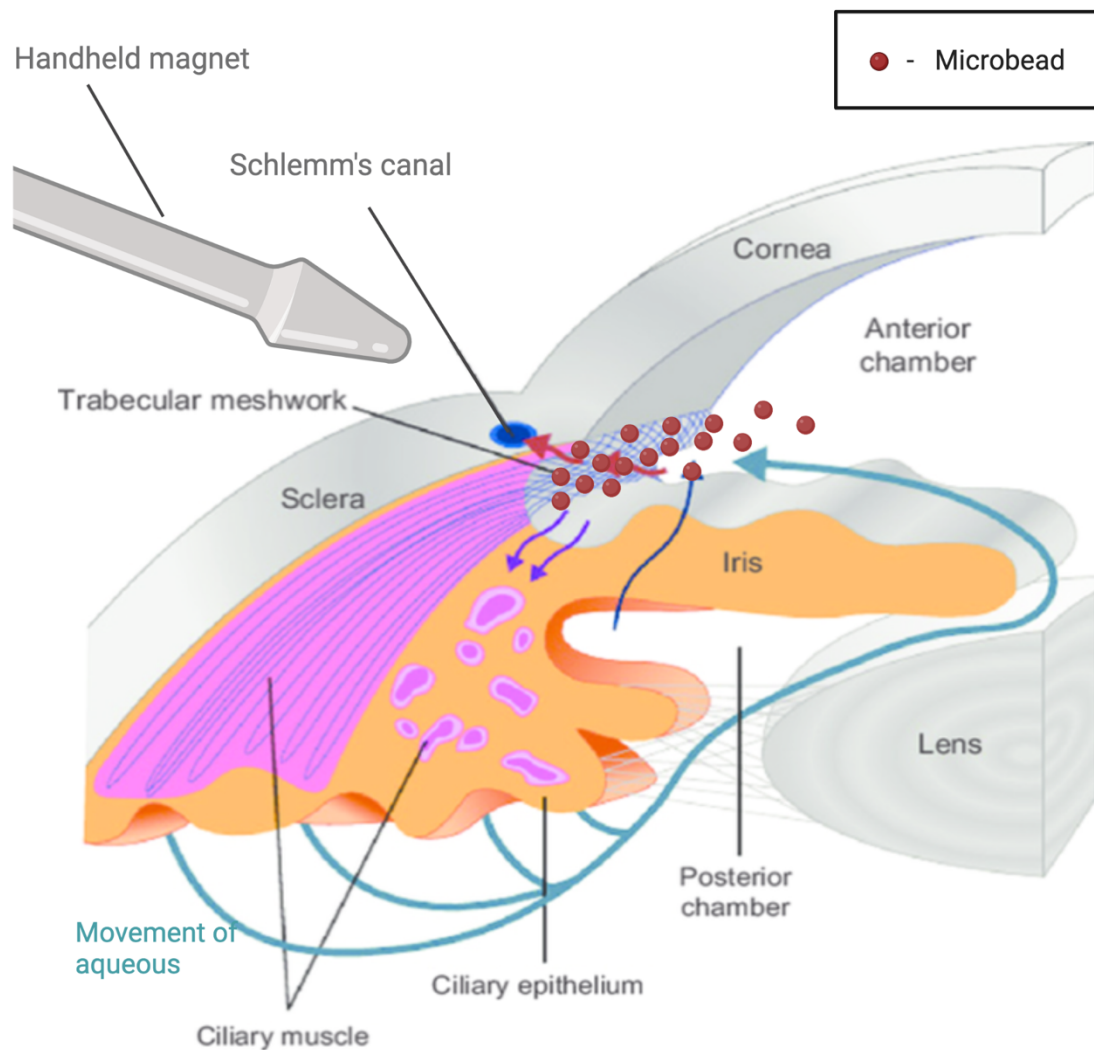


Figure 1.16: Microbeads blocking aqueous outflow by obstructing the trabecular meshwork.

Edited from Crawley et al., 2012.

1.7.3. Models selected

Based on the many advantages of the technique and the existing expertise available within our group, the magnetic microbead model was considered to be the most suitable choice for the project proposed in this thesis. However, considering it has not yet been widely applied to mice, it was sensible to also incorporate other more well-established models. The retinal explant was a preferred model in this respect. The accessibility of the technique, the ability to obtain data after a few days, and the wealth of literature on mouse retinas and BDNF make this a very appropriate choice. Another *in vivo* model would also be highly desirable considering that the BDNF delivery in this mouse model is dependent on the normal,

physiological production and circulation of platelets. The cost of buying laser equipment unfortunately excludes the laser trabeculoplasty method. And while it would certainly be fascinating to see how a cross with the DBA/2J strain would progress, this was also considered unsuitable. Aside from the major concerns over the true cause of the RGC degeneration in these mice, there would be substantial costs incurred purchasing and maintaining another transgenic colony alongside the *Rosa26-LSL-Bdnf-myc-IG/Pf4iCre* mice, and coordinating cross breeding to have sufficient numbers of animals with the multiple different genotype combinations needed to collect reliable data was simply impractical.

The ONC model requires minimal additional equipment and, although there are limitations directly translating this mechanism of axon injury to clinical glaucoma, it is an extremely reliable procedure to cause RGC degeneration. The extensive library of previous ONC studies across species with different neuroprotective methods also make this method an important benchmark when considering how the results of the *Rosa26-LSL-Bdnf-myc-IG/Pf4iCre* fit into the wider research in the field. ONC was therefore selected as the third model to be used for this project. The combination of retinal explants, ONC and magnetic microbead models should ensure that sufficient data can be collected from both *ex vivo* and *in vivo* models and provide a broad assessment of this novel transgenic model.

1.8. Summary

There is now a wealth of data showing the neuroprotective properties of BDNF in RGCs. This knowledge is obviously valuable considering the desperate need for new glaucoma treatments. However, despite several decades of encouraging results, there are still no BDNF/TrkB-based treatments based in clinical practice. While this state of affairs has generated understandable frustration and even concerns, much has been learned during this time about the design of promising strategies to overcome the difficulties associated with BDNF and TrkB signalling. With a suitable method of delivery and control of the concentration to prevent TrkB downregulation, successful approaches now appear to be within reach. Furthermore, platelets as natural, circulating and therefore ubiquitous BDNF reservoir are emerging as promising vehicles.

The primary aim of this project will be to use the unique *Rosa26-LSL-Bdnf-myc-IG/Pf4iCre* transgenic mouse to determine if BDNF carried by platelets demonstrably deploy a neuroprotective effect on mouse RGCs in experimental glaucoma models. To achieve this

goal, the project brought together a combination of different glaucoma models in order to balance their different strengths and limitations: retinal explants, optic nerve crush and microbead ocular hypertensive models. The morphology of RGC dendrites was scrutinised to detect changes in cell health and to study the cell connectome. These detailed investigations were complemented by measurements of cell survival using RGC counts to provide a wider assessment of the neuroprotection. Circulating levels of BDNF were measured using ELISA of proven sensitivity and specificity and in later experiments, methods were explored to try and enhance BDNF release from platelets in a potentially relevant clinical perspective.

Chapter 2. Methods and Materials

2.1. Animals

2.1.1. Animal husbandry

All animals in this study were approved by the Cardiff University Ethical Review Board, and all experiments were performed within the guidelines of the Home Office Animals (Scientific Procedures) Act, 1986. All animals were housed in the licenced facility at Cardiff University. Animals were housed in M3 cages (48 x 15 x 13cm, 510cm² floor space) with 1 - 5 adult mice per cage. Different mouse lines were housed separately, but within the different mouse lines, mixed genotypes were housed together (i.e. homozygous/heterozygous/wild type mice were not separated). Environmental conditions were controlled to maintain a room temperature of 20-24°C, and a humidity of 55% +/- 10%. They were maintained on a 12-hour light/dark cycle, from 06:00 to 18:00, and had access to food *ad libitum*.

2.1.2. Rosa26-LSL-Bdnf-myc-IG/Pf4iCre Mouse

The *Rosa26-LSL-Bdnf-myc-IG/Pf4iCre* Mouse was kindly provided by Professor Yves Barde's group. The model was developed by Dr Xinsheng Nan, Cardiff University, who also provided the information on the resulting phenotype and protocols for genotyping. The development of the model has been described in detail (Dingsdale et al., 2021) but due to its central role in this research project, a description is also included here.

To generate the Rosa26-LSL-BDNF-myc-IG mice, “The pZDonor-Mouse-Rosa26 plasmid (Sigma-Aldrich, D9196) was used as the backbone of a Rosa26 targeting vector. We inserted a 4185 bp PCR fragment, containing chimeric intron–exon-loxP-NeopA-loxP-MCS-IRES-eGFPpA amplified from the pCAGfloxedNeolRESeGFP plasmid (gift from Professor Meng Li, Cardiff University) as a template, to the EcoRI/XmaI site to generate pZDR-LSL-IG. To generate pZDR-LSL-BDNF-myc-IG, a fragment containing the BDNF-myc coding sequence was isolated by double digestion with EcoRI/SacI from pCMV-BDNF-myc (constructed by adding one myc-tag copy at the C-terminus of WT mouse BDNF following the deletion of the last three amino acids⁵⁵) and inserted into the PmeI site of pZDR-LSL-IG. Mouse ES cells E14TG2a were cultured in gelatin coated flasks or Petri dishes in GMEM medium (ThermoFisher Scientific, 11710035) with LIF (homemade) and 10% FCS (Biosera, FB-1001/500). To generate Rosa26LSL-BDNF-myc-IG mouse ES cells, cells were transfected with pZDR-LSL-BDNF-myc-IG and pCMV-RosaL6 ELDmut and pCMV-RosaR4 KKRmut (gifts from Charles Gersbach, Addgene plasmid #37198 and #3719956) in a 10:1:1 ratio. Transfection was performed in Nucleofector solution P3 (Lonza, V4XP-3024) using 4DNucleofector X Unit (Lonza, AAF-1002X), program CG104. 5'-homologous recombination was confirmed by generation of a 2.2 kb PCR fragment using primer pair (GTGGAGCCGTTCTGTGAGAC and GTCATAGCCG AATAGCCTCTCCAC), 3' homologous recombination by a 1.3 kb PCR fragment using primer pair (TCGAG CTGGACGCGACGTAAAC and TTGGGGGAGGAG ACATCCACCTGG). Rosa26-LSL-BDNF-myc-IG mice (BDNF-myc hereafter) were generated by injection of Rosa26-LSL-BDNFmyc-IG mouse ES cells into C57BL/6 blastocysts. Germline transmission was genotyped by PCR as above. Subsequent genotyping was conducted by PCR using two primer pairs (Bdnf pair: GAACTACCCAATCGTATGTTTCG and CTACAAGTCTTCTTCAGAAATAA GCTT; Rosa26 pair: AAGGGAGCTGCAGTGGAGTA and GTCCCTCCAATTTTACACC) to identify heterozygotes (140 bp and 275 bp products), homozygotes (140 bp), and wild-type animals (275 bp).”(Dingsdale et al., 2021b)

In summary, the model was created by inserting a myc tagged *Bdnf* gene, preceded by a stop cassette flanked by loxP sites, into the C57BL/6 mouse *Rosa26* locus that would be conditionally expressed in the presence of Cre recombinase (Figure 2.1). The *Rosa26* locus is located on chromosome 6 and is a widely used target for knock-in models as genes inserted at this site are ubiquitously expressed without disrupting functionally relevant gene function. Platelet specific BDNFmyc expression is achieved by crossing the *Rosa26-LSL-BDNFmyc-IG* with *PF4-Cre* mice (The Jackson Laboratory, 008535, C57BL/6 background), to remove the Neo-pA cassette. The Cre-recombinase activity of the PF4-Cre line has been extensively investigated and shown to be confined to megakaryocytes (Tiedt et al., 2007). These mice

express BDNFmyc in the presence of the mouse PF4 codon-optimised Cre recombinase (iCre) that also includes a nuclear localisation signal.

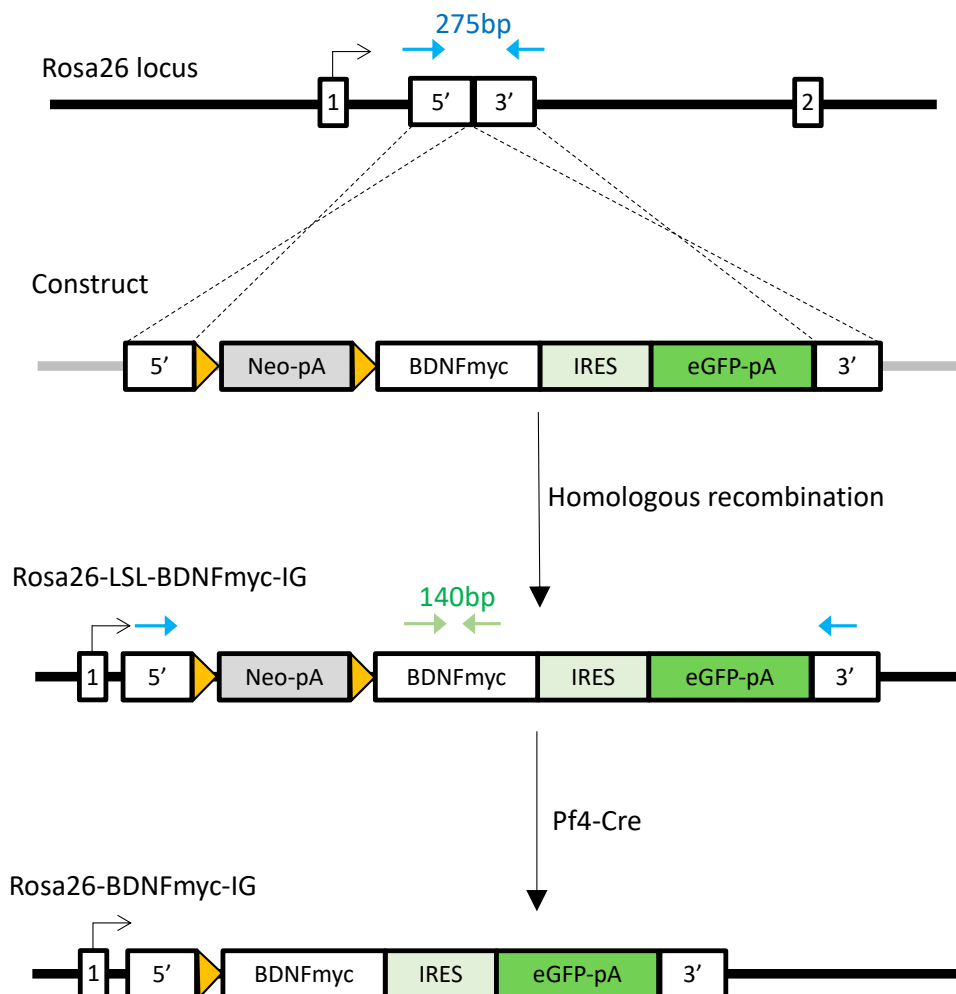


Figure 2.1: Generation of a mouse model expressing a myc tagged BDNF in platelets.

The construct used here was comprised of a 5' end homologous recombination arm (5'), a neo resistant gene with a polyA signalling sequence (Neo-pA) flanked by loxP sites (yellow triangle) on both ends, *Bdnf* coding sequence fused with *myc* tag coding sequence in frame (BDNFmyc), an Internal Ribosome Entry Site (IRES), eGFP reporter gene with a polyA signalling sequence (eGFP-pA) and the 3' end homologous recombination arm (3'). The Neo-pA stop cassette is removed in the presence of Pf4-Cre, allowing expression of the construct. Reproduced and edited with permission from Xinsheng Nan, Cardiff University.

Breeding pairs were set-up using homozygous and heterozygous BDNFmyc pairings, with Pf4-Cre-positive and Pf4-Cre-negative animals. When bred from heterozygous parents, intra-litter genotypes were expected at mendelian ratios. At the time of weaning litters, ear notch tissue biopsies were taken from mice for genotyping by PCR (see below). PCR was performed for the BDNF recombination (140 bp) and Rosa-26 wild type (275 bp), and then separately for

the PF4-Cre product (420 bp) with Jarid c/d (302 bp on Y chromosome, 331 bp on X chromosome) used as an internal control for the reaction.

As expected, Cre-negative animals were found to have serum and plasma BDNF levels equivalent to wild-type mice, whereas BDNFmyc; Cre-positive mice have concentrations that were similar to the range seen in humans.

The *Rosa26-Bdnf-myc/PF4iCre* mouse is hereafter referred to as:

B Cre+	Cre positive (either homozygous or heterozygous BDNFmyc)
B+/+ Cre+	Homozygous <i>BDNFmyc</i> , Cre-positive
B+/- Cre+	Heterozygous <i>BDNF</i> , Cre-positive
WT	Wild type, Cre-negative (irrespective of <i>BDNFmyc</i> genotype)

2.1.3. C57BL/6J Mice

8-week-old C57BL/6J mice were purchased from Charles River Laboratories (MA, USA) and habituated for 7 days before being used for experiments or set up into mating pairs.

2.1.4. Genotyping - DNA Extraction

Genotyping for the *Rosa26-LSL-Bdnf-myc-IG/Pf4iCre* mouse line was performed by PCR from ear notch tissue biopsies. DNA Extraction was performed using PCR BIO Rapid Extract PCR Kit (PCR Biosystems, PB10.24-40). A master mix was made containing for each tissue sample:

- 5X PCR BIO Rapid Extract Buffer A 20 µL
- 10X PCR BIO Rapid Extract Buffer B 10 µL
- Double distilled water 70 µl

Tissue samples were kept in Eppendorf tubes and were centrifuged at high speed for 1 min to ensure sample was at the bottom of the tubes, before adding 100 µL of the master mix to each. Samples were then incubated at 60°C for 30 minutes on a thermomixer at 1100rpm, followed by incubation at 95°C for 10 minutes (no shaker). 400 µL of ddH₂O were added to each sample before centrifuging at high speed again for 1 minute to pellet debris at the bottom. Supernatant was removed and stored at -20°C or used immediately for PCR.

2.1.5. Genotyping - PCR Reaction

All primers for PCR reaction were made up to 100µM concentration in TE buffer. Separate primer mixes and samples were used for *Rosa26/Bdnf-myc* reactions and the *iCre/Jarid1* reactions. Mixes were made with equal volumes of the relevant primers for each reaction (Table 2.1 and Table 2.2).

Table: 2.1 Primers for BDNF/Rosa26 PCR reaction

Primers	Sequence	PCR product
Bdnf-pFt	GAAGTACCCAATCGTATGTTTCG	Bdnf-myc PCR product 140 bp
myc-pR	CTACAAGTCTTCTTCAGAAATAAGCTT	
Rosa26 WT - Forward	AAGGGAGCTGCAGTGGAGTA	PCR product 275 bp
Rosa26 WT - Reverse	GTCCCTCCAATTTTACACC	

Table 2.2 Primers for iCre/Jarid1 PCR reaction

Primers	Primer sequence	PCR product
Pf4pro-F2g	CCAAGTCCTACTGTTTCTCACTC	iCre PCR product 420bp
iCre-Rg	TGCACAGTCAGCAGGTT	
Jarid1c/d - Forward	CTGAAGCTTTTGGCTTTGAG	Jarid1c/d 302bp(Y) and 331bp(X)
Jarid1c/d - Reverse	CCACTGCCAAATTCTTTGG	

A PCR reagent mix was made for each reaction containing the following volumes for per sample to be tested:

- 2X PCRBIO HS Taq Mix Red 10 µl
- ddH₂O 8.6 µl
- Primer mix 0.4 µl

19µl of respective PCR mixes was added to PCR tubes, with 1µL of samples made from the DNA extraction procedure above. Tubes were then centrifuged at high speed for 1 min to ensure all of the sample was at the base of the tubes and bubbles removed. The PCR reaction was then performed with the relevant program:

Bdnf/Rosa and iCre/Jarid1

- 95°C for 3min
- (95°C for 30 seconds, 60°C for 30 seconds, 68°C for 1 minute) x35 cycles

- 4°C for infinite1

2% agarose gel was made using 1X TAE buffer with 5µl of Ethyl bromide in 100ml. In a 20 well gel, 15µL of sample was added to each well, with 10µL of 100bp ladder. The gel was then run at 120V for roughly 50 minutes.

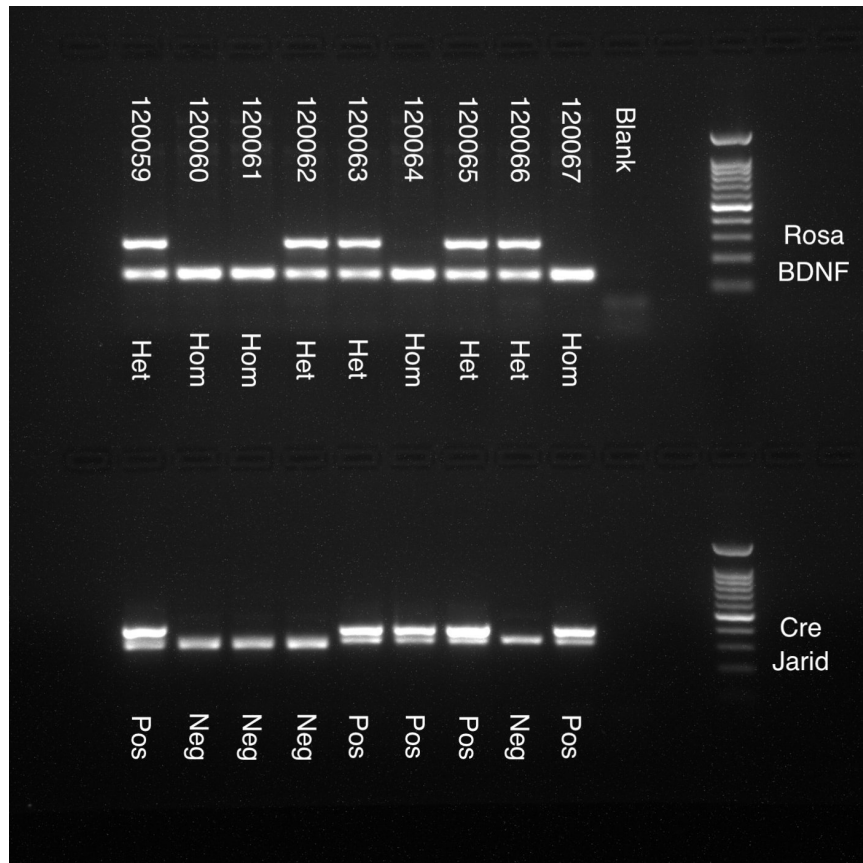


Figure 2.2: Example PCR results for genotyping the *Rosa26-Bdnf-myc/Pf4iCre* Mouse. Animal ID numbers used to label each well, with *Rosa26/BDNF* (top row) and *iCre/Jarid* (bottom row) below.

2.2. Tissue harvest and dissection

2.2.1. Enucleation and dissection

Mice were transported to the dissection laboratory with individual health checks before and after the transfer. Mice were then culled by cervical dislocation in accordance with United Kingdom Home Office regulations in all experiments with the exception of those where blood samples were taken by cardiac puncture (see section 2.10). Once death was confirmed, eyes were immediately enucleated and transferred into Hank's Balanced Salt Solution (HBSS,

Gibco, 24020-091, Fisher Scientific). A mark on the temporal cornea was made with a handheld cauteriser prior to enucleation, allowing orientation of the tissue during dissection. Under a dissecting microscope, the eye was then dissected using Pierse Notched Forceps (Duckworth & Kent Ltd, 2-100E) and straight Vannas Scissors (Duckworth & Kent Ltd, 1-110). The globe was punctured at the limbus using a 26G needle then cut circumferentially at the ora serrata, allowing removal of the cornea, lens and vitreous. The retina could then be removed from the sclera and choroid, cutting the optic nerve to separate it completely. Four cuts were then made in the retina cup to allow it to be flat mounted and used for experiments, with a longer cut made at the temporal edge for orientation.

2.3 Retina immunohistochemistry

2.3.1. Cryosection preparation

Following enucleation, whole eyes were immediately transferred to PFA 4% for 30 minutes (unless otherwise stated) and the globe punctured at the ora serrata to allow PFA to reach the internal structures more rapidly. The tissue samples were then cryoprotected by transferring to 30% sucrose solution overnight until the tissue had sunk to the bottom of the tube. Samples were then frozen in OCT Embedding Matrix (CellPath, KMA-0100-00A, Fisher Scientific) in a mould on dry ice. The samples could then be stored at -80°C until ready to be sectioned. 10-16µm slices were cut using a Leica CM3050 S Cryostat and transferred directly onto microscope slides. These were then left to air dry for 3 hours before proceeding to immunostaining.

2.3.2. Retinal flat mount preparation

The retina was dissected and removed from the eye as described in section 2.2.1. Once flattened out, it was immediately transferred to 4% PFA in PBS solution for a minimum of 30 minutes. The procedure was usually performed in 24 well plates but can also be completed in an Eppendorf tube.

After the required protocols had been completed, the retina was transferred to a microscope slide, and carefully positioned to ensure the retina was correctly orientated with the ganglion cell layer up and unfolded before mounting as described in 2.3.3.

2.3.3. Immunohistochemistry protocol

The following method was used for all immunohistochemistry procedures on both prepared cryosections and for retinal flat mounts unless otherwise stated. For each step, retina flat mounts were left on a rocker, whereas for the cryosections, the process was performed directly on the slides, with the slides stationary in a moisture chamber.

The samples were permeabilised with 0.1% Triton in PBS for one hour at room temperature, followed by blocking with 5% normal horse serum in 0.1% Triton-PBS for a further hour at room temperature. The samples were then washed three times with PBS for 10 minutes. Primary antibodies were diluted in 0.1% Triton-PBS and left overnight at room temperature.

After 12 hours, the samples were washed three times with PBS for 2 minutes before the secondary antibody was added, also diluted in 0.1% Triton-PBS. This was left for 3 hours at room temperature. The samples were then washed again three times with PBS before having the nuclear stain (Hoechst 1:1000 in 0.1% Triton-PBS) applied for 15 minutes. After a final set of washes with PBS, the samples were mounted with FluorSave Reagent (Millipore, 345789, Sigma-Aldrich) and left to dry for 1 hour before being stored at 4°C until they were taken for confocal imaging.

Antibody dilutions for commonly used protocols are as follows.

Primary antibodies

- Anti-RBPMS rabbit, Novus NBP2-20112 - 1:1000

Secondary antibodies

- Goat anti-Rabbit IgG (H+L), Cross-Adsorbed Ready Probes, Secondary Antibody, Alexa Fluor 594, R37117, Thermo Fisher – 1:500

2.4. Retina DiOlistics

2.4.1 Choice of technique

There are several methods that can be used for visualising the dendritic structure of RGCs. DiOlistics involves firing dye coated particles at the tissue from a gene gun that can penetrate into the cells. This spread of the fired particles results in a random selection of RGCs being

hit and labelled by the dye. Using a combination of two different dyes, a higher yield of cells can be achieved as separating channels of overlapping cells stained by different colours allows clear visualisation of their morphology. When considering the planned experiments, DiOlistics has several advantages over alternative methods. In particular, DiOlistics is not dependent on the health of the cells (Honig and Hume, 1986) in the same way as other methods such as biolistics, which rely on transfection and the expression of fluorescent proteins. The intended research project will involve glaucoma models intended to compromise the health of RGCs and DiOlistics can therefore, be justified as the more appropriate method. Furthermore, DiOlistics is a faster and simpler process to perform. Alternative strategies for investigating the dendritic structure may also include the use of genetic mouse strains that express fluorescence in a minority of RGCs such as Thy1-YFP lines (Leung et al., 2011). While these models are very useful, they would require additional costs and breeding with the B Cre⁺ mouse line. Additionally, the genetic models can overrepresent healthy neurons as they rely on the ability to translate mRNAs. The DiOlistics method can be used immediately on any retinas from any strain of mouse without the need for prior preparation.

2.4.2. Bullet preparation

2mg of 1-1-dioctadecyl-3,3,3,3-tetramethylindocarbocyanine per- chlorate (DiI, Invitrogen, D282, Thermo Fisher) and 4mg of 3,3-dioctadecyloxacarbocyanine perchlorate (DiO, Invitrogen, D275, Thermo Fisher) were weighed out in separate 1.5mL Eppendorf tubes, as well as 80mg of Tungsten particles (Tungsten M-25 Microcarrier, 1.7 μ m, Bio-Rad, 1652269). Under a fume hood, 400 μ L of methylene chloride (European Pharmacopoeia (EP), M1550000, Sigma-Aldrich) was added to each dye. The Tungsten particles were then transferred to a clean glass slide and grinded with a razor blade to ensure any clumps were removed and the Tungsten formed a fine powder. This was then separated into two equal piles and small quantities of DiI added to one, and DiO to the other. After each addition of dye, the particles were left to dry for 5 minutes, before being broken up with the razor blade again. This process was repeated until all 400 μ L of each dye had been added to their respective piles. Finally, the two piles of dye-coated Tungsten were combined and mixed well with the razor blade. The mixture was then funnelled into 12 inches of Tefzel tubing (BioRad, 1652441) until the internal surface was fully coated by the particles. The prepared tubing was stored in the dark until it was needed. At which time, 12mm sections of the tubing were cut off as bullets to be loaded into the gene gun (Figure 2.3).

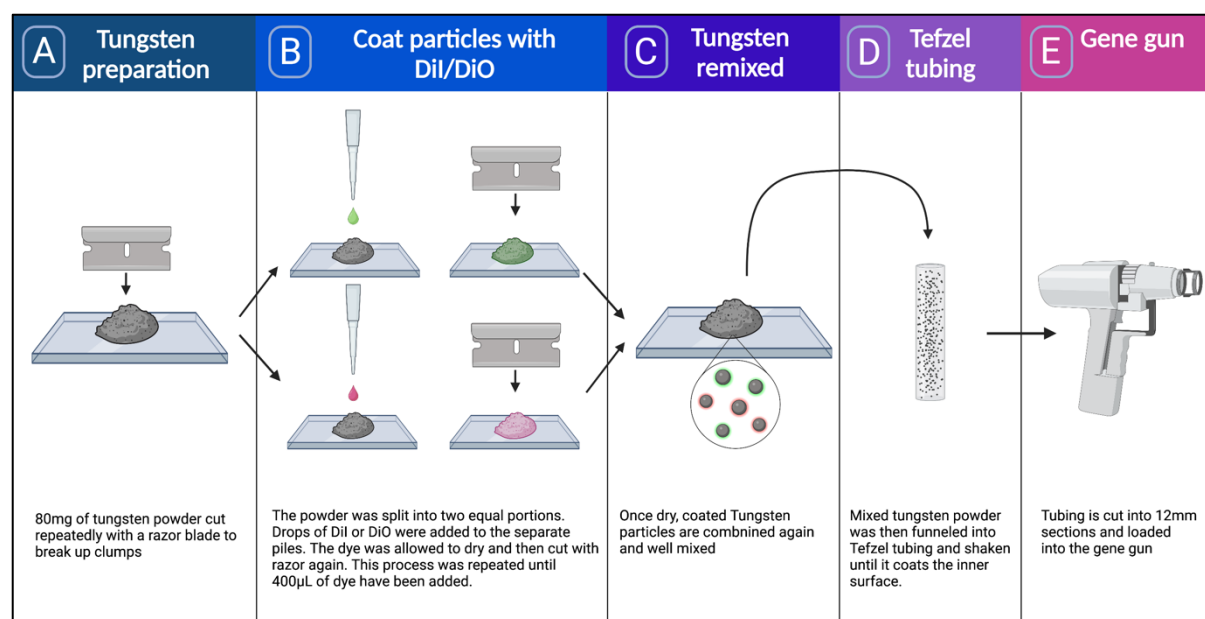


Figure 2.3: Preparation of ‘bullets’ for DiOlistic labelling

(A) 80mg of Tungsten powder is prepared by cutting repeatedly with a razor blade to remove any clumps. (B) The tungsten powder is divided into two equal piles. Either DiI and DiO (prepared in methylene chloride) are added to the separate piles and allowed to dry. Once dry, the powder was cut again with a razor blade to remove clumps. The process was repeated until 400 μ L of dye had been added to each. (C) Once dry, the coated Tungsten particles were combined and mixed well. (D) Mixed tungsten powder was funneled into Tefzel tubing and shaken until the inner surface was coated. (E) The tubing was cut into 12mm ‘bullets’ and loaded into the gene gun to be used for labelling.

2.4.3. DiOlistics Gene gun shooting and retina preparation

The retina was dissected from the globe as described in Section 2.2.1 and transferred to a microscope slide. Once flattened out and correctly positioned, the HBSS media was removed from the slide. A Falcon Cell Culture Insert, 3.0 μ m pore size (Falcon, 353092, Fisher Scientific) was then placed over the retina prior to shooting with the gene gun to help disperse the Tungsten particles and block larger clumps. The Helios gene gun (BioRad, 1652432) was pressurised to 100-120 psi from a helium cylinder and positioned with the gene gun spacer directly over the cell culture insert. Once shot, Neurobasal-A media was added to the slide and the retinas were transferred to an incubator at 37°C for 30 minutes. After incubation, the Neurobasal-A media was removed, and the retinas were fixed in 4% PFA for 30 minutes. The samples were then washed with PBS before having the nuclear stain (Hoechst 1:1000 in PBS) applied for 15 minutes. After a final set of washes with PBS, the samples were mounted with FluorSave Reagent (Millipore, 345789, Sigma-Aldrich) and left to dry for 1 hour before being stored at 4°C until they were taken for confocal imaging.

The staining produced by this DiOlistics method will leak significantly from the cells if left beyond 48 hours. Therefore, all confocal imaging must be performed within this time.

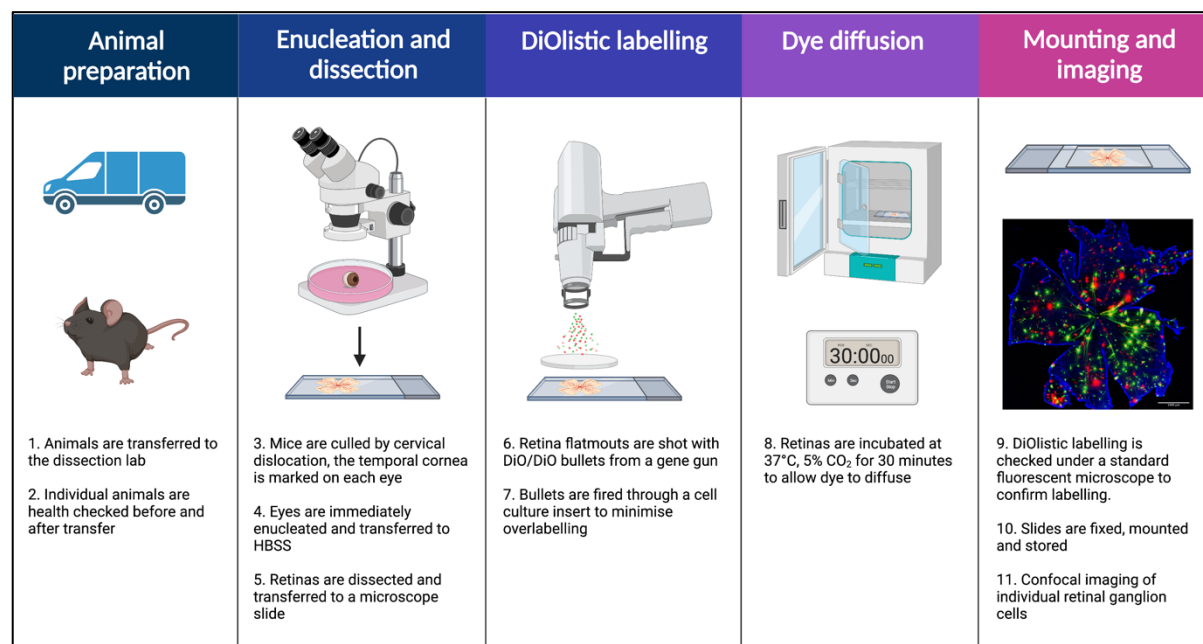


Figure 2.4: Overview of DiOlistic labelling method.

Created with Biorender.com

2.5. Confocal Microscopy

Prepared tissue samples were imaged on an LSM 780, Carl Zeiss confocal microscope. Retinas prepared using the DiOlistics method were imaged using a 20x objective to collect a z-stack of images. RGCs were identified by their location in the ganglion cell layer of the retina and their morphological features, namely, a dendritic tree extending into the inner plexiform layer, and a clear axon projecting to the optic nerve. If these features were not present, the cell was not included for analysis as there would be a high risk of including other retina cell types such as amacrine cells. Bistratified RGCs were also excluded. The entire cell was imaged including the cell axon, and the full dendritic tree. Z-stacked 1024 x 1024 images were obtained in 1.68 μm steps using separate channels for each dye (DiI 543nm laser with 565–615nm bandpass filter; DiO 488nm argon laser with 500–530nm bandpass filter). The resulting images had a resolution of 3.37 pixels/ μm .

Retinal flat mounts and cryo sections were also imaged on the same Carl Zeiss confocal microscope. Images were captured using a 20x objective or 60x objective depending on the target. Z-stacks of 1024 x 1024 images were acquired, with separate collection of respective channels.

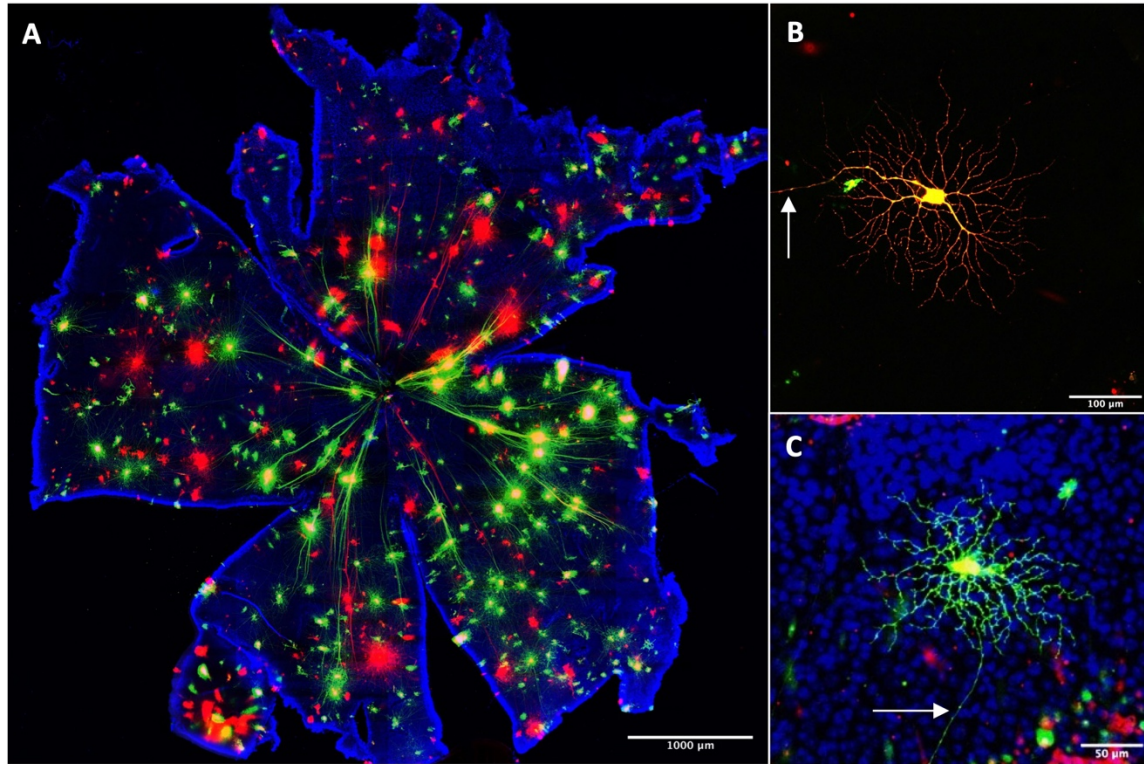


Figure 2.5: Confocal imaging of DiOlistically labelled retinas.

(A) Multichannel overview image demonstrating the orientation of axons towards to optic nerve head at the centre of the retina. **(B,C)** Example images of RGCs, identified by the dendritic tree and the axon. White arrow indicates RGC axon.

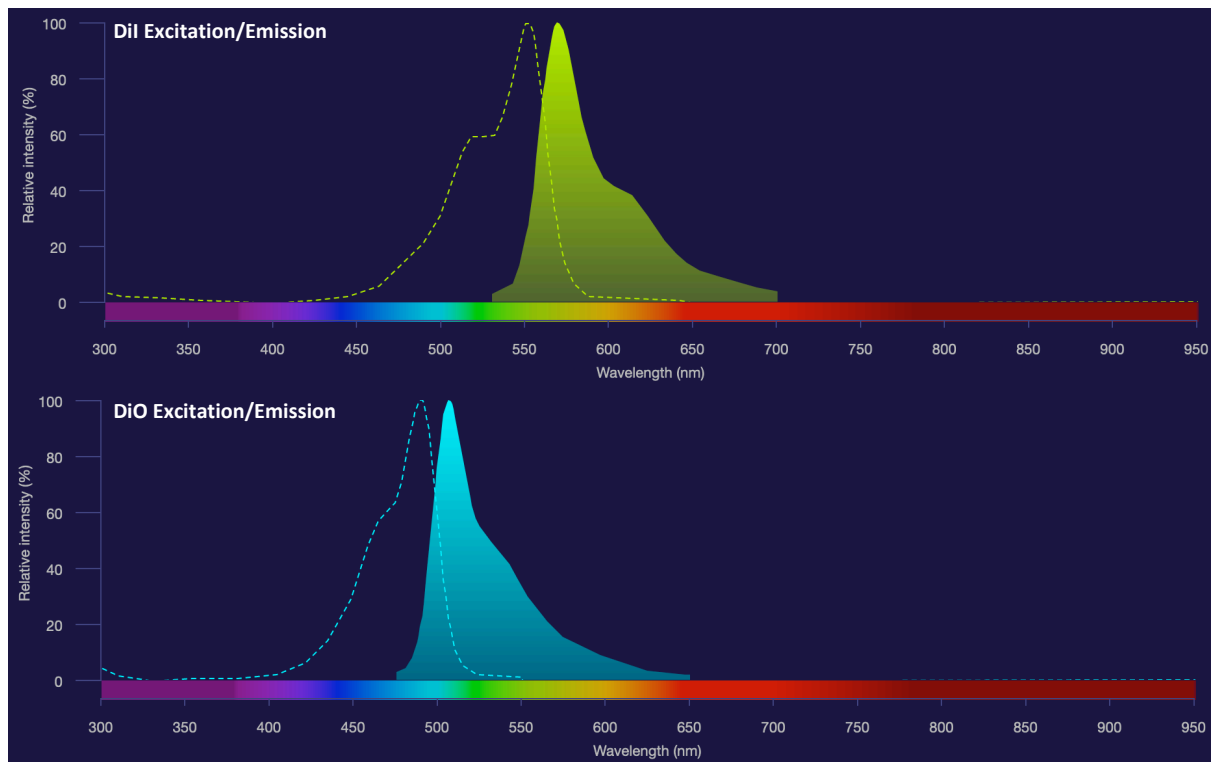


Figure 2.6: Excitation and emission ranges for DiI and DiO

2.6. RGC Locations

RGC locations were recorded when imaging on the confocal microscope as (x, y) coordinates in micrometres relative to the optic nerve head. The position of the long temporal cut of the retina was then measured relative to the horizontal using FIJI, and this angle was then used to transpose the RGC coordinates, correcting for the rotation of the retina on the slide. The following equations were used to convert the original (x, y) RGC coordinates to the new, corrected RGC coordinates, (x', y') , based on the angle of the temporal cut:

$$x' = x \cos \theta - y \sin \theta$$

$$y' = x \sin \theta + y \cos \theta$$

For right eyes, X' positions were then multiplied by -1 so that right and left eyes could be shown with a standardised nasal and temporal orientation, in a left eye configuration.

2.7. Imaris Image Analysis and Neuronal Reconstruction

All RGC confocal images were analysed using Imaris software (version 9.3.1, Bitplane, Zurich, Switzerland), using the Filament Tracer module to trace RGC dendritic fields. A region of interest (ROI) was demarcated around the dendritic field and automatically traced to reconstruct the dendritic arbour. The constructed filament was then reviewed and manually corrected to remove any incorrectly traced sections that may include debris or adjacent cells. Any dendrites that had been missed by the automated process were manually added. The statistical parameters were exported for data analysis, with Sholl analysis intervals set at $10\mu\text{m}$.

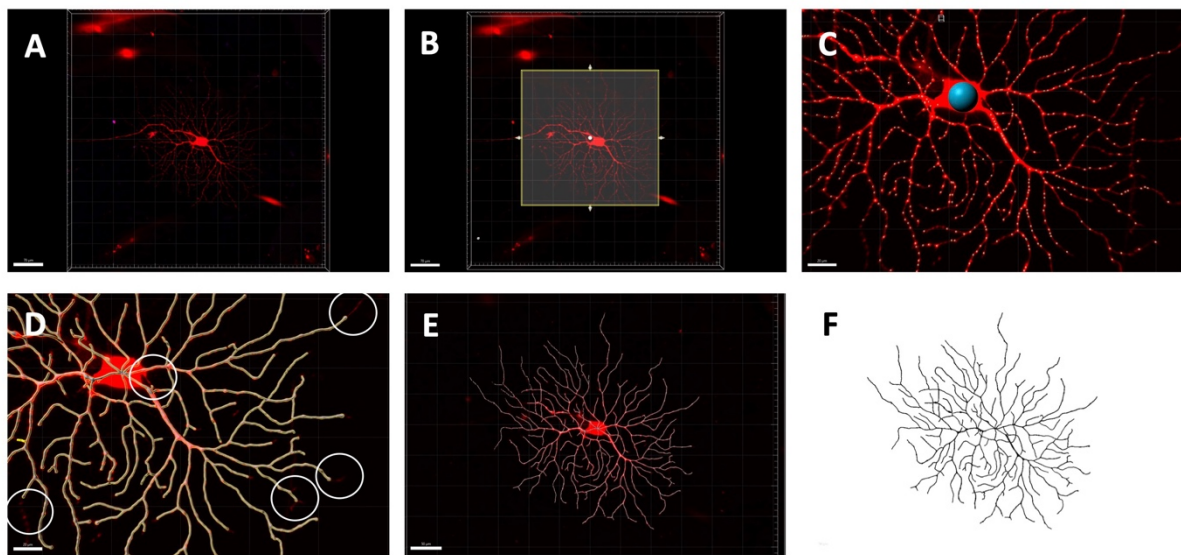


Figure 2.7: Neuronal reconstruction using Imaris Filament Tracer module.

(A) Raw confocal z-stack image is imported into Imaris and the channel of interest is selected. (B) A region of interest is drawn around the dendritic field of the cell. (C) The cell body is calculated based on specified thresholds and dendrites are detected and marked with 'seed points.' (D, E) Seed points are used to calculate dendritic branching and a reconstruction of the dendritic tree is produced. The reconstructed filament is then reviewed and manually edited to address any areas missed/incorrect areas of the automatic tracing (example areas shown in white circles). (F) Data from the completed filament is exported to be used for Sholl analysis.

2.8. Sholl analysis

Dendritic morphology is most commonly assessed using Sholl analysis (Sholl, 1953). This is a standard measure of dendritic complexity as a function of distance from the cell body and quantifies the number of dendrites intersecting concentric rings at set intervals from the cell soma ($10\mu\text{m}$ for this project). The data from all RGCs from a given experimental group is

combined, with mean number of dendritic intersections plotted at each interval. The vast differences in the dendrite morphology of RGC subtypes means that the Sholl profiles of individual cells can be quite variable, but when averaged together, the curve from an adult mouse typically peaks at around 20 intersections at approximately 60µm from the soma. After this point, the curve gradually declines with the final dendrites at approximately 250µm. Because of the wide variability in cell types, and the associated size of standard deviations on the Sholl curves, standard error of the mean (SEM) is used instead to aid with visual inspection of the graphs. A loss of dendritic complexity is seen as a left and downward shift of the Sholl curve. The initial portion of the curve represents the primary and secondary dendrites (Figure 2.7 C), typically preserved even in cases of moderate degeneration (Tribble et al., 2014). The significance of the difference between the two curves is assessed at every 10µm interval by two-tailed Mann-Whitney U test. If $p < 0.05$, this is indicated by a (*) below the axis at the corresponding x value (Figure 2.7 D).

Besides the Sholl curve itself, there are other parameters that can be assessed that provide additional details of the dendritic arbour:

Area Under Curve

The area under curve (AUC) represents the area until the Sholl curve and gives an overall measure of dendrite complexity, allowing comparison of different curves through a single numerical value (Figure 2.7 E). This is an extremely valuable measurement, and often the used as the primary outcome of Sholl assessments to demonstrate differences between groups.

Maximum number of intersections

The maximum number of intersections reached at any point on the Sholl curve, indicating the highest point of complexity.

Total dendrite length

The sum total of all the branches within the dendritic tree measured in µm.

Field area

The area of the dendritic field measured in µm². This is determined using the 'Convex Hull' function of the Imaris software once the filament has been traced.

Branching index

This analysis provides a comparison of dendrite branches based on their branching level, ie. primary, secondary, tertiary, quaternary, etc. The dendritic atrophy that occurs in glaucoma and its experimental models begins with loss of the outer dendrites, with the primary and secondary dendrites usually preserved until later stages. Counting the mean number of branches at different levels can therefore help to highlight subtle changes in the outer branches.

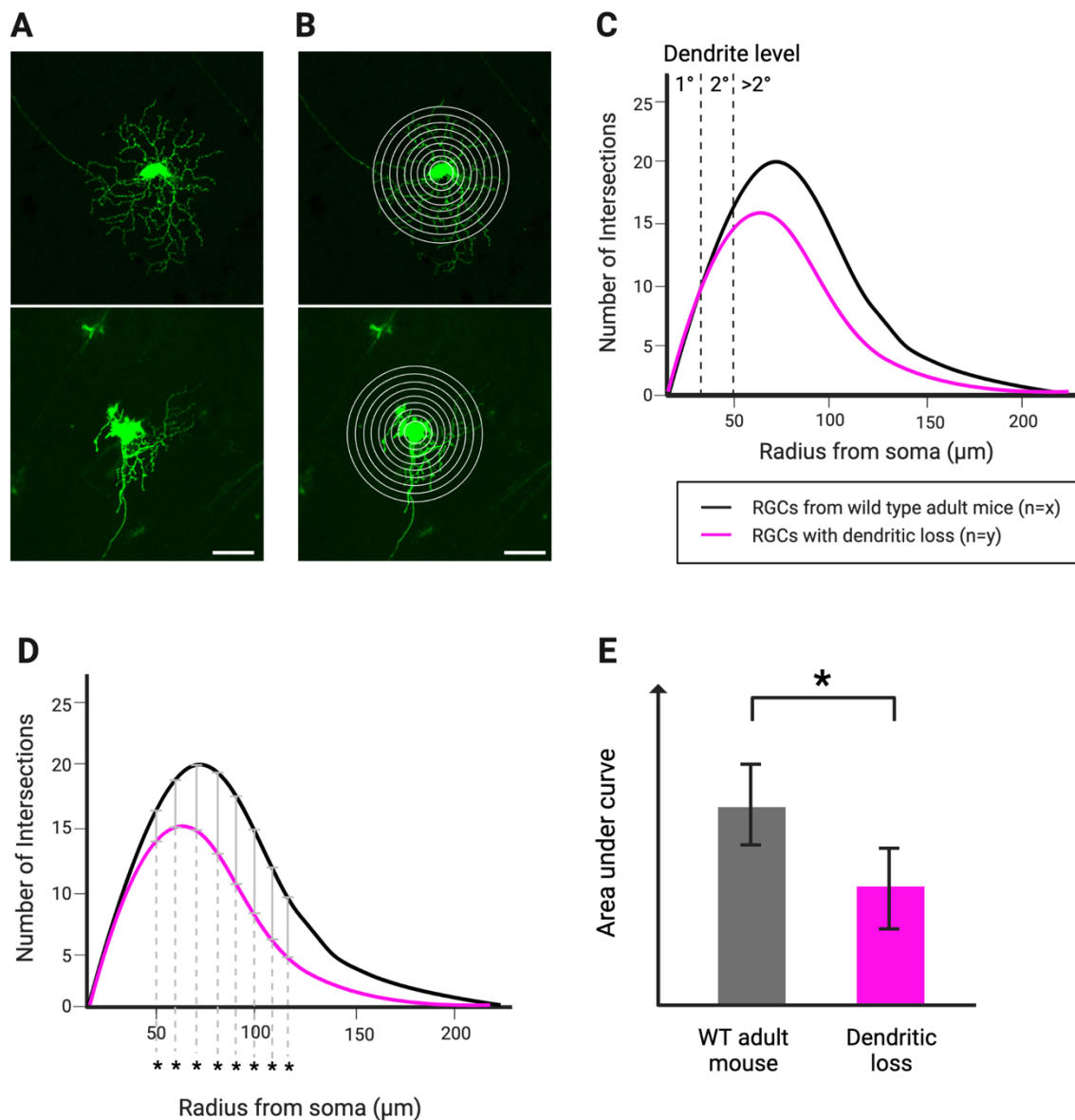


Figure 2.8: Conceptual Sholl analysis of mouse retina ganglion cells, plotting number of intersections against distance from soma.

(A) Example RGCs from a wild type adult mouse and an RGC with dendritic loss. **(B)** Quantification of dendrites intersecting concentric rings at $10\mu\text{m}$ intervals from the cell soma. **(C)** Mean number of intersections are plotted on Sholl curve. A left, downward shift in RGCs with dendritic loss. N = number of RGCs in each group. **(D)** Significance of the difference between curves is calculated at every $10\mu\text{m}$ interval. If $p < 0.05$, this is indicated by a (*) below

the x axis. **(E)** Area under the Sholl curve is calculated and mean values used to compare overall dendrite complexity between groups.

2.9. RGC count

The most common approach to determine the success of a given intervention on RGCs is with a cell count before and after the treatment. This can be used to indicate an increase in the proportion of RGCs able to survive the stresses produced by a given glaucoma model. Performing an accurate cell count requires a method of highlighting and identifying the RGC population in a way that can distinguish them from neighbouring cell populations.

Since Santiago Ramón y Cajal used Golgi silver staining method to visualise and describe RGCs (Cajal, 1893), there have been several methods developed to try and accurately identify RGCs in different settings. Cells can be retrogradely labelled by injection of tracers into areas of the brain targeted by RGCs such as the superior colliculus. However, this method relies on active axonal transport, which can be compromised in disease models. Therefore, they cannot differentiate between cell loss and failure of transport. Additionally, it requires invasive procedures to administer the tracers, either by bilateral injection into the superior colliculi to capture both ipsilateral and contralateral RGC projections, or by unilateral injection of the optic nerve. Nevertheless, tracers such as FluoroGold have proven to be very effective for this method and are often considered as a benchmark for testing other labelling methods (Mead et al., 2014).

Counting myelinated RGC axons in optic nerve is possible but can overestimate the number as efferent neurons with thin myelin sheaths are difficult to distinguish from axons of small RGCs. It also needs additional preparation of samples and electron microscopy that are time consuming and costly.

Another more commonly used method to identify and count RGCs is through immunohistochemical labelling of cells based on a specific marker, usually applied to a retinal wholemount or section (Mead et al., 2014). There are several markers that have been proposed that each have different strength and limitations. Thy-1 was widely used but it is downregulated in the diseased retina (Huang et al., 2006) and can therefore, underestimate the cell number. In contrast, Beta III tubulin and Islet-1 localise to amacrine cells as well as RGCs and are prone to overestimating RGC numbers (Mead et al., 2014). This is especially important in disease models in which amacrine cells are less likely to die, such as an optic nerve crush. Brain-specific homeobox/POU domain protein 3A (Brn3a) exclusively stains RGCs, but does not stain intrinsically photosensitive RGCs (Nadal-Nicolás et al., 2012),

meaning it can also underestimate total RGC numbers. RNA binding protein with multiple-splicing (RBPMS) has been shown to be a robust marker of RGCs, with almost 100% of RGCs being labelled (Kwong et al., 2010), around 20% more than with Brn3a labelling (Rodriguez et al., 2014). As result, RBPMS has become a preferred marker for RGC counts (Masin et al., 2021) and was used in this project.

Flat-mounted retinas were fixed in 4% PFA and labelled for RBPMS using the protocol described in Section 2.3.3. Slides were then imaged on the LSM 780, Carl Zeiss confocal microscope at 10x magnification. For each quadrant of the retina, 3 x 0.33mm² sample images were taken at 500um, 1000um and 1500um from the optic nerve head (method based on (Mead et al., 2018)). Cells were counted manually on Fiji Version: 2.3.0/1.53f with the aid of the Cell Counter plugin. The mean number of RGCs/image was calculated for each of the 3 radial distances, and a mean composite count for all 3 distances calculated to produce a final cells/mm² mean value for each retina.

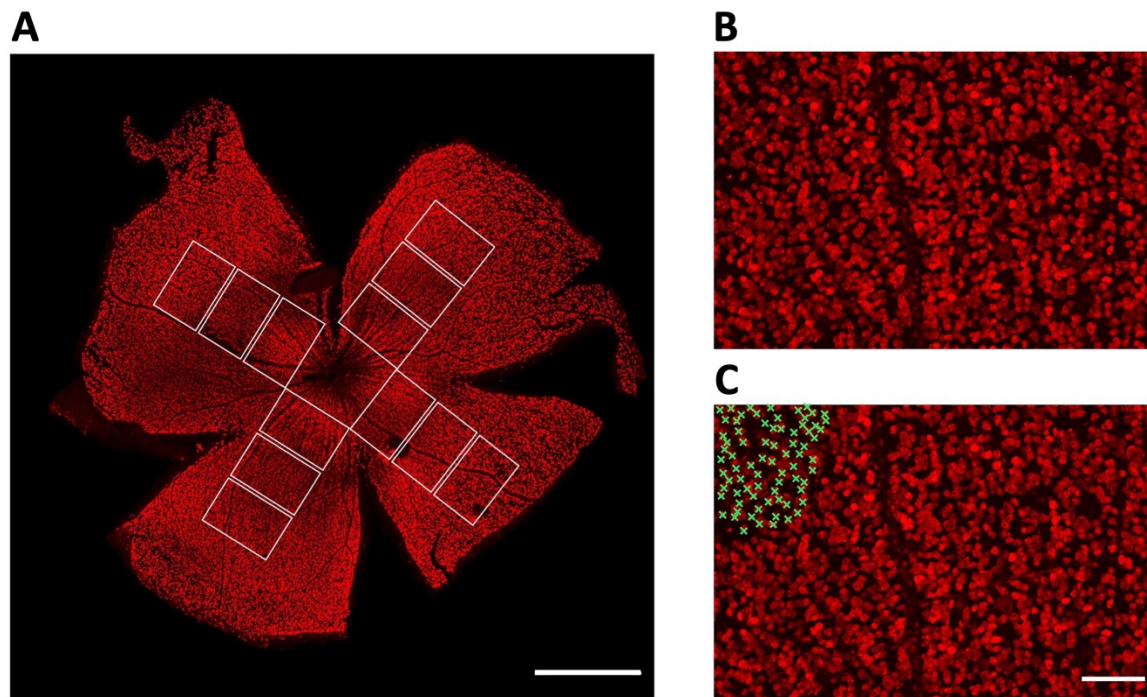


Figure 2.9: RGC counting method using RBPMS labelling.

(A) Flat mounted retina showing RBPMS labelling. 3 x 0.33mm² sample images were taken at 500um, 1000um and 1500um from the optic nerve head for each quadrant. Scale bar = 1000µm. **(B)** example sample image for counting. Scale bar = 100µm. **(C)** Cells were counted manually using Fiji Cell counter plugin.

2.10. Blood collection and sample preparation

2.10.1. Blood sampling

Blood samples were taken by cardiac puncture, immediately after the animal had been sacrificed using CO₂. This was performed using a 25G needle and a 1mL syringe. CO₂ was used as a Schedule 1 method as cervical dislocation can cause rupture of large blood vessels in the neck, reducing the volume of blood that can be collected.

2.10.2. Serum sample preparation

Whole blood samples were transferred to an Eppendorf tube and left to rest at room temperature for 1 hour, followed by 1 hour at 4°C (no other buffers or reagents were added to collected blood). The sample was then centrifuged at 2000 G for 10 min at 4°C. The serum was then collected (top, straw-coloured portion) from the top of the tube, taking care to leave a small amount remaining to ensure other components separated by centrifuging, such as red blood cells, were not disturbed. The collected serum samples were then centrifuged again at 2000 G for 10 min at 4°C to remove further cells before being aliquoted in new tubes and stored at -80°C until needed.

2.10.3. Plasma sample preparation

Blood was collected by cardiac puncture, drawn up into a syringe containing 20µL of 500mM EDTA. After the blood had been collected, the syringe was inverted to ensure the EDTA and blood were well mixed. The sample was then transferred to a 1.5mL Eppendorf tube and centrifuged at 2000 G for 10 minutes at 4°C. The top 2/3 of plasma was then carefully removed and transferred into a new tube before being recentrifuged again at 2000 G for 10 minutes at 4°C for further purification. This plasma could then be collected, taking care not to disturb any remaining debris in the base of the tube, and aliquoted for storage at -80°C until needed.

2.10.4. Washed platelet sample preparation

Blood was collected by cardiac puncture, drawn up into a syringe containing 100 μ L of Acid-citrate-dextrose (ACD) buffer and drawn up to a final volume of 500 μ L. After the blood had been collected, the syringe was inverted to ensure the EDTA and blood were well mixed. The samples were then centrifuged at 2000 G for 5 minutes at room temperature with no brake. Platelet-rich plasma was then carefully removed from the top of the tube and transferred to a new tube, taking care not to disturb the other components separated by centrifuging, such as red blood cells and centrifuged again at 200 G for 5 minutes at room temperature with no brake to clear out more cells. The top fraction was then transferred to a new tube again, before being centrifuged at 900 G for 10 minutes at room temperature with no brake and platelets collected at the top of the tube. The platelet-poor plasma was discarded, the platelets resuspended in 0.3mL Tyrodes buffer containing 1/10 ACD buffer, followed by a final centrifugation at 800 G for 10 minutes at room temperature with no brake, before being resuspended again in Tyrodes buffer containing 1/10 ACD buffer. The milky platelet suspension was then allowed to rest at room temperature. “Sandy”-looking samples were discarded as they indicated that the platelets had been activated.

2.11. BDNF ELISA (Enzyme-linked Immunosorbent Assay)

In order to quantify the BDNF concentration in serum, plasma and isolated platelets, ELISA was performed using the Fujifilm Mature BDNF ELISA Kit *Wako*, High Sensitive, 298-83901, and completed as per manufacturer instructions. The kit used was based on a “sandwich” ELISA principle using a monoclonal, capture antibody targeting the N-terminal sequence of BDNF cleaved off its precursor sequence.

Samples were diluted as appropriate with the buffer solution included with the ELISA kit. Wild type mouse serum was diluted 4-fold, whereas serum from B Cre⁺ mice was diluted 100-fold, due to the substantially higher BDNF concentration.

The BDNF standard solution was prepared by reconstituting BDNF (provided with the kit) with the volume of purified water specified with each kit to make a stock solution of 10ng/mL. This was then mixed with Buffer solution to create a series of standard solutions, prepared as per kit instructions listed in Table 2.3. However, when investigating wild type mouse serum, the

concentration of BDNF was extremely low and a modified set of standard solutions that covered a smaller range was used.

Table 2.3: Recombinant BDNF Standards for ELISA

Concentration of standard solution (pg/mL)	Volume of standard solution	Volume of Buffer
500	Stock solution (10 ng/mL) : 20 μ L	380 μ l
	↓	
50.0	Standard solution (500 pg/mL) : 50 μ L	450 μ l
20.0	Standard solution (50.0 pg/mL) : 100 μ L	150 μ l
8.00	Standard solution (20.0 pg/mL) : 100 μ L	150 μ l
3.20	Standard solution (8.00 pg/mL) : 100 μ L	150 μ l
1.28	Standard solution (3.20 pg/mL) : 100 μ L	150 μ l
0.512	Standard solution (1.28 pg/mL) : 100 μ L	150 μ l
0.205	Standard solution (0.512 pg/mL) : 100 μ L	150 μ l
0		150 μ l

The Fujifilm ELISA kit contains a 96-well Anti-body coated plate. The solution initially filling the plate was discarded and the wells were washed 4 times with the Wash Solution (1X) included in the kit. With each wash, the plate was inverted to remove the solution and then blotted against clean paper towels to remove any excess liquid retained in the wells. 50 μ L of diluted standard solution and diluted samples was added to respective wells, with triplicate wells used for each standard and sample. The plate was then covered and agitated on a microplate shaker for 2 hours at room temperature (20-25°C).

The solution was then discarded and the wells washed 4 times with Wash Buffer as above. 50 μ L of Biotin-conjugated antibody solution was added to each well, the plate covered and incubated on a shaker again for 1 hour at room temperature. The solution was then discarded, the wells washed 4 times as above and 50 μ L of Peroxidase-conjugated Streptavidin Solution added to each well. The plate was then covered and placed on a shaker for 30 minutes at room temperature. Following a final series of 4 washes with the Wash Buffer, 50 μ L of mixed luminescent reagents 1 and 2 (1:1) were added to each well. The plate was shaken for 1 minute using the shaker and then the luminescence was measured using a 96-well microplate

reader (FLUOstar Omega, BMG Labtech). Measurements were performed 10 minutes after the addition of the luminescent reagent. The standard solutions were used to make a standard curve converting luminescence to BDNF concentration that could be applied to the experimental samples.

2.12. Exercise tracking

Custom tracking equipment was constructed to monitor the activity of mice continuously over several days in experiments designed to investigate changes in serum and plasma BDNF concentrations. Peripheral BDNF has been associated with depression, and therefore, in an effort to reduce the stress that mice can experience from isolation, cages were constructed that housed two mice, separated by a barrier that could allow a degree of social interaction. The barrier was made with small perforations and allowed feeding from a communal food hopper. Mice could therefore still see, smell and interact with each other throughout the experiment, while still allowing tracking of individual activity.

Exercise wheels (PLUTEO Silent Hamster Running Wheel, 13cm/5.1 Inch) were attached to both walls of RB3R cages (48 x 28 x 20cm). The removable, central barrier was made from 3mm Perspex and cut using a handheld fret saw, with two rows of 4mm diameter holes along the length of the barrier. Brackets were constructed from PVC and secured to the cage walls with M3 16mm nuts and bolts. The edges of the components were sanded and rounded to ensure there were no sharp edges that may cause injury to the mice, and all materials used were non-absorbent to ensure cages could be safely cleaned. 8 cages were constructed to house a total of 16 mice. The experiment would be designed to track exercise activity of 8 mice, with an additional 8 mice used as controls. The control cages were constructed in the same way as the exercise group to standardise conditions, except for the exercise wheel which had been fixed in place.

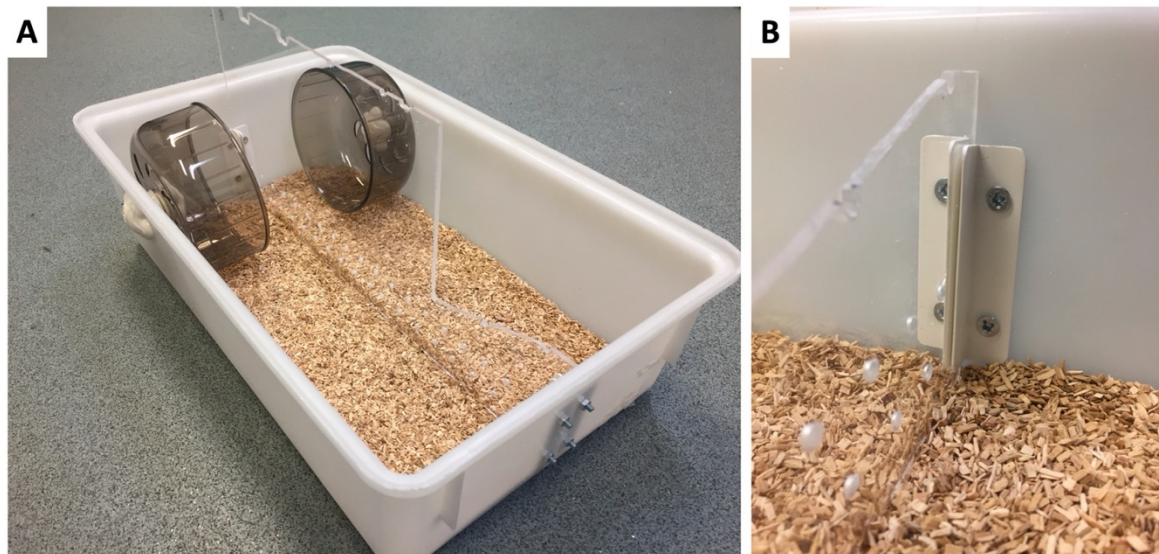


Figure 2.10: Base of modified RB3R cages for exercise tracking experiments
(A) added exercise wheels and clear Perspex barrier. (B) Brackets on cage wall keep barrier securely in place but can be easily removed to allow cleaning.

Rotations of the exercise wheels were monitored using an infrared sensor (Infrared Obstacle Avoidance Sensor Module, 3 wire, Frienda, Frienda-Obstacle-431S) mounted to the outside of the cage. The mounting apparatus was constructed from hand cut 3mm Perspex arms and secured to the outside of the cage (Figure 2.10 B). Using the interruption of the infrared beam as a trigger allowed all the electronic equipment and components to be outside of the cage and prevent the possibility of any wires being chewed by the mice. The sensors were also potted with silicone to prevent short-circuiting.

Sensors were connected to a Raspberry pi 4B Model B (LABISTS) via a breadboard using an electronic circuit designed specifically for this project (Figure 2.10 D). The Raspberry pi was connected to an uninterruptable power supply (Tecnoware UPS ERA PLUS 800 Together On - Uninterruptable power supply) to prevent loss of data in the event of power failure. Using a Python script, the input from 8 exercise wheel sensors was tracked. The time and date of each revolution from each cage was logged as well as a running count of the total number of rotations for each wheel (Figure 2.10 C). At the end of the experiment, all data was collected and processed using RStudio (Version 1.2.1335). To account for false positive triggering of the sensors, a limit was set to exclude events where the time interval was less than 0.275 seconds. The time interval of the updated results was used to calculate the revolutions per minute (RPM).

The full details of the cage construction, electronic circuit, python and R scripts are included in Appendix 2.

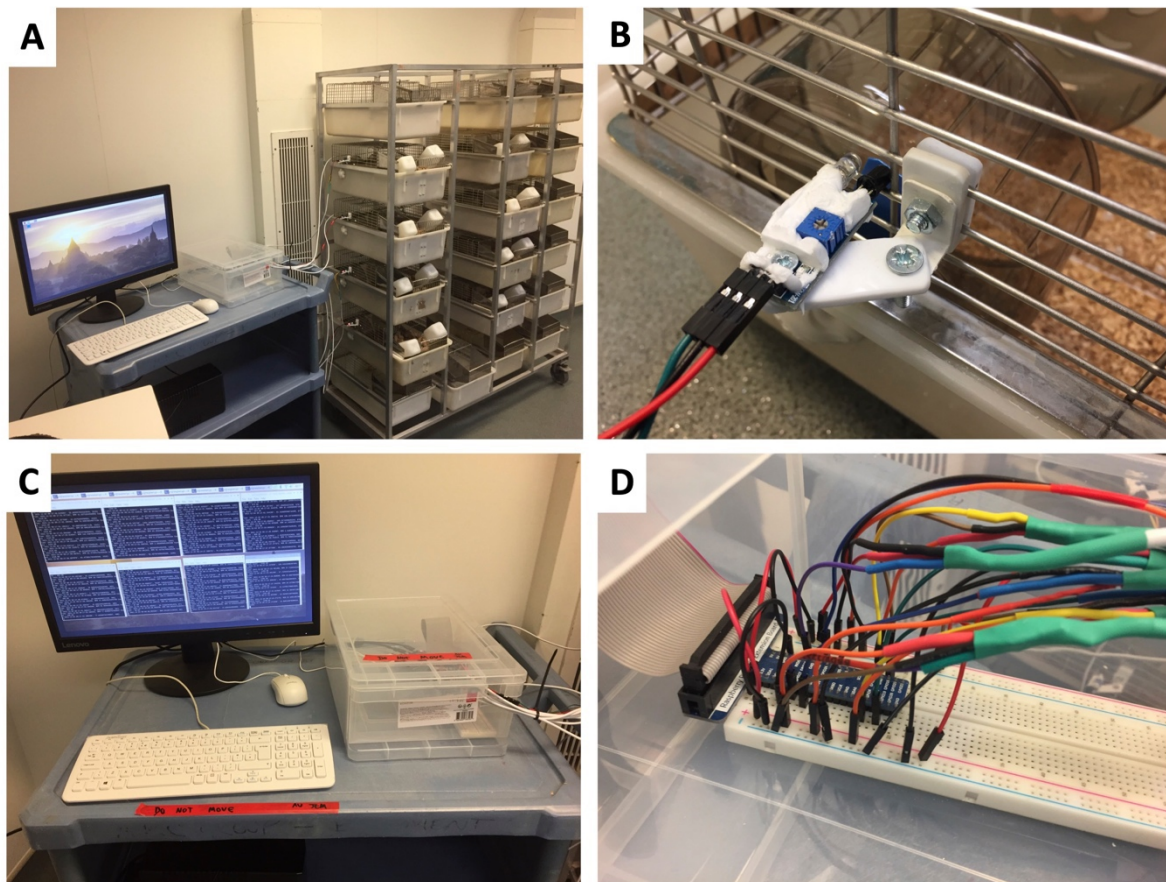


Figure 2.11: Exercise tracking equipment

(A) Apparatus of exercise experiment showing multiple cages with monitoring equipment. (B) Each exercise cage had a sensor secured externally that would trigger when the IR beam was interrupted by the exercise wheel. The sensor component was potted using silicone sealant to prevent short circuit. (C) The sensors were connected to a Raspberry pi 4B so that input from multiple cages could be simultaneously monitored. (D) An external breadboard was used to build the circuit to allow modifications and additional of other components as needed during the early phases of the experiments.

2.13. Statistical Analysis

Statistical analysis was completed using GraphPad Prism 9 and RStudio Version 1.2.1335. Data from the Imaris filament tracing of RGCs was used to plot a Sholl analysis showing the number of dendrite intersections plotted against the distance from the cell soma at 10 μ m intervals. All Sholl plots displayed the mean values \pm standard error of the mean (SEM). For all other data, data is displayed as mean values \pm standard deviation (SD)

Shapiro-Wilk test was performed on datasets to determine the normality of the data. Normally distributed data was then analysed using unpaired t-test, and non-normally distributed data analysed using Mann-Whitney-U test. For Sholl analysis, two-tailed Mann-Whitney U test was performed at each interval distance. Kruskal-Wallis test was used for analysis of non-parametric data when there were more than two groups, for example when assessing outcomes for homozygous, heterozygous and wild type animals within a given experiment. Significant results are denoted as follows: * = $p < 0.05$, ** = $p < 0.01$, *** = $p < 0.001$.

Power calculations were performed using G*Power (Faul et al., 2007). As a possible impact of BDNF in B Cre+ mice had not been investigated before, the expected effect size, if any, could only be estimated based on the degree of deterioration seen in previous studies that had examined dendrite complexity following BDNF treatments. The AUC in the Binley et al., 2016 retinal explant experiment was increased by 75.8 +/- 14.8 % with BDNF supplementation compared to controls at 72 hour, suggesting that if BDNF released from platelets would reach the RGCs, there may be a measurable impact with regard towards preserving dendritic complexity. Using the G*Power, the following sample sizes were calculated based on an A priori power analysis of Wilcoxon-Mann-Whitney test of the means of two groups, with an alpha value of 0.05 and power value of 0.90. Control group mean AUC (SD) was estimated at 1400 +/- 700, based on preliminary trials.

Table 2.4 Power calculations determining recommended RGC sample size based on estimated effect size

% change in AUC	Effect size	Recommended sample size per group
40%	0.8	36
35%	0.7	46
30%	0.6	63
25%	0.5	90
20%	0.4	113

The sample size based on the power calculation must be balanced with the time needed to process large numbers of retinas, the limited time window for imaging the DiOlistic labelling and animal costs. Eighty RGCs per group were assumed to be an acceptable compromise, corresponding to an effect size of 0.53. Assuming an average of 10 RGCs per retina, this would mean at least 8 retinas would be used per group for experiments requiring Sholl analysis based on DiOlistics.

Chapter 3. Baseline characteristics

3.1 Introduction

Given the complexities of BDNF actions detailed above, it was important to first establish baseline characteristics of the retina in the B Cre⁺ mice compared to WT and to independently validate the presence of BDNF in platelets by measuring serum BDNF concentrations using a new BDNF ELISA kit (see above), not used in previous studies with the B Cre⁺ line (Dingsdale et al., 2021).

3.2 Physical characteristics

At 12 weeks the mean weight of B Cre⁺ mice was 27.06 ± 4.51 g in males and 21.01 ± 1.21 g in females, not significantly different from wild type mice with weights of 27.22 ± 1.73 g for males and 21.01 ± 0.55 g in females (n = 8 males, 8 females for both groups). This suggests that these mice have not developed any overt abnormalities in terms of food intake regulation which is unexpected given that BDNF levels and TrkB signalling are critical in the regulation of food intake in both mice (Lyons et al., 1999; Kernie, 2000) and humans (Yeo et al., 2004).

3.3 Retinal features

3.3.1. Introduction

Given the role of BDNF in RGCs (see Chapter 1), baseline retina RGC counts were performed, as well as immunostaining for TrkB to determine if the chronic exposure to elevated BDNF has caused any changes in expression in the retina compared to WT controls.

3.3.2. Experimental setup

Retinas from B Cre⁺ and WT mice were collected and prepared for immunolabelling as described in Chapter 2.3. Flat mounted retinas were labelled for RBPMS for cell counting using anti-RBPMS rabbit, Novus NBP2-20112 as a primary antibody (1:1000 dilution, overnight, room temperature) and Goat anti-Rabbit, Alexa Fluor Plus 594, Thermo Fisher R37117 (1:500, 3 hours, room temperature) as a secondary antibody. Cryo sections were used to investigate the distribution of TrkB as described in Chapter 2, using anti-TrkB goat, R&D Systems AF1494 as a primary antibody (1:1000 dilution, overnight, room temperature)

and Donkey anti-goat, Alexa Fluor 594, Invitrogen as a secondary (1:500 dilution, 3 hours room temperature).

3.3.3. Results

There was no significant difference between the RGC count of the B Cre⁺ mice and WT controls ($n = 5$ for each group, B Cre⁺ 3303 ± 93 , WT 3237 ± 89 , $p = 0.283$). Similarly, there was no difference in TrkB distribution on retina cryosections, although this was not formally quantified. (Figure 3.2).

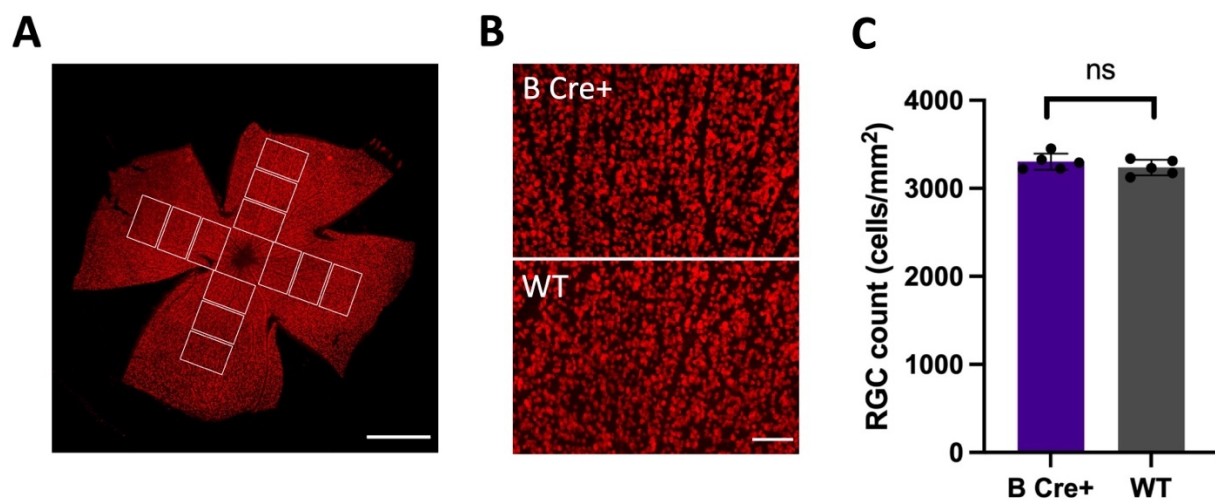


Figure 3.1: RGC count of B Cre⁺ mice and WT controls based on RBPMS labelling. (A) Example flat mounted retina with RBPMS labelling, scale bar = 1000µm. (B) Example images for RGC count B Cre⁺ mice and WT controls, scale bar = 100µm. (C) Column scatter graph showing RGC count/mm². Points show values from individual retinas, columns show means, error bars show standard deviation.

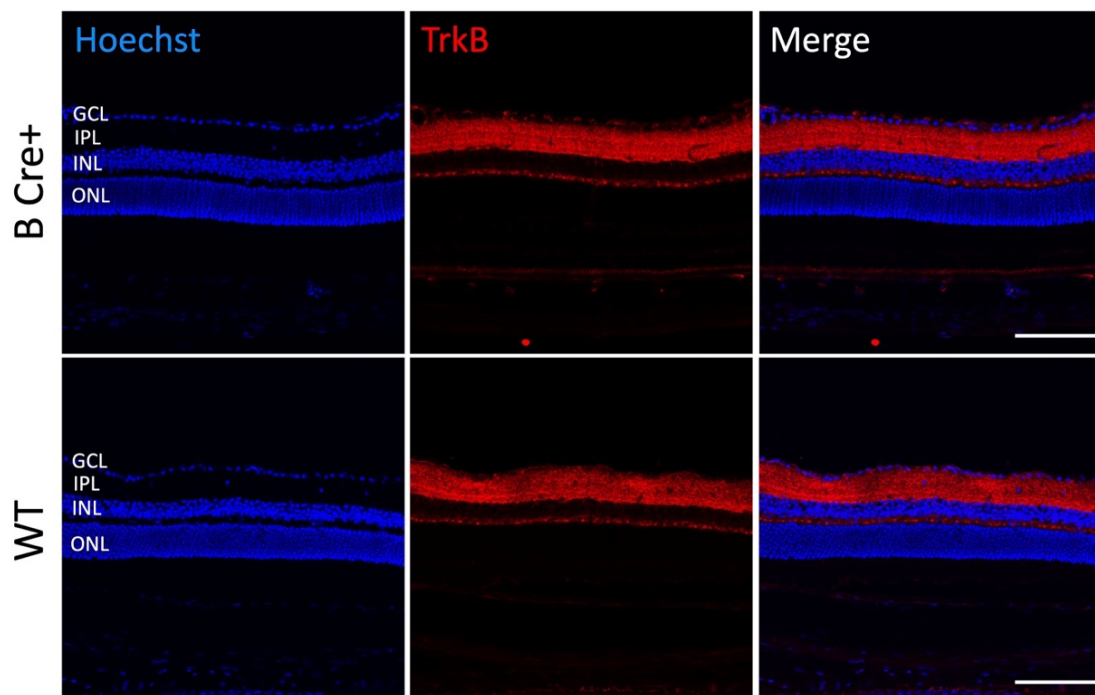


Figure 3.2: Immunolabelling of retina cryosections showing TrkB (red) in B Cre⁺ mice and Wild type (WT) controls.

16µm retina cryosections labelled for TrkB (red) and with Hoechst nuclear stain (blue). No qualitative difference was seen in TrkB labelling between B Cre⁺ and WT mice. Retinal layers – ganglion cell layer (GCL), inner plexiform layer (IPL), inner nuclear layer (INL), outer nuclear layer. Scale bar = 100µm.

3.3.4. Discussion

There are two important conclusions to draw from these results. Firstly, the equal RGC counts are consistent with normal retinal development in the B Cre⁺ mice. Even though there has been additional BDNF present throughout the developmental period there has not been an increase in RGC number due to the prevention of programmed RGC death, nor has there been cell loss from prolonged exposure and p75^{NTR} pathway activation. This is largely in keeping with previous work using gene knockout models and BDNF supplementation that has suggested that BDNF is but one of many factors involved in this process, and that these different elements have some regulatory capacity if one factor is missing or in excess. Secondly, the similarities in TrkB distribution and retina morphology further suggest there has been relatively normal retinal development and there has not been a downregulation of TrkB from chronic BDNF exposure.

It is worth noting that the antibody used labels multiple forms, including internalised TrkB, and is not specific to cell surface TrkB that is accessible for binding through BDNF. While adjusting the protocol to reduce/avoid using detergents and limit staining of intracellular TrkB may have been of interest, a more effective way to try and evaluate the availability of the TrkB pathway would be to administer saturating concentrations of BDNF and then label for phosphorylated TrkB. This method has been used successfully to investigate the regulation and interactions of Trk receptors in neurons differentiated from human embryonic stem cells (Ateaque et al., 2022). A further experiment was attempted by adding high dose BDNF to retinal explants for 1 hour and then labelling for phosphorylated TrkB. Unfortunately, the staining was minimal in these experiments and insufficient to draw any meaningful conclusions. After several unsuccessful attempts, it was agreed that continuing this line of enquiry further and the sacrifice of additional animals was not justified at this time. The later experiments using models of RGC degeneration would provide more valuable data and should be prioritised. Without the additional information into the activation of TrkB, at this stage, it was most appropriate to simply say that total TrkB expression had not been grossly reduced in the B Cre⁺ retinas.

3.4. Serum BDNF concentration

3.4.1. Introduction

BDNF has been notoriously difficult to detect in small concentrations with any accuracy. This is despite extensive work adapting and refining the methods. Kolbeck et al., 1999 assessed the sensitivity and specificity of nine BDNF antibodies to determine the most suitable pair of antibodies for a sandwich immunoassay. The highest sensitivity (5-10 pg/mL) was achieved using biotinylated mAB#1 bound to streptavidin-coated plates and m#Ab9 conjugated to peroxidase. No cross reactivity was detected to NGF, NT3 or NT4. This method has been used by the Barde lab group and collaborators, becoming a core technique for BDNF investigations (Naegelin et al., 2018a; Dingsdale et al., 2021a). Serum concentrations in the B Cre⁺ mouse were determined by Dingsdale et al., 2021 using an ELISA method based on these antibodies (B^{+/+} Cre⁺ 32.3 ± 3.70ng/mL, B^{+/-} Cre⁺ 10.6 ± 1.45ng/mL, Cre⁻ (WT phenotype) undetectable) .

To confirm the B Cre⁺ mouse results, ELISA of serum samples was repeated using a new commercially available kit from Fujifilm WAKO (Fujifilm WAKO Pure Chemical Corporation, Japan), that was reported to be more sensitive than this previous method. This new ELISA kit

can also be completed within approximately 4 hours (compared with 12 hours for the previous method) making it a very attractive option. The accuracy of the Fujifilm WAKO ELISA kit was validated with additional experiments that included measuring serum from C57BL6/J mice (Charles River), avoiding the *Rosa26-LSL-Bdnf-myc-IG/Pf4iCre* line (even if Cre negative) to ensure that any BDNF detected was not as a consequence of any unexpected, low-level expression of the BDNF construct. Furthermore, serum from a pooled sample of C57BL6/J serum was incubated with antibodies to either BDNF, or other members of the neurotrophin families (NGF and NT3), to exclude cross-reactivity with other neurotrophins. If the ELISA kit was specific to BDNF, incubation with antibodies to other neurotrophins should not have any effect on the signal, whereas the anti-BDNF antibodies should remove BDNF from the serum and cause loss of the signal.

3.4.2. Experimental setup

Mice were culled using CO₂ and blood collected and prepared for serum as described in Chapter 2.8. ELISA was then performed using the Fujifilm WAKO mature BDNF High Sensitivity kit as described in Chapter 2.9.

For the assessment of serum BDNF concentration in *Rosa26-BDNF-Myc/PF4iCre* mice, serum was collected from 9 B Cre⁺ mice (5 B^{+/+} Cre⁺ and 4 B^{+/-} Cre⁺) and 3 WT Cre⁻ mice (age 11-15 weeks). For the validation experiments, serum was collected from 24 C57BL6/J mice age 8-12 weeks (Charles River, 12 male, 12 female). A pooled serum sample was made from the combined serum of 9 mice (4 female, 5 male) and used to assess the specificity of the ELISA kit using antibodies to deplete neurotrophins from the serum (Figure 3.3). Protein G Sepharose 4 Fast Flow Beads (GE Healthcare) were centrifuged at 12,000 G and then washed with PBS 3 times (resuspended in PBS and centrifuged at 12,000 G for 20 seconds again). For each sample, 60µL of Protein G Sepharose beads were resuspended in 300µL of PBS with 30µg of antibody to either BDNF (Ab#9), NGF, NT3 or PBS only as a control. The anti-NGF (Korsching and Thoenen, 1983) and anti-NT3 antibodies (Gaese et al., 1994) had been raised at the Max-Planck Institute and were kindly provided by Prof. Yves Barde. Samples were then incubated for 1 hour on ice, vortexing intermittently to allow the antibodies to bind to the beads. The beads were then washed again (3x 12,000 G for 20 seconds and resuspension in PBS) to remove any excess unbound antibodies. Pooled serum samples (at 1/4 dilution with ELISA kit buffer) were then incubated for 3 hours on ice with the respective bead-bound antibodies, vortexing intermittently, to allow binding of the respective neurotrophins. Finally, samples were centrifuged to at 12,000 G for 20 seconds 3 times, with

serum collected and transferred to a new tube each time to remove all beads and the bound neurotrophin from the samples. BDNF concentrations from prepared serum samples were then measured using the Fujifilm ELISA kit as described in Chapter 2.

3.4.3. Results

ELISA results confirmed the presence of elevated BDNF concentrations in the B Cre⁺ mouse (Figure 3.4). Mean BDNF concentrations were measured at 25.74 \pm 11.36 ng/mL (n = 5) for homozygous (B^{+/+} Cre⁺) and 17.02 \pm 6.44 ng/mL (n = 4) for heterozygous (B^{+/-} Cre⁺) mice, in line with previous reports (Figure 3.4). The mean BDNF was slightly lower in the B^{+/-} Cre⁺ animals compared to B^{+/+} Cre⁺ although the difference did not reach significance. However this may have been due to the smaller sample size considering that B^{+/-} Cre⁺ concentration was significantly lower Dingsdale et al. (2021). A very small amount of BDNF was detected in the serum of WT, Cre⁻ animals (mean 3.06 \pm 0.16 pg/mL, n = 3).

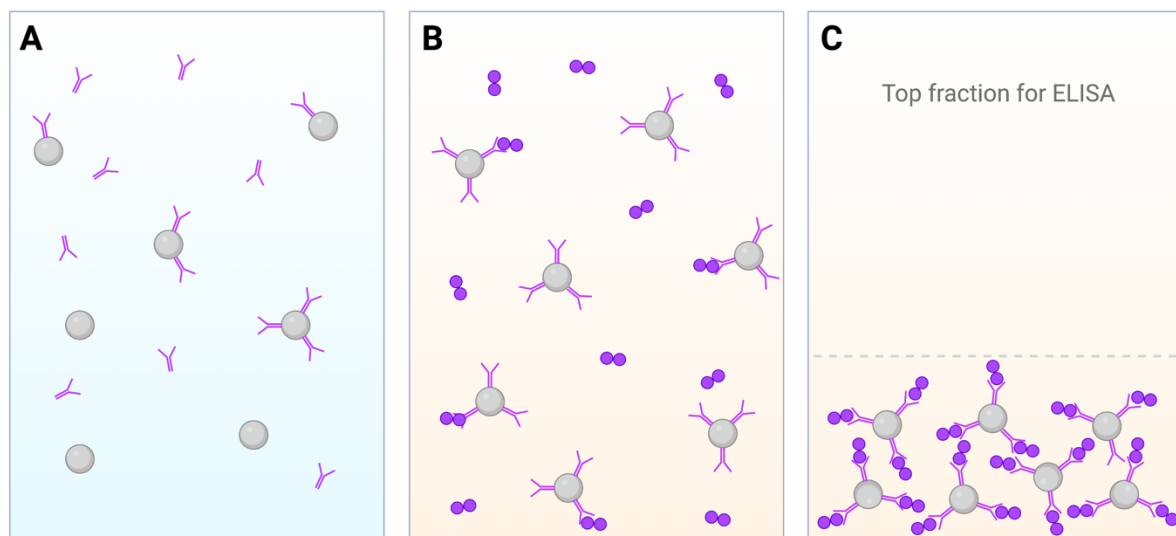


Figure 3.3: Depletion of serum BDNF to validate ELISA specificity. (A) Protein G Sepharose beads are washed and then resuspended with antibodies to neurotrophins for 1 hour. Antibodies will bind to the surface of the beads. (B) Beads are then resuspended in serum and the neurotrophin will be bound to the antibodies in the bead surface. (C) When centrifuged, the beads and the bound neurotrophin will be pelleted to the bottom of the tube, depleting the sample. The top fraction of the serum is removed and used for ELISA measurement. Created using Biorender.com

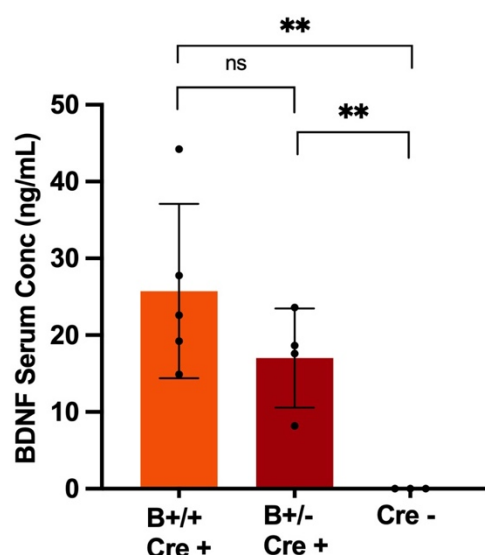


Figure 3.4: BDNF levels in the serum of homozygous (B+/+ Cre+), heterozygous (B+/- Cre+) and Cre -.

* = $p < 0.05$, ** = $p < 0.01$, *** = $p < 0.001$

A detectable level of BDNF was also found in serum samples from all Charles River C57BL/6/J mice. Mean BDNF concentration was $7.21 \text{ pg/mL} \pm 2.96$, with a concentration of $8.15 \pm 3.26 \text{ pg/mL}$ in males and $6.28 \pm 2.45 \text{ pg/mL}$ in females ($p = 0.13$) (Figure 3.5 A, B). Of note, a small number of samples showed a wider than expected spread of the triplicate measurements, suggesting inaccuracy in the ELISA reading and the position of the sample in the 96 well plate may have been a factor. One sample was in a corner well, while two others were next to a sample of B Cre+ mouse serum that had a raw luminescence several thousand times higher. Despite the 96 well plate being opaque, there appeared to have been a small degree of overspill luminescence from the neighbouring well. This effect was minimal and only seen when a sample of extremely high concentration was next to a well of very low concentration. However, considering the low levels of BDNF in C57BL/6J serum is, and the importance that subtle differences in concentration may have, caution should be taken to carefully consider the layout of plates in their experiments to avoid interaction of neighbouring wells.

Regarding the antibody depletion experiments, there was a significant reduction in the ELISA signal following incubation with anti-BDNF antibodies ($p = 0.0001$, one-way ANOVA), while the signal was retained in the other groups (Figure 3.5 C, D). This was an important result that confirms the Fujifilm ELISA kit is not only highly sensitive but also highly specific. It shows that the signal is not due to cross-reactivity with other members of the neurotrophin family, nor is it due to an artefact related to some other component of serum.

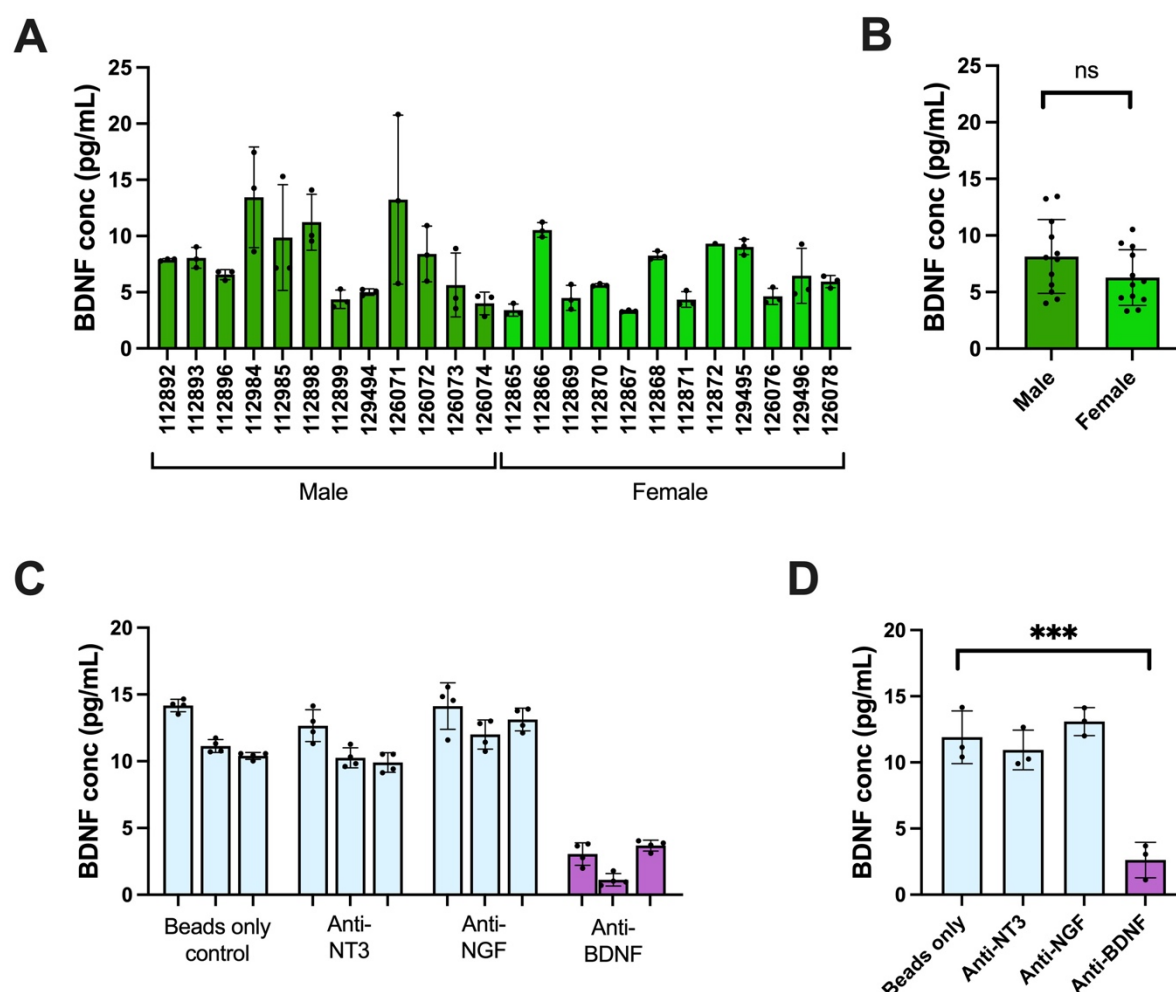


Figure 3.5: ELISA results showing further investigation of serum BDNF concentration in C57BL/6J mice

(A) Serum concentration of male and female C57BL/6J mice. Points represent individual ELISA readings; column represents the mean of the triplicates for each serum sample. (B) Mean serum BDNF concentration for male and female C57BL/6J mice. $P = 0.1275$, unpaired t-test. (C) BDNF concentration of a pooled serum sample following incubation with protein G beads alone, or protein G beads bound with antibodies to different neurotrophins, NGF, NT-3 or BDNF. Points represent individual ELISA readings; column represents the mean of the triplicates for each serum sample. (D) Mean BDNF concentrations of a pooled serum sample, incubated with protein G beads alone, or beads bound with antibodies to different neurotrophins. Points represent triplicate means for each sample, column represents group mean. $P = 0.0001$, One-way ANOVA.

3.4.4. Discussion

These findings are consistent with the previous studies in this model, showing BDNF serum concentrations similar to that seen in humans in the B Cre⁺ mouse. Previous work with this

model also found a lower mean in heterozygous animals and it is likely that the result from the ELISA presented here would reach significance with increased numbers.

The Fujifilm WAKO mature BDNF ELISA kit is highly sensitive and specific, able to measure serum concentrations within the range of 3-10pg/mL. The previous immunoassay method reported a sensitivity of 5-10pg/mL (Kolbeck et al., 1999), but failed to detect BDNF in mouse serum (Chacón-Fernández et al., 2016). It is possible that this was because the serum concentration is at the lower limit of the sensitivity of this method, whereas the Fujifilm WAKO kit documentation reports sensitivity of 0.2pg/mL (this lower limit has not been verified here, however the standard curve using the Mature BDNF Standard within the kit does include a concentration of 0.205pg/mL).

This kit is therefore a suitable test to be used throughout this project, but is also an extremely valuable tool for wider research on BDNF as it could in principle be used to measure BDNF in fluids such as CSF and aqueous humour to a level of accuracy that may not have been possible before. The confirmation of BDNF in C57BL/6J serum is also an interesting finding that has several implications. Given the absence of BDNF in mouse megakaryocytes and platelets, this low level of BDNF is likely to originate from another peripheral source such as skeletal muscle. This provides support for studies that had theorised the presence of low levels of circulating BDNF in mice, such as the Fulgenzi et al., 2020 work on interactions between skeletal muscle and TrkB in pancreatic β -cells. Now that serum BDNF can be measured in the mouse, it could be a valuable model to investigate other sources of peripheral BDNF that are usually masked by the dominant expression in megakaryocytes and platelets.

3.5. Summary

The B Cre⁺ mice have no overt deficits in physical health or behaviour, and based on these small number of investigations, the retina appears grossly normal with baseline RGC counts equal to WT mice. The measurements of serum BDNF concentration validated the results of Dingsdale et al., 2021, confirming that these mice express humanised levels of BDNF. They are therefore appropriate to be used for the planned experiments investigating the responses of RGCs in the context of glaucoma models.

The Fujifilm WAKO mature BDNF ELISA kit was confirmed to be a sensitive and specific method of measuring BDNF in very low concentrations, demonstrated by the detection of low levels of BDNF in WT mouse serum. This supports the use of this kit as a valuable tool in

future research, and opens the door for using mouse models in the investigation of other sources of peripheral BDNF.

Chapter 4. Development of Models and Techniques

4.1. Short introduction

Accurate assessments of RGC morphology depends on robust experimental models with reliable endpoint readouts. In this chapter, assessments were made of the central methods and models used in the intended project. Preliminary trials using the three selected glaucoma models were performed using WT mice. The purpose of these trials was to finalise protocols, to demonstrate that glaucomatous damage could be induced and to establish whether the procedures had been learned to a sufficient standard. While dendritic atrophy in mouse retinal explant and ONC models is well documented, this has not yet been shown in the mouse magnetic microbead model. It is well established in rats, and while RGC loss had been confirmed in mice with this model (Ito et al., 2016a), dendrite changes were yet to be determined.

4.2. Retinal Explants

4.2.1. Introduction

The first of the glaucoma models to be evaluated was the retinal explant. This technique has become an effective and established tool in glaucoma research, and has also been used to demonstrate the impact of BDNF *in vitro* by previous members of our research group (Binley et al., 2016a), thus allowing comparisons with studies using the B Cre+ mouse line.

4.2.2. Experimental setup

5 female C57BL/6 mice, age 5 months, were included in the experiment. Mice were culled by cervical dislocation before the eyes were immediately enucleated and dissected as described in Chapter 2.2. Retinas were transferred onto culture inserts (Millicell, Cell Culture Inserts 0.4µm), and flat mounted with the ganglion cell layer facing upwards. The culture inserts were positioned in a 6 well plate, supplemented with cell culture media. (10 mL of cell culture media

contains 100 μ L N-2 supplement (100X), 200 μ L B-27 supplement (50X), 100 μ L Pen/Strep (10000 U/mL), 25 μ L GlutaMAX supplement (200 mM), 9.565 mL Neurobasal-A Medium) 1.5mL of media was added to each well, ensuring that media made contact with the insert below, maintaining an air-tissue interface on the superior surface. The retinas were then kept in an incubator at 37°C, 5% CO₂ for either 48 or 72 hours, with culture media being changed after 48 hours.

At the end of the required number of days, the retinas were transferred to a microscope slide. This was achieved by cutting a small section of the culture insert surrounding the retina, thus avoiding damage to the tissue during transfer. The retinas were then labelled using DiOlistics as described in Chapter 2.4.

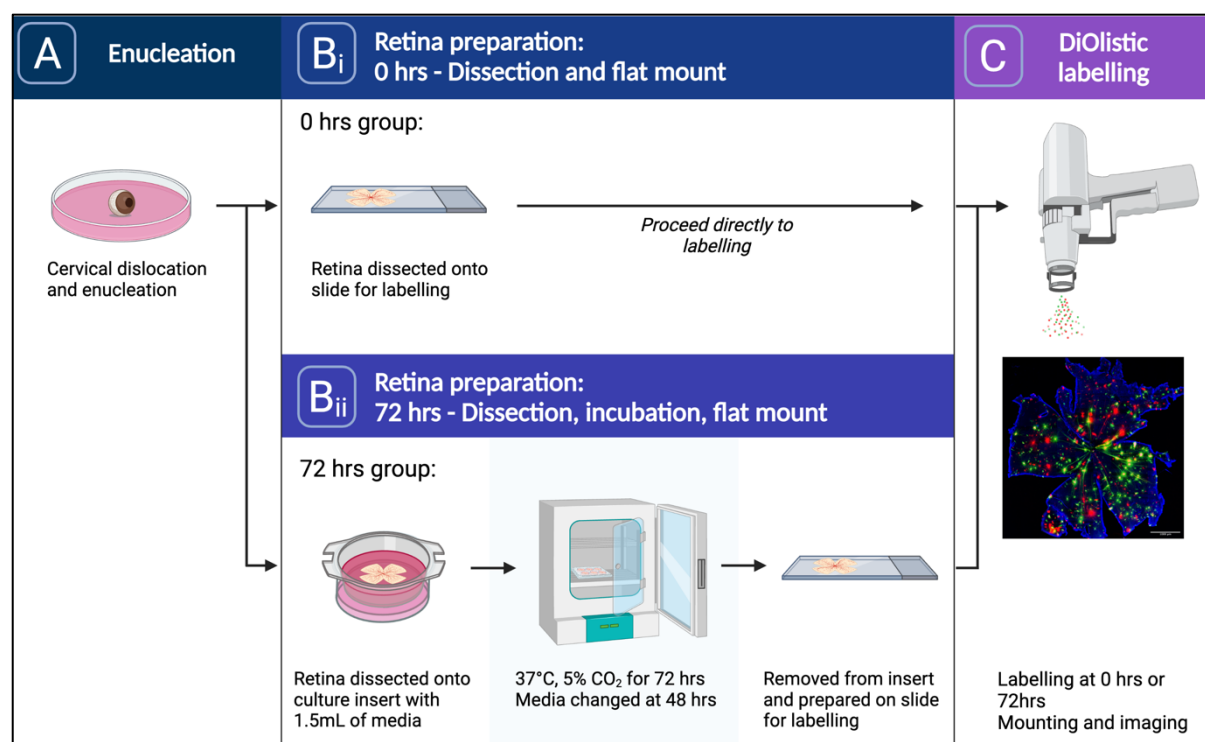


Figure 4.1: Overview of retinal explant method

(A) Animals are sacrificed by cervical dislocation and eyes enucleated. **(B_i)** Retinas are then dissected and placed directly on a slide for labelling at 0 hrs or **(B_{ii})** transferred to a culture insert and incubated for 72 hrs. **(C)** DiOlistic labelling performed followed by mounting of slides and imaging. Created with BioRender.com.

4.2.3. Results

As expected, analysis revealed a marked reduction in Sholl AUCs as the post-mortem time interval increased: $53.24\% \pm 26.12\%$ at 48 hours ($P = 0.004$, ANOVA with Tukey post hoc) versus $46.94\% \pm 25.43\%$ at 72 hours ($P < 0.001$, ANOVA with Tukey post hoc) compared to the 0 hours baseline. While this change from baseline was significant, the difference between these two timepoints was comparatively small and not found to be significant ($p = 0.882$, ANOVA with Tukey post hoc). Binley et al., 2016 reported a similar finding when assessing the extent of dendritic atrophy seen in retinal explants, with the most significant change in the Sholl curve and AUC seen within the first few days, and a much smaller change seen between 48 and 72 hours.

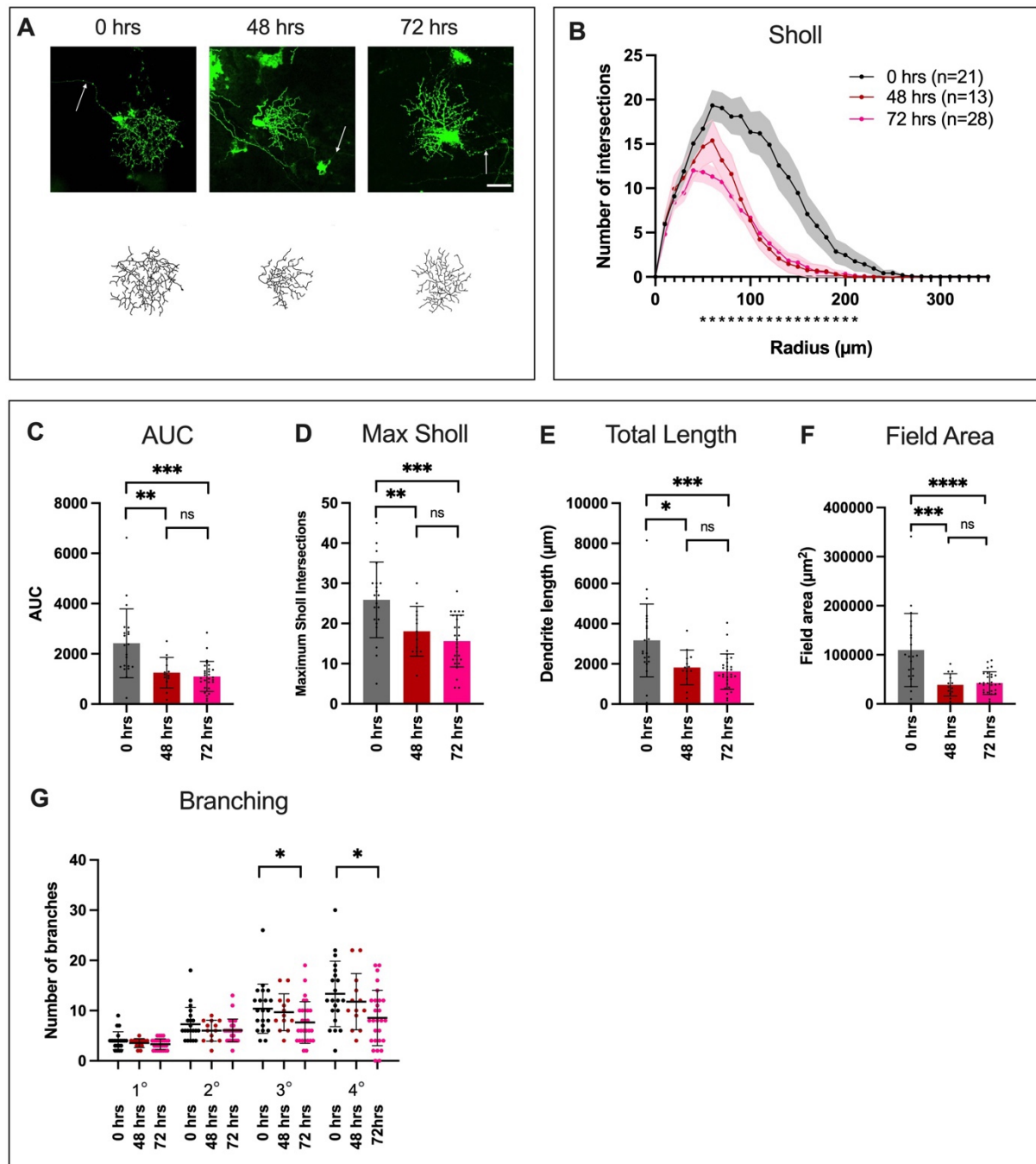


Figure 4.2: Sholl analysis comparing RGCs in retinal explants over time.

(A) Representative examples RGCs and dendrite reconstructions from experiment groups. White arrow indicates RGC axon, scale bar = $50\mu\text{m}$. (B) Sholl analysis showing mean at each interval (line) \pm SEM. 0 hrs (black), 48 hrs (red) and 72 hrs (pink). Two-tailed Mann-Whitney U test at each interval distance, * = $P < 0.05$, n=number of RGCs. (C) Area under the Sholl curve. (D) Maximum number of Sholl intersections. (E) Total dendrite length (μm). (F) Dendrite field area (μm^2). (G) Number of dendrites at each branching level. For Column Scatterplots E-J data points represent individual cells, columns represent means for group and error bars correspond to SD, * = $p < 0.05$, ** = $p < 0.01$, *** = $p < 0.001$.

4.2.4. Discussion

While the numbers of animals and individual RGCs are relatively small, this preliminary experiment was sufficient to demonstrate the expected dendritic atrophy using a straightforward protocol also used in previous studies. It was adopted as the protocol of choice for subsequent studies of the B Cre⁺ mice using the 72-hour end point.

4.3. Optic Nerve Crush

4.3.1. Introduction

The optic nerve crush (ONC) model has been used in glaucoma research for decades, and represents a step up in complexity from the retinal explants, both physiologically in terms of the *in vivo* nature of the model, and the technical skill required for its use. While all methods of (ONC) aim to cause a mechanical injury to the nerve, there are several different variations on the procedure. A common method is to use an anterior approach, making an incision in the conjunctiva, and gently dissecting the tissues to expose the optic nerve (Cameron et al., 2020; Templeton and Geisert, 2012). This method is relatively fast and technically simpler than other variations that, for example, use a supraorbital approach (Mead et al., 2021). The supraorbital approach exposes a longer section of the optic nerve, and allows the dural sheath to be opened to separate the nerve and artery before performing the crush. This arguably makes the crush procedure more reliable but it is a much more complex technique. To reach the optic nerve, the surgeon must first navigate past the Harderian gland and avoid damage to the retro-orbital venous sinus or the large blood vessels along the orbital rim, with even slight injuries resulting in bleeding. The main skin incision requires suturing, often with additional surgical glue to cover the sutures and prevent them being dislodged by the mice after the procedure. The more straightforward anterior approach is faster and simpler, but without separating the dural sheath, there is a risk of occluding the arterial supply. This could result in an arterial occlusion and ischaemic retinal damage, rather than the neuronal degeneration that is intended. However, this risk can be mitigated by performing the crush injury at least 1.5-2mm behind the globe, and by examining the eye after each procedure to assess for evidence of vascular occlusion. On balance, the anterior approach was considered the most suitable for the intended project and a trial was performed.

4.3.2. Experimental setup

4 WT male mice were used for this experiment, aged 11 months. A left eye ONC procedure was performed on all 4 animals.

The method for the ONC procedure was broadly based on Cameron et al., 2020, with some adjustments made to suit the available surgical space and equipment. Mice were anaesthetised using isoflurane and positioned on a temperature-controlled heat pad. A lubricating ointment (Viscotears Liquid Gel, Bausch & Lomb) was then applied to the fellow eye, to prevent exposure keratopathy during the procedure. Topical oxybuprocaine hydrochloride 0.4% (Bausch & Lomb) was applied to the eye undergoing the procedure for anaesthesia, followed by Povidone Iodine 5% (Bausch & Lomb) to sterilise the area.

The inferior-temporal conjunctiva was grasped using Pierse Notched micro-cupped forceps (Duckworth & Kent) and Vannas scissors (Duckworth & Kent) were then used to make an incision. By lifting the grasped conjunctiva, an incision can be safely made through the conjunctiva and tenons capsule while staying clear of the underlying sclera and the episcleral veins. The inferior-temporal approach is used so that a channel can be made in the space between the extraocular muscles (Figure 4.5 A).

The globe is rotated nasally and blunt dissection used to expose the optic nerve. The nerve is then grasped and crushed for 5 seconds using Dumont cross-action N5 forceps, with only the pressure from the self-clamping action to crush the nerve. Using the cross-action forceps allows a consistent force to be applied across the different procedures. Once the crush is completed, the tissues were repositioned and chloramphenicol drops applied.

At the end of the procedure, lubricating ointment and a coverslip were placed on the surface of the eye to allow examination of the retina (Figure 4.5 C). If there were any signs of arterial occlusion or the lens had become cloudy, the animals were excluded from the experiment. Once the procedure was completed, the mouse was transferred to an incubator until they had fully recovered from the anaesthetic.

After 7 days, the mice were culled by cervical dislocation and the eyes immediately enucleated. Retinas were dissected and RGCs labelled by DiOlistics as described in Chapter 2.4.

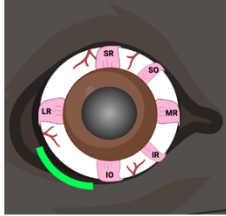
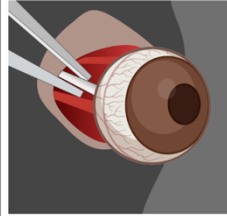
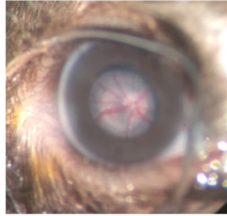


A Animal preparation	B Incision and crush	C Retina check	D Observation	E Mounting and imaging
 <ol style="list-style-type: none"> 1. Animals are anaesthetised using isoflurane 2. Topical anaesthetic is applied to the eye 3. Incision made through conjunctiva and tenon's capsule at inferior temporal quadrant, in the space between the extraocular muscles 	 <ol style="list-style-type: none"> 4. Blunt dissection is used to carefully expose the optic nerve 5. Optic nerve is crushed for 5 seconds using Dumont N5 cross action forceps 	 <ol style="list-style-type: none"> 6. Using Viscotears and a coverslip and coverslip, the retina is examined to exclude vascular occlusion 	 <ol style="list-style-type: none"> 7. Observation for 7 days 	 <ol style="list-style-type: none"> 8. Dissection, DiOlistic labelling and Sholl analysis

Figure 4.3: Overview of Optic nerve crush procedure

(A) Anatomy of mouse extraocular muscles, demonstrating larger spacing between the muscles on the temporal side to access optic nerve. SR- superior rectus, SO – superior oblique, MR – medial rectus, IR – inferior rectus, IO – inferior oblique, LR – lateral rectus Edited from (Ruiz-Ederra and Verkman, 2006). **(B)** Exposure of the optic nerve and crush injury using forceps, taken from (Cameron et al., 2020) **(C)** Examination of the mouse retina and optic disc after the nerve crush injury, confirming that the vascular supply has not been compromised (original image). **(D)** Observation for 7 days. **(E)** Preparation of retinas for DiOlistics.

4.3.3. Results

Following ONC injury, a significant decrease was seen in the Sholl curve, with AUC measuring $2031 \pm 863.3\mu\text{m}^2$ and $1465 \pm 636\mu\text{m}^2$ in the fellow eye control and ONC eye respectively ($p = <0.001$) (Figure 4.4). A significant decrease was also in the maximum number of Sholl intersections (25.12 ± 8.61 and 19.68 ± 6.67 , $p = <0.001$) and the total dendrite length (2986 ± 1199 and 2157 ± 920 , $p = <0.001$). There was no evidence of vascular occlusion in any of the four mice included in this trial.

4.3.4. Discussion

This method of ONC produced a significant retraction of the dendrites at 7 days, and is in line with previous reports that ONC causes changes in dendrite morphology (Kalesnykas et al., 2012). It demonstrates that the ONC procedure can be performed to a consistent standard and is suitable for larger experiments with the B Cre+ mouse model. The anterior approach was also quick and effective and, providing the eye is properly examined at the end of the procedure, it was reliable a method for inducing predictable RGC degeneration.

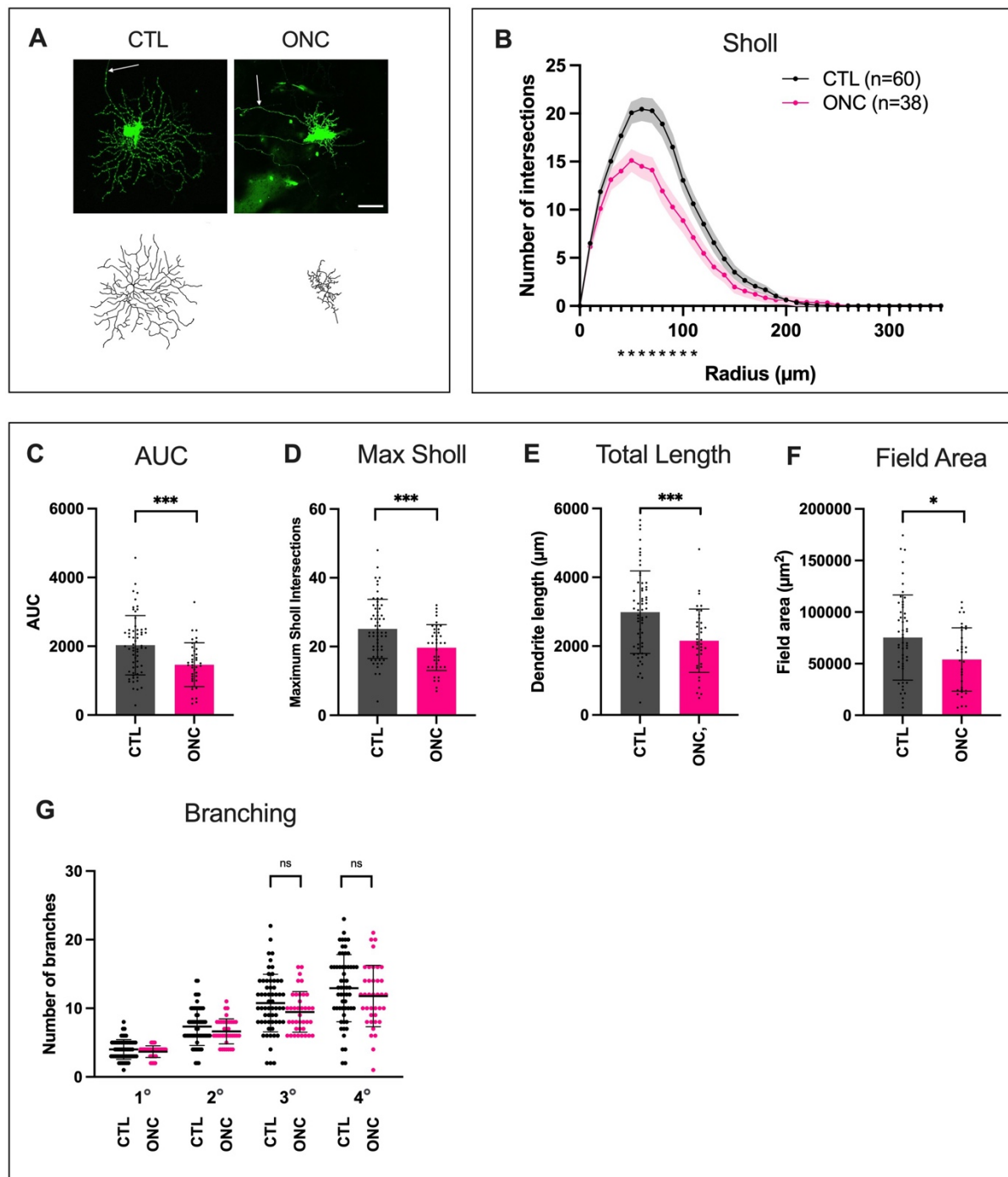


Figure 4.4: Analysis of RGCs 7 days after Optic Nerve Crush injury.

(A) Representative examples RGCs and dendrite reconstructions from experiment groups, fellow eye control (CTL) and optic nerve crush eye (ONC). White arrow indicates RGC axon, scale bar = 50 μm . (B) Sholl analysis showing mean at each interval (line) \pm SEM. CTL (black) and ONC eye (pink). Two-tailed Mann-Whitney U test at each interval distance, * = $P < 0.05$, n=number of RGCs. (C) Area under the Sholl curve. (D) Maximum number of Sholl intersections. (E) Total dendrite length (μm). (F) Dendrite field area (μm^2). (G) Number of dendrites at each branching level. For Column Scatterplots E-J data points represent individual cells, columns represent means for group and error bars correspond to SD, * = $p < 0.05$, ** = $p < 0.01$, *** = $p < 0.001$.

4.4. Microbead model

4.4.1. Introduction

The microbead model has been successfully used in different species for many years to induce the sustained elevation of IOP as a model for glaucoma. Multiple refinements of the technique have been developed involving to the size and material of microbeads used as well as the approach and equipment used to make the injection.

Dendritic atrophy has been well established in the rat magnetic microbead model (Williams, 2016) as a marker of glaucomatous changes but, the evidence in the mouse microbead model is far more limited. (Ito et al., 2016b) only assessed RGC and axon count and did not assess dendrite morphology. However more recently, the same method was used on B6.Cg.Tg [Thy1-YFPH]2Jrs/J mice (transgenic mouse line expressing yellow fluorescent protein in RGCs) to investigate the role of adenosine monophosphate-activated protein kinase (AMPK) in RGC dendrite retraction (Belforte et al., 2021). While this study did report a reduction in the Sholl curve in the ocular hypertensive group, it is worth noting that the size of the change in the Sholl curve appeared to be much smaller than that seen in the rat magnetic microbead models. The Sholl peak reduced from approximately 28 to 24 intersections, a peak that is still higher than the baseline peak for the mice in this chapter, as well as other previously published work (Bevan et al., 2020). Therefore, prior to proceeding to the B Cre⁺ mouse experiments, dendritic atrophy in response to the IOP elevation must also be confirmed in the WT mouse. This is of particular relevance when using C57BL/6 mice as they have often been noted to be more resilient to RGC damage compared to other mouse strains. This was described by Cone et al., 2010 when using a polystyrene bead model, who found that RGC layer loss in response to the glaucoma model was reduced in older C57BL/6 mice compared to CD1 and DBA/2J strains. This was also commented on by Ito et al., 2016 in their description of the mouse magnetic microbead model using C57BL/6 mice. While gradual loss of RGCs was seen in the first 3 weeks after injection, a significant increase in RGC death was not observed between weeks 3 and 6. The resistant nature of the C57BL/6 mice was postulated as a possible explanation and longer periods of elevated IOP may be required to study further RGC loss at later time points. Unfortunately, due the B Cre⁺ model being developed on a C57BL/6 background it is not possible to use alternative strains. This possible resistance further supports the use of retinal DiOlistics and assessment of RGC morphology as an outcome measure as this is a sensitive marker of early degeneration that precedes cell death.

When deciding on the most appropriate method of microbead model to use in the intended experiments with the B Cre+ mice, several factors must be considered. Colleagues at Cardiff University have established a reliable protocol for the rat microbead model (Morgan and Tribble, 2015; Tribble, Otmani, Kokkali, et al., 2021a), but there are important differences in the mouse. The mouse eye has an axial length of 3.38mm, compared to 6.29mm in the rat, and approximately one eighth of the volume (Hughes, 1979; Remtulla and Hallett, 1985). However, in principle, a similar method should be applicable.

Injection volume and concentration

Functional estimations of the mouse eye indicated that the anterior chamber volume is approximately 7µL (Zhang et al., 2002). Therefore, a smaller volume of beads needed to be injected than the 8µL often used in the rat model. There is some variation in practice but a volume of 1-2µL of microbeads has been commonly used in the mouse for microbead injections (Ito et al., 2016a; Jassim and Inman, 2019).

In order to have sufficient numbers of beads to occlude the trabecular meshwork in such a small volume, the concentration of the bead mixture must also be considered, and this is notably variable between different groups. Regarding the magnetic M450 Dynabeads, a concentration of 2.7×10^6 beads/µl was used to sustain IOP elevation in the rats. In the method described by Ito et al., 2016 for the mouse model, 1.5µL of beads at a concentration of 1.6×10^6 was used, giving a final total of 2.4×10^6 beads. A summary of the variations in beads, concentrations and methods used in previous rodent experiments are listed in Table 4.1 and Table 4.2.

Injection apparatus

There are also variations in the equipment used for the injection whereby Morgan and colleagues have previously used a Nanofill Hamilton syringe, injected by hand, a microsyringe pump with a pulled and bevelled glass needle is an alternative (Ito et al., 2016b). This approach turned out to give a finer control over the injection speed and volume as well as customisation of the needle tip. However, the position of the injector apparatus is relatively fixed. The handheld Hamilton syringe has the advantage of being more mobile, allowing the researcher freedom to adjust and adapt the angle of injection as necessary. Considering the successful results achieved on rats, the Nanofil Hamilton syringe was the first method to be used in the mouse model.

Choice of anaesthetic

The primary choice for anaesthetic in these procedures was between an intraperitoneal (IP) injection or an inhaled anaesthetic. Tribble et al., 2021 had used an IP injection containing ketamine (37.5 mg/kg) and medetomidine hydrochloride (1.25mg/kg) for their rat model, and Ito et al., 2016 used a similar cocktail of ketamine (20mg/mL), xylazine (2mg/mL) and acepromazine (0.4mg/mL) mixed together and delivered by IP injection at 1µL/g of body weight. There are several advantages to this method of anaesthesia. Firstly, there is more flexibility when handling the mouse and adjusting the position as the animal is not connected to an inhalation mask. The mask itself can also limit some angles of approach to the eye, as a correctly fitting mask that covers the mouth and nose will be close to the surgical field. Additionally, the longer recovery period can be utilised to allow the beads time to settle in the iridocorneal angle, rather than becoming dislodged. After consultation with the Cardiff University veterinarian, a combination of ketamine (75mg/kg) and medetomidine hydrochloride (1mg/kg) was selected, followed by Atipamezole 1mg/kg by subcutaneous injection for reversal at the end of the procedure. While this method was effective, there were some concerns regarding the slow recovery of the mice from the anaesthetic. The dose was reduced but some mice continued to have laboured breathing and occasionally oral secretions. Therefore, an alternative method using inhaled isoflurane (initiation 4%, maintenance 2.5%) was trialled. This has been used in both mouse and rat microbead models and despite the limitations created by the mask, there are other advantages. The depth of anaesthesia is easier to control, and the recovery is much faster. In practice, the mask did not cause significant obstruction when injecting if time was spent to plan the approach beforehand, and to arrange the surgical equipment appropriately.

Table 4.1 Summary of magnetic microbead models in rats. Edited from (Tribble, Otmani, Kokkali, et al., 2021b)

Protocol	Bead Details	Bead Preparation	Bead Concentration	Injection Details	Time Frame
Samsel et al., 2011	5- μ m diameter ferromagnetic microspheres (Corpuscular, Inc., Cold Spring, NY)	Sterilized by gamma irradiation	30 mg/mL	0–20 μ L delivered by unilateral tunnel injection	42 days, with up to 3 repeat injections
Williams, 2016	Dynabead M-450 Epoxy, 4.5- μ m diameter (Thermo Fisher Scientific)	Washed in 1-M Tris buffer solution (pH 11) for 24 hours at 4°C, reconstituted in BSS, sterilized by gamma irradiation	30 mg/mL	10 μ L delivered by unilateral tunnel injection	16 days with repeat injections, if necessary
Tribble et al., 2018	4.5- μ m diameter paramagnetic polystyrene microspheres (Kisker Biotech, Steinfurt, Germany)	4 \times centrifugation (1600g) and washing in BSS, sterilized by gamma irradiation	30 mg/mL (4.7×10^5)	10 μ L delivered by unilateral tunnel injection	0 days of OHT (followed by 14 days of return to NT); repeat injections undertaken, if necessary, with 1 week intervals
Tribble et al., 2021	Dynabead M-450 Epoxy, 4.5- μ m diameter (Thermo Fisher Scientific)	2 \times centrifugation (1000g) and washing in HBSS	$\sim 1.6 \times 10^6$ beads/ μ L	6–8 μ L delivered per eye by bilateral tunnel injection; no repeat injections	14 days OHT

Table 4.2 Summary of magnetic microbead models in mice

Protocol	Bead Details	Bead Preparation	Bead Concentration	Injection Details	Time Frame
Jassim and Inman, 2019	COMPEL COOH-Modified 8 μm diameter (Bangs Laboratories, Fishers, USA)	Not specified	Not specified	1 μL injected using glass-pulled micropipette and microsyringe pump	4 weeks
Ito et al., 2016	Dynabead M-450 Epoxy, 4.5- μm diameter (Thermo Fisher Scientific)	Washed in 0.02 M NaOH in 10x Tris buffer, 4x wash in diH ₂ O, 4x wash in BSS	$\sim 1.6 \times 10^6$ beads/ μL	1.5 μL delivered by unilateral tunnel injector	6 weeks

The planned experiments with the B Cre⁺ mice were an additional reason to avoid ketamine in the induction of anaesthesia as ketamine is known to have a rapid onset antidepressant effect. All antidepressants, including ketamine, increase expression and signalling of BDNF through its receptor, TrkB (Ateaque and Barde, 2021; Casarotto et al., 2021). Indeed, Casarotto et al., 2021 have reported that antidepressants, including ketamine bind to the transmembrane domain of TrkB thereby stabilising a conformation of TrkB transmembrane dimers that potentiating TrkB signalling. Given this context, the use of ketamine with the B Cre⁺ mouse model could be a confounding factor.

4.4.2. Experimental setup

Taking all of the elements into consideration, the following method was adopted for the microbead model, performed using C57Bl/6J mice (Charles River) (see Figure 4.7 for procedure overview).

Intraocular Pressure Measurement Method

IOP was measured using a TonoLab rebound tonometer (Icare, Vantaa, Finland) on awake animals. Mice were scruffed, taking care not to apply the scruff too high so that it would cause additional pressure on the eyes, but high enough to ensure the head can be held in place to allow the IOP to be measured. One drop of Oxybuprocaine Hydrochloride 0.4% Minims (Bausch & Lomb, PL03468/0053) was applied to each eye to anaesthetise the cornea before IOP was measured. IOP was taken as the average of 5 sets tonometer readings, each of which consists of 6 individual IOP measurements with a single value for the set displayed by the TonoLab tonometer. Animals were habituated to the tonometry procedure for 2 weeks prior to the surgical intervention to familiarise them with the process and to obtain baseline IOP measurements. Following the procedure, IOP was measured at day 1, 3, 5 and 7, and then weekly up until 4 weeks. All measurements were taken between 09:00am - 10:00am to account for IOP variation in circadian rhythms.

Microbead Preparation

The M450 Dynabeads were selected as a suitable microbead to use for the experiments after the successful results in the rat models, and the benefits previously described that include a clear visual axis, allowing for other retinal investigations in future if required. Under a sterile hood, 500µl of M450 Dynabeads were drawn up and transferred to a sterile Eppendorf tube, shaking bottle well before drawing up to ensure the beads are well mixed. The beads were

then centrifuged for 3 minutes at 5700g at room temp. The supernatant was discarded, and the bead pellet resuspended in 500µL of sterile Balanced Salt Solution (BSS). The beads were then centrifuged for 3 minutes at 3200g at room temp and resuspended in BSS twice more. After the final centrifuge step, the beads were resuspended in 125µL of BSS. This will produce a bead mix for injection with concentration of 2.7×10^6 beads/µl, 240mg/ml. The mixture was then sterilised further with UV light.

Intracameral Injection of Microbeads

The initial experiments were based on the method used for the rat model, with some variations made to account for the smaller anatomical structures and smaller volumes. The animal is anaesthetised using isoflurane and positioned on a temperature-controlled heat pad throughout the procedure. Lubricating ointment (Viscotears Liquid Gel, Bausch & Lomb, PL13757/0020) is applied to the eye not being injected in order to prevent exposure keratopathy. Topical anaesthetic, oxybuprocaine hydrochloride 0.4%, (Bausch & Lomb, PL03468/0053), is applied to the procedure eye, followed by topical povidone-iodine 5% (Bausch & Lomb, PL03468/0020). Titanium forceps are then used to elevate the globe, providing sufficient position and access to the globe (non-magnetic forceps must be used to prevent interaction with the magnet used later)

8µL of previously prepared and washed M450 Epoxy Dynabeads (Invitrogen, 14011, Thermo Fisher Scientific) are drawn up into a 100µL Nanofil Hamilton syringe with an attached 33G needle immediately before injection. The Nanofil Hamilton syringe with a 33G needle is then used to make a tunnelled incision through the cornea into the anterior chamber of the eye. 1.5µL of microbeads are slowly injected over 15-30 seconds into the anterior chamber and positioned into the iridocorneal angle using an external magnet (Neodymium Boron magnet, strength c.0.45T). The magnet is held in place, opposite to the site of entry in order to prevent loss of beads in the event of reflux when the needle is being removed. A tunnelled incision is used as this will become self-sealing, and no suturing or other closure method will be required (this method is routinely used for cataract surgery in ophthalmology theatres). The external magnet can be used again until the microbeads are distributed into an even ring around the iridocorneal angle. Topical chloramphenicol 0.5% (Bausch & Lomb, PL03468/0069) is applied to the eye at the end of the procedure and the animal moved to a warmed area and monitored until they have fully recovered.

Post-operative period

Following the procedure, IOP was measured at day 1, 3, 5 and 7, and then weekly up until 4 weeks. All measurements were taken between 09:00am - 10:00am to account for IOP

variation in circadian rhythms. If there were any signs of infection in the eye or other health concerns, the mice were culled. Additionally, the mice were also culled if the IOP reached $>30\text{mmHg}$ as this may be causing pain to the animal. At the end of the 4-week post-operative period, mice were culled by cervical dislocation and the retinas prepared for DiOlistic labelling and Sholl analysis as described in Chapter 2.



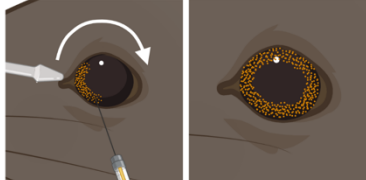

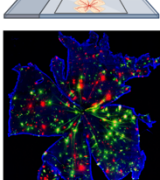
A Habituation	B Baseline IOP	C Microbead injection	D IOP Monitoring	E Dissection and labelling
 Handling and habituation	 Baseline IOP measurements for 2 weeks	 <ul style="list-style-type: none"> - Anaesthetise using isoflurane - Topical oxybuprocaine and Povidone - Magnetic microbeads injected into anterior chamber - Distribution of the beads using an external magnet - Formation of a 360° ring of beads - Post-operative chloramphenicol 	 IOP measurements: <ul style="list-style-type: none"> - Day 1 - Day 3 - Day 5 - Day 7 - Day 14 - Day 21 - Day 28 	 Retina dissection and DiOlistic labelling

Figure 4.5: Overview of magnetic microbead model. (A) Habituation and handling to acclimatise animals. (B) 2 weeks of baseline IOP measurements with further handling to ensure animals are relaxed during the procedure. (C) Under anaesthetic, injection of microbeads into the anterior chamber and positioning of the beads using an external magnet (grey bar). This magnet is then slowly moved around the eye (white arrow) until a full 360° ring of beads is formed. (D) Post-operative IOP monitoring over a subsequent 4-week period. (E) Mice are culled and retinas prepared for DiOlistic labelling and imaging of RGCs.

4.4.3. Results

The microbead model turned out to be extremely challenging. Despite consistent success with rats (Tribble, Otmani, Kokkali, et al., 2021b), IOP profiles in mice were highly variable and attained IOP elevations $\geq 16\text{mmHg}$ in only a small number of mice (12/71). Even when this pressure was reached, it was rarely sustained beyond a few days. The 33G needle allowed smooth injection of the magnetic microbeads, but created a large corneal incision. The size of this incision was manageable in the rat, but the smaller size of the mouse eye and the thinner cornea meant that when the needle was removed, there was significant reflux through the wound. This leakage not only prevented the formation of a pressurised anterior chamber, but the flow of aqueous out the incision also allowed the microbeads to become dislodged from their position in the iridocorneal angle. Several strategies were used to try and address this

problem. The length of the corneal tunnel was varied to try and achieve a better seal, an air bubble was injected into the anterior chamber to force the beads to remain in the angle, and a small injection of viscoelastic (Viscoat, Alcon) was used to try and create a seal at the injection site. None of these methods were able to resolve the issues (Figure 4.8).

A 35G needle was used to make a smaller incision through the cornea. While this reduced leakage from the wound, the smaller diameter also meant the needle quickly became blocked by the beads. In view of the cost of these needles this was not a sustainable approach. A disposable needle from TSK (TSK Laboratory, Japan) of approximately 34G could be attached to a syringe via a Luer fit. This was improved on the 33G needle but the wound was still larger than desired, and the microbeads often collected and settled in the dead space area if the needle attachment. This caused a lot of wastage of the beads and resulted in BSS alone being injected.

In view of these considerations, the decision was therefore made to move to glass needles. These needles, made from glass capillary tubes, must be pulled and bevelled by the experimenter which can be time consuming. However, they have the advantage of being able to make large numbers of needles that can be shaped to meet the specific requirements of the project (Figure 4.9). The capillary tubes (Capillary Glass, 1.0mm OD, 0.58mm ID, 7.62c (3 inches long) – 1B100-3, World Precision Instruments) were pulled using a Micropipette puller (Model P-80/PC Flaming/Brown Micropipette Puller, Shutter Instrument Co., USA, Settings: Heat 789, Pull 50, Velocity 70, Time 80), and then shaped using a Micropipette beveler (BV-10 Micropipette Beveler, World Precision Instruments) to make tri-beveled tips. Once shaped, the needles were flushed with 70% ethanol followed by sterile BSS, and sterilised further with UV light. The prepared needles were kept in a sealed container until use. To perform the microbead injection, the glass needles were attached to the 100µL Nanofil Hamilton syringe using a specialised glass pipette holder (1.00mm Glass Pipette Holder for NANOFIL Syringe, World Precision Instruments, NFINHD-G10). The additional equipment used allowed smaller incisions to be made in the cornea, and several attempts produced a clear ring of magnetic beads with an apparently maintained anterior chamber. But despite these changes, the IOP was still inconsistent and could only produce a moderate rise in around 40% of mice.

Trials with the magnetic microbead model included a total of 79 mice. Across these trials, the RGC data was collated from all mice that achieved a successful IOP rise of ≥ 16 mmHg at any point in the 4-week post-operative period. This combined Sholl analysis showed that even when only the most successful IOP rises were included, there was no difference in the dendrite

complexity between the ocular hypertensive (OHT) eyes, and the fellow eye controls. Nor was there any difference in any of the additional sub analyses (Figure 4.10).

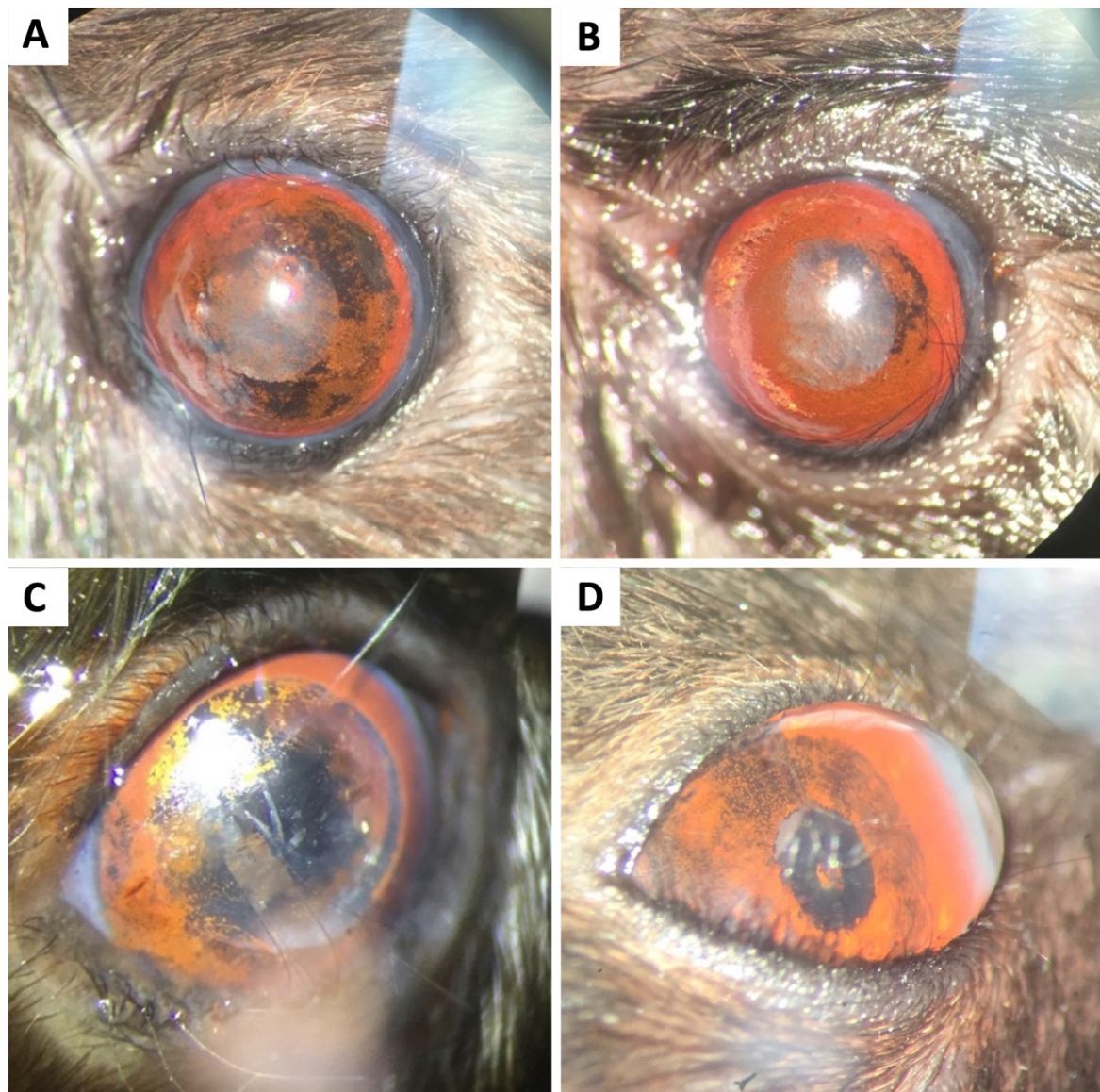


Figure 4.6: Examples of magnetic microbead injection attempts and alternative strategies attempted to improve the results. None of the examples pictured here were able to achieve a sustained rise in IOP.

(A) 1.5 μ L of prepared beads injected into the anterior chamber and distributed using an external magnet to produce a 360° ring in beads in the iridocorneal angle. (B) Increased volume of beads injecting to cause a much thicker ring of beads. (C) air bubble injected to direct beads into the iridocorneal angle, and to act as a tamponade in the days immediately post-operative to keep the beads in place. (D) A droplet of anaesthetic on the surface acted as a form of gonio lens, allowing direct visualisation of the iridocorneal angle. A full examination confirmed good positioning of the beads.

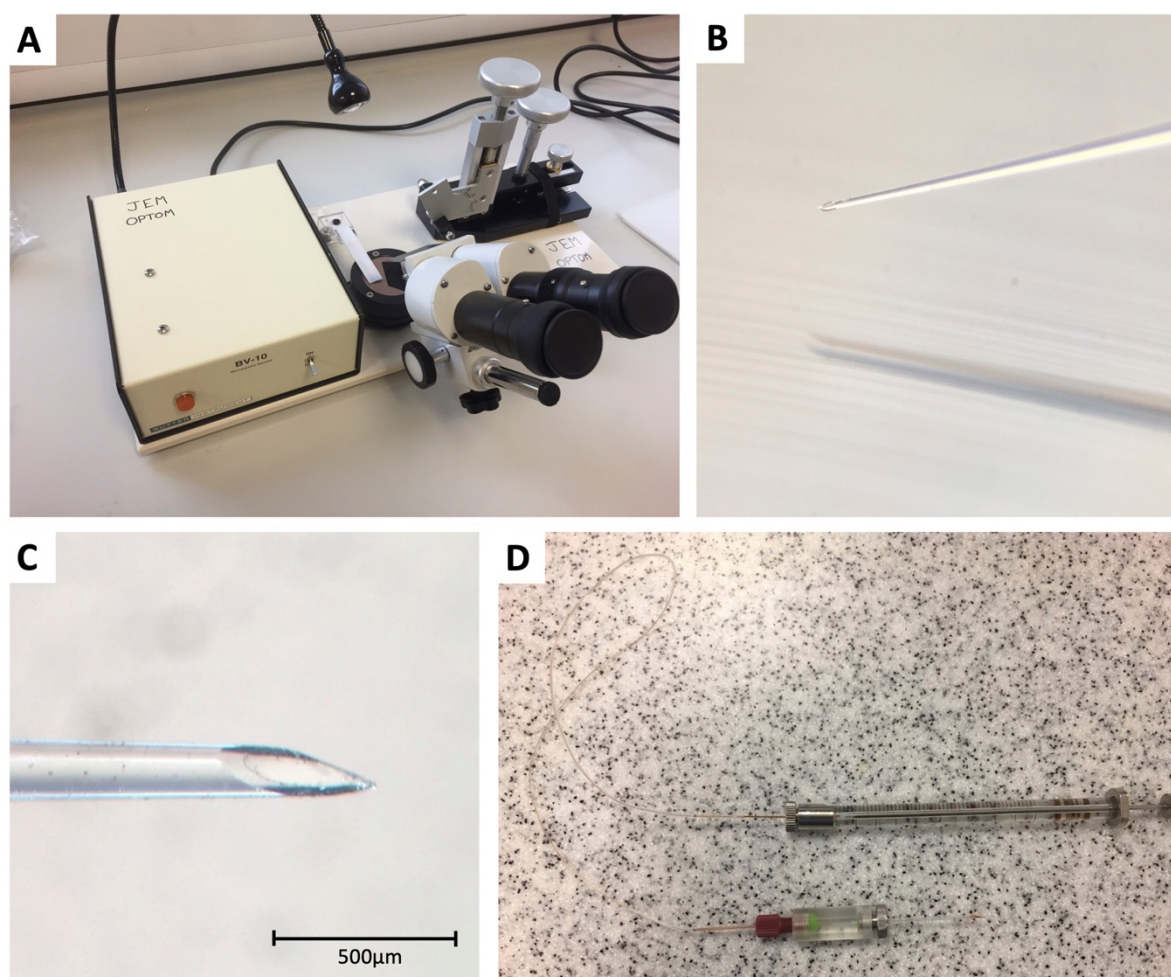


Figure 4.7: Preparation of glass needles and injection equipment

(A) WPI Micropipette beveler. (B) Pulled glass capillary tube bevelled under direct visualisation. (C) Tri-bevelled shape and quality of needle tip confirmed by examination under microscope. (D) Prepared glass needle attached to 100µL Hamilton syringe via WPI glass pipette holder.

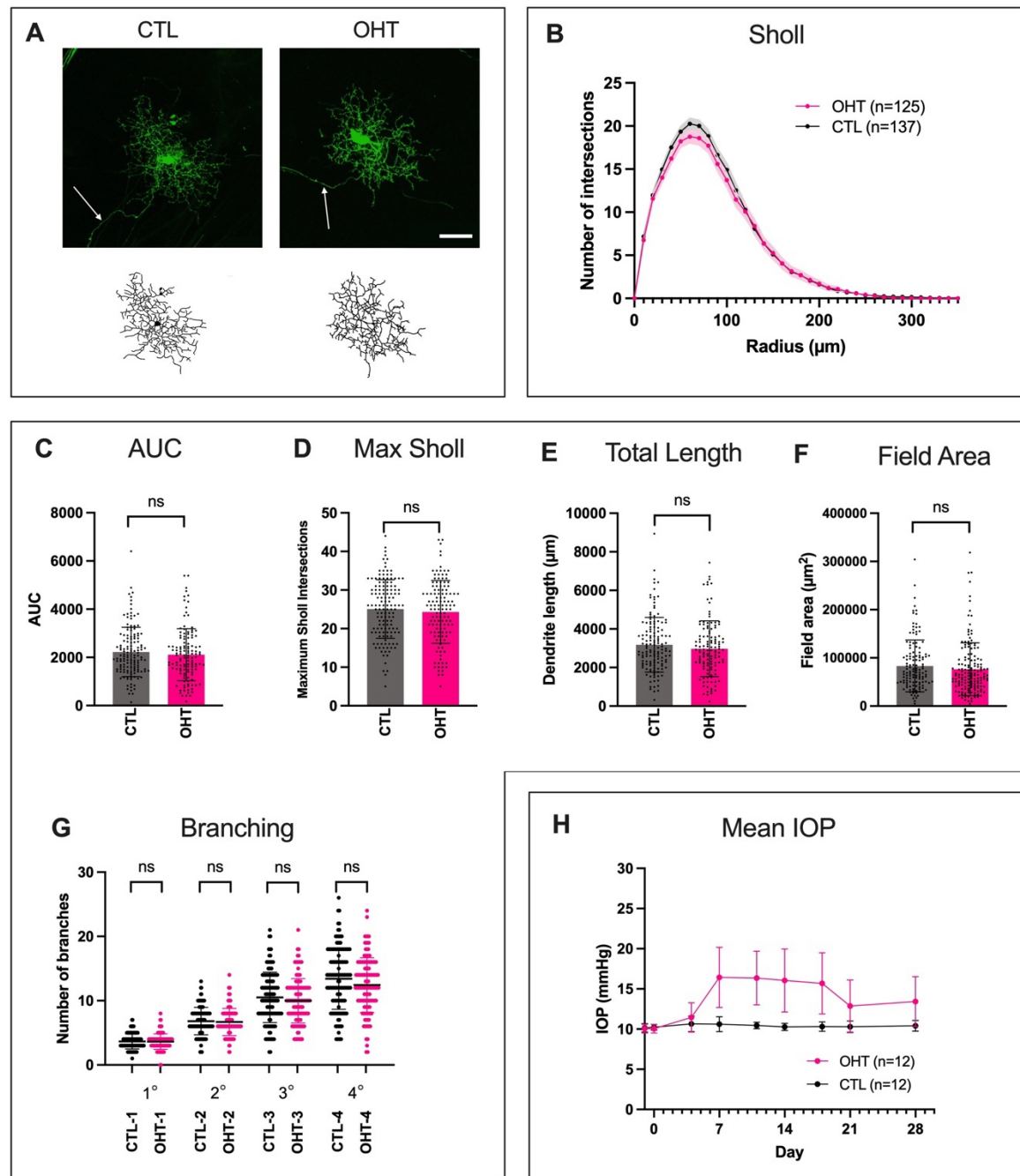


Figure 4.8: Collated Sholl analysis of mice achieving IOP ≥ 16 mmHg across different microbead trials. No difference was seen between Ocular hypertension eyes (OHT) and fellow eye controls (CTL). (A) Representative examples RGCs and dendrite reconstructions from experiment groups, fellow eye control (CTL) and optic nerve crush eye (OHT). White arrow indicates RGC axon, scale bar = 50 μ m. **(B)** Sholl analysis showing mean at each interval (line) \pm SEM, CTL (black) and OHT eye (pink). Two-tailed Mann-Whitney U test at each interval distance, * = $P < 0.05$ (no points were significant), n=number of RGCs. **(C)** Area under the Sholl curve. **(D)** Maximum number of Sholl intersections. **(E)** Total dendrite length (μ m). **(F)** Dendrite field area (μ m²). **(G)** Number of dendrites at each branching level. For Column Scatterplots E-J data points represent individual cells, columns represent means for group and error bars correspond to SD, * = $p < 0.05$, ** = $p < 0.01$, *** = $p < 0.001$. **(H)** Mean IOP against time, error bars show SD. Microbead injection performed at day 0.

4.4.4. Discussion

The somewhat erratic nature of the results, the lack of sustained IOP rise and the absence of changes in the Sholl curves prompted the need for a re-evaluation of the microbead model on these mice. Other glaucoma models such as episcleral vein cauterization and laser to the trabecular meshwork have indicated that it is possible for the mouse eye to maintain an elevated IOP, and this has also been reported by Ito et al., (2016) using magnetic microbeads. There are several reasons for why the IOP may have been so inconsistent during the attempts summarised here. Firstly, the beads may have been incorrectly positioned leading to insufficient occlusion of the trabecular meshwork. After adjusting the position of the beads with the external magnet, a full 360° ring of beads in the AC was achieved in the majority of procedures. However, only a small amount of open trabecular meshwork is needed for the IOP to normalise, and if some of the beads dislodged shortly after the procedure then the pressure will not be able to be sustained. Finer control of the injection would be preferable as this would allow small quantities of beads to be injected and positioned in a stepwise approach. Ideally this would be performed using a microinjector pump, but this was unfortunately not available. Secondly, there may have been some leakage from the corneal wound. This would essentially have created a valve that allowed aqueous humour to leak out if the pressure rises. This was certainly apparent in some of the early trials using the larger needles, but the change to the glass needles was intended to address this issue. Furthermore, IOP measurement was avoided on day 1 to allow the cornea to heal. Even with these additional measures, the IOP rise was still extremely inconsistent, and a leak from the wound is probably not the main cause of the failure of the model.

With the aid of a second person during the procedure, a microinjector pump, and potentially time spent with another group to learn the procedure in more depth, the model may be achievable. However, as alluded to above, the C57BL/6 mouse has been noted to be surprisingly resistant to glaucomatous damage in hypertensive models. Even when Ito et al., (2016) achieved elevated IOPs of approximately 20mmHg from weeks 1-6, they reported that the C57BL/6 was more resistant to change than other strains and unfortunately, the B Cre+ mouse has been developed on the background of C57BL/6. Considering the previous published reports as well as the dendrite data presented here, the model may not be able to reliably and consistently produce the significant changes in RGC dendrites needed to act as a useful disease model. If the WT mice do not show a large enough reduction in dendrite complexity, then it would not be possible to determine any protective effect from BDNF. From a 3Rs perspective, the numbers of mice that would need to be sacrificed in order to develop

this technique is also extremely difficult to defend when an optimised procedure appears to be unlikely to produce the required disease features.

Discussions with other researchers have revealed anecdotal reports of similar difficulties. Attempts to use C57BL/6 mice that were abandoned due to lack of damage induced by the hypertensive models, resulting in changes to other strains or alternative methods. However, there is conflicting data with other published studies reporting more success (Sappington et al., 2010; Frankfort et al., 2013; Mukai et al., 2019). The dendrite data presented here contributes to the debates and growing impression that C57BL/6 strains are not suitable for glaucoma studies. The data are informative for the wider research community regarding the use of this strain for the development of experimental glaucoma and suggest a reappraisal for work with this model in the context of glaucoma.

It is unclear why the C57BL/6 mouse may be resistant to changes in hypertensive models. It is notable that this trait appears to have a stronger protective effect than many of the novel medications and treatments that the model is intended to investigate. Pigmented melanopsin cells are more resilient (Li et al., 2006), and the pigmented nature of the C57BL/6 may have some contribution to this, but there appears to be a more profound difference in this strain beyond this simple explanation. This in itself is a fascinating question and a topic worthy of a thorough and detailed investigation. Unfortunately, this lies outside the scope of this project.

4.5. Summary

Both the retinal explant and the ONC models showed a significant reduction in dendrite complexity in the WT C57BL/6 mice and are suitable to be used in the evaluation of the B Cre+ model. The magnetic microbead model failed to produce consistent IOP increases and changes in dendrite complexity and was therefore excluded. However, even without the magnetic microbead model, the combination of the *ex vivo* retinal explant and *in vivo* ONC can provide a firm platform in which to explore the effects of platelet BDNF on RGCs.

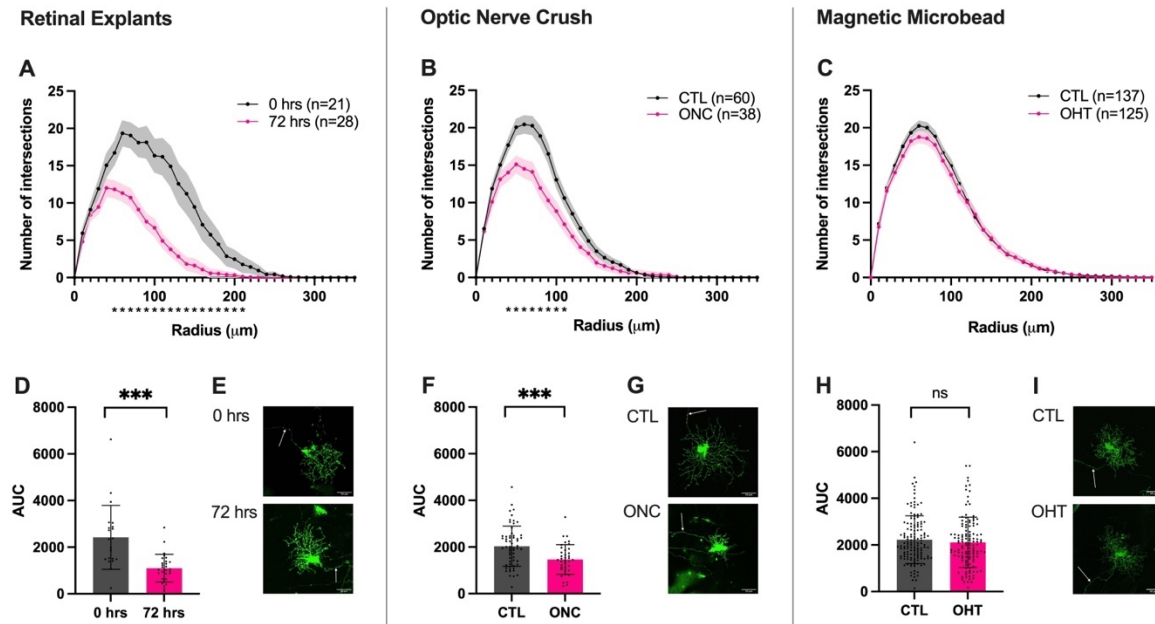


Figure 4.9: Summary of Sholl analysis results from WT mouse RGCs for each of the three experimental models.

Sholl plots for **(A)** retinal explants, **(B)** optic nerve crush and **(C)** magnetic microbead models showing mean at each interval (line \pm SEM). Two-tailed Mann-Whitney U test at each interval distance, * = $P < 0.05$, n=number of RGCs. Area under curve scatter column graphs and example RGC images for retinal explants **(D, E)**, optic nerve crush **(F, G)** and magnetic microbead models **(H, I)**. For Column Scatterplots data points represent individual cells, columns represent means for group and error bars correspond to SD, * = $p < 0.05$, ** = $p < 0.01$, *** = $p < 0.001$.

Chapter 5. Investigating the Effect of Platelet BDNF on Retinal Ganglion Cells Using a Retinal Explant Model

5.1. Short Introduction

The aim for the experiments described in this chapter was to determine if a neuroprotective effect could be observed and quantified in retinas from B Cre⁺ animals, and if so, how it would compare with the effects of direct supplementation of media with *E. coli* recombinant BDNF (100ng/mL, Regeneron/Amgen partners) or the TrkB activator ZEB85 (50µg/mL, Zebra Biologics), both used at saturating concentrations. The dendrite complexity was used as the primary outcome, as assessed using DiOlistics labelling and Sholl analysis. The DiOlistics work was supplemented with experiments monitoring global RGC numbers by performing cell counts using RBPMS (RNA-binding protein with multiple splicing) staining on retinal flat mounts.

5.2. Experimental setup

The methodology of the explant experiment followed the structure used in Binley et al., 2016 and Merkouris et al., 2018 and is described in detail in Chapter 4.3. Briefly, mice were culled by cervical dislocation and the eyes immediately enucleated. The retinas were then dissected out from the eyes and laid out flat on a culture insert with the RGC layer face-up. Retinas were then labelled using either DiOlistics or immunostaining as required at 0 hours, or after 72 hours in culture with media changed after 48 hours. All experiments used a combination of male and female mice, with left and right eyes from individual animals separated across the different experimental groups.

5.3. Results

5.3.1. Analysis of RGC Dendrite Morphology – Comparison of Genotypes

An initial experiment sought to determine if there was an effect on the dendrite complexity of the B Cre⁺ mouse RGCs compared to WT Cre⁻ controls, and if so, to determine if there was

a difference between homozygous (B^{+/+} Cre⁺) and heterozygous (B^{+/-} Cre⁺) genotypes. 4 mice were included for each of the homozygous, heterozygous and Cre-negative wild types (WT), both sexes, age 4-5 months. For each animal, one retina was labelled at 0 hours and the other labelled after 72 hours *ex vivo* in culture.

Sholl analysis demonstrated significant preservation of dendritic complexity in both B^{+/+} Cre⁺ and B^{+/-} Cre⁺ genotypes after 72 hours in culture (Figure 5.2, Figure 5.3) with a higher Sholl curve compared to the lower, left-shifted peak of the WT Cre⁻ controls. The Sholl AUC was significantly larger in both B^{+/+} Cre⁺ ($p=0.0043$) and B^{+/-} Cre⁺ ($p=0.0048$) groups compared to WT Cre⁻ (Mean AUC $1775\pm597.1\mu\text{m}^2$, $1808\pm824.0\mu\text{m}^2$ and $1378\pm770.5\mu\text{m}^2$ respectively), with no significant difference in baseline at 0 hours. A similar pattern was also seen with decreases in the sub-analysis of maximum Sholl intersections, total dendrite length, and dendrite field area. Furthermore, these differences were manifested with a preservation in the more peripheral quaternary dendrite branches, without significant differences from WT Cre⁻ in those more proximal to the cell soma.

No significant difference was seen between B^{+/+} Cre⁺ and B^{+/-} Cre⁺ genotypes in the Sholl analysis, AUC or any of the additional sub-analyses. This similarity between the genotypes is notable when considering the serum BDNF concentration is lower in the B^{+/-} Cre⁺ mice. However, the concentration in B^{+/-} Cre⁺ mice is still several thousand times greater than the levels found in WT mice. It is possible that with such a dramatic increase from baseline, there is a threshold where a maximum effect is reached, and the additional difference in BDNF concentration between the B^{+/+} Cre⁺ and B^{+/-} Cre⁺ genotypes beyond this does not confer any further change. Based on these findings, it was considered reasonable to use B^{+/+} Cre⁺ and B^{+/-} Cre⁺ mice together as a single group in subsequent experiments (collectively referred to as B Cre⁺ mice).

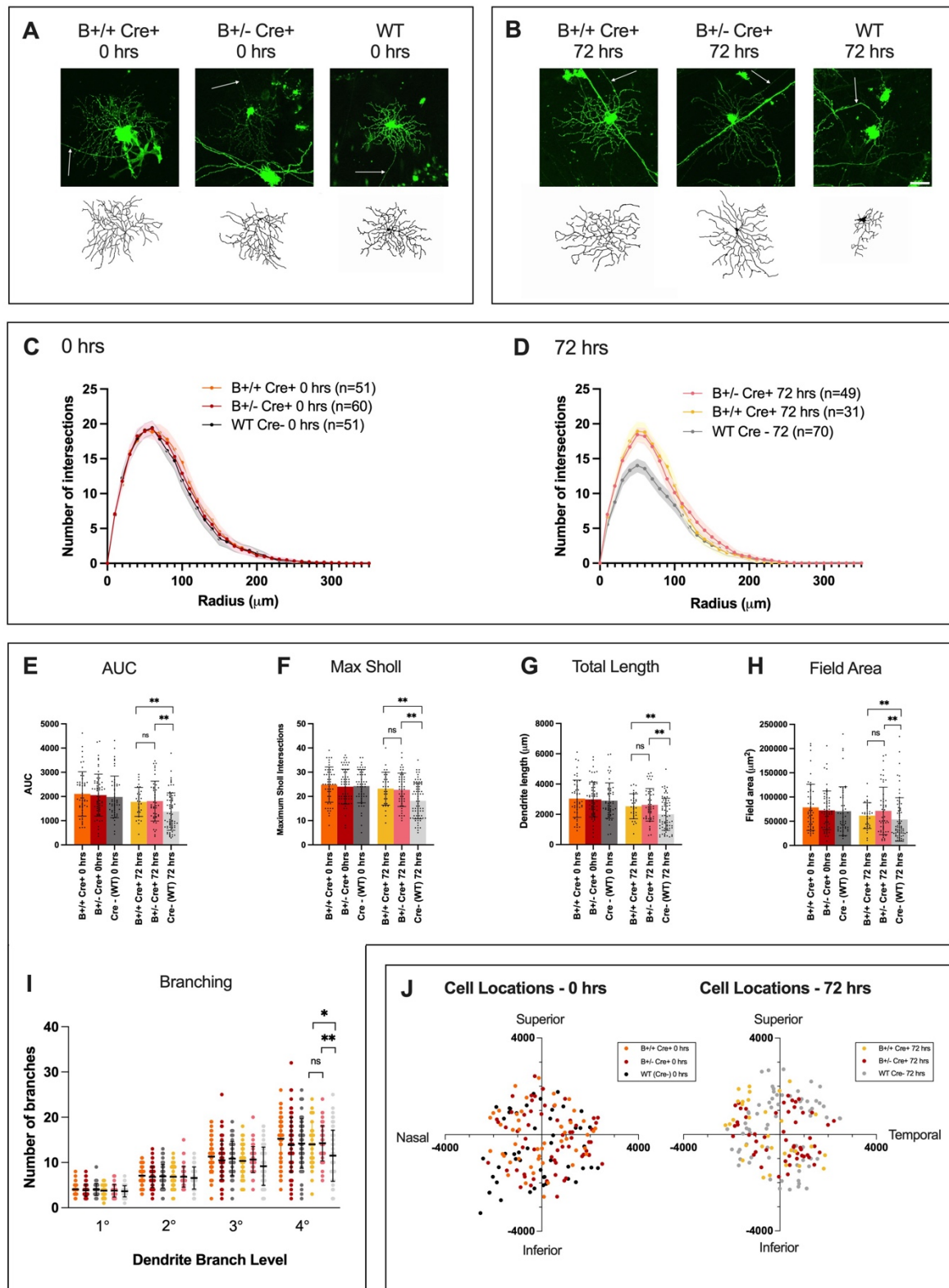


Figure 5.1: Preservation of RGC dendrite complexity in B Cre+ mouse retinas was seen in both homozygous and heterozygous genotypes. Analysis by time point

Representative examples RGCs from experiment groups and dendrite reconstructions at **(A)** 0 hrs and **(B)** 72 hrs. White arrow indicates RGC axon, scale bar = 50μm. **(C-D)** Sholl analysis

showing mean at each interval (line) \pm SEM. B+/+ Cre+ (orange), B+/- Cre+ (red) and WT (grey) are shown on separate plots showing results at 0 hrs and 72 hrs. Two-tailed Mann-Whitney U test at each interval distance, * = $P < 0.05$, n=number of RGCs. **(E)** Area under the Sholl curve. **(F)** Maximum number of Sholl, **(G)** Total length of all dendrites (μm). **(H)** Dendrite field area (μm^2). **(I)** Number of dendrites at each branching level. **(J)** Retina locations of RGCs included in analysis in μm relative to the optic nerve head. For Column Scatterplots F-I data points represent individual cells, columns represent means for group and error bars correspond to SD, * = $p < 0.05$, ** = $p < 0.01$, *** = $p < 0.001$.

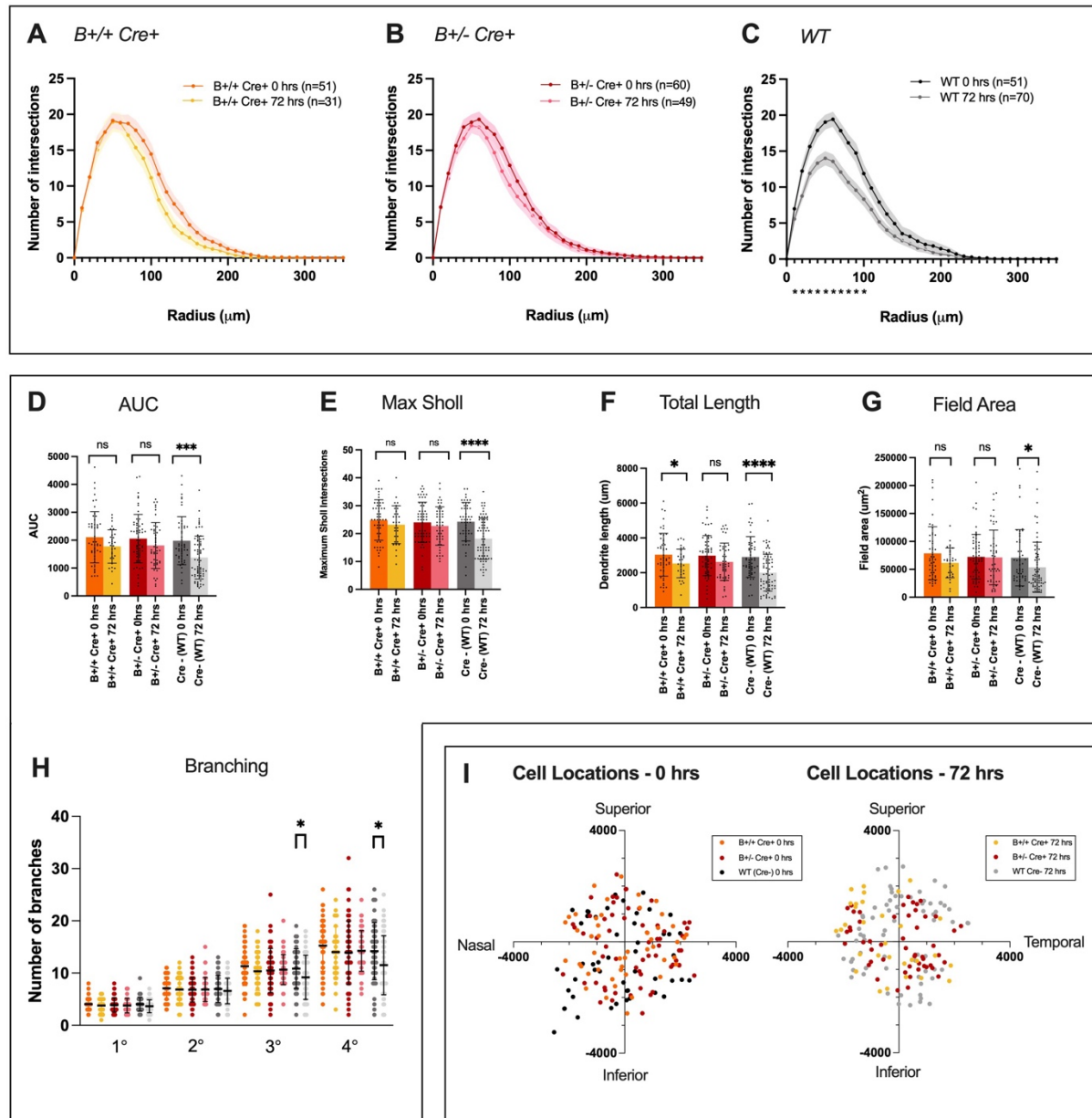


Figure 5.2: Preservation of RGC dendrite complexity in B Cre+ mouse retinas was seen in both homozygous and heterozygous genotypes. Analysis by genotype.

(A-C) Sholl analysis showing mean at each interval (line) \pm SEM. B+/+ Cre+ (orange), B+/- Cre+ (red) and WT (grey) are shown on separate plots showing results at 0 hrs and 72 hrs. Two-tailed Mann-Whitney U test at each interval distance, * = $P < 0.05$, n=number of RGCs. **(D)** Area under the Sholl curve. **(E)** Maximum number of Sholl, **(F)** Total length of all dendrites (μm). **(G)** Dendrite field area (μm^2). **(H)** Number of dendrites at each branching level. **(I)** Retina locations of RGCs included in analysis in μm relative to the optic nerve head. For Column

Scatterplots F-I data points represent individual cells, columns represent means for group and error bars correspond to SD, * = $p < 0.05$, ** = $p < 0.01$, *** = $p < 0.001$.

5.3.2. Analysis of RGC Dendrite Morphology – Comparison with media supplementation

In order to expand upon these findings, further retinal explant experiments were performed now including the additional experimental groups with media supplemented with *E. coli* recombinant BDNF (100ng/mL) and the TrkB agonist ZEB85 (50µg/mL) as repeats of the Merkouris et al., 2018 studies. All other aspects of the protocol remained consistent, allowing data from all trials to be combined for a cumulative analysis. In order to have sufficient cells for the most accurate Sholl analysis, the final results were obtained by pooling data from three experimental runs. These runs included the initial experiment comparing the different genotype groups, and two subsequent experiments that each used the following groups:

0 hrs

- WT retina
- B Cre⁺ mouse retinas

72 hrs

- WT retina, standard media (CTL)
- B Cre⁺ retina, standard media
- WT retina, BDNF (100ng/mL) supplemented media
- WT retina, ZEB85 (50µg/mL) supplemented media

All experiments used a combination of male and female mice, with left and right eyes from individual animals separated across the different experimental groups. The final data included results from 28 B Cre⁺ retinas (12 at 0 hours and 16 at 72 hours) and 36 WT retinas (8 at 0 hours, 12 at 72 hours in control media, 8 at 72 hours in BDNF 100ng/mL media and 8 at 72 hours in ZEB85 50µg/mL media), both sexes, aged 2-5 months.

RGCs from explants supplemented with BDNF (100ng/mL) and ZEB85 (50µg/mL) both showed preservation of the complexity of the dendritic field compared to the WT retinas in standard media, replicating the results of Merkouris et al., 2018. The retinas of B Cre⁺ mice in standard media also continued to show preservation of the dendrites throughout the

experiments. Furthermore, this preservation was not significantly different from the BDNF and ZEB85 media (Figure 5.3). Sholl AUC was measured as $1733 \pm 833.0 \mu\text{m}^2$, $1763 \pm 909.0 \mu\text{m}^2$, $1776 \pm 924.9 \mu\text{m}^2$ and $1451 \pm 809.3 \mu\text{m}^2$, representing a decrease from baseline of 14.2% ($p=0.006$), 14.8% ($p=0.014$) and 16.2% ($p<0.0001$) in the BDNF media, ZEB85 media and B Cre+ groups respectively, compared to 31.6% in the WT control group. The other morphological parameters including maximum Sholl intersections and total dendrite length showed a similar configuration to the AUC, however, the majority of these results did not reach significance.

To avoid potential errors from pseudoreplication, the data were further analysed using mean values for each retina, rather than individual RGCs. Weighted means and standard deviations were then calculated for each group, weighted according to the number of RGCs per retina, and statistical significance determined by a weighted two-sample t test (Bland and Kerry, 1998). Analysis by retina continued to show a significant preservation of the Sholl curve and AUC in all treatment groups. After 72 hours in culture, the weighted mean Sholl AUCs were $1811 \pm 258 \mu\text{m}^2$, $1776 \pm 435 \mu\text{m}^2$, $1763 \pm 256 \mu\text{m}^2$ and $1406 \pm 315 \mu\text{m}^2$, representing a decrease from baseline of 14.3% ($p=0.0011$), 14.0% ($p=0.0403$) and 14.6% ($p=0.0211$) in the B Cre+, BDNF media and ZEB85 media groups respectively, compared to 31.9% in the WT control group. The other morphological parameters including maximum Sholl intersections and total dendrite length showed a similar configuration to the AUC, though changes in dendrite field area did not reach significance.

To assess whether there was any variation between RGC subtypes, all cells were categorised as either ON-centre or OFF-centre based on the sublamina level within the IPL that the dendritic tree was found (ON-centre cells arborise in sublamina b, OFF-centre cells arborise in sublamina a). The analysis of these subgroups (Figure 5.4) showed that the OFF-centre RGCs had lower AUCs in multiple groups but the difference was not significant. It is important to acknowledge that the number of cells included for the analysis was relatively low, especially for the BDNF (100ng/mL) and ZEB85 (50 $\mu\text{g/mL}$) groups following the division into ON and OFF subgroups. With such low cell numbers, it is difficult to make any assertions based on the analysis of those groups.

These observations showed that RGC dendritic pruning is reduced in the retinas from B Cre+ mice in the retinal explant model. Furthermore, the effect is comparable to that seen with direct supplementation of BDNF and a TrkB agonist.

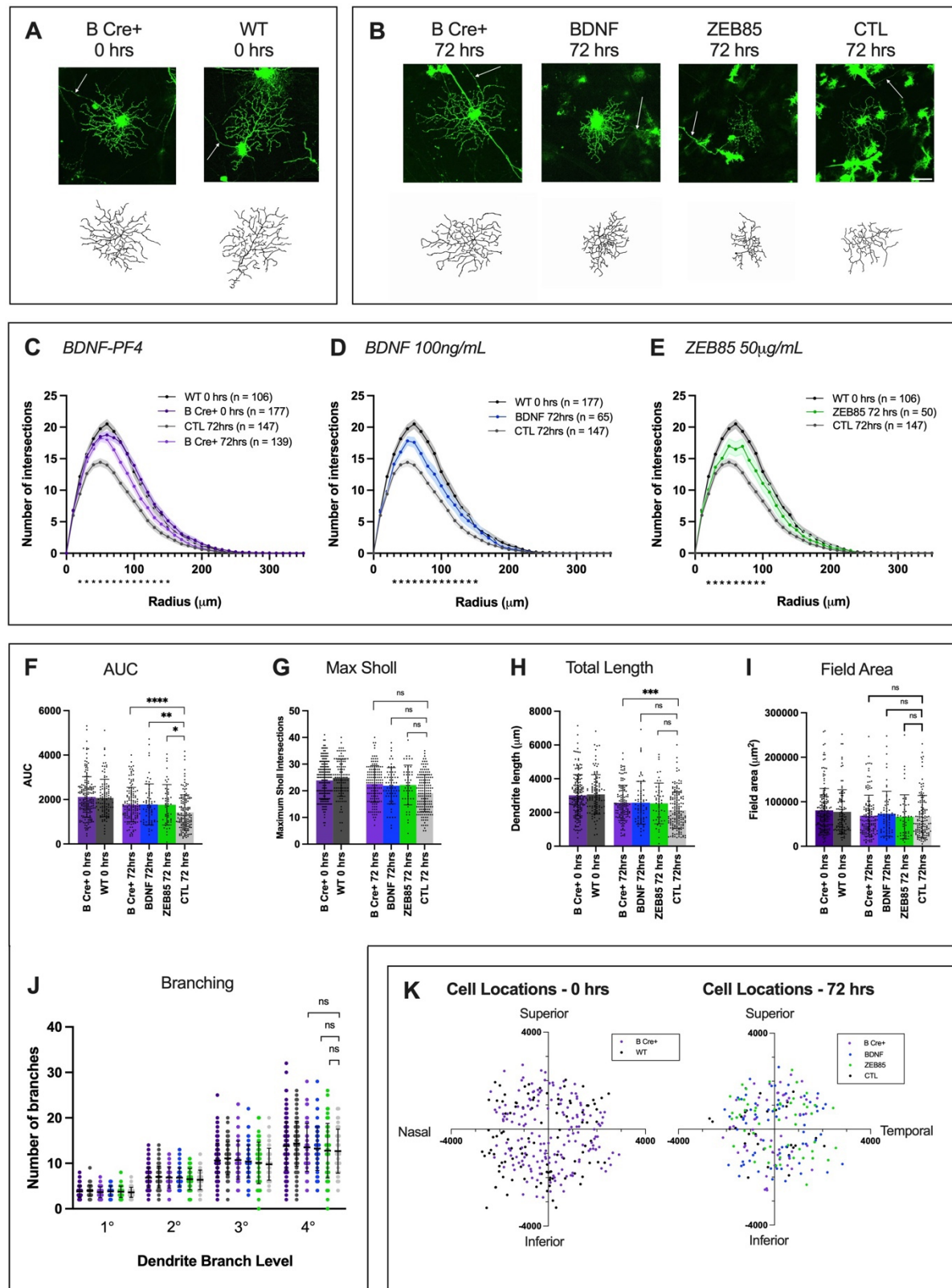


Figure 5.3: Preservation of RGC dendrite complexity in B Cre+ mouse retinas and with supplementation of BDNF and ZEB85.

Representative example RGCs and dendrite reconstructions at **(A)** 0 hrs and **(B)** 72 hrs. White arrow indicates RGC axon, scale bar = 50µm. **(C-E)** Sholl analysis showing mean at each interval (line) ± SEM. B Cre+ (purple), BDNF 100ng/mL (blue) and ZEB85 50µg/mL (green) are shown on separate curves with the WT 0 hrs and CTL 72hrs results included in all plots in

grey. Two-tailed Mann-Whitney U test at each interval distance comparing 72-hour result to CTL 72 hrs, * = $P < 0.05$, n =number of RGCs. **(F)** Area under the Sholl curve. **(G)** Maximum number of Sholl intersections. **(H)** Total length of all dendrites (μm). **(I)** Dendrite field area (μm^2). **(J)** Number of dendrites at each branching level. **(K)** Retina locations of RGCs included in analysis in μm relative to the optic nerve head. For Column Scatterplots D-H data points represent individual cells, columns represent means for group and error bars correspond to SD, * = $p < 0.05$, ** = $p < 0.01$, *** = $p < 0.001$.

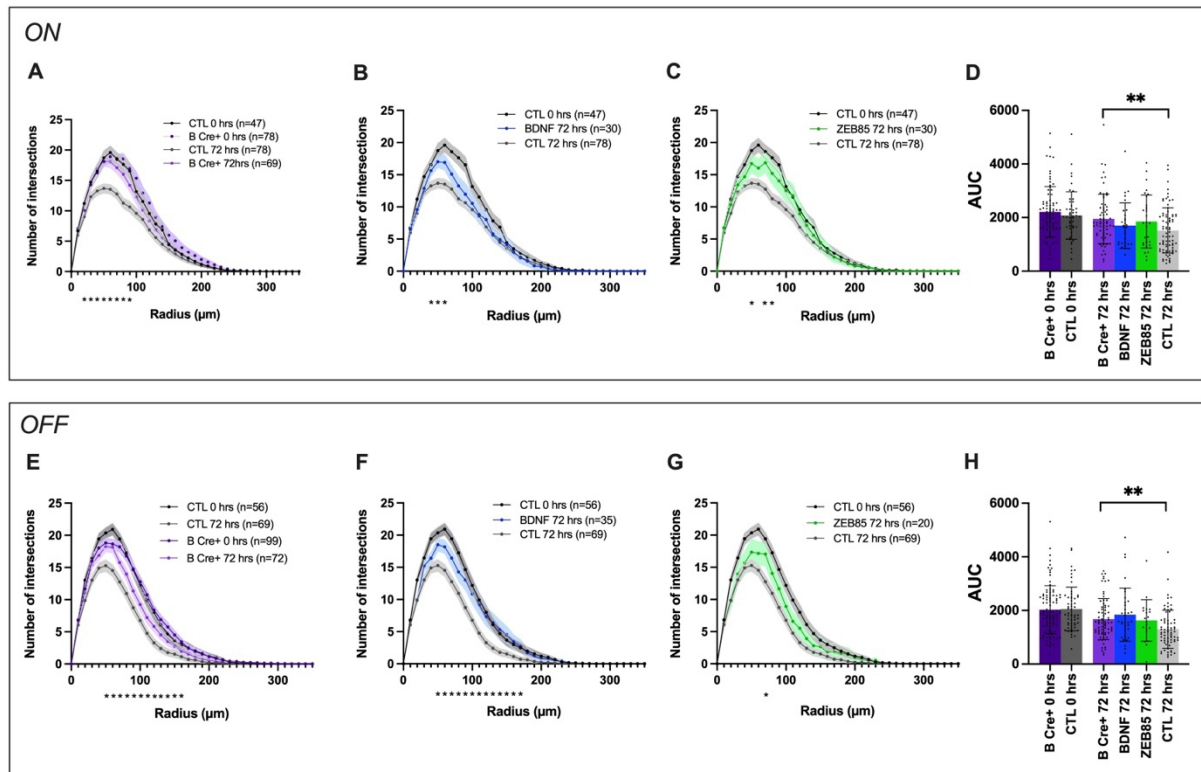


Figure 5.4: Sholl analysis of separated ON and OFF-centre RGCs

ON-centre Sholl analysis showing mean at each interval (line) \pm SEM, n =number of RGCs. **(A)** B Cre+ (purple), **(B)** BDNF 100ng/mL (blue) and **(C)** ZEB85 50 $\mu\text{g}/\text{mL}$ (green) are shown on separate curves with the WT 0 hrs and CTL 72hrs results included in all plots in grey. **(H)** Area under the Sholl for ON-centre RGCs. OFF-centre Sholl analysis showing mean at each interval (line) \pm SEM. **(E)** B Cre+ (purple), **(F)** BDNF 100ng/mL (blue) and **(G)** ZEB85 50 $\mu\text{g}/\text{mL}$ (green) are shown on separate curves with the WT 0 hrs and CTL 72hrs results included in all plots in grey. **(H)** Area under the Sholl for OFF-centre RGCs. Column scatterplots represent individual data points with columns representing mean and error bars corresponding to SD.

5.3.3. Analysis of global RGC loss by measurement of cell count

In order to investigate the impact of BDNF more widely in the retinas of these mice, the experiment was repeated with RGC cell count now used as the primary outcome instead of dendrite morphology. Flat mounted retinas were labelled for RBPMS and then imaged using

confocal microscopy. RBPMS positive cells were then counted manually on sample images. The method for immunolabelling and cell counting is described in detail in Chapter 2.

Retinal explants were prepared with 6 retinas in each of the experimental groups (B Cre+ 0 hrs, WT 0 hrs, B Cre+ 72 hrs, BDNF (100ng/mL) 72hrs, ZEB85 (50µg/mL) 72hrs and CTL media 72hrs), both sexes age 2-6 months. All steps were completed with retinas in individual wells of a 24 well plate on a rocker using anti-RBPMS rabbit, Novus NBP2-20112 as a primary antibody (1:1000 dilution, overnight, room temperature) and Goat anti-Rabbit, Alexa Fluor Plus 594, Thermo Fisher R37117 (1:500, 3 hours, room temperature) as a secondary antibody.

There were no significant differences seen in the cell count between any of the 4 groups at the 72-hour time point (Figure 5.5). All groups showed a reduction of approximately 15% at 72 hours with B Cre+, BDNF (100ng/mL), ZEB85 (50ug/mL) and CTL showing cell counts of 2811 ± 91.33 , 2836 ± 229.9 , 2723 ± 167.7 and 2888 ± 186.0 cells/mm² respectively ($p < 0.01$ in all groups). No treatment group was able to reduce the loss of RGCs in the explant model.

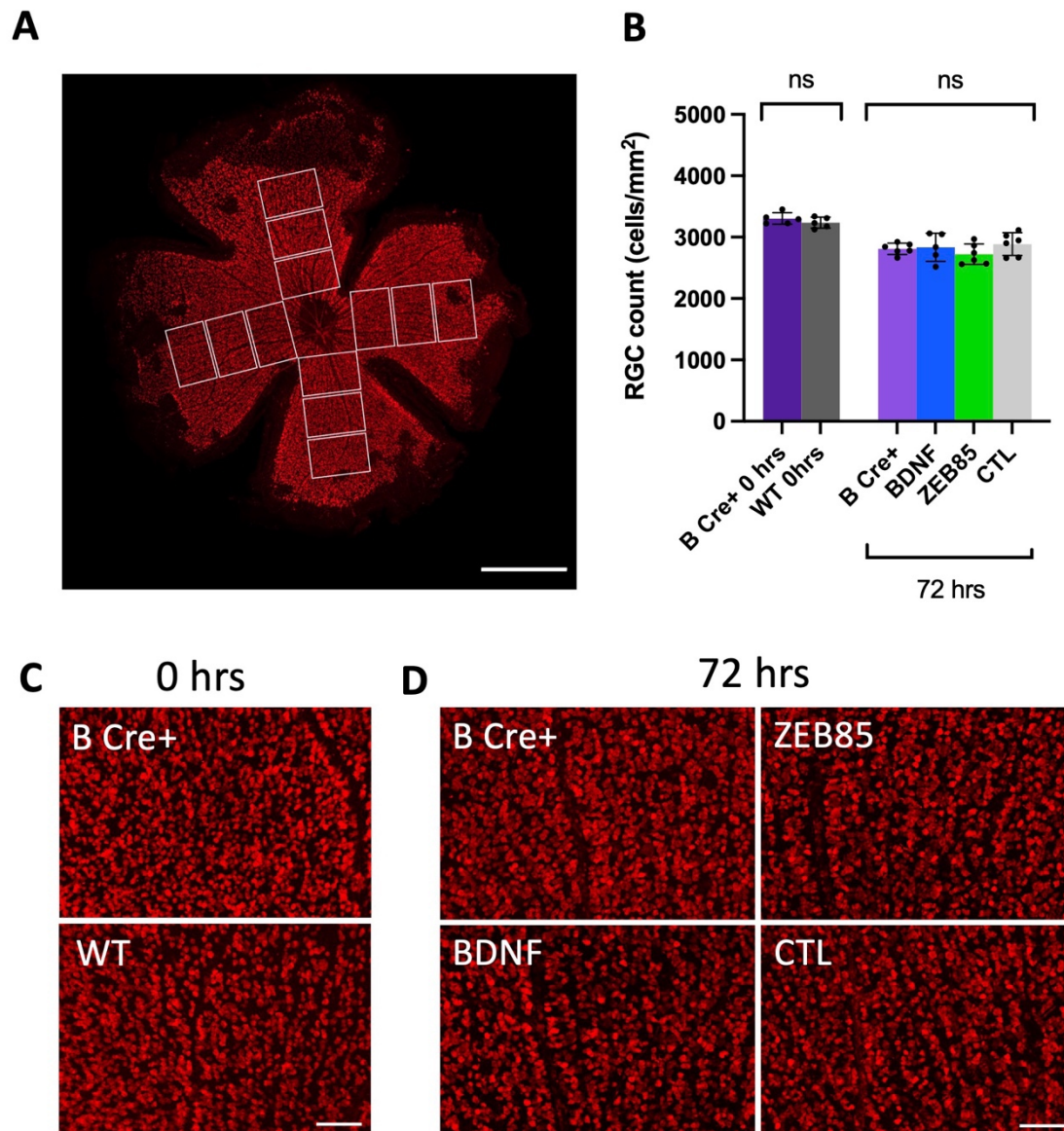


Figure 5.5: RGC cell loss in retinas explanted from B Cre⁺ mice compared with wild type retinas cultures in either control media, or supplemented with BDNF or ZEB85.

Dissected retinas were flat mounted with 4 petals and labelled for RBPMS positive cells. For each petal, 3 x 0.33mm² areas were imaged at 500µm, 1000µm and 1500µm from the optic nerve head. RBPMS cells were counted manually and an average count/mm² for each retina used for analysis. **(A)** Example retina flat mount with location of sample images used for cell counting, scale bar = 1000µm. **(B)** Column scatter plot of RGC count (cells/mm²). Points represent average count for individual retinas, columns represent means for group and error bars correspond to SD, * = $p < 0.05$, ** = $p < 0.01$, *** = $p < 0.001$. **(C)** Example images used for RGC count at 0 hours. **(D)** Example images used for RGC count at 72 hours. Scale bar = 100µm.

5.4. Discussion

The main conclusion of this chapter is that RGC dendritic pruning is reduced in the retinas from B Cre⁺ mice in the retinal explant model. Furthermore, the effect is comparable to that seen with direct media supplementation of BDNF and a TrkB agonist. This suggests that BDNF derived from platelets has been able to successfully reach the RGCs. While many other active factors may be released from platelets, the rationale for ascribing the results to BDNF is that these other factors would also be present in the platelets of WT mice. However, the BDNF pathway, activated by either platelet-derived BDNF, exogenous BDNF or ZEB85, was not found to prevent cell death.

At first, the cell count result may seem at odds to the multiple studies that have shown an improvement in cell survival with BDNF delivery in the past (Mey and Thanos, 1993a; Di Polo et al., 1998; Chen and Weber, 2001). However, there are important differences in study design that may help to explain these results. In the retinal explant model, RGC loss only becomes apparent after approximately 3 days (Binley et al., 2016; Johnson et al., 2016). Investigations of BDNF in retinal explant models in the past only showed a significant difference in cell count after 7 days, with no difference after 4 days *ex vivo* (Bull et al., 2011). In that study, it was noted that the neuroprotective effects of BDNF based on cell count were “modest” in the retinal explant model. In the experiment described in this chapter, the loss of approximately 15% of RGCs suggests that the process of cell loss is in its very early stages. Therefore, while 3 days is an appropriate duration for assessing dendrite morphology, it is too early to reliably differentiate between the groups based on cell count at this stage. It does, however, highlight a strength of the DiOlistics approach in that it is possible to detect the subtle signs of degeneration, and the benefits of neuroprotective agents, at an early stage before cell death.

The similarity of the Sholl curves from the B Cre⁺, BDNF and ZEB85 groups is striking. The BDNF and ZEB85 results were expected based on previously reported data in Merkouris et al., 2018 but the comparable effect seen in the B Cre⁺ mouse is unexpected. Prior to this work it was unclear as to whether the BDNF contained within the platelets would be able to reach the RGCs and whether the response to the acute degeneration caused by the retinal explant model would have been affected by the chronic BDNF exposure. This result has confirmed that not only can BDNF affect the RGCs in this model, but that the resulting neuroprotective effect is sizeable and apparently the maximum that can be achieved by TrkB activation. The immunolabelling of TrkB in the retina presented in Chapter 3 confirmed that there had not been extensive downregulation of TrkB in the retinas of the B Cre⁺ mouse but the functional

outcomes were still uncertain. If there had been a reduction in TrkB, this pathway and its subsequent neuroprotective effects may have been unavailable.

The preservation of the dendrite complexity is strong evidence that BDNF contained in platelets exerted a neuroprotective effect on the RGCs. When the retinas were explanted, the blood remaining in the retinal vessels would coagulate, leading to platelet activation and BDNF release. This is very different from the continuous flow of non-clotted blood through the retina under physiological conditions *in vivo*. When the retina was dissected, the main blood vessels supplying the retina were cut along with the optic nerve thus creating an opening for serum to leak from the cut end of the larger central vessels into the culture media during the experiment. Based on work mapping the vasculature of the retina (Kim et al., 2018) and the serum BDNF ELISA results from Chapter 3, a rough estimate can be made of the BDNF contained within the explant. Accounting for some loss of tissue during the dissection process, the volume of blood within a retinal explant can be estimated at approximately 2 μ L. Assuming that serum accounts for 55% of this volume, a homozygous B Cre⁺ mouse retina would be expected to contain approximately 28.3pg of BDNF within 1.1 μ L of mouse serum. Should this BDNF be able to diffuse evenly through the 1.5mL of culture media, this would correspond to a final concentration of 18.9pg/mL, unlikely that to be sufficient to activate TrkB. Instead, it would appear more likely that the BDNF concentration would be higher closer to the site of platelet activation. It may be possible to measure BDNF in the culture media using the Fujifilm ELISA kit, and this could be included in future work to clarify the media concentration of BDNF and how this may change over the 72 hours.

An additional approach is needed to provide further evidence of the neuroprotective effect seen in the B Cre⁺ retina. And it is here that the optic nerve crush model will be extremely valuable. As an *in vivo* model, it will be more representative of physiological blood flow, platelet activity and subsequent BDNF release.

Chapter 6. Investigating the Effect Platelet BDNF on Retinal Ganglion Cells Using an Optic Nerve Crush Model

6.1. Short Introduction

A possible *in vivo* neuroprotective effect of BDNF was then examined using optic nerve injury. In previous related work (see Introduction), BDNF was typically injected into the vitreous or else delivered using viral vectors. By contrast, in B Cre⁺ animals BDNF would be originating

from the intravascular space following lesions of the optic nerve. As with the previous chapters, the primary outcome was the assessment of RGC dendrite complexity using DiOlistic labelling and Sholl analysis. RGC numbers were also assessed by counting the number of RBPMS-positive cells.

6.2. Experimental setup

The ONC procedure was described in detail in Chapter 4. Briefly, mice were anaesthetised using isoflurane and the optic nerve was exposed using an inferior-temporal incision through the conjunctiva and Tenon's capsule. The nerve is then grasped and crushed for 5 seconds using cross-action N5 forceps, with only the pressure from the self-clamping action to crush the nerve. Following the crush injury, the retina was examined to ensure the lens remained clear and there were no signs of arterial occlusion. After 7 days, the mice were culled by cervical dislocation and the eyes immediately enucleated. Retinas were dissected and RGCs labelled by DiOlistics as described in Chapter 2. As with the retinal explant model, a repeat of the experiment was performed measuring the cell count of RBPMS positive cells to supplement the dendrite data.

6.3. Results

6.3.1. Analysis of RGC dendrite morphology 7 days following ONC

ONC procedures were performed on 8 B Cre⁺ (4 right eye, 4 left eye) mice and 7 WT mice (4 right eye, 3 left eye). An additional WT mouse was culled due to bleeding during the procedure. As with the retinal explant experiment, the RGCs from the B Cre⁺ mice showed preservation of the dendrite complexity following ONC, with a mean Sholl AUC of $2775 \pm 1371 \mu\text{m}^2$ and $2033 \pm 1179 \mu\text{m}^2$ for B Cre⁺ and WT respectively ($p = 0.0078$) (Figure 6.1). A similar trend was seen in the additional analysis however, only total dendrite length reached significance. These results indicated a similar trend as observed with retina explants (see Chapter 5). The shape of the Sholl curve was slightly more irregular in the ONC study, presumably due to the lower number of successfully labelled cells.

Once again, analysis was performed using mean values for each retina rather than individual RGCs to reduce the risks of errors from pseudoreplication. Following the ONC injury, the AUC was significantly higher in the B Cre⁺ mice compared to WT ($2667 \pm 690 \mu\text{m}^2$ and $1921 \pm 392 \mu\text{m}^2$ respectively, $p=0.0256$), with no significant difference in the contra-lateral eye controls. Total

dendrite length and dendrite field area were also significantly higher ($p=0.0325$, $p=0.0245$) but maximum Sholl intersections failed to reach significance but continued the trend of a higher mean value in the B Cre+ group ($p=0.0348$).

6.3.2. Analysis of RGC count 7 days following ONC

ONC procedures were performed on the right eye of an additional 5 B Cre+ mice and 5 WT mice, both sexes, age 2.5-4 months. As with the retinal explant experiments, retinas were labelled for RBPMS positive cells and counted manually as described in Chapter 2. Once again, no significant difference was found between the cell counts of B Cre+ and WT groups. However, in contrast to the retinal explant model, after 7 days there had been a substantial loss of RGCs. Both WT and B Cre+ groups showed a cell loss of approximately 50% (WT 45.14% loss, B Cre+ 54.28% loss, not significant) seven days after ONC. The ONC model should predictably induce RGC loss of approximately 50% at 7 days and 80% at 14 days, suggesting the model had been performed to an acceptable standard in these experiments. Closer examination of the cell count by sector (Figure 6.3) did not show any anomalous areas of extreme cell loss that may represent a branch vascular occlusion. Both ONC and fellow eye controls, showed a typical pattern with a slight tendency for lower cell counts in the periphery (Figure 6.3 E).

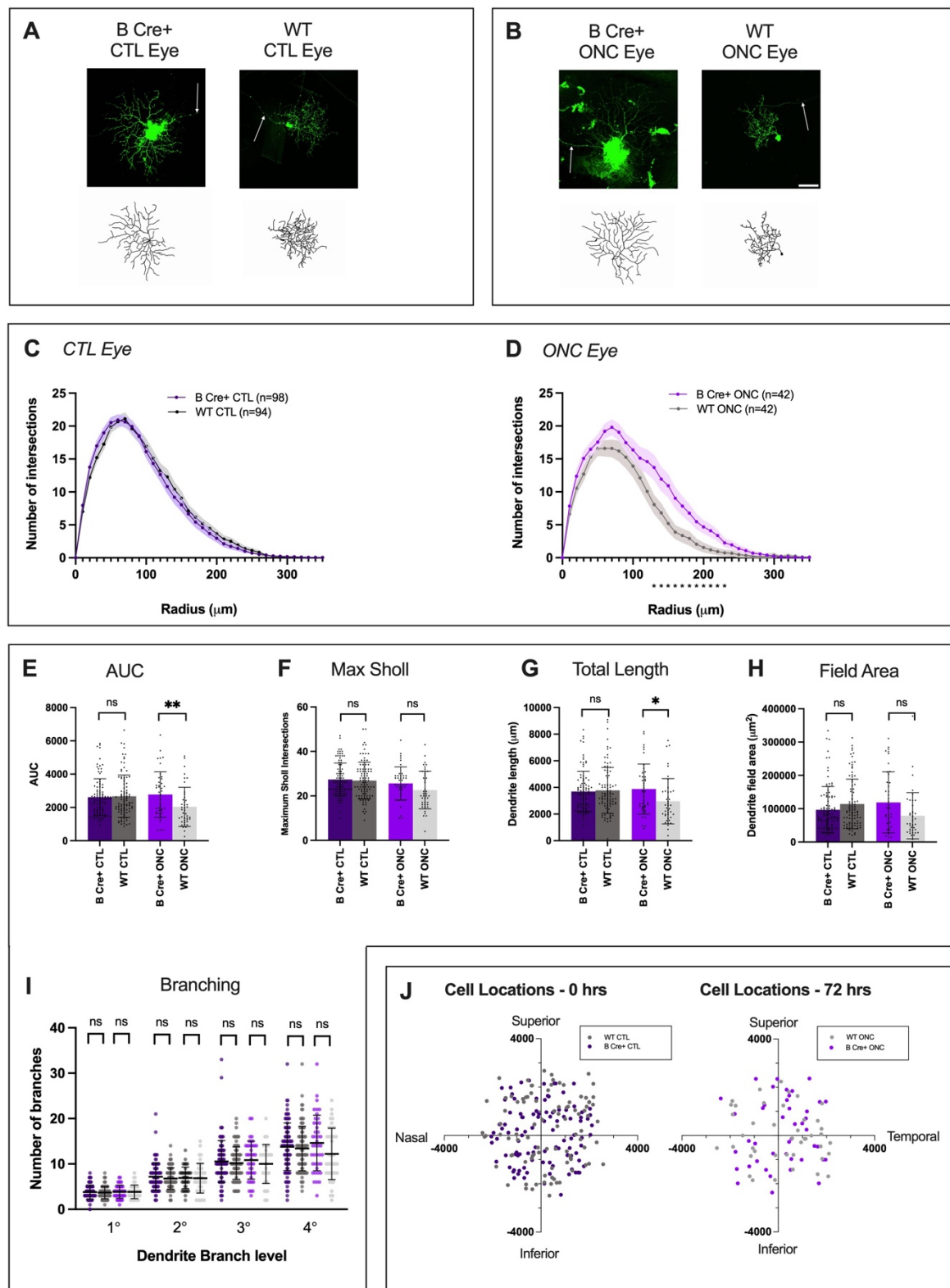


Figure 6.1: Analysis of RGCS 7 days after optic nerve crush injury.

Representative example RGCs and dendrite reconstructions at **A**) Fellow eye controls, CTL and **B**) ONC. White arrow indicates RGC axon, scale bar = 50μm. **(C, D)** Sholl analysis showing mean at each interval (line) ± SEM. B Cre+ (purple) and WT (grey). Two-tailed Mann-Whitney U test at each interval distance comparing 72-hour result to CTL 72 hrs, * = P < 0.05, n=number of RGCs. **(E)** Area under the Sholl curve. **(F)** Maximum number of Sholl intersections. **(G)** Total length of all dendrites. **(H)** Dendrite field area (μm²). **(I)** Number of

dendrites at each branching level. **(J)** Retina locations of RGCs included in analysis in μm relative to the optic nerve head. For Column Scatterplots E-H data points represent individual cells, columns represent means for group and error bars correspond to SD, * = $p < 0.05$, ** = $p < 0.01$, *** = $p < 0.001$.

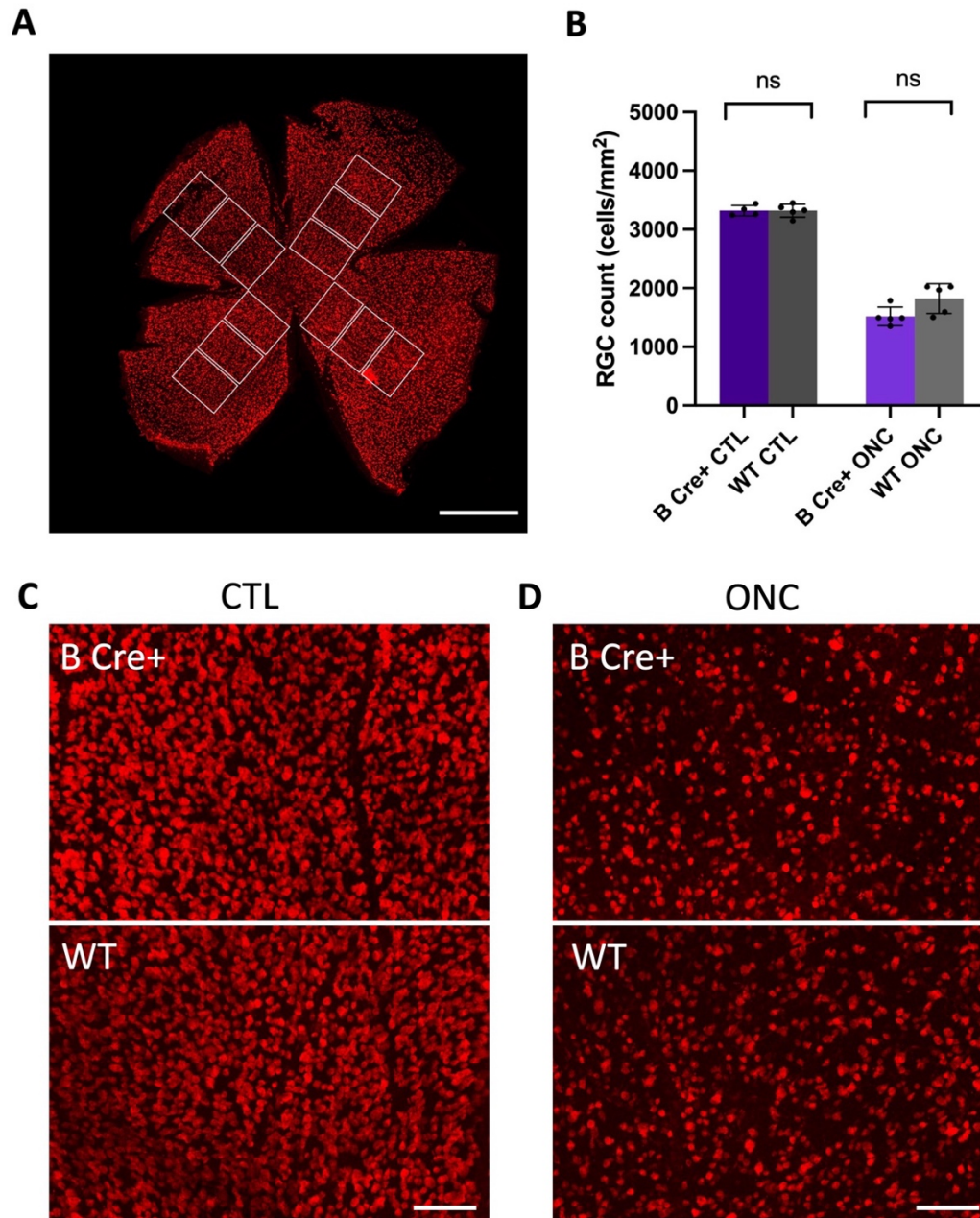


Figure 6.2: Cell count of RBPMS+ cells was reduced in B Cre+ and WT retinas after ONC. **(A)** Example retina flat mount with location of sample images used for cell counting, scale bar = 1000 μm . **(B)** Column scatter plot of RGC count (cells/mm²). Points represent average count for individual retinas, columns represent means for group and error bars correspond to SD, * = $p < 0.05$, ** = $p < 0.01$, *** = $p < 0.001$. **(C)** Example image of B Cre+

contralateral eye control, **(D)** Example image of B Cre+ ONC, **(E)** Example image of WT contralateral eye control, **(F)** Example image of WT ONC. Scale bar = 100 μ m.

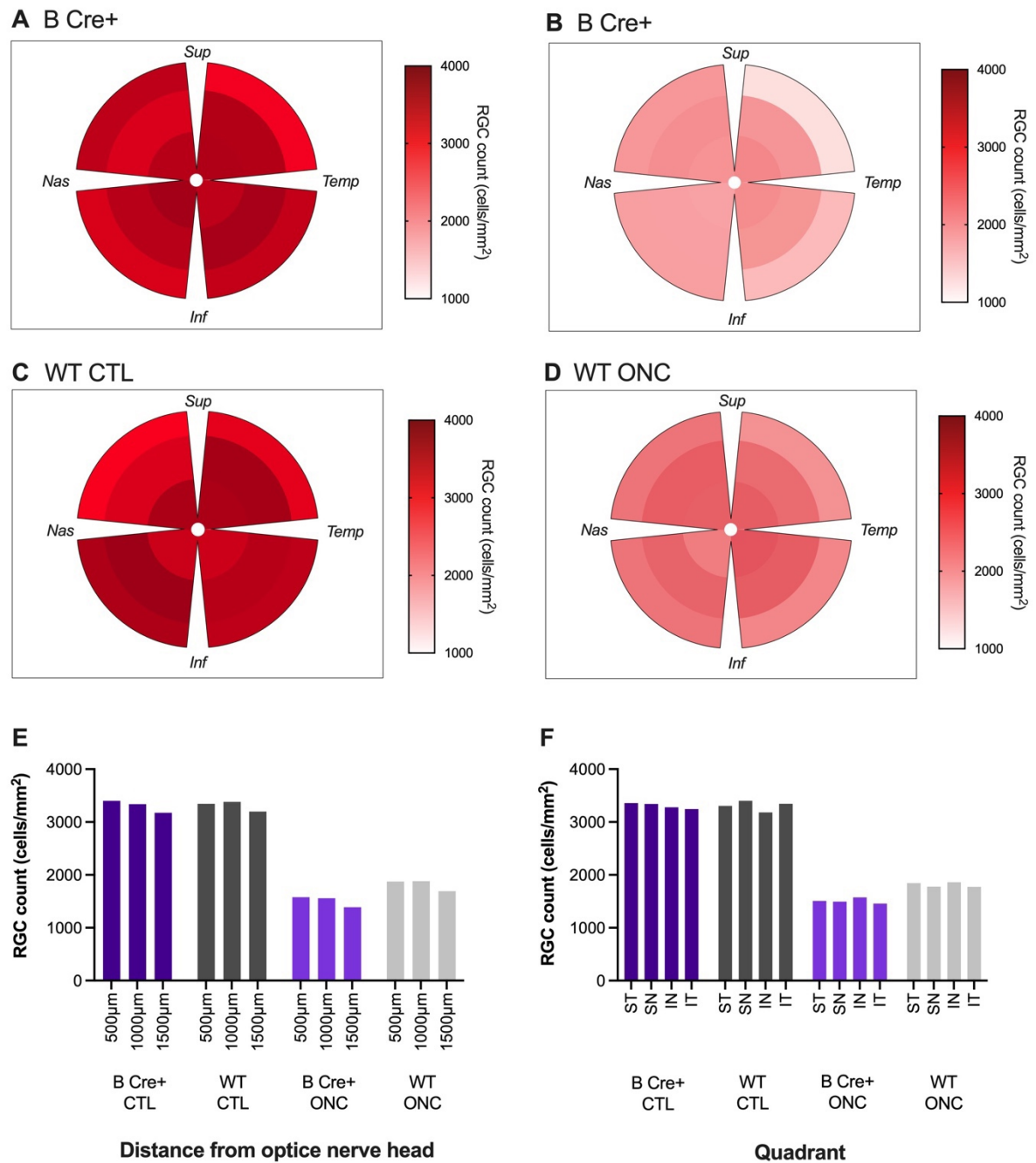


Figure 6.3: Heatmaps showing the mean cell count at different retinal locations
(A-D) Heatmaps show mean RGC count at each of the 12 sectors in the different experimental groups. Column charts show mean RGC count at by distance from optic nerve head **(E)** and by retina quadrant **(F)**, ST – superior temporal, SN – superior nasal, IN – inferior nasal, IT – inferior temporal.

6.3.3. Analysis of RGC Dendrite Morphology 3 days following ONC

The cell count data provided a possible explanation as to why the cell yield per retina was so low in the DiOlistics experiments described in Chapter 6.3.1. With approximately 50% cell loss, there is inevitably a lower probability that a Tungsten particle from the gene gun will hit an RGC. This also raises questions over how representative the few cells successfully labelled truly are. In order to address this concern, a final DiOlistics experiment was completed where the labelling of the RGCs was performed after a shorter duration to improve the cell yield. While it is widely agreed that cell loss reaches approximately 50% by 7 days, the specific nature of the RGC degeneration in the first few days appears to be less certain. Some studies have reported cell loss from the time of injury (Li et al., 2020), while others have reported an initial period where the cell count is unchanged from baseline until approximately 3-5 days, whereupon then is a sudden and rapid decrease (Daniel et al., 2018; Parrilla-Reverter et al., 2009). Changes in dendrite morphology are documented in the initial days after injury (Kalesnykas et al., 2012) but the scale of the change to be expected is somewhat uncertain. For this final ONC experiment with the B Cre⁺ mice, labelling of the RGCs was performed after 3 days. At this stage, it was hypothesised that there would have been sufficient damage from the crush injury to have produced some degeneration of the dendrites, with sufficient cells remaining to improve the number of cells per retina.

ONC was performed on the right eye of a further 5 B Cre⁺ and 5 WT mice, with DiOlistics completed using the standard method described in Chapter 2 after 3 days. The cell yield was indeed greater with an average of >10 cells/retina achieved in the ONC eye for both groups. On assessment of the RGCs, the Sholl curve on the ONC eyes was once again slightly lower and left-shifted in the WT eyes compared to the B Cre⁺ (Figure 6.4). As expected, this difference was smaller than that seen in the 7-day experiment and subsequently the difference in area under the curve, or any of the further analysis, did not reach significance.

The CTL eye for the B Cre⁺ group was noted to have a slightly lower Sholl and AUC compared to the WT. In the previous ONC and retinal explant experiments there has not been a significant difference in the baseline dendrite complexity or the cell count. The reasons for the Sholl curve being slightly reduced on this occasion are unclear. Despite this small difference in the B Cre⁺ baseline, it appeared that even after only 3 days, the trend in the changes of the Sholl curve seen in previous experiments started to emerge. However, the difference in AUC did not reach significance and as such, the impact of this data taken in isolation must be

considered limited. Nevertheless, the context of the previous 7-day results, as well as the retinal explant data, may add further weight to the small difference in the Sholl curve seen at this earlier time point.

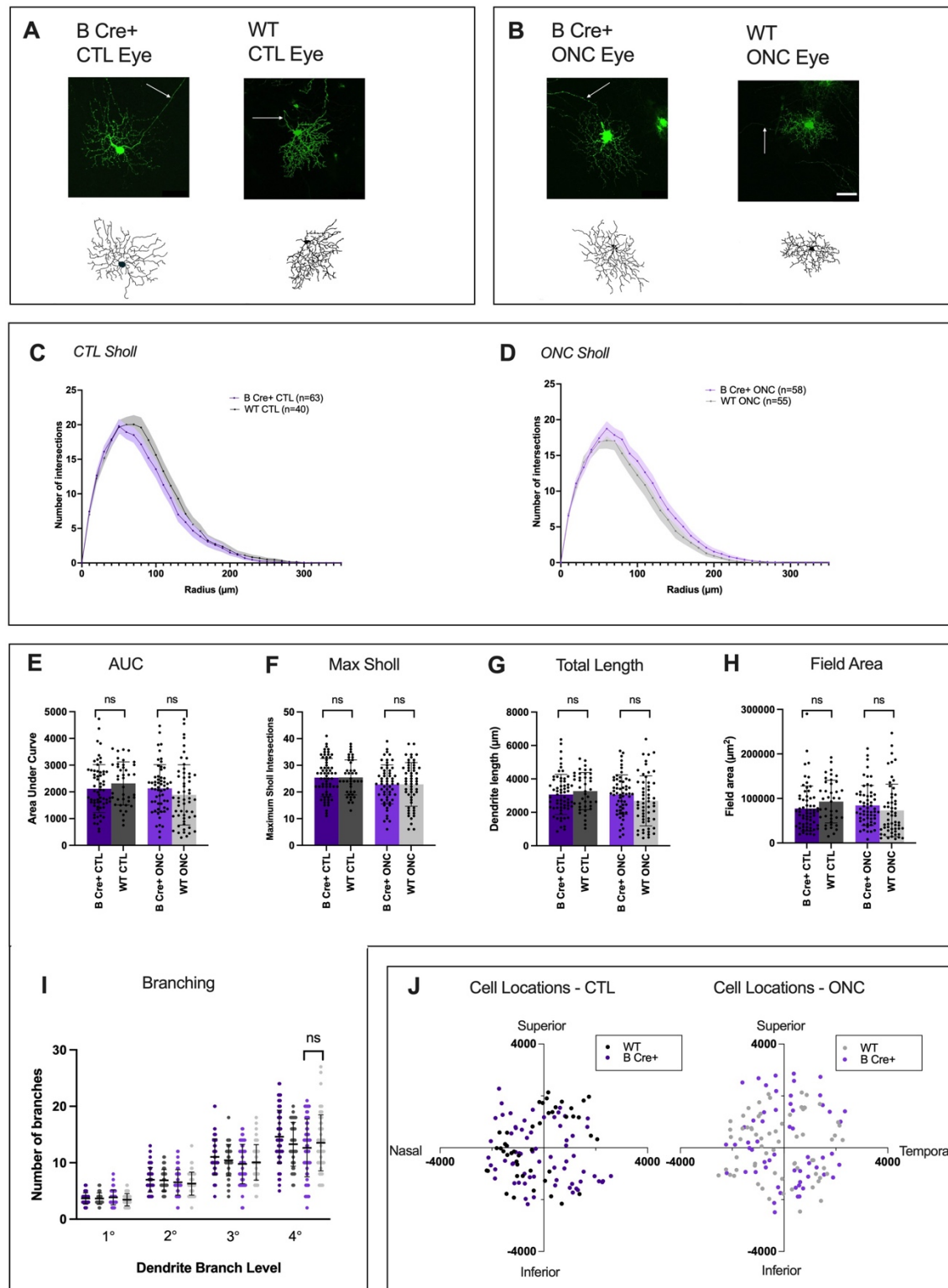


Figure 6.4: Analysis of RGCS 3 days after optic nerve crush injury.

Representative example RGCs and dendrite reconstructions at **(A)** Fellow eye controls, CTL and **(B)** ONC. White arrow indicates RGC axon, scale bar = 50 μ m. **(C, D)** Sholl analysis showing mean at each interval (line) \pm SEM. B Cre+ (purple) and WT (grey). Two-tailed Mann-Whitney U test at each interval distance comparing 72-hour result to CTL 72 hrs, * = $P < 0.05$, n=number of RGCs. **(E)** Area under the Sholl curve. **(F)** Maximum number of Sholl intersections. **(G)** Total length of all dendrites. **(H)** Dendrite field area (μ m²). **(I)** Number of dendrites at each branching level. **(J)** Retina locations of RGCs included in analysis in μ m relative to the optic nerve head. For Column Scatterplots E-H data points represent individual cells, columns represent means for group and error bars correspond to SD, * = $p < 0.05$, ** = $p < 0.01$, *** = $p < 0.001$.

6.4. Discussion

Despite the limitations of performing DiOlistic cell labelling on retinas with 50% cell loss, these *in vivo* results suggest that platelet BDNF preserved dendrite complexity in a more physiopathologically relevant setting than is the case with the retinal explants.

In spite of the preservation of the dendrite complexity, BDNF treatment did not prevent cell loss. BDNF treatment has previously shown an improvement in cell count after 7 days in ONC (Chen and Weber, 2001; Parrilla-Reverter et al., 2009) but the dose, timing and route of delivery were markedly different from the model used here. While the mean serum concentration of BDNF was 25.74 ng/mL in homozygous animals, the concentration likely to reach RGCs was bound to be dramatically lower, and certainly much lower than the large, acute doses of BDNF delivered in other studies by intravitreal injection (Mansour-Robaey et al., 1994; Parrilla-Reverter et al., 2009). The preservation of dendrite complexity without an associated preservation of cell count is likely to represent a more subtle effect from the slow, low-dose, sustained BDNF exposure in this model.

The duration of the study was another important variable when contrasting with previous work as cell survival was typically assessed at much later time points. For example, Mey and Thanos, 1993 administered BDNF by intravitreal injection and counted RGCs after 3, 5 or 7 weeks after optic nerve transection. Di Polo et al., 1998 used gene delivery by a viral vector to cause rat Muller cells to express BDNF and assessed the retinas 16 days after an axotomy injury. It is possible that a small difference in cell count in the B Cre+ mouse may become apparent at later time points. The cell yield with the DiOlistics approach was already limited at 7 days post injury, and by 16 days with an estimated 10-15% of cells remaining, it is unlikely that there would be sufficient cells labelled for a reliable analysis. As such, 7 days appeared to be close to the limit for the ONC experiment when using this method, but in further work, a shift to focus on cell count in a longer duration model of RGC degeneration would be valuable.

The preservation of dendrites without associated cell survival could be explained, in part, by considering the role of BDNF in the CNS. Unlike NGF in the PNS, BDNF is not a major survival factor for most CNS neurons as previously suggested (Rauskolb et al., 2010) and discussed in Chapter 1. The mice with CNS specific *Bdnf* knockout did not suffer the degeneration of peripheral ganglia seen in with the global *Bdnf* knockout models and were able to live to adulthood, demonstrating that BDNF was not essential for prolonged postnatal survival. In the adult CNS in particular, BDNF's role seems to be primarily related to the preservation and modulation of connectivity (Lu et al., 2013). It is hypothesised that rather than a gradual retraction of dendrites as the cell degenerates, the presence of BDNF preserves the dendrite complexity throughout the period of cell degeneration but cell death still occurs at the same time point.

In summary, the combination of the ONC and retinal explant experiments suggested that an increase in circulating BDNF can lead to a neuroprotective effect in the CNS. As humans and other primates naturally contain comparatively high levels of BDNF stored in platelets (see Chapter 1), the possibility to increase BDNF release from platelets was explored in the next Chapter. This would have clinical applications, for example in the context of developing new approaches to treat glaucoma.

Chapter 7. Stimulation of BDNF release from platelets

7.1 Short introduction

The results of the retinal explant and ONC experiments suggested that platelet BDNF can preserve dendrite integrity in CNS neurons. This final results chapter describes pilot studies exploring methods of increasing BDNF release from platelets, with a view to applying this knowledge to humans in conditions such as glaucoma where the neuroprotective effects of BDNF described in the previous chapters would be desirable. As humans already express BDNF in their platelets, methods would need to be found to stimulate release of additional BDNF from the platelet reservoir by triggering activation.

Platelets can be activated in response to a variety of stimuli, both chemical and mechanical (Estevez and Du, 2017; Yun et al., 2016). This activation is not a binary process, but a more of a continuum, with different stimuli affecting the proportion of circulating platelets that are

activated (Leiter et al., 2019). Theoretically, if the correct stimulus was used, this proportion could be increased, with a corresponding increase in the release of bioavailable BDNF. However, the nature of this stimulus and the degree of subsequent activation achieved requires careful consideration. Too little activation would result in insufficient release of BDNF to have any effect, whereas too much could precipitate coagulation and thrombus formation, risking serious harm to the patient. The correct stimulus might be able to reach this “Goldilocks” zone and use this platelet store of BDNF as a safe and effective neuroprotective treatment. In order to determine the nature of this required stimulus, it is worth considering known scenarios that induce states of moderate/low-level platelet activation such as exercise.

There is extensive evidence for the benefits of exercise on mood and cognition. The mechanisms that lead to these benefits are multi-factorial but BDNF is thought to play an important role. Both BDNF mRNA and protein concentrations are increased in the hippocampus following voluntary exercise in rats (S A Neeper et al., 1995; Russo-Neustadt, 1999; Soya et al., 2007), and BDNF has also been shown to be essential for exercise-induced brain plasticity and cognitive function, an effect that can be prevented by blocking TrkB (using a short-interfering mRNA) over a 3 week period (Intlekofer et al., 2013). Neuronal BDNF production increases in response to activity but there is evidence that peripheral BDNF may also contribute. Circulating BDNF increases following exercise in both humans and rats, a finding supported by multiple meta-analyses. This is seen after acute exercise sessions (Dinoff et al., 2017; Szuhany et al., 2015) and regular regimens however, resistance training does not seem to have the same effect (Dinoff et al., 2016). These meta-analyses included studies using either plasma or serum as an outcome, with serum being far more common. It is important to note that there are also examples of studies that failed to show changes in BDNF following exercise (Forti et al., 2014; Baird et al., 2018; Rezola-Pardo et al., 2020). In Dinoff et al., 2016 only half of the reported studies (9/18) in the meta-analysis observed an increase in resting BDNF, and these studies may have been influenced by including populations with a lower baseline BDNF such as Parkinson’s disease, obesity and metabolic syndrome. Similar criticism also applies to the meta-analysis performed by Szuhany et al., 2015. Nevertheless, in another recent meta-analysis, Y. Wang et al., 2022 focused on healthy subjects in randomised controlled trials. They also concluded that both acute and long-term physical exercise can increase circulating BDNF. Broadly, it appears that acute aerobic exercise transiently increases circulating BDNF, while longer-term exercise training seems to have small and variable effects on resting concentrations (Walsh and Tschakovsky, 2018).

Recent work by Leiter et al., 2019 has provided a useful insight into the association of platelet activation following exercise. Although an underlying mechanism and causality have not yet

been established, the observation of platelet activation adds further support for this being the primary cause of the increased BDNF. It is within this debate that the B Cre⁺ mouse could be extremely valuable, given the ability to effectively isolate the platelet contribution in an experimental study. A series of experiments were therefore designed to compare exercising and non-exercising B Cre⁺ mice and measure the BDNF concentrations in the blood. The primary aim would be to show more definitively that exercise causes BDNF to be released from platelets and therefore, support the use of exercise as a therapeutic intervention.

7.2. Exercise tracking – serum BDNF following 7 days of exercise, WT mice

7.2.1. Introduction

As the degree to which each animal exercises varies, it was necessary to monitor each animal's activity. This was achieved using a system counting the number of rotations of an exercise wheel in the cages. In order to accurately monitor individuals, this would require mice to be housed in separate cages with their own exercise wheels. However, social isolation can have an impact on the propensity to exercise. In order to minimise the impact of social isolation, cages were constructed with a clear, perforated Perspex barrier separating two mice in a shared cage, each with its own exercise wheel and tracking apparatus. This allowed individual exercise tracking while still allowing the mice to see and smell their neighbour and to have some degree of social interaction. The details of the construction of the exercise tracking equipment are described in detail in Chapter 2.10. In brief, an infrared sensor was mounted on the outside of the cages to record the rotations of the exercise wheel, with the inputs from 8 exercise wheels (4 cages) recorded using a Raspberry Pi 4B. A second set of cages had the exercise wheels fixed in place to allow a non-exercising control group, with an otherwise identical environment. Mice were allowed to exercise *ad libitem* during the course the experiment (Figure 7.1).

The first experiment tracked the exercise of WT mice over 7 days, with serum BDNF measurements taken at the end of the experiment. This followed an experimental paradigm that has been used in several previous studies of BDNF and exercise. This initial trial was primarily a test of the tracking equipment, but was also an opportunity to investigate the effects in WT mice. Importantly, the minimal levels of BDNF in mouse serum have meant that in the past, mice could not be used for these types of studies (see previous Chapter about BDNF ELISA). Serum collection is simpler and more reliable than plasma collection and was

considered appropriate for this first trial. With the absence of BDNF in mouse platelets, there was expected to be little difference between serum and plasma concentrations.

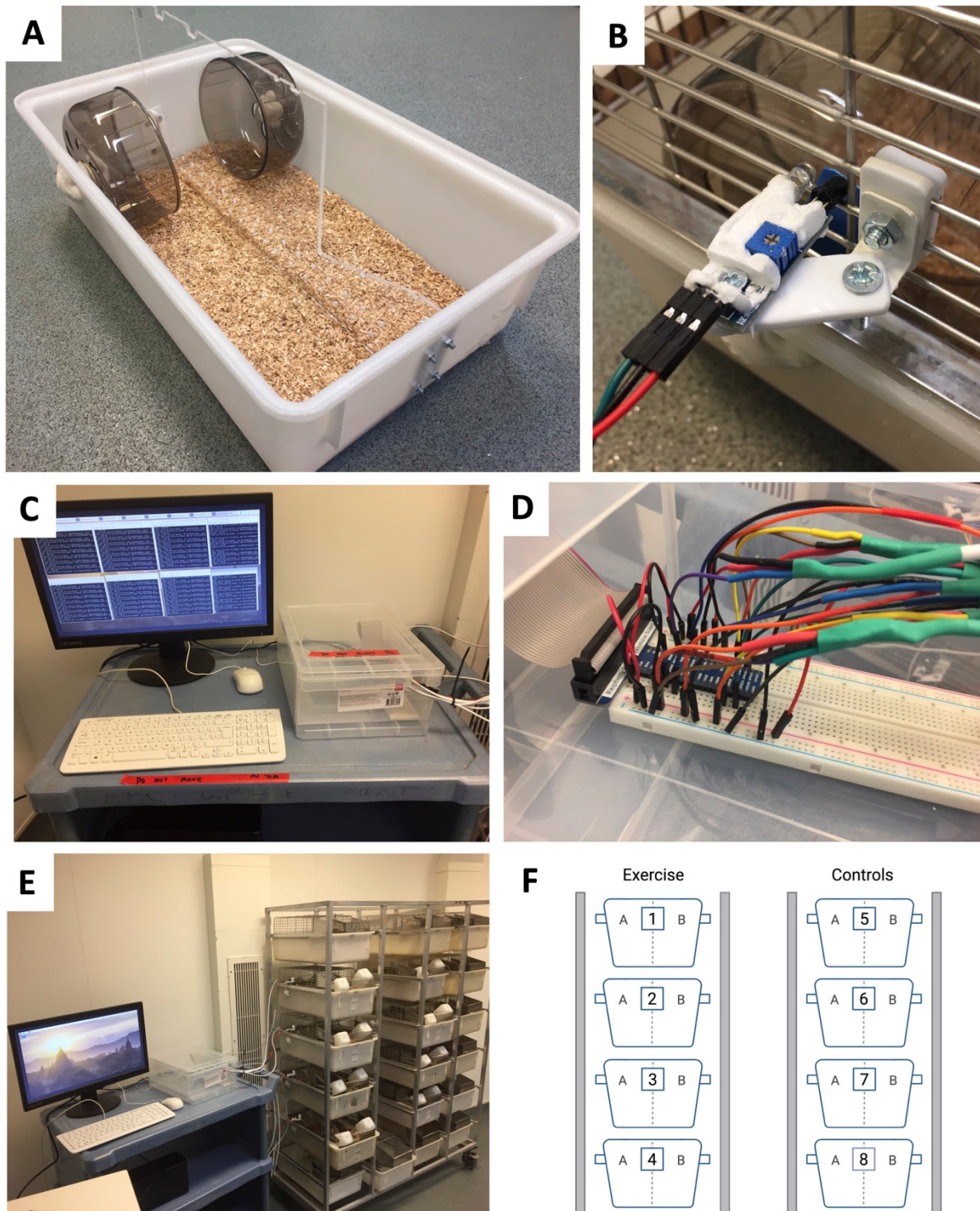


Figure 7.1: Customised exercise tracking equipment

(A) Cages constructed to house two mice, each with their own exercise wheel, separated by a clear, perforated, Perspex divider. (B) Infrared sensor attached using a customised mounting bracket. Sensor has been potted in silicone sealant to reduce the risk of short circuit.

(C) A Raspberry pi adjacent to cages allowing recording and simultaneous tracking from all 8 sensors. (D) An external breadboard was used to allow easy adjustments and additions to be made to the circuit when necessary. (E, F) Cage layout and numbering with one column of 4 cages (housing 8 mice) for exercise tracking and one column for the non-exercising controls.

7.2.2. Experimental set up

16 C57BL/6J mice (Charles River) were included in the experiment, with 8 mice in the exercise group, and 8 mice in the non-exercising controls (4 male and 4 females for each group, age 10 weeks). Mice were allowed to exercise *ad libitum* for 7 days, with wheel rotations continuously monitored through the Raspberry Pi. At the end of 7 days, mice were culled by CO₂ and blood extracted by cardiac puncture. Serum was then prepared from these samples and BDNF concentration measured using the High Sensitivity Fujifilm Wako mature BDNF ELISA kit.

7.2.3. Results

No difference was seen in the serum BDNF concentration after 7 days in WT mice, with mean serum BDNF concentration measured at 6.66 ± 2.41 pg/mL in the exercise group and 7.27 ± 3.34 pg/mL in the control group (Figure 7.2). Cardiac puncture was unsuccessful for the mouse in Cage 2B and so could not be included. On further analysis there did not appear to be any influence attributable to cage position or any difference between males and females. Samples from cages 5A, 5B and 6A had wide variation between the individual ELISA repeats suggesting some inaccuracy. Even if these anomalous results were removed, there was still no significant difference between the two groups.

There was a negative correlation between serum BDNF and total number of wheel revolutions (R squared = 0.677, $p = 0.0230$, Figure 7.3D) and between serum BDNF concentration and mean RPM (R squared = 0.7448, $p = 0.0124$, Figure 7.3F). The mean RPM values were higher than expected and the distributions seen on the histograms (Appendix 5.1) also showed considerable variation. One possible explanation is the false positive triggering of the IR sensors. Cage 3B conversely had a very low number of total revolutions. The sensor was checked and confirmed to be in alignment with the wheel indicator. However, the weight of the mouse in the wheel caused the wheel marker to contact the edge of the cage and generate a noise that deterred the mouse from using the wheel. The wheel position was corrected to adjust for the animal weight and this resolved the issue in later experiments. Of note, this individual actually had the highest BDNF concentration of the exercise group. The full data from the individual exercise tracking cages is shown in Appendix 5.1.

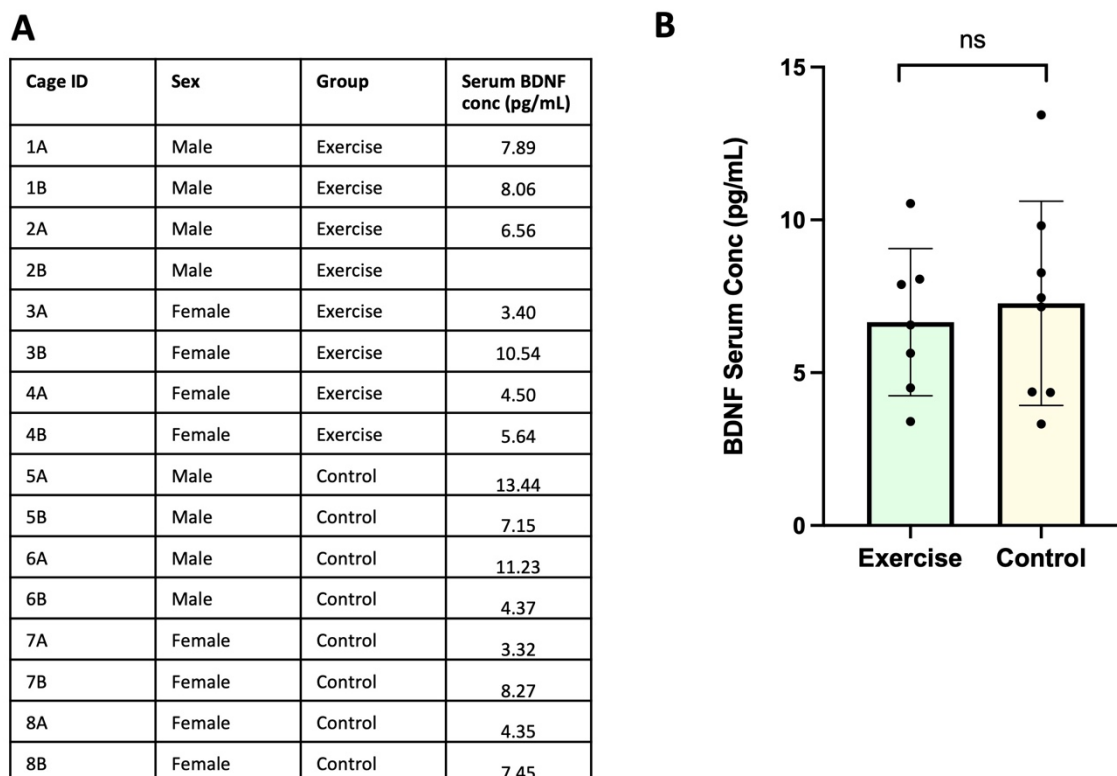


Figure 7.2: Serum BDNF concentration after 7 days of voluntary exercise compared to controls in WT mice.

(A) Individual serum BDNF concentrations (pg/mL). No sample could be obtained from the mouse in cage 2B. **(B)** Column scatterplot represent individual data points with columns representing mean and error bars corresponding to SD.

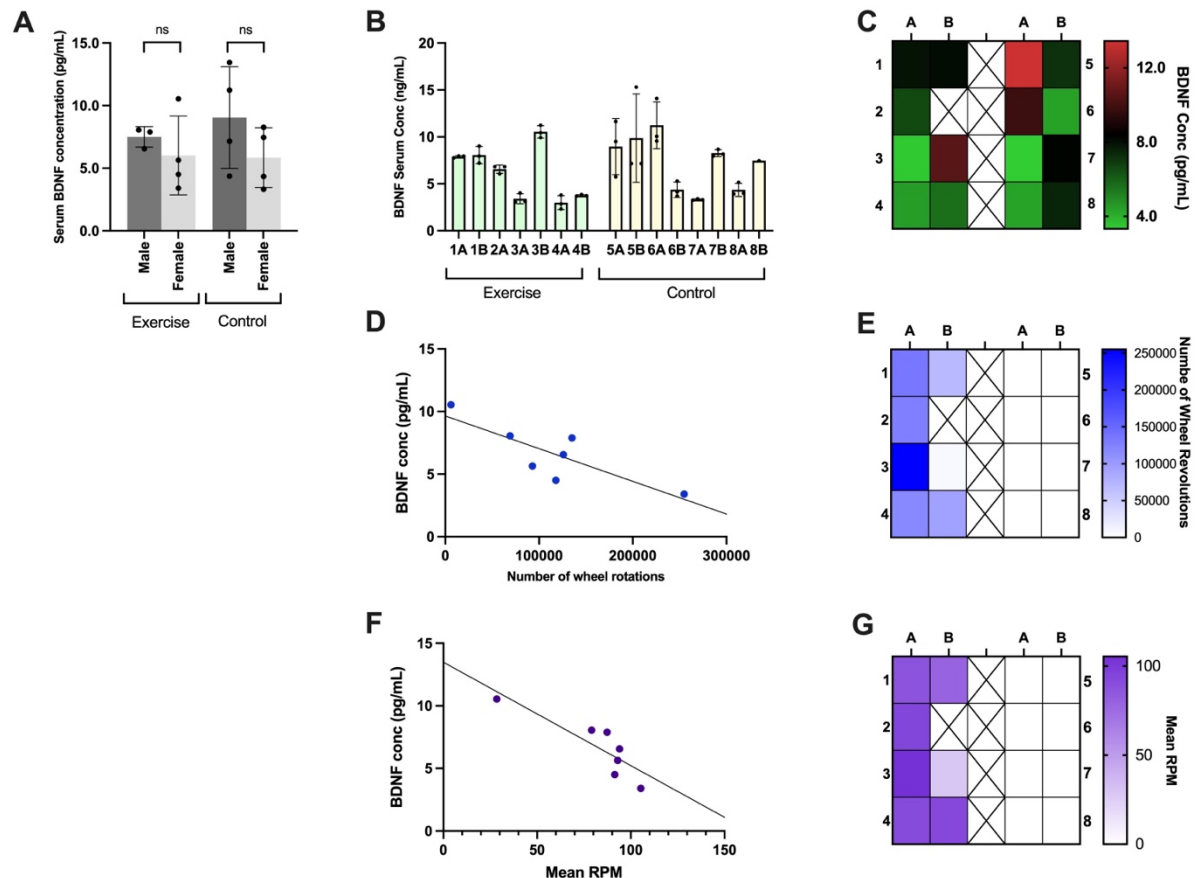


Figure 7.3: Further analysis of exercise tracking experiment 1

(A) BDNF serum concentration in exercise group and control comparing males and females. (B) BDNF serum concentration in exercise group and control showing individual ELISA results from each mouse. (C) Heat map of serum BDNF concentration in relation to cage location. (D) serum BDNF concentration (pg/mL) compared to number of wheel rotations. $R^2=0.677$, $p=0.023$. (E) Heatmap of number of wheel rotations in relation to cage location, (F) Serum BDNF concentration (pg/mL) compared to mean RPM. $R^2=0.745$, $p=0.012$. (G) Heatmap of mean RPM by cage location.

7.2.4. Discussion

This first test of the exercise tracking apparatus was reasonably successful. The position of the sensors may have made the precise values of the total revolutions and mean RPM inaccurate, but they were able to confirm which mice were using the wheels and the times that they were most active. The equipment required some small modifications, but worked sufficiently to be used for further experiments investigating BDNF release from platelets in B Cre+ mice.

Despite the activity in the exercising group, no difference was found in the serum BDNF concentration. It was hypothesised from [Fulgenzi et al., 2020](#) work that low levels of BDNF may have been derived from smooth muscle and there may have been a small increase with exercise. The current data did not support this, however the variation in serum BDNF concentrations between individual mice are such that much larger cohorts would be needed in future experiments to continue exploring peripheral sources of BDNF in WT mice.

7.3. Exercise tracking – serum BDNF following 7 days of exercise, B Cre⁺ mice

7.3.1. Introduction

Having completed a first exploratory trial, the experiment was then repeated using the B Cre⁺ mice to investigate the effect on exercise on BDNF release from platelets.

7.3.2. Experimental setup

The same protocol as the previous experiment was used for B Cre⁺ mice, comparing 8 mice undergoing exercise *ad libitum* for 7 days with 8 mice in the non-exercising control group. A mixture of male and females and HOM and HET animals were included (age 2.5-3.5 months).

7.3.3. Results

No difference was seen in the serum BDNF between exercise and control groups, with mean concentrations measured at $25.25 \pm 9.92\text{pg/mL}$ and $22.07 \pm 11.52\text{pg/mL}$ respectively ($p = 0.580$). Cardiac puncture was unsuccessful in mouse 112070 (cage 8A) therefore, no serum sample was collected. Further analysis showed that triplicates ELISA measurements closely clustered in all samples suggesting a reliable measurement, with the exception of 112060 (cage 5B). Sample 108981 (cage 2A) has a notably low concentration for a homozygous mouse. It is possible this was a heterozygous animal and an error had been made at the time of tissue biopsy or genotyping. Even if this result were to be excluded as an anomaly, the difference between the groups was still not significant. The mean concentration for males in

both groups was slightly lower but this is most likely a reflection of the heterozygous mice in the male groups, whereas females were all homozygous.

A problem was discovered with the positioning of two of the tracking sensors in the first two days and needed to be adjusted. Data related to the exercise is shown for the remaining 5 days after this adjustment was made as it was not possible to reliably compare individuals before this time. Even so, the number of revolutions was notably different between individuals. While some variation is to be expected, the spread of values and mean RPM raises ongoing concerns of false positive triggering of the sensors in some cages. There was no correlation between the number of wheel rotations or RPM to BDNF concentration. However, considering the suspected inaccuracies in the exercise tracking during this experiment, the main conclusion is that modifications need to be made to how the IR sensors are secured to the cages. The full data from the individual exercise tracking cages is shown in Appendix 5.2.

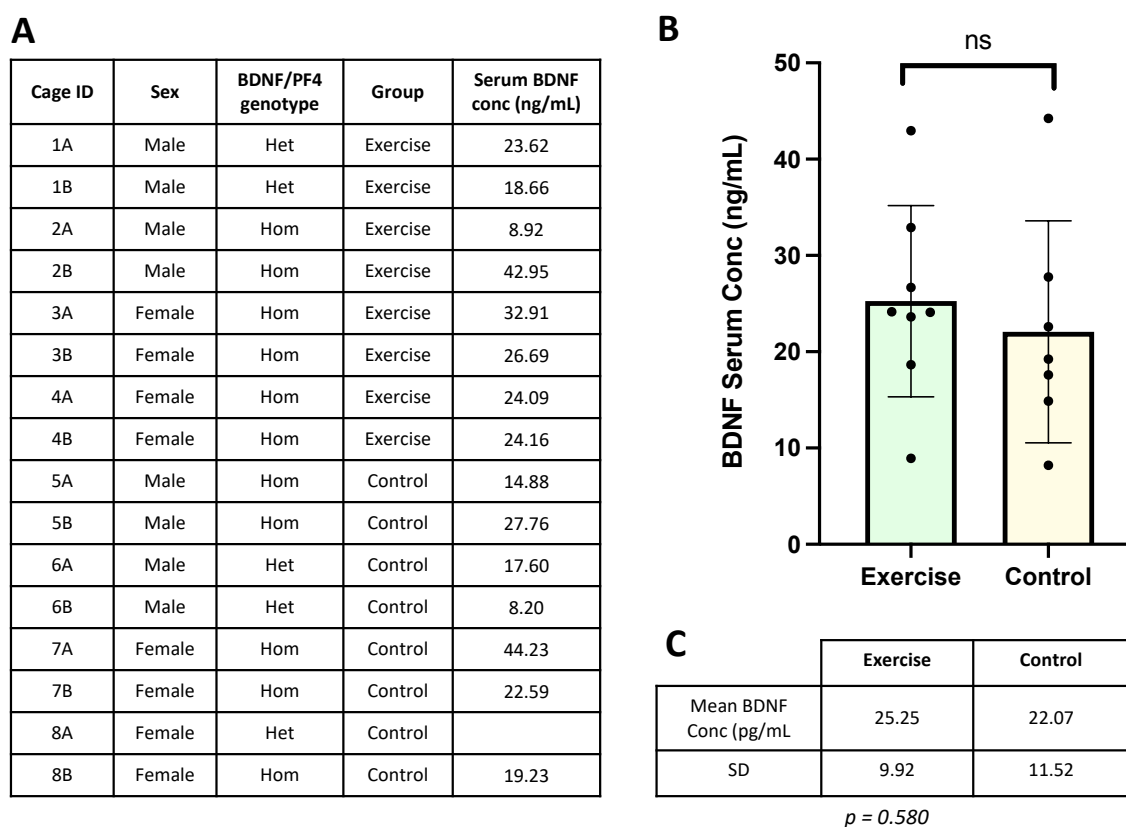


Figure 7.4: Serum BDNF concentration after 7 days of voluntary exercise compared to controls in B Cre⁺ mice

(A) Individual serum BDNF concentrations (ng/mL). No sample could be collected from the mouse in cage 8A. (B) Column scatterplot represent individual data points with columns representing mean and error bars corresponding to SD. (C) Mean and SD of individual groups.

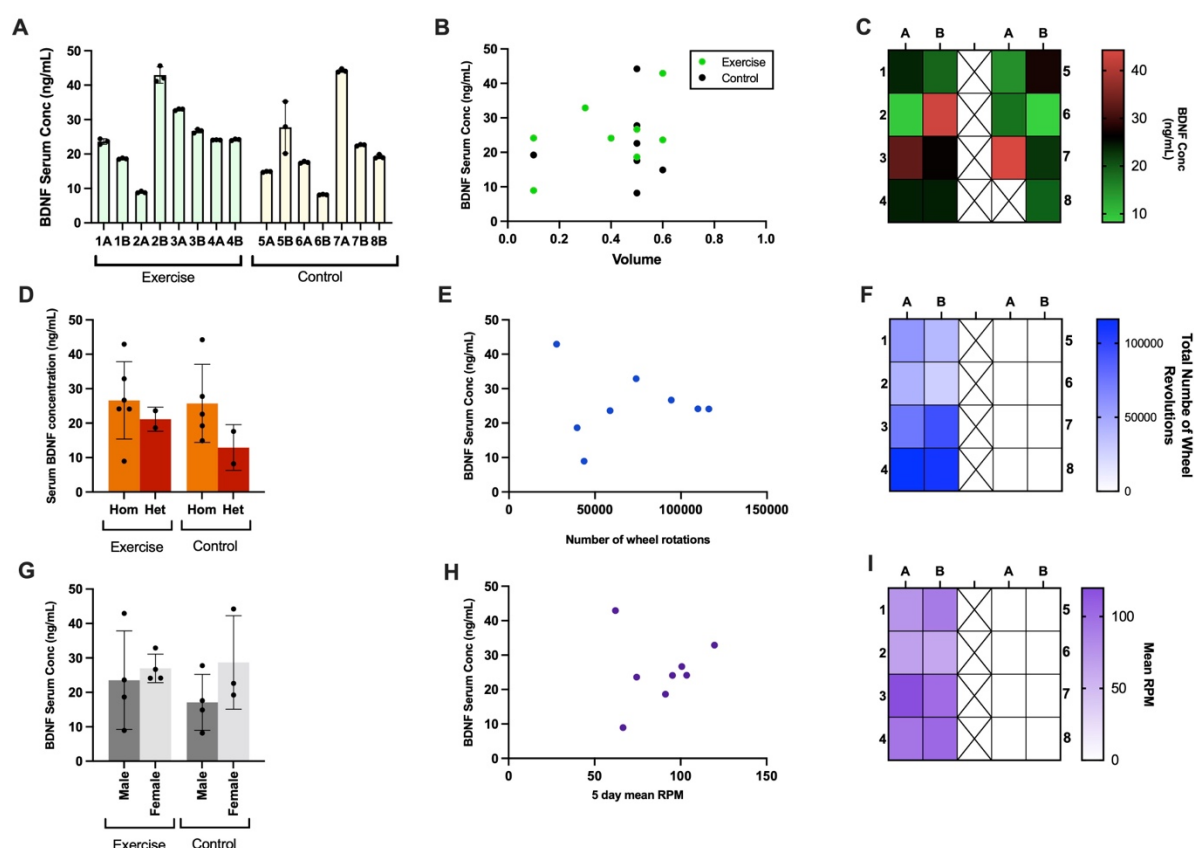


Figure 7.5: Further data analysis of exercise tracking experiment 2

Column scatterplots represent individual data points with columns representing mean and error bars corresponding to SD (**A**) Plasma BDNF concentrations. Points show values from individual ELISA wells, columns show mean values for each individual. (**B**) Blood volume collected compared to plasma BDNF concentration (ng/mL). (**C**) Heatmap of plasma BDNF concentration in relation to cage location. (**D**) Plasma BDNF concentrations for homozygous and heterozygous animals. (**E**) Number of wheel revolutions compared to plasma BDNF concentration (ng/mL). (**F**) Heatmap of number of exercise wheel revolutions in relation to cage location. (**G**) Plasma BDNF concentrations for male and females. (**H**) Mean RPM compared to plasma BDNF concentration (ng/mL). (**I**) Heatmap of mean RPM in relation to cage location.

7.3.4. Discussion

The results of the experiments with running wheels mostly highlight the challenges related to measurement of BDNF as a function of exercise. The range of serum BDNF in both WT and B Cre⁺ mice are quite large, as is also the case in humans (see in particular Naegelin et al. 2018 and power calculations therein related to cohort comparisons). Much larger numbers of mice will be needed in future experiments to confidently detect possible changes in the levels of serum or plasma BDNF related to physical exercise.

7.4. Exercise tracking – plasma BDNF following 3 days of exercise, B Cre+ mice

7.4.1. Introduction

BDNF levels were also determined in plasma and the timing of blood collection adjusted, given previous results that platelet activation in response to exercise may peak early. In particular, Leiter et al., 2019 reported a peak of platelet activation after 4 days of running, which had returned to normal by day 7. It is therefore possible that a change in BDNF due to exercise-induced platelet activation would have also returned to normal. Leiter et al. measured activation at day 0, 1, 4 and 7, leaving the exact timing of peak activation unclear. As this was primarily a “proof-of-concept” type of experiment, 3 days of exercise was selected.

7.4.2. Experimental set up

6 B Cre+ mice were included in each of the exercise and control groups, with each group containing 2 males and 4 females, equal numbers of homozygous and heterozygous, aged 2.5 – 3.5 months. Continuous exercise tracking was performed over 3 days, after which mice were culled by CO₂ and blood samples collected immediately after death by cardiac puncture, between 09:00 – 10:30am. Blood was collected directly into a syringe containing 20uL or 500mM EDTA. Plasma samples were then prepared as described in Chapter 2.8.3 and stored at -80°C until ready for measurement. BDNF levels were measured using the Fujifilm Mature BDNF ELISA Kit Wako, High Sensitive, with plasma samples diluted at 1/50 with buffer as the concentration was expected to be lower than serum.

Following the concerns in the previous sections over the positioning and stability of the exercise tracking sensors in the last experiments, some modifications were also made to the apparatus. IR sensors were now mounted to crab clamps (TRIXES Crab Clamp Mount Stand Desk Wall Panel Holder Clip Professional 1/4" and 3/8" Thread) on the outside of the cages. This simultaneously allowed a more secure mounting for the sensors, but also made them easier to be removed which reducing the risk of damaging the components in the process.



Figure 7.6: Alterations made to IR sensor mounting

IR sensors were attached to a Crab Clamp mount, allowing a greater range of motion to position the sensor, greater stability when aligned, and more convenient removal at the end of the experiment

7.4.3. Results

Plasma samples were successfully collected from all 12 animals. One individual (127970, cage 8A) was found to have a concentration of 20.44 ng/mL, equivalent to serum concentrations and suggesting the blood had clotted and platelets activated during the collection process. This sample was therefore excluded from further analysis. In the remaining samples, mean plasma BDNF concentration was 2.19 ± 1.28 and 1.28 ± 0.60 ng/mL in the exercise and control groups respectively, however, this difference was not significant ($p=0.253$).

On further analysis, there was little variation between the different ELISA wells for a given individual suggesting the ELISA had been reliable. There was no significant difference seen between homozygous and heterozygous animals in either group, nor was there any particular pattern or clustering of plasma BDNF concentration or exercise activity based on the cage position. In this experiment all 6 exercising mice recorded a relatively similar number of total revolutions (mean wheel revolutions 45472, SD ± 4738). Additionally, there was no correlation between the number of wheel revolutions and the plasma BDNF concentration. The distribution was once again tending towards a negative correlation (increased rotations associated with reduce BDNF levels) but this was not significant.

Of note, there was a moderate negative correlation between the volume of blood collected during cardiac puncture and the measured plasma BDNF concentration ($p = 0.0464$, $R^2 = 0.372$). The concentrations of all 11 samples included in the analysis was more than 10 times lower than that of serum, suggesting that platelet activation had not been profound. Nevertheless, there may have been a small amount of activation in occurring in a small proportion of the platelets. The lower volume of blood collected was generally an indication of a more difficult cardiac puncture, which may have added a few more seconds to the procedure before the needle was removed and the blood thoroughly mixed with EDTA. It is possible that there may have been some platelet activation in the needle or even in the heart itself during this time. Clearly, the measured concentration of BDNF is quite sensitive to any variation in the collection process. The full data from the individual exercise tracking cages is shown in Appendix 5.3.

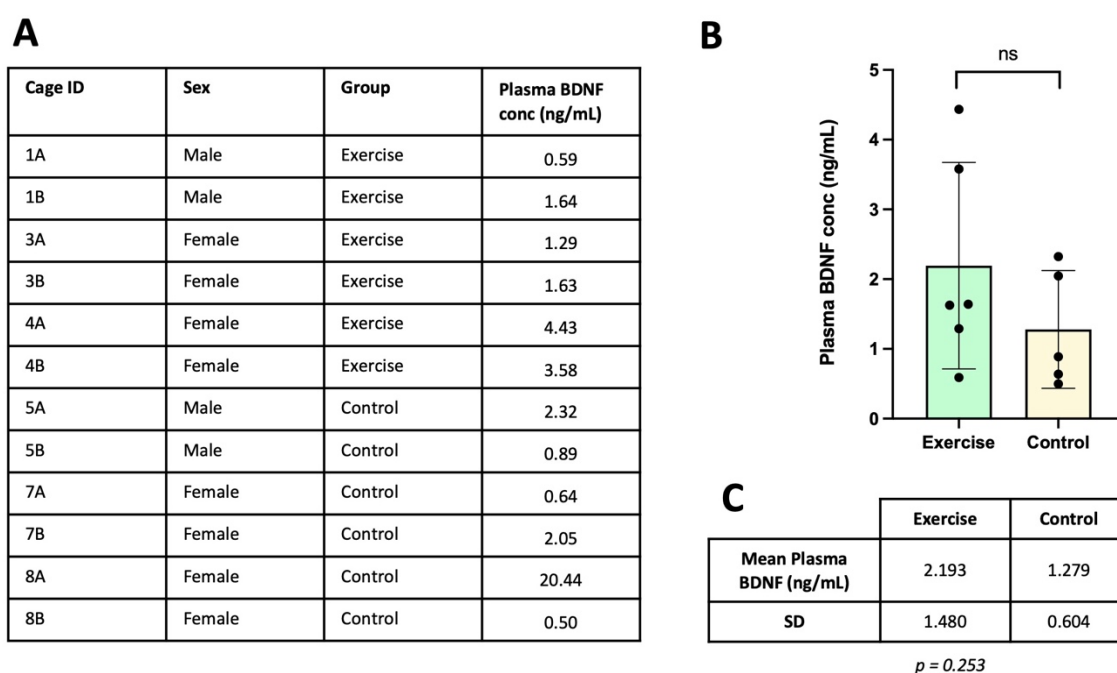


Figure 7.7: Plasma BDNF concentration after 3 days of voluntary exercise compared to controls

(A) Individual plasma BDNF concentrations (ng/mL). Sample from 8A was anomalously high and excluded from additional analysis (B) Column scatterplot represent individual data points with columns representing mean and error bars corresponding to SD. (C) Mean and SD of individual groups.

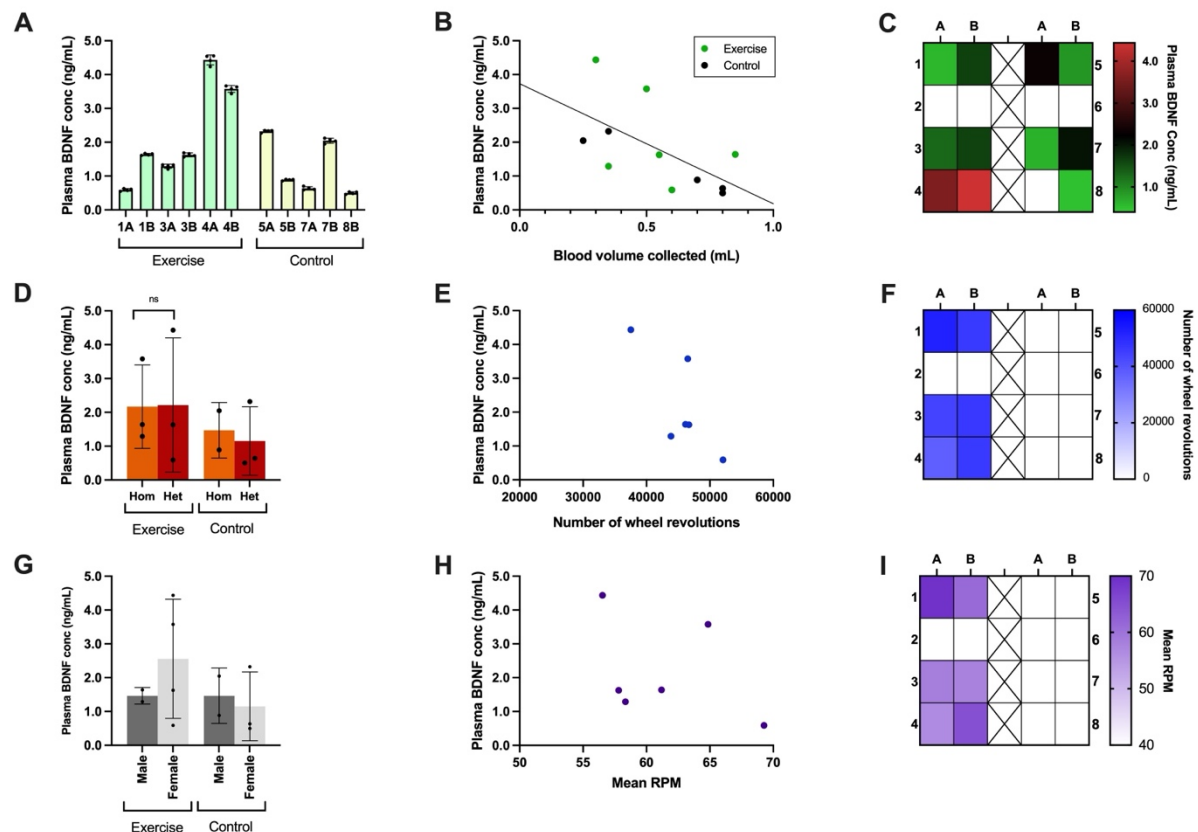


Figure 7.8: Further analysis of exercise tracking experiment 3

Column scatterplots represent individual data points with columns representing mean and error bars corresponding to SD (A) Plasma BDNF concentrations. Points show values from individual ELISA wells, columns show mean values for each individual. (B) Blood volume collected compared to plasma BDNF concentration (ng/mL). (C) Heatmap of plasma BDNF concentration in relation to cage location. (D) Plasma BDNF concentrations for homozygous and heterozygous animals. (E) Number of wheel revolutions compared to plasma BDNF concentration (ng/mL). (F) Heatmap of number of exercise wheel revolutions in relation to cage location. (G) Plasma BDNF concentrations for male and females. (H) Mean RPM compared to plasma BDNF concentration (ng/mL). (I) Heatmap of mean RPM in relation to cage location

7.4.4. Discussion

Despite several variations of the exercise experiments, clearly significant elevations in BDNF levels following exercise could not be detected, be that in plasma or serum. It is clear that given probable small differences attributable to exercise, much larger groups of mice should be envisaged in future experiments. Based on a power calculation using the means and standard deviation provided by this preliminary trial, at least 34 mice would be needed in each group in a larger scale experiment, plus additional mice to account for errors during plasma collection. Additionally, the equipment and protocol may need to be optimised in order to detect such small changes in BDNF concentration.

With the exception of the one excluded sample (127970, cage 8A) all others blood samples were in a relatively small range, suggesting that the blood collection had been performed correctly. Nevertheless, the negative correlation between the collected blood volume and the BDNF concentration does raise some concerns, and it is clear that even a very small amount of activation could influence the outcome of this experiment. When mice are culled by CO₂, the cardiac puncture must be performed within seconds of death, with any delay potentially leading to a more difficult collection of the blood and a poorly prepared sample. An ideal solution may be to perform the cardiac puncture on an anaesthetised animal as this tends to give a more successful draw and is the method preferred by other groups that have a greater focus on plasma content. This exsanguination procedure was not covered by the corresponding project licence and thus could not be completed at this time.

Another consideration relates to the timing of a potential BDNF peak. If the levels of plasma BDNF would be elevated in response to exercise, it is unclear if they would persist long enough to allow detection. The exercise tracking data shows that the mice were most active at the beginning of the night between 20:00 – 02:00. They later had shorter bursts of exercise up until 08:00 (when lights were turned on) but were much less active in this time. It is possible that by the time the blood samples were taken at 09:00 – 10:00 the BDNF concentration had returned to normal. BDNF is known to have a short half-life in plasma (0.92 minutes) (Poduslo and Curran, 1996). However, this value was calculated by intravenous injection of radiolabelled BDNF. The duration of sustained plasma concentration in this case is more likely to be due to the underlying processes of the platelets as opposed to the diffusion properties of the unbound protein. From the available literature, there are some suggestions that changes in BDNF levels may be short-lived following cessation of exercise in humans, with levels returning to baseline within 30 minutes for serum and 60 minutes for plasma (Gilder et al., 2014). This issue highlights the importance of exercise tracking if using voluntary exercise. For example, it may be preferable to collect the blood samples at approximately 02:00, immediately after the most active period. Unfortunately, the mice had to be transferred to another building for the blood collection which limited the procedure to normal working hours during the day. Another alternative would be to use forced exercise on a treadmill instead of voluntary exercise. This would allow complete control over the time interval from cessation of exercise to blood collection, as well as creating the opportunity to determine a dose response based on set periods and intensities of exercise.

Even with these adjustments made, the degree of platelet activation induced by exercise may still present challenges. Leiter et al., 2019 used flow cytometry to detect the activation of

platelets, first gating for cells marked for CD61, and then for CD62P within that population. Platelet activation was then reported as a percentage of activated platelets relative to the control group. While the percentage increase was significant, the overall number of activated platelets is very low, and it may be that the amount of additional BDNF released into plasma is still extremely small. The work with the WT mouse serum has shown that the High Sensitivity ELISA kit is capable of detecting extremely small concentrations, but that subtle change may be easily superseded by additional factors, be that environmental or limitations of the experiment protocol.

7.5. Stimulation of BDNF release by ultrasound

7.5.1. Introduction

While it is well documented and accepted that physical exercise has profound benefits for many aspects of health in humans (Rosenbaum et al., 2014; Khodadad Kashi et al., 2022; Yu et al., 2022), patient adherence with advised exercise regimes tends to be limited. There are many reasons for this, but for patients with age-related conditions such as glaucoma, mobility problems may be a further limiting factor. It is therefore worth considering other strategies to try and stimulate platelets to release BDNF.

Mechanical shear stress is a major factor triggering platelet activation. For example, Fujimura et al., 2002 assessed BDNF release from platelets *in vitro* and concluded that “shear stress stimulation also induced BDNF release and did so in proportion to the potency of shear stress”. There are methods of artificially producing a similar shear stress that could not only avoid some of the challenges resulting from exercise implementation (see protocol), but also allow for a more controlled approach. One such method could be the use of ultrasound.

Ultrasound consists of pressure waves with frequencies of 20kHz or greater, generated by piezoelectric transducers that convert an applied voltage into a mechanical movement (Husseini and Pitt, 2009). As well as having widespread applications in medical imaging, the pressure waves can induce biomechanical effects on the targeted tissues by acoustic cavitation. Acoustic cavitation involves the formation and subsequent collapse of microbubbles in response to a driving pressure wave. As the ultrasound waves pass through imperfections in the fluid, the repeated compression and rarefaction will create small gas pockets that act as cavitation nuclei (Choi et al., 2020a). These nuclei are typically located at the boundary of a fluid and within gas-filled crevices, such as cellular cytoplasm, and can also

be enhanced by delivering exogenous microbubbles into the circulation. Cavitation can be defined as stable or inertial (Figure 7.12). In stable cavitation, the microbubbles will continuously expand and contract around the same resting radius (Gogate and Kabadi, 2009). At increasing acoustic pressures, nonlinear bubble oscillations can be induced, creating strong shear forces and viscous shear near the surface of the bubble. These forces can disrupt the surrounding environment, including cellular membranes, and with sufficient energy can lead to cell death (O'Brien, 1986). Above a certain threshold, bubbles will expand to the point where they become unstable. At this point, the bubble will collapse and implode, releasing energy in a shockwave. This is known as inertial cavitation, which releases a huge amount of thermal energy that can trigger sonochemical reactions, generating reactive oxygen species (ROS) (Riesz and Berdahl, 1985) and, in some cases, produce light by sonoluminescence (Suslick and Flannigan, 2008). The energy released is also more than sufficient to disrupt cell membranes (Choi et al., 2020).

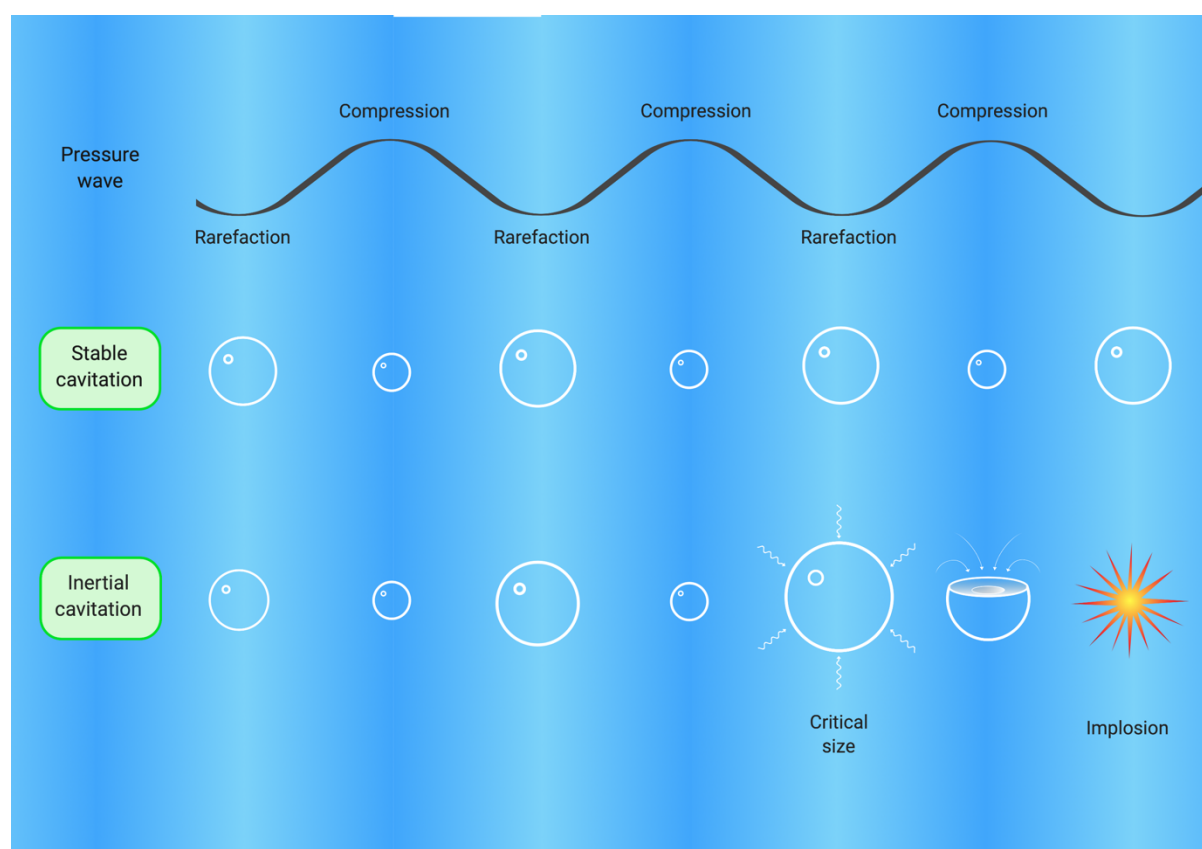


Figure 7.9: Illustration of stable and inertial acoustic cavitation
Edited from Choi et al., 2020

The disruption of cell membranes can increase drug transportation through tissues and into cells and has been demonstrated in several different settings. Mitragotri et al., 1995 showed that 20kHz ultrasound facilitated transdermal delivery of medium and high molecular weight proteins. Importantly, three hours after ultrasound, the skin regained its transport resistance suggesting that no permanent damage had been done to the tissue. The evolution of this concept has led to Acoustic Cluster Therapy (ACT), where a dispersion of microbubbles/microdroplets are injected intravenously with a drug followed by application of low power insonation from a regular medical imaging ultrasound over the target area (Park, 2016). The insonation causes rapid evaporation of the droplets, generating large bubbles that induce the biomechanical effects increasing the uptake of the drug into the surrounding tissue. This can increase the drug concentration in the target area without risking the harmful side effects of increasing the systemic dose. The results of this technique have been extremely encouraging with clinical trials in oncology patients already underway (Sontum, Per Christian and Phoenix Solutions, 2019).

The applications for ultrasound in drug delivery have been taken further by using it in combination with nanoparticles. Carrier vehicles can be used to transport toxic medications such as those used in chemotherapy with release then triggered by ultrasound. Pluronic polymers are capable of forming micelles by spontaneous arrangement of amphiphilic block copolymers in aqueous solution. They have a hydrophobic core with a hydrophilic shell, in which hydrophobic drugs to be encapsulated. Ultrasound-induced acoustic cavitation can then disrupt the polymeric micelles and release the medication contained inside (Amin et al., 2017). Re-encapsulation has been reported to be completed within 0.6 seconds of the cessation of ultrasound (Husseini et al., 2002), minimising any interaction of the drug with tissues downstream. Advances in the development of nanocarriers have improved the stability, loading capacity and circulation time, allowing the technique to be modified to suit a specific treatment, with additional modifications being used to stimulate release of their contents in response to other stimuli, including light, temperature, enzymes and magnetic fields. The hydrophobic nature of many cancer drugs makes them particularly suited for this form of delivery, and there are several varieties of polymeric micelles being evaluated for clinical trials, with Genexolt-polymeric micelle having been granted FDA approval (Cabral and Kataoka, 2014).

There are many advantages to this approach. Concentrating ultrasound to a target area allows a high concentration of the drug to be released locally, with minimal systemic distribution. Ultrasound is non-invasive, requiring only contact with the skin using a water-soluble gel, and the waves can penetrate deep into the body, giving it an advantage over optical techniques.

Using platelets as a delivery vehicle instead of micelles would carry these same advantages, with the added benefit of avoiding administration of an exogenous drug preparation because it would utilise the existing source of BDNF already in circulation. The ability of ultrasound to activate platelets has been known since the late 1970s. These investigations were part of a general interest in the biological effects of ultrasound as it was becoming an increasingly prevalent tool in clinical practice at the time. Within the parameters used for diagnostic imaging, there were no substantial risks identified, but there was clear evidence that platelets could be activated under the correct conditions. By the late 1990s, ultrasound induced activation had been proposed as method of stopping traumatic bleeding by helping to stimulate the formation of an initial haemostatic plug (Martin et al., 1999; Vaezy et al., 1999). Platelet aggregation following activation was found to be dependent on the frequency of ultrasound delivered, with aggregation increasing as frequency decreased (from 3.0 to 0.75MHz).

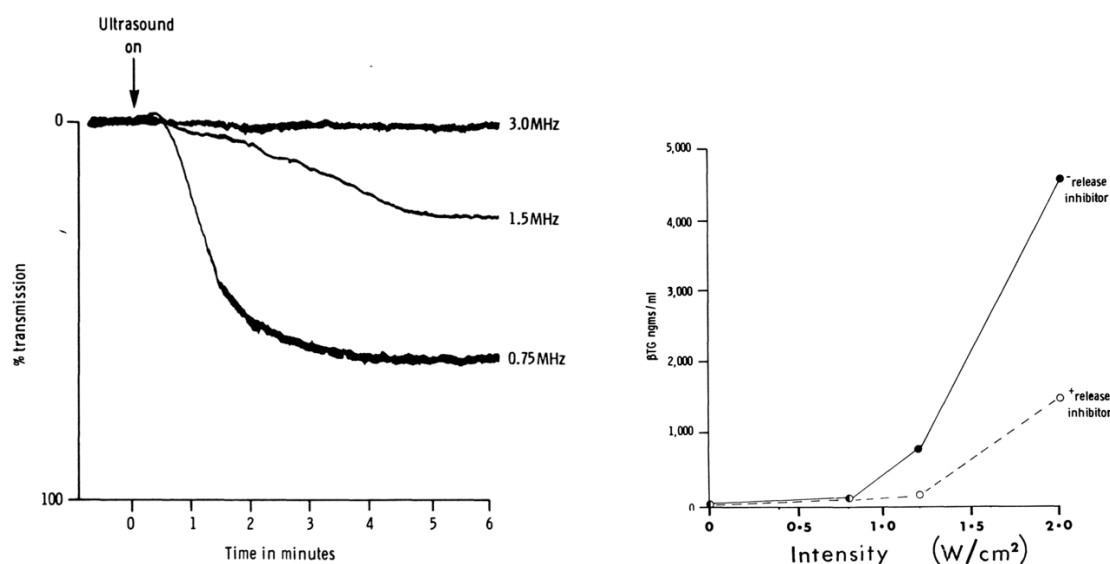


Figure 7.10: Platelet aggregation induced by 1.8 W/cm² of ultrasound at different frequencies. Aggregation is inferred from light transmission through the sample. As a large number of individual platelets aggregate to become a smaller number of large particles, percentage of light transmitted increases. Taken from Williams, 1983.

They postulated that this was the result of two distinct effects. Firstly, ultrasonic cavitation disrupts a small proportion of the platelets directly, causing the release of active substances. These substances will then in turn activate adjacent undamaged platelets leading to further aggregation (Chater et al., 1977). This work was taken further by Otto et al., 2001 who showed that ultrasound-induced aggregation of platelet rich plasma (PRP), using 35kHz for 5 seconds, was well correlated with ADP-induced aggregation, suggesting that the effects are mediated by similar pathways.

Since BDNF is released from platelets on activation, it can be reasoned that ultrasound could be used to provide targeted activation of platelets and the release of BDNF. This possibility was explored with a small pilot experiment in which platelets were exposed to ultrasound *in vitro* to determine if this enhanced BDNF release.

7.5.2. Experimental setup

Due to the small volume of platelets that can be obtained from a blood sample from mice, platelets were instead collected from rats. Brown Norway rats aged 18 weeks were sacrificed by CO₂ and blood collected by cardiac puncture immediately after death. These rats were being used for another research project by Gloria Cimaglia (PhD Fellow, Cardiff University) who kindly allowed blood samples to be taken at the time of Schedule 1. Blood was drawn up to a final volume of 1500µL into a syringe containing 300µL of ACD buffer (1/5 of final volume), and washed platelets prepared as described in Chapter 2. This method followed an established protocol for preparing washed platelet samples (Dingsdale et al., 2021b). The purity of the platelet preparation was not formally tested in this experiment.

Three 200µL samples were taken from the prepared platelets from each animal to be used for three treatment groups (Figure 7.14). This allowed platelet counts to remain consistent across the experimental groups for each animal. One sample was exposed to ultrasound for 20 seconds by applying KY gel to the ultrasound probe and holding this adjacent to the Eppendorf tube containing the washed platelet sample. The pulser/receiver was set to a frequency of 20 KHz with energy 16µJ. This ultrasound signal was then delivered via 2.25MHz probe, with an oscilloscope used to monitor the signal. The ultrasound probes, pulser/receiver module and oscilloscope were kindly loaned to the project by Dr Xin Yang (School of Engineering, Cardiff University). The second platelet sample was left to rest at room temperature for 5 min to act as a negative control, and the third sample had Thrombin (0.01 U/mL) and Calcium chloride (2mM) added to cause activation of the platelets and act as a positive control.

After treatment, samples were centrifuged at 900g for 10 min at room temp (no brake) to pellet the platelets. The supernatant was then collected into a new tube and the platelet pellet resuspended in 20µL of RIPA buffer. Both the lysed platelets and the supernatant were stored at -80C until ready for use. This method was applied to samples from all 4 rats and then BDNF of both the lysed platelets and the supernatant from all individuals and groups were measured using a Fujifilm BDNF colorimetric ELISA.

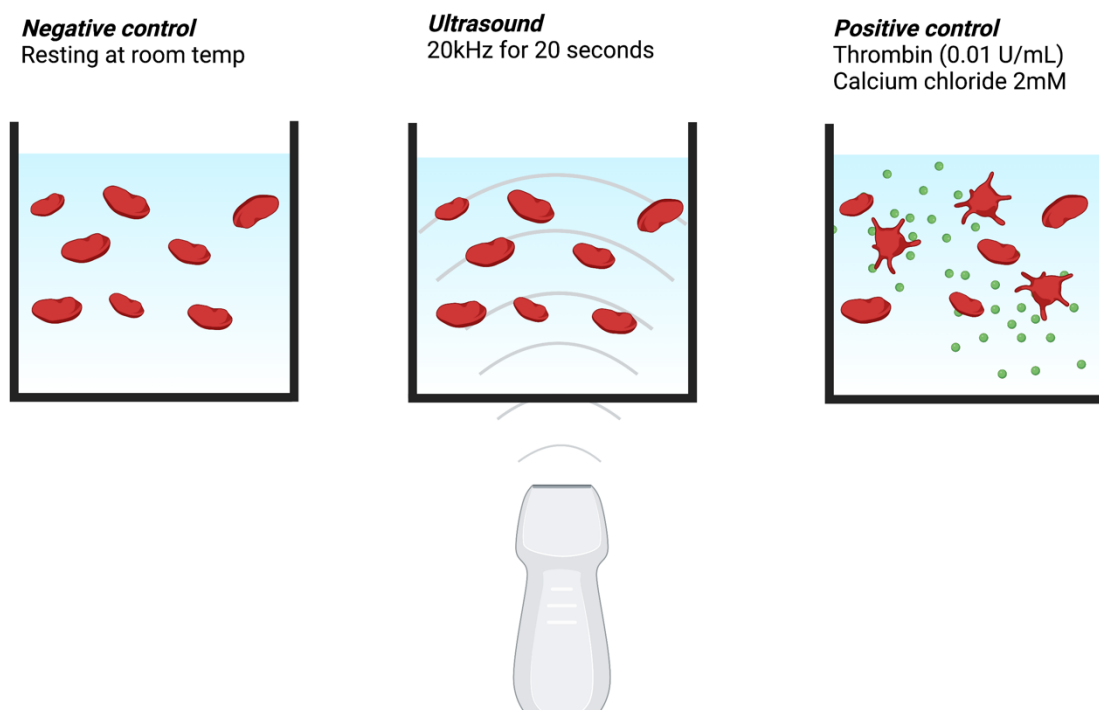


Figure 7.11: Experimental setup for ultrasound stimulated BDNF release from platelets Platelets isolated from each individual rat were divided in to three samples. One as a negative control, one exposed to ultrasound and one with platelet activation stimulated by thrombin and calcium chloride as a positive control. Created using Biorender.com

7.5.3. Results

BDNF was detectable in the platelet pellet from all samples. Its levels were dramatically reduced following addition of thrombin and calcium in the positive control, confirming that BDNF was released following chemical activation (Figure 7.15). This was confirmed by an increased concentration in the supernatant. The BDNF concentration of the lysed platelet pellet in the ultrasound samples showed a reduced BDNF concentration compared to the negative control in three out of the four groups (Figure 7.15A), which may suggest BDNF a portion of BDNF has been released from these platelets. A corresponding increase in the supernatant concentration was not seen but considering the size of the change in the platelet concentration this may be due to the limits in sensitivity of the ELISA and dilutions used.

The difference in mean BDNF concentrations between resting control and ultrasounded pellets was not significantly different, due to Sample 4 having a higher BDNF concentration in pellet exposed to ultrasound compared to the negative, resting control. However, the negative

control was also noted to have a slightly higher level of BDNF in the supernatant. This could represent a small degree of platelet activation inadvertently occurring during the preparation of the negative control, leading to an artificially low concentration measured in the platelet pellet.

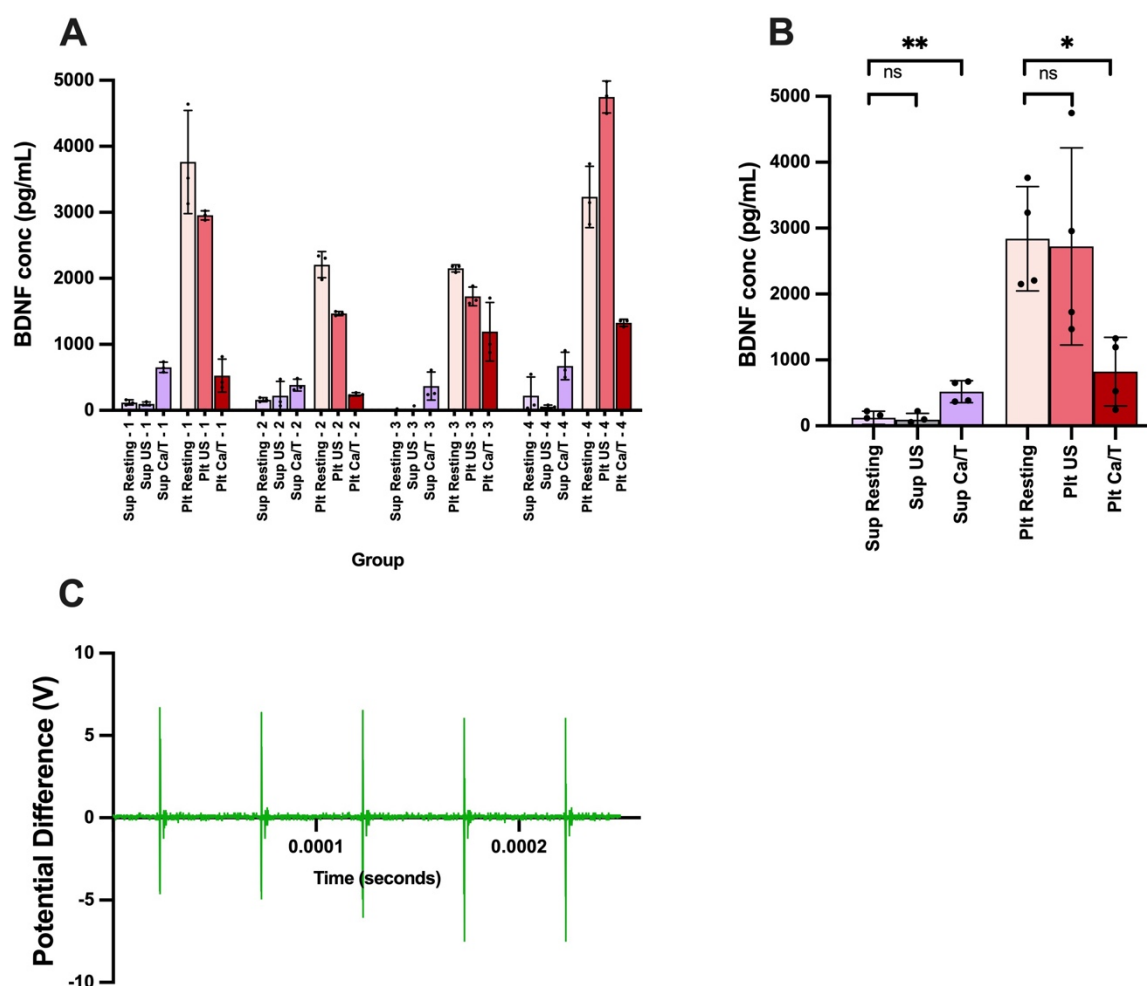


Figure 7.12: Exposure of rat platelets to ultrasound in vitro led to a decrease in the concentration of BDNF remaining within platelets in 3 of 4 samples

(A) Individual results of the BDNF ELISA for each sample. For each rat there was a resting sample (Resting), an ultrasounded sample (US) and a sample activated with calcium and thrombin (Sup Ca/T). After treatment, the supernatant (Sup) and lysed platelet pellet (Plt) were tested separately. **(B)** Mean BDNF concentration by group, Comparison of resting and ultrasounded samples - supernatant $p=0.565$ paired t test, platelet pellet $p=0.847$ paired t test. Comparison of resting and positive control (Ca/T) – supernatant $p=0.009$ paired t test, platelet pellet $p=0.023$ paired t test. **(C)** Oscilloscope readout of the ultrasound pulse delivered to the platelets.

7.5.4. Discussion

The experiment performed here was intended as a proof-of-concept and it would be premature to draw firm conclusions at this stage. Nevertheless, the results of this pilot experiment, while

preliminary, indicate a promising way forward to control the release of platelet stored BDNF. BDNF is obviously already known to be released during the course of platelet activation, together with a range of growth factors and cytokines (see Introduction), and 20kHz would be expected to produce the required physical effects needed to activate the platelets. While a minimal level of platelet activation may have been considered a negative result in the previous studies aiming at achieving haemostasis, it may be a desirable outcome for the intended application of ultrasound discussed here. The small decrease in BDNF in samples 1-3 is consistent with a small degree of platelet activation, leading to a partial release of BDNF from platelets. This raises the possibility of using small, targeted pulses of ultrasound to control the temporal and spatial parameters of BDNF release in humans. However, as a pilot experiment, the protocol used here was not sufficient to conclusively confirm that platelet activation had occurred and more investigations are needed.

Using the handheld probe means the ultrasound delivery may have been variable between samples. Future experiments should be completed in collaboration with a group with the engineering and technical experience in ultrasound required for a more accurate assessment. Ultrasound equipment with fine control over frequency, amplitude and subsequently energy delivered is required, as well as monitoring of the ultrasound waves delivered to the target and any changes in temperature. Additionally, this experiment was limited by the small volume of platelets available. Rats provided a much greater volume than mice, but it would be preferable to obtain human samples so that larger volumes can be used. The BDNF concentration in the supernatant was extremely low, and it was not possible to accurately determine if the BDNF decrease in the platelets would match the increase in the supernatant. Access to human platelets would increase the volume used and the number of samples. Performing a platelet count and standardising this between samples would also be essential for further studies. If higher platelet counts are used (achieved by adjustments in the volume of the buffer used to resuspend the platelets) BDNF may be more readily detectable in the supernatant. Finally, an assessment of the purity of the platelet preparation should be performed. While the previous assessments performed on this transgenic mouse model showed no evidence of significant expression of the BDNF construct in other blood cell types (discussed in Chapter 1.6), it would still be a requirement to ensure the quality of the platelet preparation and demonstrate the results were not influenced by other cell types.

Despite the limitations and provisional nature of this experiment, the findings are enough to support continued study of this concept. Further work will focus on exploring this concept in more depth and providing a detailed description of the ultrasound parameters, and resulting forces, required for optimal BDNF release.

Chapter 8. General Discussion

8.1. Main Findings

The principal findings reported in this thesis are that dendritic atrophy of lesioned RGCs was significantly reduced in a transgenic mouse model expressing BDNF in platelets, both in *ex vivo* and *in vivo* models. Furthermore, this reduction was of similar magnitude when compared with direct media supplementation of BDNF or the TrkB agonist, ZEB85, in the retinal explant model, as reported here and in previous studies.

Previous studies with this mouse model did not show evidence of expression of additional BDNF in other blood cell types (Section 1.6, Dingsdale et al., 2021). Additionally, the Cre-recombinase activity of the Pf4-associated Cre strain from Jackson Laboratory has been extensively investigated and found to be confined to megakaryocytes (Tiedt et al., 2007). In these studies, expression of Cre protein by Western blot was undetectable in tissue from spleen, thymus and brain. This was further investigated by crossing these mice with ROSA26-lacZ reporter mice, where expression of β -galactosidase is activated on Cre-mediate deletion of a premature polyadenylation signals. Staining samples with X-Gal could then be used to identify areas of Cre activity. Bone marrow cryosections showed that Cre activity was restricted to megakaryocytes, and was absent from other inspected organs. As the construct used in the B Cre⁺ transgenic mice is also inserted into the same *Rosa26* locus as the *ROSA26-lacZ* reporter, it is likely that expression is similarly specific to megakaryocytes. Furthermore, the difference between serum and plasma BDNF concentrations (approximately 20ng/mL and 2ng/mL respectively) is strong evidence that the BDNF is primarily contained within platelets, and released on activation. While BDNF expression has not been examined in the liver, spleen or other tissues, it is highly likely that platelets are the source of the additional BDNF in the B Cre⁺ mouse. Therefore, it is also highly likely that platelet-derived BDNF was responsible for the significant neuroprotective effect on damaged CNS neurons.

It is important to acknowledge that these findings were derived from acute and marked axonal injury, either by transection (retinal explants) or nerve crush. It is notable that the baseline RGC counts and dendritic arborisation were not different in B Cre⁺ mice. This may suggest that chronic exposure to low levels of BDNF during the lifetime of the animals may have led to desensitisation of the corresponding signalling pathways. The introduction of the acute

lesion created a new situation that then allowed the impact of the platelet BDNF to be revealed. Unfortunately, it turned out not to be possible to test the effect of platelet BDNF in a chronic ocular hypertensive model with a slower, more gradual deterioration in RGCs over a longer period as is known to occur in human glaucoma, owing to the difficulties of using the microbead model in mice.

8.2. Platelet BDNF in different species

These results suggest that in the mouse, platelet BDNF makes a significant contribution to the protection of lesioned CNS neurons, a conclusion based on the comparison made between WT littermates and Cre-expressing mice (see Methods), thus allowing causality to be firmly established, as well as the assumption that the additional BDNF was primarily expressed in platelets. As mice are widely used as experimental models in lesion of the nervous system, it would seem likely that whatever is reported would not take into consideration the potential neuroprotective effects of endogenous BDNF in humans and even in rats, a factor that is absent in WT mice. In this context it is interesting that in a well-established model of nerve lesion (facial nerve section), the number of motor neurons surviving in the facial nucleus is significantly higher in rats compared with mice (Sendtner et al., 1992). This work also demonstrated that recombinant BDNF applied to the lesioned axons of motoneurons prevented the death of these neurons.

More generally, there are considerable differences in the levels of serum BDNF across different species (see Figure 8.1, Table 8.1). At least in humans, rats and mice the origin of these differences could be traced to the presence or absence of significant transcription of the *BDNF* gene in megakaryocytes (Chacon-Fernandes et al., 2016). Humans have the highest mean serum BDNF concentrations of any species recorded (Naegelin et al., 2018b) and aside from the B Cre⁺ mouse, the next highest concentrations are found in other primates (Mori et al., 2003), with all species having mean concentrations relatively close to those seen in humans. A close examination of these results and of the corresponding genomic analyses also suggests that primates closer to humans tend to have BDNF serum concentrations closer to what is thought to be the norm in humans, in spite of considerable variations between single human individuals (Naegelin et al., 2018). Other mammals typically have serum BDNF concentrations around 10-20 times lower than primates, with rats at about 1-4 ng/mL, and pigs and dogs lower still. As discussed above, mouse serum BDNF had previously been described as undetectable with conventional BDNF ELISAs.

Table 8.1: Summary of published serum BDNF concentrations reported in different species

Mean serum BDNF concentration reported in the reference publication is provided, including the standard deviation (SD) and the number of samples included in the study.

Species	Mean serum BDNF conc (ng/mL)	SD	Number of samples	Reference
Human	32.69	8.33	259	Naegelin, 2018
BDNF Cre Mouse HOM	25.74	11.36	5	AW data
BDNF Cre Mouse HET	17.02	6.44	4	AW data
Japanese macaque (<i>Macaca fuscata</i>)	15.9	6.3	5	Mori, 2003
Common squirrel monkey (<i>Saimiri sciureus</i>)	13.4	1.7	2	Mori, 2003
Lar gibbon (<i>Hylobates lar</i>)	19.1	5.9	2	Mori, 2003
Bornean orangutan (<i>Pongo pygmaeus</i>)	20.4	0	1	Mori, 2003
Chimpanzee (<i>Pan troglodytes</i>)	18	7.9	9	Mori, 2003
Rat	1		5	Radka, 1997
Rat	1.25			Klein, 2011
Rat	2.985	0.372	8	Elfving, 2010
Rat	4.336	1.119	5	Karege, 2002
Dog	0.4		33	Moesta, 2019
Dog	0.1		9	Sechi, 2015
Pig	0.015		6	Rault, 2018
Pig (plasma)	0.994	0.186	12	Klein, 2011
Mouse	0.0067	0.0024	22	AW data

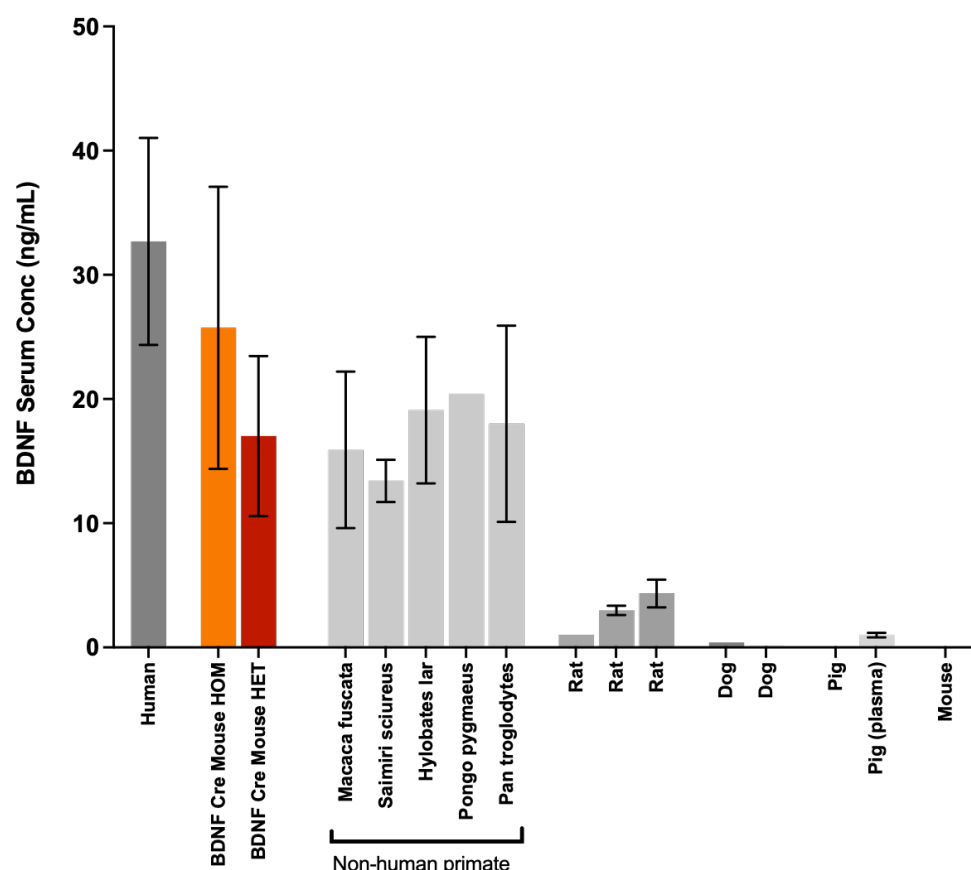


Figure 8.1: Serum BDNF concentrations reported in different species

These observations invite the speculation that the development of a larger source of circulating BDNF during the course of evolution may have been beneficial for long-lived species. Primates rely on a high degree of manual dexterity for climbing, grasping and gathering food in general. The necessarily complex behaviour of hunter/gatherers makes them more prone to limb injuries in particular and it is conceivable that the delivery at the site of injury of neuroprotectants such as BDNF may have favoured peripheral nerve regeneration. In the event of trauma, platelet activation would release BDNF and other platelet factors at the site of injury thereby promoting nerve regeneration. The notion that BDNF may have been optimised early during the course of evolution is supported by comparative genomic analyses: based on many hundred species, it turned out that the amino acid sequence encoding the mature BDNF protein is identical in all mammals analysed so far, with only small differences in more distant species (Götz et al., 1992). From this, it has been estimated that BDNF may have evolved as a result of gene duplication approximately 600 million years ago well before other neurotrophins such as NGF which shows, by comparison, more sequence variation between species.

8.3. BDNF access to the nervous system

The relationship between the CNS and peripherally derived BDNF has been extensively discussed in the context of a range of neurological disorders and the results in this thesis raise further questions regarding the observed correlations. Since the BBB presents an obstacle to the diffusion of proteins such as BDNF (Pardridge, W et al., 1994), it is important to consider that in lesion experiments, the BBB/BRB may not be intact, certainly not in the lesion models used here. In response to the lesion, blood platelets are bound to release their contents, including BDNF in the case of B Cre⁺ animals.

It is also important to consider that that platelet BDNF may also reach the nervous system in the absence of lesion. Platelets are known to be the major source of extracellular (or micro-) vesicles found in the blood, between 60 and 90% according to [Brisson et al., \(2017\)](#). The presence of BDNF in extracellular vesicles purified from human blood has already been demonstrated (Aatonen et al., 2014) and it is conceivable that such vesicles may help the delivery of BDNF through the BBB (discussed in Matsumoto et al., 2018). While there is no direct experimental evidence for this scenario, and in particular, no direct ultrastructural evidence, this possibility could be also investigated functionally. As it is conceivable that one of the consequences of physical exercise may be an increase formation of such platelet-derived extracellular vesicles and/or vesicles originated from younger platelets known to be released from the spleen as a result of increased activity of the sympathetic system, this mechanism could also explain the benefit of physical exercise. In the absence of ultrastructural data, the B Cre⁺ animals described in this study could be used before and after exercise and the levels of TrkB phosphorylation in structures such as the hippocampus compared with WT animals.

8.4. Clinical applications

Confirmation of BDNF movement across the BBB would also have significant implications for how BDNF could be delivered in the treatment of neurodegenerative conditions. The findings in the B Cre⁺ mice suggest that BDNF from platelets may be able to exert a neuroprotective effect on CNS neurons. However, as humans already contain equivalent levels of BDNF in platelets, the emphasis of further work should be on methods of increasing BDNF release from platelets in order to make these findings have clinical relevance. The hypothesis would be that humans have a baseline level of free, BDNF circulating under normal physiological conditions. If platelets could be stimulated to release additional BDNF from the platelet

reservoir then this increase in available BDNF may provide a neuroprotective effect, analogous to the effect seen in the B Cre⁺ mice. The key concept would be whether an increase from baseline of the BDNF (packaged in extracellular vesicles) from platelets could be beneficial, rather than an absolute presence or absence. However, the degree of any benefit would be substantially more work to determine.

From a clinical standpoint, the prescription of regular exercise is unlikely to be followed with useful adherence, especially in an elderly population that may have coexisting mobility issues. It is here that a targeted approach, such as ultrasound, that could be delivered in the clinic is more attractive. Further work is needed to define the optimal parameters required, but the results on ultrasound-stimulated release from platelets are a useful proof of concept that support further investigation in this area. The relevance of these findings is further supported by the promising results of many preclinical studies using platelet lysate in the treatment of neurodegenerative conditions (reviewed in [Burnouf et al., 2022](#); [Nebie et al., 2022](#)). Since the lysates contain a cocktail of platelet-derived factors from within the platelets, it is not clear which one, or combination of agents is responsible for this effect. But considering the neuroprotective effects of BDNF and the amount contained within platelets, it is certainly a potential candidate.

The successful action of the low-dose delivery of platelet-derived BDNF also prompts reflection on the administration of BDNF used in previous studies. Many studies have used BDNF concentrations that are far above those found under normal physiological conditions in the CNS (see Chapter 6.4). While these concentrations would likely achieve maximum activation of the TrkB pathway, they would increase TrkB downregulation and loss of the neuroprotective effects. Ateaque et al. (2022) have demonstrated that phosphorylation of TrkB following prolonged exposure to very low concentrations of BDNF (40 nM) can be recovered upon BDNF re-exposure at 24 hours, a recovery that is not possible with exposure to BDNF at 1 nM concentrations and higher. For extended use, BDNF may be most effective in repeated low doses rather than being present at sustained high concentrations. Small, controlled pulses of BDNF released from platelets by ultrasound could be an example of this principle.

8.5. Conclusion and outlook

The use of B Cre⁺ animals and comparisons with littermates lacking expression of BDNF in circulating platelets was strongly suggestive of a neuroprotective effect of a platelet-derived

growth factor in a lesion model. This work has implications for the use of mouse models and their limitations when the results are extrapolated to humans, given the absence of BDNF in WT mice. In future experiments it will be important to explore the role of BDNF-containing, platelet-derived extracellular vesicles in more depth. Such investigations could shed new light on the benefits of exercise and also support new strategies for developing and delivering BDNF-based treatments.

References

- Aatonen, M. T., Öhman, T., Nyman, T. A., Laitinen, S., Grönholm, M. and Siljander, P. R.-M. (2014) 'Isolation and characterization of platelet-derived extracellular vesicles.' *Journal of Extracellular Vesicles*, 3(1) p. 24692.
- Abu-Hassan, D., Ascott, T. and Kelley, M. (2014) 'The Trabecular Meshwork: A Basic Review of Form and Function.' *Journal of Ocular Biology*, 2(1).
- Aihara, M., Lindsey, J. D. and Weinreb, R. N. (2003) 'Aqueous Humor Dynamics in Mice.' *Investigative Ophthalmology & Visual Science*, 44(12) p. 5168.
- Almasieh, M., Wilson, A. M., Morquette, B., Cueva Vargas, J. L. and Di Polo, A. (2012) 'The molecular basis of retinal ganglion cell death in glaucoma.' *Progress in Retinal and Eye Research*, 31(2) pp. 152–181.
- Amin, M. C. I. M., Butt, A. M., Amjad, M. W. and Kesharwani, P. (2017) 'Polymeric Micelles for Drug Targeting and Delivery.' *In Nanotechnology-Based Approaches for Targeting and Delivery of Drugs and Genes*. Elsevier, pp. 167–202.
- An, J. J., Gharami, K., Liao, G.-Y., Woo, N. H., Lau, A. G., Vanevski, F., Torre, E. R., Jones, K. R., Feng, Y., Lu, B. and Xu, B. (2008) 'Distinct Role of Long 3' UTR BDNF mRNA in Spine Morphology and Synaptic Plasticity in Hippocampal Neurons.' *Cell*, 134(1) pp. 175–187.
- Anastasia, A. and Hempstead, B. L. (2013) 'BDNF function in health and disease.' *Nature Reviews Neuroscience* p. 1.
- Anderson, D. and Normal Tension Glaucoma Study (2003) 'Collaborative normal tension glaucoma study.' *Current Opinion in Ophthalmology*, 14(2) pp. 86–90.
- Anderson, S. R., Zhang, J., Steele, M. R., Romero, C. O., Kautzman, A. G., Schafer, D. P. and Vetter, M. L. (2019) 'Complement Targets Newborn Retinal Ganglion Cells for Phagocytic Elimination by Microglia.' *The Journal of Neuroscience*, 39(11) pp. 2025–2040.
- Ateaque, S. and Barde, Y.-A. (2021) 'A new molecular target for antidepressants.' *Cell Research*, 31(5) pp. 489–490.
- Ateaque, S., Merkouris, S., Wyatt, S., Allen, N. D., Xie, J., DiStefano, P. S., Lindsay, R. M. and Barde, Y. (2022) 'Selective activation and down-regulation of Trk receptors by neurotrophins in human neurons co-expressing TrkB and TrkC.' *Journal of Neurochemistry*, May, p. jnc.15617.
- Baaten, C. C. F. M. J., ten Cate, H., van der Meijden, P. E. J. and Heemskerk, J. W. M. (2017) 'Platelet populations and priming in hematological diseases.' *Blood Reviews*, 31(6) pp. 389–399.
- Baden, T., Euler, T. and Berens, P. (2020) 'Understanding the retinal basis of vision across species.' *Nature Reviews Neuroscience*, 21(1) pp. 5–20.

Bai, Y., Dergham, P., Nedev, H., Xu, J., Galan, A., Rivera, J. C., ZhiHua, S., Mehta, H. M., Woo, S. B., Sarunic, M. V., Neet, K. E. and Saragovi, H. U. (2010) 'Chronic and Acute Models of Retinal Neurodegeneration TrkA Activity Are Neuroprotective whereas p75NTR Activity Is Neurotoxic through a Paracrine Mechanism.' *Journal of Biological Chemistry*, 285(50) pp. 39392–39400.

Bai, Y., Xu, J., Brahimi, F., Zhuo, Y., Sarunic, M. V. and Saragovi, H. U. (2010) 'An Agonistic TrkB mAb Causes Sustained TrkB Activation, Delays RGC Death, and Protects the Retinal Structure in Optic Nerve Axotomy and in Glaucoma.' *Investigative Ophthalmology & Visual Science*, 51(9) p. 4722.

Baird, J. F., Gaughan, M. E., Saffer, H. M., Sarzynski, M. A., Herter, T. M., Fritz, S. L., den Ouden, D. B. and Stewart, J. C. (2018) 'The effect of energy-matched exercise intensity on brain-derived neurotrophic factor and motor learning.' *Neurobiology of Learning and Memory*, 156, December, pp. 33–44.

Bamji, S. X., Majdan, M., Pozniak, C. D., Belliveau, D. J., Aloyz, R., Kohn, J., Causing, C. G. and Miller, F. D. (1998) 'The p75 Neurotrophin Receptor Mediates Neuronal Apoptosis and Is Essential for Naturally Occurring Sympathetic Neuron Death.' *Journal of Cell Biology*, 140(4) pp. 911–923.

Barde, Y. A., Edgar, D. and Thoenen, H. (1982a) 'Purification of a new neurotrophic factor from mammalian brain.' *The EMBO Journal*, 1(5) pp. 549–553.

Barde, Y. A., Edgar, D. and Thoenen, H. (1982b) 'Purification of a new neurotrophic factor from mammalian brain.' *The EMBO Journal*, 1(5) pp. 549–553.

Bathina, S. and Das, U. N. (2015) 'Brain-derived neurotrophic factor and its clinical implications.' *Archives of Medical Science*, 6 pp. 1164–1178.

Baxter, G. T., Radeke, M. J., Kuo, R. C., Makrides, V., Hinkle, B., Hoang, R., Medina-Selby, A., Coit, D., Valenzuela, P. and Feinstein, S. C. (1997) 'Signal Transduction Mediated by the Truncated trkB Receptor Isoforms, trkB.T1 and trkB.T2.' *The Journal of Neuroscience*, 17(8) pp. 2683–2690.

Belforte, N., Agostinone, J., Alarcon-Martinez, L., Villafranca-Baughman, D., Dotigny, F., Cueva Vargas, J. L. and Di Polo, A. (2021) 'AMPK hyperactivation promotes dendrite retraction, synaptic loss, and neuronal dysfunction in glaucoma.' *Molecular Neurodegeneration*, 16(1) p. 43.

Bennett, J. L., Zeiler, S. R. and Jones, K. R. (1999) 'Patterned Expression of BDNF and NT-3 in the Retina and Anterior Segment of the Developing Mammalian Eye,' 40(12) p. 10.

Best, M. G., Vancura, A. and Wurdinger, T. (2017) 'Platelet RNA as a circulating biomarker trove for cancer diagnostics.' *Journal of Thrombosis and Haemostasis*, 15(7) pp. 1295–1306.

Bevan, R. J., Hughes, T. R., Williams, P. A., Good, M. A., Morgan, B. P. and Morgan, J. E. (2020) 'Retinal ganglion cell degeneration correlates with hippocampal spine loss in experimental Alzheimer's disease.' *Acta Neuropathologica Communications*, 8(1) p. 216.

-
- Bhide, P. and Frost, D. (1991) 'Stages of growth of hamster retinofugal axons: implications for developing axonal pathways with multiple targets.' *The Journal of Neuroscience*, 11(2) pp. 485–504.
- Binley, K. E., Ng, W. S., Barde, Y.-A., Song, B. and Morgan, J. E. (2016a) 'Brain-derived neurotrophic factor prevents dendritic retraction of adult mouse retinal ganglion cells.' Kirik, D. (ed.) *European Journal of Neuroscience*, 44, July, pp. 2028–2039.
- Binley, K. E., Ng, W. S., Barde, Y.-A., Song, B. and Morgan, J. E. (2016b) 'Brain-derived neurotrophic factor prevents dendritic retraction of adult mouse retinal ganglion cells.' Kirik, D. (ed.) *European Journal of Neuroscience*, 44, July, pp. 2028–2039.
- Bland, J. M. and Kerry, S. M. (1998) 'Weighted comparison of means.' *BMJ*, 316(7125) pp. 129–129.
- Brady, R., Zaidi, S. I. A., Mayer, C. and Katz, D. M. (1999) 'BDNF Is a Target-Derived Survival Factor for Arterial Baroreceptor and Chemoafferent Primary Sensory Neurons.' *The Journal of Neuroscience*, 19(6) pp. 2131–2142.
- Brisson, A. R., Tan, S., Linares, R., Gounou, C. and Arraud, N. (2017) 'Extracellular vesicles from activated platelets: a semiquantitative cryo-electron microscopy and immuno-gold labeling study.' *Platelets*, 28(3) pp. 263–271.
- Brubaker, R. F. (1991) 'Flow of Aqueous Humor in Humans,' (13) December, p. 22.
- Bueker, E. D. (1948) 'Implantation of tumors in the hind limb field of the embryonic chick and the developmental response of the lumbosacral nervous system.' *The Anatomical Record*, 102(3) pp. 369–389.
- Bueller, J. A., Aftab, M., Sen, S., Gomez-Hassan, D., Burmeister, M. and Zubieta, J.-K. (2006) 'BDNF Val66Met Allele Is Associated with Reduced Hippocampal Volume in Healthy Subjects.' *Biological Psychiatry*, 59(9) pp. 812–815.
- Bull, N. D., Johnson, T. V., Welsapar, G., DeKorver, N. W., Tomarev, S. I. and Martin, K. R. (2011) 'Use of an Adult Rat Retinal Explant Model for Screening of Potential Retinal Ganglion Cell Neuroprotective Therapies.' *Investigative Ophthalmology & Visual Science*, 52(6) p. 3309.
- Burnouf, T. and Walker, T. L. (2022) 'The multifaceted role of platelets in mediating brain function.' *Blood*, 140(8) pp. 815–827.
- Cabral, H. and Kataoka, K. (2014) 'Progress of drug-loaded polymeric micelles into clinical studies.' *Journal of Controlled Release*, 190, September, pp. 465–476.
- Cajal, R. y (1893) 'La rétine des vertébrés.' *La Cellule*, 9 pp. 119–257.
- Caldeira, M. V., Melo, C. V., Pereira, D. B., Carvalho, R., Correia, S. S., Backos, D. S., Carvalho, A. L., Esteban, J. A. and Duarte, C. B. (2007) 'Brain-derived Neurotrophic Factor Regulates the Expression and Synaptic Delivery of α -Amino-3-hydroxy-5-methyl-4-isoxazole Propionic Acid Receptor Subunits in Hippocampal Neurons.' *Journal of Biological Chemistry*, 282(17) pp. 12619–12628.

Cameron, E., Xia, X., Galvao, J., Ashouri, M., Kapiloff, M. and Goldberg, J. (2020) 'Optic Nerve Crush in Mice to Study Retinal Ganglion Cell Survival and Regeneration.' *BIO-PROTOCOL*, 10(6).

Caracciolo, L., Marosi, M., Mazzitelli, J., Latifi, S., Sano, Y., Galvan, L., Kawaguchi, R., Holley, S., Levine, M. S., Coppola, G., Portera-Cailliau, C., Silva, A. J. and Carmichael, S. T. (2018) 'CREB controls cortical circuit plasticity and functional recovery after stroke.' *Nature Communications*, 9(1) p. 2250.

Carter, B. D., Zirrgiebel, U. and Barde, Y.-A. (1995) 'Differential Regulation of p21^{ras} Activation in Neurons by Nerve Growth Factor and Brain-derived Neurotrophic Factor.' *Journal of Biological Chemistry*, 270(37) pp. 21751–21757.

Casarotto, P. C., Giryck, M., Fred, S. M., Kovaleva, V., Moliner, R., Enkavi, G., Biojone, C., Cannarozzo, C., Sahu, M. P., Kaurinkoski, K., Brunello, C. A., Steinzeig, A., Winkel, F., Patil, S., Vestring, S., Serchov, T., Diniz, C. R. A. F., Laukkanen, L., Cardon, I., Antila, H., Rog, T., Piepponen, T. P., Bramham, C. R., Normann, C., Lauri, S. E., Saarma, M., Vattulainen, I. and Castrén, E. (2021) 'Antidepressant drugs act by directly binding to TRKB neurotrophin receptors.' *Cell*, 184(5) pp. 1299-1313.e19.

Cellerino, A., Carroll, P., Thoenen, H. and Barde, Y.-A. (1997) 'Reduced Size of Retinal Ganglion Cell Axons and Hypomyelination in Mice Lacking Brain-Derived Neurotrophic Factor.' *Molecular and Cellular Neuroscience*, 9(5–6) pp. 397–408.

Cepko, C. (2014) 'Intrinsically different retinal progenitor cells produce specific types of progeny.' *Nature Reviews Neuroscience*, 15(9) pp. 615–627.

Chacón-Fernández, P., Säuberli, K., Colzani, M., Moreau, T., Ghevaert, C. and Barde, Y.-A. (2016) 'Brain-derived Neurotrophic Factor in Megakaryocytes.' *Journal of Biological Chemistry*, 291(19) pp. 9872–9881.

Chalupa, Leo and Williams, Robert (2008) *Eye, Retina, and Visual System of The Mouse*. MIT Press.

Chang, L. K., Putcha, G. V., Deshmukh, M. and Johnson, E. M. (2002) 'Mitochondrial involvement in the point of no return in neuronal apoptosis.' *Biochimie*, 84(2–3) pp. 223–231.

Chater, B. and Williams, A. (1977) 'Platelet Aggregation Induced in Vitro by Therapeutic Ultrasound.' *Thromb Haemost.*, 38(03) pp. 0640–0651.

Chen, H. and Weber, A. J. (2001) 'BDNF Enhances Retinal Ganglion Cell Survival in Cats with Optic Nerve Damage,' 42(5) p. 9.

Choi, V., Rajora, M. A. and Zheng, G. (2020a) 'Activating Drugs with Sound: Mechanisms Behind Sonodynamic Therapy and the Role of Nanomedicine.' *Bioconjugate Chemistry*, 31(4) pp. 967–989.

-
- Choi, V., Rajora, M. A. and Zheng, G. (2020b) 'Activating Drugs with Sound: Mechanisms Behind Sonodynamic Therapy and the Role of Nanomedicine.' *Bioconjugate Chemistry*, March, p. acs.bioconjchem.0c00029.
- Chou, T.-H., Park, K. K., Luo, X. and Porciatti, V. (2013) 'Retrograde Signaling in the Optic Nerve Is Necessary for Electrical Responsiveness of Retinal Ganglion Cells.' *Investigative Ophthalmology & Visual Science*, 54(2) p. 1236.
- Ciammola, A., Sassone, J., Cannella, M., Calza, S., Poletti, B., Frati, L., Squitieri, F. and Silani, V. (2007) 'Low brain-derived neurotrophic factor (BDNF) levels in serum of Huntington's disease patients.' *American Journal of Medical Genetics Part B: Neuropsychiatric Genetics*, 144B(4) pp. 574–577.
- Ciferri, S., Emiliani, C., Guglielmini, G. and Orlacchio, A. (2000) 'Platelets release their lysosomal content in vivo in humans upon activation.' *Thromb Haemost.*, 83(1) pp. 157–64.
- Clawson, C. C., Rao, G. H. R. and White, J. G. (1975) 'Platelet Interaction With Bacteria.' *American Journal of Pathology*, 81(2) p. 10.
- Cohen, S. (1960) 'Purification of a nerve-growth promoting protein from the mouse salivary gland and its neuro-cytotoxic antiserum.' *Proceedings of the National Academy of Sciences*, 46(3) pp. 302–311.
- Cohen-Cory, S. and Fraser, S. E. (1995) 'Effects of brain-derived neurotrophic factor on optic axon branching and remodelling in vivo.' *Nature*, 378(6553) pp. 192–196.
- Cone, F. E., Gelman, S. E., Son, J. L., Pease, M. E. and Quigley, H. A. (2010) 'Differential susceptibility to experimental glaucoma among 3 mouse strains using bead and viscoelastic injection.' *Experimental Eye Research*, 91(3) pp. 415–424.
- Cone, F. E., Steinhart, M. R., Oglesby, E. N., Kalesnykas, G., Pease, M. E. and Quigley, H. A. (2012) 'The effects of anesthesia, mouse strain and age on intraocular pressure and an improved murine model of experimental glaucoma.' *Experimental Eye Research*, 99, June, pp. 27–35.
- Coppinger, J. A., O'Connor, R., Wynne, K., Flanagan, M., Sullivan, M., Maguire, P. B., Fitzgerald, D. J. and Cagney, G. (2007) 'Moderation of the platelet releasate response by aspirin.' *Blood*, 109(11) pp. 4786–4792.
- Crawley, L., Zamir, S. M., Cordeiro, M. F. and Guo, L. (2012) 'Clinical Options for the Reduction of Elevated Intraocular Pressure.' *Ophthalmology and Eye Diseases*, 4, January, p. OED.S4909.
- Creel, D. and Wiikop, C. J. (1974) 'Asymmetric visually evoked potentials in human albinos: evidence for visual system anomalies,' 13 p. 11.
- Croll, S. D., Chesnutt, C. R., Rudge, J. S., Acheson, A., Ryan, T. E., Siuciak, J. A., DiStefano, P. S., Wiegand, S. J. and Lindsay, R. M. (1998) 'Co-infusion with a TrkB-Fc Receptor Body Carrier

Enhances BDNF Distribution in the Adult Rat Brain.’ *Experimental Neurology*, 152(1) pp. 20–33.

Daniel, S., Clark, A. and McDowell, C. (2018) ‘Subtype-specific response of retinal ganglion cells to optic nerve crush.’ *Cell Death Discovery*, 4(1) p. 67.

Dargusch, R., Piasecki, D., Tan, S., Liu, Y. and Schubert, D. (2008) ‘The role of Bax in glutamate-induced nerve cell death: Bax and nerve cell death.’ *Journal of Neurochemistry*, 76(1) pp. 295–301.

Davies, A. M., Thoenen, H. and Barde, Y.-A. (1986) ‘Different factors from the central nervous system and periphery regulate the survival of sensory neurones.’ *Nature*, 319(6053) pp. 497–499.

De Moraes, C. G., John, S. W. M., Williams, P. A., Blumberg, D. M., Cioffi, G. A. and Liebmann, J. M. (2022) ‘Nicotinamide and Pyruvate for Neuroenhancement in Open-Angle Glaucoma: A Phase 2 Randomized Clinical Trial.’ *JAMA Ophthalmology*, 140(1) p. 11.

Dengler-Crish, C. M., Smith, M. A., Inman, D. M., Wilson, G. N., Young, J. W. and Crish, S. D. (2014) ‘Anterograde transport blockade precedes deficits in retrograde transport in the visual projection of the DBA/2J mouse model of glaucoma.’ *Frontiers in Neuroscience*, 8, September, p. 290.

Dhani, S., Zhao, Y. and Zhivotovsky, B. (2021) ‘A long way to go: caspase inhibitors in clinical use.’ *Cell Death & Disease*, 12(10) p. 949.

Di Polo, A., Aigner, L. J., Dunn, R. J., Bray, G. M. and Aguayo, A. J. (1998) ‘Prolonged delivery of brain-derived neurotrophic factor by adenovirus-infected Muller cells temporarily rescues injured retinal ganglion cells.’ *Proceedings of the National Academy of Sciences*, 95(7) pp. 3978–3983.

Díaz-Coránguez, M., Ramos, C. and Antonetti, D. A. (2017) ‘The inner blood-retinal barrier: Cellular basis and development.’ *Vision Research*, 139, October, pp. 123–137.

Dieni, S., Matsumoto, T., Dekkers, M., Rauskolb, S., Ionescu, M. S., Deogracias, R., Gundelfinger, E. D., Kojima, M., Nestel, S., Frotscher, M. and Barde, Y.-A. (2012) ‘BDNF and its pro-peptide are stored in presynaptic dense core vesicles in brain neurons.’ *Journal of Cell Biology*, 196(6) pp. 775–788.

Dingsdale, H., Nan, X., Garay, S. M., Mueller, A., Sumption, L. A., Chacón-Fernández, P., Martinez-Garay, I., Ghevaert, C., Barde, Y.-A. and John, R. M. (2021a) ‘The placenta protects the fetal circulation from anxiety-driven elevations in maternal serum levels of brain-derived neurotrophic factor.’ *Translational Psychiatry*, 11(1) p. 62.

Dingsdale, H., Nan, X., Garay, S. M., Mueller, A., Sumption, L. A., Chacón-Fernández, P., Martinez-Garay, I., Ghevaert, C., Barde, Y.-A. and John, R. M. (2021b) ‘The placenta protects the fetal circulation from anxiety-driven elevations in maternal serum levels of brain-derived neurotrophic factor.’ *Translational Psychiatry*, 11(1) p. 62.

Dinoff, A., Herrmann, N., Swardfager, W. and Lanctôt, K. L. (2017) 'The effect of acute exercise on blood concentrations of brain-derived neurotrophic factor in healthy adults: a meta-analysis.' Foxe, J. (ed.) *European Journal of Neuroscience*, 46(1) pp. 1635–1646.

Dinoff, A., Herrmann, N., Swardfager, W., Liu, C. S., Sherman, C., Chan, S. and Lanctôt, K. L. (2016) 'The Effect of Exercise Training on Resting Concentrations of Peripheral Brain-Derived Neurotrophic Factor (BDNF): A Meta-Analysis.' Hills, R. K. (ed.) *PLOS ONE*, 11(9) p. e0163037.

Domenici, L., Origlia, N., Falsini, B., Cerri, E., Barloscio, D., Fabiani, C., Sansò, M. and Giovannini, L. (2014) 'Rescue of Retinal Function by BDNF in a Mouse Model of Glaucoma.' Barnes, S. (ed.) *PLoS ONE*, 9(12) p. e115579.

Drager, U. C. and Olsen, J. F. (1981) 'Ganglion cell distribution in the retina of the mouse,' 20(3) p. 9.

Drum, K., Forbed, M., Wang, S. and Johnson, J. (1996) 'Treatment with BDNF does not prevent normal chick retinal ganglion cell in ovo.' *Soc Neurosci Abstr*, 22 p. 998.

Egan, M. F., Kojima, M., Callicott, J. H., Goldberg, T. E., Kolachana, B. S., Bertolino, A., Zaitsev, E., Gold, B., Goldman, D., Dean, M., Lu, B. and Weinberger, D. R. (2003) 'The BDNF val66met Polymorphism Affects Activity-Dependent Secretion of BDNF and Human Memory and Hippocampal Function.' *Cell*, 112(2) pp. 257–269.

Ellis, E. M., Gauthier, G., Sivyer, B. and Murphy, G. J. (2016) 'Shared and distinct retinal input to the mouse superior colliculus and dorsal lateral geniculate nucleus.' *Journal of Neurophysiology*, 116(2) pp. 602–610.

Erickson, J. T., Conover, J. C., Borday, V., Champagnat, J., Barbacid, M., Yancopoulos, G. and Katz, D. M. (1996) 'Mice Lacking Brain-Derived Neurotrophic Factor Exhibit Visceral Sensory Neuron Losses Distinct from Mice Lacking NT4 and Display a Severe Developmental Deficit in Control of Breathing.' *The Journal of Neuroscience*, 16(17) pp. 5361–5371.

Ernfors, P., Lee, K.-F. and Jaenisch, R. (1994) 'Mice lacking brain-derived neurotrophic factor develop with sensory deficits.' *Nature*, 368(6467) pp. 147–150.

Esposito, D., Patel, P., Stephens, R., Perez, P., Chao, M., Kaplan, D. and Hempstead, B. L. (2001) 'The Cytoplasmic and transmembrane Domains of the p75 and TrkA receptors regulate high affinity binding to Nerve Growth Factor.' *Journal of Biological Chemistry*, 276(35) pp. 32687–32695.

Estevez, B. and Du, X. (2017) 'New Concepts and Mechanisms of Platelet Activation Signaling.' *Physiology*, 32(2) pp. 162–177.

Fang, J., Wang, X., Xu, Z. and Jiang, F. (2010) 'Neuroprotective effects of bis(7)-tacrine against glutamate-induced retinal ganglion cells damage.' *BMC Neuroscience*, 11(1) p. 31.

-
- Faul, F., Erdfelder, E., Lang, A.-G. and Buchner, A. (2007) 'G*Power 3: A flexible statistical power analysis program for the social, behavioral, and biomedical sciences.' *Behavior Research Methods*, 39(2) pp. 175–191.
- Fernandes, K. A., Harder, J. M., Fornarola, L. B., Freeman, R. S., Clark, A. F., Pang, I.-H., John, S. W. M. and Libby, R. T. (2012) 'JNK2 and JNK3 are major regulators of axonal injury-induced retinal ganglion cell death.' *Neurobiology of Disease*, 46(2) pp. 393–401.
- Flynn, T. H., Mitchison, N. A., Ono, S. J. and Larkin, D. F. P. (2008) 'Aqueous Humor Alloreactive Cell Phenotypes, Cytokines and Chemokines in Corneal Allograft Rejection: Aqueous Humor Alloreactive Cell.' *American Journal of Transplantation*, 8(7) pp. 1537–1543.
- Forti, L. N., Njemini, R., Beyer, I., Eelbode, E., Meeusen, R., Mets, T. and Bautmans, I. (2014) 'Strength training reduces circulating interleukin-6 but not brain-derived neurotrophic factor in community-dwelling elderly individuals.' *AGE*, 36(5) p. 9704.
- Frank, L., Ventimiglia, R., Anderson, K., Lindsay, R. M. and Rudge, J. S. (1996) 'BDNF Down-regulates Neurotrophin Responsiveness, TrkB Protein and TrkB mRNA Levels in Cultured Rat Hippocampal Neurons.' *European Journal of Neuroscience*, 8(6) pp. 1220–1230.
- Frankfort, B. J., Khan, A. K., Tse, D. Y., Chung, I., Pang, J.-J., Yang, Z., Gross, R. L. and Wu, S. M. (2013) 'Elevated Intraocular Pressure Causes Inner Retinal Dysfunction Before Cell Loss in a Mouse Model of Experimental Glaucoma.' *Investigative Ophthalmology & Visual Science*, 54(1) p. 762.
- Frost, D. O., Ma, Y.-T., Hsieh, T., Forbes, M. E. and Johnson, J. E. (2001) 'Developmental changes in BDNF protein levels in the hamster retina and superior colliculus.' *Journal of Neurobiology*, 49(3) pp. 173–187.
- Fujieda, H. and Sasaki, H. (2008) 'Expression of brain-derived neurotrophic factor in cholinergic and dopaminergic amacrine cells in the rat retina and the effects of constant light rearing.' *Experimental Eye Research*, 86(2) pp. 335–343.
- Fujimura, H., Altar, C., Chen, R., Nakamura, T., Nakahashi, T., Kambayashi, J., Sun, B. and Tandon, N. (2002) 'Brain-derived Neurotrophic Factor Is Stored in Human Platelets and Released by Agonist Stimulation.' *Thrombosis and Haemostasis*, 87(04) pp. 728–734.
- Fujimura, Hironobu, Altar, Anthony, Chen, Ruoyan, Nakamura, Takashi, Nakahashi, Takeshi, Kambayahsi, Jun-ichi, Sun, Bing, and Tandon, Narendra N. (2002) 'Brain-derived Neurotrophic Factor is Stored in Human Platelets and Released by Agonist Stimulation.' *Thromb Haemost*, 87(04) pp. 728–734.
- Fukuda, T., Asou, E., Nogi, K. and Goto, K. (2017) 'Evaluation of mouse red blood cell and platelet counting with an automated hematology analyzer.' *Journal of Veterinary Medical Science*, 79(10) pp. 1707–1711.
- Fulgenzi, G., Hong, Z., Tomassoni-Ardori, F., Barella, L. F., Becker, J., Barrick, C., Swing, D., Yanpallewar, S., Croix, B. S., Wess, J., Gavrilova, O. and Tessarollo, L. (2020) 'Novel metabolic role for BDNF in pancreatic β -cell insulin secretion.' *Nature Communications*, 11(1) p. 1950.

-
- Gaese, F., Kolbeck, R. and Barde, Y.-A. (1994) 'Sensory ganglia require neurotrophin-3 early in development.' *Development*, 120(6) pp. 1613–9.
- Gao, H., Qiao, X., Hefti, F., Hollyfield, J. G. and Knusel, B. (1997) 'Elevated mRNA Expression of Brain-Derived Neurotrophic Factor in Retinal Ganglion Cell Layer After Optic Nerve Injury.' *Investigative Ophthalmology*, 38(9) p. 8.
- García, M., Forster, V., Hicks, D. and Vecino, E. (2003) 'In Vivo Expression of Neurotrophins and Neurotrophin Receptors Is Conserved in Adult Porcine Retina In Vitro.' *Investigative Ophthalmology & Visual Science*, 44(10) p. 4532.
- Ghaffariyeh, A., Honarpisheh, N., Heidari, M. H., Puyan, S. and Abasov, F. (2011) 'Brain-Derived Neurotrophic Factor as a Biomarker in Primary Open-Angle Glaucoma.' *Optometry and Vision Science*, 88(1) pp. 80–85.
- Gilder, M., Ramsbottom, R., Currie, J., Sheridan, B. and Nevill, A. M. (2014) 'Effect of fat free mass on serum and plasma BDNF concentrations during exercise and recovery in healthy young men.' *Neuroscience Letters*, 560, February, pp. 137–141.
- Gilley, J., Adalbert, R., Yu, G. and Coleman, M. P. (2013) 'Rescue of Peripheral and CNS Axon Defects in Mice Lacking NMNAT2.' *Journal of Neuroscience*, 33(33) pp. 13410–13424.
- Gogate, P. R. and Kabadi, A. M. (2009) 'A review of applications of cavitation in biochemical engineering/biotechnology.' *Biochemical Engineering Journal*, 44(1) pp. 60–72.
- Gomes, A., Correia, S. S., Carvalho, A. L. and Duarte, C. B. (2003) 'Regulation of AMPA receptor activity, synaptic targeting and recycling: role in synaptic plasticity.' *Neurochem Res.*, 28(10) pp. 1459–73.
- Gorski, J. A., Zeiler, S. R., Tamowski, S. and Jones, K. R. (2003) 'Brain-Derived Neurotrophic Factor Is Required for the Maintenance of Cortical Dendrites.' *The Journal of Neuroscience*, 23(17) pp. 6856–6865.
- Götz, R., Raulf, F. and Scharf, M. (1992) 'Brain-Derived Neurotrophic Factor Is More Highly Conserved in Structure and Function than Nerve Growth Factor During Vertebrate Evolution.' *Journal of Neurochemistry*, 59(2) pp. 432–442.
- Gremmel, T., Frelinger, A. and Michelson, A. (2016) 'Platelet Physiology.' *Seminars in Thrombosis and Hemostasis*, 42(03) pp. 191–204.
- Grozdanic, S. D., Betts, D. M., Sakaguchi, D. S., Allbaugh, R. A., Kwon, Y. H. and Kardon, R. H. (2003) 'Laser-Induced Mouse Model of Chronic Ocular Hypertension.' *Investigative Ophthalmology & Visual Science*, 44(10) p. 4337.
- Guillery, R. W., Okoro, A. N. and Witkop, C. J. (1975) 'Abnormal visual pathways in the brain of a human albino.' *Brain Research*, 96(2) pp. 373–377.
- Hallböök, F., Ibáñez, C. F. and Persson, H. (1991) 'Evolutionary studies of the nerve growth factor family reveal a novel member abundantly expressed in xenopus ovary.' *Neuron*, 6(5) pp. 845–858.

Hamburger, V., Brunso-Bechtold, J. and Yip, J. (1981) 'Neuronal death in the spinal ganglia of the chick embryo and its reduction by nerve growth factor.' *The Journal of Neuroscience*, 1(1) pp. 60–71.

Harada, T., Harada, C., Nakamura, K., Quah, H.-M. A., Okumura, A., Namekata, K., Saeki, T., Aihara, M., Yoshida, H., Mitani, A. and Tanaka, K. (2007) 'The potential role of glutamate transporters in the pathogenesis of normal tension glaucoma.' *Journal of Clinical Investigation*, 117(7) pp. 1763–1770.

Hare, W. A., WoldeMussie, E., Lai, R. K., Ton, H., Ruiz, G., Chun, T. and Wheeler, L. (2004) 'Efficacy and Safety of Memantine Treatment for Reduction of Changes Associated with Experimental Glaucoma in Monkey, I: Functional Measures.' *Investigative Ophthalmology & Visual Science*, 45(8) p. 2625.

Hartwig, J. H. (1992) 'Mechanisms of actin rearrangements mediating platelet activation.' *Journal of Cell Biology*, 118(6) pp. 1421–1442.

Heijl, A., Leske, C., Bengtsson, Bo, Hyman, L., Bengtsson, Boel and Hussein, M. (2002) 'Reduction of Intraocular Pressure and Glaucoma Progression: Results From the Early Manifest Glaucoma Trial.' *ARCH OPHTHALMOL*, 120 p. 12.

Heijnen, H. F. G., Debili, N., Vainchencker, W., Breton-Gorius, J., Geuze, H. J. and Sixma, J. J. (1998) 'Multivesicular Bodies Are an Intermediate Stage in the Formation of Platelet α -Granules.' *Blood*, 91(7) pp. 2313–2325.

Henneberger, C., Jüttner, R., Rothe, T. and Grantyn, R. (2002) 'Postsynaptic Action of BDNF on GABAergic Synaptic Transmission in the Superficial Layers of the Mouse Superior Colliculus.' *Journal of Neurophysiology*, 88(2) pp. 595–603.

Hofer, M. M. and Barde, Y.-A. (1988) 'Brain-derived neurotrophic factor prevents neuronal death in vivo.' *Nature*, 331(6153) pp. 261–262.

Hohn, A., Leibrock, J., Bailey, K. and Barde, Y.-A. (1990) 'Identification and characterization of a novel member of the nerve growth factor/brain-derived neurotrophic factor family.' *Nature*, 344(6264) pp. 339–341.

Hong, E. J., McCord, A. E. and Greenberg, M. E. (2008) 'A Biological Function for the Neuronal Activity-Dependent Component of Bdnf Transcription in the Development of Cortical Inhibition.' *Neuron*, 60(4) pp. 610–624.

Honig, M. G. and Hume, R. I. (1986) 'Fluorescent carbocyanine dyes allow living neurons of identified origin to be studied in long-term cultures.' *Journal of Cell Biology*, 103(1) pp. 171–187.

Howell, G. R., Libby, R. T., Jakobs, T. C., Smith, R. S., Phalan, F. C., Barter, J. W., Barbay, J. M., Marchant, J. K., Mahesh, N., Porciatti, V., Whitmore, A. V., Masland, R. H. and John, S. W. M. (2007) 'Axons of retinal ganglion cells are insulted in the optic nerve early in DBA/2J glaucoma.' *Journal of Cell Biology*, 179(7) pp. 1523–1537.

Huang, W., Fileta, J., Guo, Y. and Grosskreutz, C. L. (2006) 'Downregulation of Thy1 in Retinal Ganglion Cells in Experimental Glaucoma.' *Current Eye Research*, 31(3) pp. 265–271.

Hughes, A. (1979) 'A schematic eye for the rat.' *Vision Research*, 19(5) pp. 569–588.

Husseini, G. A. and Pitt, W. G. (2009) 'Ultrasonic-Activated Micellar Drug Delivery for Cancer Treatment.' *Journal of Pharmaceutical Sciences*, 98(3) pp. 795–811.

Husseini, G. A., Rapoport, N. Y., Christensen, D. A., Pruitt, J. D. and Pitt, W. G. (2002) 'Kinetics of ultrasonic release of doxorubicin from pluronic P105 micelles.' *Colloids and Surfaces B: Biointerfaces*, 24(3–4) pp. 253–264.

Igarashi, Tsutomu, Miyake, K., Kobayashi, M., Kameya, S., Fujimoto, C., Takahashi, Hisatomo, Igarashi, Toru, Miyake, N., Iijima, O., Hirai, Y., Okada, T. and Takahashi, Hiroshi (2016) 'Tyrosine triple mutated AAV2-BDNF gene therapy in a rat model of transient IOP elevation.' *Molecular Vision*, 22 pp. 816–826.

Igarashi, Tsutomu, Nakamoto, K., Kobayashi, M., Suzuki, H., Arima, T., Tobita, Y., Takao, K., Igarashi, Toru, Okuda, T., Okada, T. and Takahashi, H. (2021) 'Brain-derived Neurotrophic Factor in the Aqueous Humor of Glaucoma Patients.' *Journal of Nippon Medical School*, 88(2) pp. 128–132.

Igarashi, Tsutomu, Nakamoto, K., Kobayashi, M., Suzuki, H., Tobita, Y., Igarashi, Toru, Okuda, T., Okada, T. and Takahashi, H. (2020) 'Serum brain-derived neurotrophic factor in glaucoma patients in Japan: An observational study.' *Journal of Nippon Medical School*.

Inman, D. M. and Harun-Or-Rashid, M. (2017) 'Metabolic Vulnerability in the Neurodegenerative Disease Glaucoma.' *Frontiers in Neuroscience*, 11, March.

Intlekofer, K. A., Berchtold, N. C., Malvaez, M., Carlos, A. J., McQuown, S. C., Cunningham, M. J., Wood, M. A. and Cotman, C. W. (2013) 'Exercise and Sodium Butyrate Transform a Subthreshold Learning Event into Long-Term Memory via a Brain-Derived Neurotrophic factor-Dependent Mechanism.' *Neuropsychopharmacology*, 38(10) pp. 2027–2034.

Italiano, J. E., Richardson, J. L., Patel-Hett, S., Battinelli, E., Zaslavsky, A., Short, S., Ryeom, S., Folkman, J. and Klement, G. L. (2008) 'Angiogenesis is regulated by a novel mechanism: pro- and antiangiogenic proteins are organized into separate platelet α granules and differentially released.' *Blood*, 111(3) pp. 1227–1233.

Ito, Y. A., Belforte, N., Cueva Vargas, J. L. and Di Polo, A. (2016a) 'A Magnetic Microbead Occlusion Model to Induce Ocular Hypertension-Dependent Glaucoma in Mice.' *Journal of Visualized Experiments*, (109) March, p. 53731.

Ito, Y. A., Belforte, N., Cueva Vargas, J. L. and Di Polo, A. (2016b) 'A Magnetic Microbead Occlusion Model to Induce Ocular Hypertension-Dependent Glaucoma in Mice.' *Journal of Visualized Experiments*, (109) March, p. 53731.

Jansen, P., Giehl, K., Nyengaard, J. R., Teng, K., Lioubinski, O., Sjoegaard, S. S., Breiderhoff, T., Gotthardt, M., Lin, F., Eilers, A., Petersen, C. M., Lewin, G. R., Hempstead, B. L., Willnow,

-
- T. E. and Nykjaer, A. (2007) 'Roles for the pro-neurotrophin receptor sortilin in neuronal development, aging and brain injury.' *Nature Neuroscience*, 10(11) pp. 1449–1457.
- Jassim, A. H. and Inman, D. M. (2019) 'Evidence of Hypoxic Glial Cells in a Model of Ocular Hypertension.' *Investigative Ophthalmology & Visual Science*, 60(1) p. 1.
- Jeon, C.-J., Strettoi, E. and Masland, R. H. (1998) 'The Major Cell Populations of the Mouse Retina.' *The Journal of Neuroscience*, 18(21) pp. 8936–8946.
- Ji, J., Chang, P., Pennesi, M. E., Yang, Z., Zhang, J., Li, D., Wu, S. M. and Gross, R. L. (2005) 'Effects of elevated intraocular pressure on mouse retinal ganglion cells.' *Vision Research*, 45(2) pp. 169–179.
- Johnson, D., Richardson, T. and Epstein, D. (1989) 'Trabecular meshwork recovery after phagocytic challenge.' *Current Eye Research*, 8(11) pp. 1121–1130.
- Johnson, J., Barde, Y., Schwab, M. and Thoenen, H. (1986) 'Brain-derived neurotrophic factor supports the survival of cultured rat retinal ganglion cells.' *The Journal of Neuroscience*, 6(10) pp. 3031–3038.
- Johnson, T. V., Oglesby, E. N., Steinhart, M. R., Cone-Kimball, E., Jefferys, J. and Quigley, H. A. (2016) 'Time-Lapse Retinal Ganglion Cell Dendritic Field Degeneration Imaged in Organotypic Retinal Explant Culture.' *Investigative Ophthalmology & Visual Science*, 57(1) p. 253.
- Johnson, T. V. and Tomarev, S. I. (2010) 'Rodent models of glaucoma.' *Brain Research Bulletin*, 81(2–3) pp. 349–358.
- Jones, K. R., Fariñas, I., Backus, C. and Reichardt, L. F. (1994) 'Targeted disruption of the BDNF gene perturbs brain and sensory neuron development but not motor neuron development.' *Cell*, 76(6) pp. 989–999.
- Jones, K. R. and Reichardt, L. F. (1990) 'Molecular cloning of a human gene that is a member of the nerve growth factor family.' *Proceedings of the National Academy of Sciences*, 87(20) pp. 8060–8064.
- Jourdi, H. and Kabbaj, M. (2013) 'Acute BDNF Treatment Upregulates GluR1-SAP97 and GluR2-GRIP1 Interactions: Implications for Sustained AMPA Receptor Expression.' Baudry, M. (ed.) *PLoS ONE*, 8(2) p. e57124.
- Kaisho, Y., Yoshimura, K. and Nakahama, K. (1990) 'Cloning and expression of a cDNA encoding a novel human neurotrophic factor.' *FEBS Letters*, 266(1–2) pp. 187–191.
- Kalesnykas, G., Oglesby, E. N., Zack, D. J., Cone, F. E., Steinhart, M. R., Tian, J., Pease, M. E. and Quigley, H. A. (2012) 'Retinal Ganglion Cell Morphology after Optic Nerve Crush and Experimental Glaucoma.' *Investigative Ophthalmology & Visual Science*, 53(7) p. 3847.
- Karlsson, M. and Hallböös, F. (1998) 'Kainic acid, tetrodotoxin and light modulate expression of brain-derived neurotrophic factor in developing avian retinal ganglion cells and their tectal target.' *Neuroscience*, 83(1) pp. 137–150.

Kernie, S. G. (2000) 'BDNF regulates eating behavior and locomotor activity in mice.' *The EMBO Journal*, 19(6) pp. 1290–1300.

Khodadad Kashi, S., Mirzazadeh, Z. S. and Saatchian, V. (2022) 'A Systematic Review and Meta-Analysis of Resistance Training on Quality of Life, Depression, Muscle Strength, and Functional Exercise Capacity in Older Adults Aged 60 Years or More.' *Biological Research For Nursing*, August, p. 109980042211209.

Kim, T.-H., Son, T., Lu, Y., Alam, M. and Yao, X. (2018) 'Comparative Optical Coherence Tomography Angiography of Wild-Type and rd10 Mouse Retinas.' *Translational Vision Science & Technology*, 7(6) p. 42.

King, S. M. and Reed, G. L. (2002) 'Development of platelet secretory granules.' *Seminars in Cell & Developmental Biology*, 13(4) pp. 293–302.

Kishino, A., Katayama, N., Ishige, Y., Yamamoto, Y., Ogo, H., Tatsuno, T., Mine, T., Noguchi, H. and Nakayama, C. (2001) 'Analysis of effects and pharmacokinetics of subcutaneously administered BDNF.' *Neuroreport*, 12(5) pp. 1067–1072.

Knox, D. L. (2007) 'Optic Nerve Hydropic Axonal Degeneration and Blocked Retrograde Axoplasmic Transport: Histopathologic Features in Human High-Pressure Secondary Glaucoma.' *Archives of Ophthalmology*, 125(3) p. 347.

Ko, M.-L., Hu, D.-N., Ritch, R., Sharma, S. C. and Chen, C.-F. (2001) 'Patterns of retinal ganglion cell survival after brain-derived neurotrophic factor administration in hypertensive eyes of rats.' *Neuroscience Letters*, 305(2) pp. 139–142.

Koh, J.-Y., Gwag, B. J., Lobner, D. and Choi, D. W. (1995) 'Potentiated Necrosis of Cultured Cortical Neurons by Neurotrophins.' *Science*, 268(5210) pp. 573–575.

Kolb, H. (1997) 'Amacrine cells of the mammalian retina: Neurocircuitry and functional roles.' *Eye*, 11(6) pp. 904–923.

Kolbeck, R., Bartke, I., Eberle, W. and Barde, Y.-A. (1999) 'Brain-Derived Neurotrophic Factor Levels in the Nervous System of Wild-Type and Neurotrophin Gene Mutant Mice.' *Journal of Neurochemistry*, 72(5) pp. 1930–1938.

Kolbeck, R., Jungbluth, S. and Barde, Y.-A. (1994) 'Characterisation of Neurotrophin Dimers and Monomers.' *European Journal of Biochemistry*, 225(3) pp. 995–1003.

Kong, C., Chan, C., Shahidullah, M. and Do, C. (2002) 'The mechanism of aqueous humour formation.' *Clinical and Experimental Optometry*, 85(6) pp. 335–349.

Korsching, S. and Thoenen, H. (1983) 'Nerve growth factor in sympathetic ganglia and corresponding target organs of the rat: correlation with density of sympathetic innervation.' *Proceedings of the National Academy of Sciences*, 80(11) pp. 3513–3516.

Koskela, T. K., Reiss, G. R., Brubaker, R. F. and Ellefson, R. D. (1989) 'Is the High Concentration of Ascorbic Acid in the Eye an Adaptation to Intense Solar Irradiation?' *Investigative Ophthalmology & Visual Science*, 30(10) pp. 2265–2267.

-
- Krabbe, K. S., Nielsen, A. R., Krogh-Madsen, R., Plomgaard, P., Rasmussen, P., Erikstrup, C., Fischer, C. P., Lindegaard, B., Petersen, A. M. W., Taudorf, S., Secher, N. H., Pilegaard, H., Bruunsgaard, H. and Pedersen, B. K. (2007) 'Brain-derived neurotrophic factor (BDNF) and type 2 diabetes.' *Diabetologia*, 50(2) pp. 431–438.
- Kwong, J. M. K., Caprioli, J. and Piri, N. (2010) 'RNA Binding Protein with Multiple Splicing: A New Marker for Retinal Ganglion Cells.' *Investigative Ophthalmology & Visual Science*, 51(2) p. 1052.
- Laske, C., Stransky, E., Leyhe, T., Eschweiler, G. W., Maetzler, W., Wittorf, A., Soekadar, S., Richartz, E., Koehler, N., Bartels, M., Buchkremer, G. and Schott, K. (2007a) 'BDNF serum and CSF concentrations in Alzheimer's disease, normal pressure hydrocephalus and healthy controls.' *Journal of Psychiatric Research*, 41(5) pp. 387–394.
- Laske, C., Stransky, E., Leyhe, T., Eschweiler, G. W., Maetzler, W., Wittorf, A., Soekadar, S., Richartz, E., Koehler, N., Bartels, M., Buchkremer, G. and Schott, K. (2007b) 'BDNF serum and CSF concentrations in Alzheimer's disease, normal pressure hydrocephalus and healthy controls.' *Journal of Psychiatric Research*, 41(5) pp. 387–394.
- Leake, P. A., Akil, O. and Lang, H. (2020) 'Neurotrophin gene therapy to promote survival of spiral ganglion neurons after deafness.' *Hearing Research*, 394, September, p. 107955.
- Lebrun-Julien, F., Morquette, B., Douillette, A., Saragovi, H. U. and Di Polo, A. (2009) 'Inhibition of p75NTR in glia potentiates TrkA-mediated survival of injured retinal ganglion cells.' *Molecular and Cellular Neuroscience*, 40(4) pp. 410–420.
- Lee, R., Kermani, P., Teng, K. K. and Hempstead, B. L. (2001) 'Regulation of Cell Survival by Secreted Proneurotrophins.' *Science*, 294(5548) pp. 1945–1948.
- Leibrock, J., Lottspeich, F., Hohn, A., Hofer, M., Hengeler, B., Masiakowski, P., Thoenen, H. and Barde, Y.-A. (1989) 'Molecular cloning and expression of brain-derived neurotrophic factor.' *Nature*, 341(6238) pp. 149–152.
- Leiter, O., Seidemann, S., Overall, R. W., Ramasz, B., Rund, N., Schallenberg, S., Grinenko, T., Wielockx, B., Kempermann, G. and Walker, T. L. (2019) 'Exercise-Induced Activated Platelets Increase Adult Hippocampal Precursor Proliferation and Promote Neuronal Differentiation.' *Stem Cell Reports*, 12(4) pp. 667–679.
- Leung, C. K., Weinreb, R. N., Li, Z. W., Liu, S., Lindsey, J. D., Choi, N., Liu, L., Cheung, C. Y., Ye, C., Qiu, K., Chen, L. J., Yung, W. H., Crowston, J. G., Pu, M., So, K. F., Pang, C. P. and Lam, D. S. C. (2011) 'Long-Term In Vivo Imaging and Measurement of Dendritic Shrinkage of Retinal Ganglion Cells.' *Investigative Ophthalmology & Visual Science*, 52(3) p. 1539.
- Levi-Montalcini, R. and Booker, B. (1960) 'Destruction of the sympathetic ganglia in mammals by an antiserum to a nerve-growth protein.' *Proceedings of the National Academy of Sciences*, 46(3) p. 8.

Li, L., Huang, H., Fang, F., Liu, L., Sun, Y. and Hu, Y. (2020) 'Longitudinal Morphological and Functional Assessment of RGC Neurodegeneration After Optic Nerve Crush in Mouse.' *Frontiers in Cellular Neuroscience*, 14, April, p. 109.

Li, R. S., Chen, B.-Y., Tay, D. K., Chan, H. H. L., Pu, M.-L. and So, K.-F. (2006) 'Melanopsin-Expressing Retinal Ganglion Cells Are More Injury-Resistant in a Chronic Ocular Hypertension Model.' *Investigative Ophthalmology & Visual Science*, 47(7) p. 2951.

Libby, R. T., Anderson, M. G., Pang, I.-H., Robinson, Z. H., Savinova, O. V., Cosma, I. M., Snow, A., Wilson, L. A., Smith, R. S., Clark, A. F. and John, S. W. M. (2005) 'Inherited glaucoma in DBA/2J mice: Pertinent disease features for studying the neurodegeneration.' *Visual Neuroscience*, 22(5) pp. 637–648.

Libby, R. T., Smith, R. S., Savinova, O. V., Zabaleta, A., Martin, J. E., Gonzalez, F. J. and John, S. W. M. (2003) 'Modification of Ocular Defects in Mouse Developmental Glaucoma Models by Tyrosinase.' *Science*, 299(5612) pp. 1578–1581.

Lindsay, R. M., Thoenen, H. and Barde, Y.-A. (1985) 'Placode and neural crest-derived sensory neurons are responsive at early developmental stages to brain-derived neurotrophic factor.' *Developmental Biology*, 112(2) pp. 319–328.

Liu, P., Huang, H., Fang, F., Liu, L., Li, L., Feng, X., Chen, W., Dalal, R., Sun, Y. and Hu, Y. (2021) 'Neuronal NMNAT2 Overexpression Does Not Achieve Significant Neuroprotection in Experimental Autoimmune Encephalomyelitis/Optic Neuritis.' *Frontiers in Cellular Neuroscience*, 15, October, p. 754651.

Liu, X., Ernfors, P., Wu, H. and Jaenisch, R. (1995) 'Sensory but not motor neuron deficits in mice lacking NT4 and BDNF.' *Nature*, 375(6528) pp. 238–241.

Lom, B., Cogen, J., Sanchez, A. L., Vu, T. and Cohen-Cory, S. (2002) 'Local and Target-Derived Brain-Derived Neurotrophic Factor Exert Opposing Effects on the Dendritic Arborization of Retinal Ganglion Cells *In Vivo*.' *The Journal of Neuroscience*, 22(17) pp. 7639–7649.

Lom, B. and Cohen-Cory, S. (1999) 'Brain-Derived Neurotrophic Factor Differentially Regulates Retinal Ganglion Cell Dendritic and Axonal Arborization *In Vivo*.' *The Journal of Neuroscience*, 19(22) pp. 9928–9938.

Lu, B., Nagappan, G., Guan, X., Nathan, P. J. and Wren, P. (2013) 'BDNF-based synaptic repair as a disease-modifying strategy for neurodegenerative diseases.' *Nature Reviews Neuroscience*, 14(6) pp. 401–416.

Lyons, W. E., Mamounas, L. A., Ricaurte, G. A., Coppola, V., Reid, S. W., Bora, S. H., Wihler, C., Koliatsos, V. E. and Tessarollo, L. (1999) 'Brain-derived neurotrophic factor-deficient mice develop aggressiveness and hyperphagia in conjunction with brain serotonergic abnormalities.' *Proceedings of the National Academy of Sciences*, 96(26) pp. 15239–15244.

Ma, Y.-T., Hsieh, T., Forbes, M. E., Johnson, J. E. and Frost, D. O. (1998) 'BDNF Injected into the Superior Colliculus Reduces Developmental Retinal Ganglion Cell Death.' *The Journal of Neuroscience*, 18(6) pp. 2097–2107.

-
- Machlus, K. R. and Italiano, J. E. (2019) 'Megakaryocyte Development and Platelet Formation.' *In Platelets*. Elsevier, pp. 25–46.
- Maes, M. E., Schlamp, C. L. and Nickells, R. W. (2017) 'BAX to basics: How the BCL2 gene family controls the death of retinal ganglion cells.' *Progress in Retinal and Eye Research*, 57, March, pp. 1–25.
- Maisonpierre, P. C., Belluscio, L., Squinto, S., Furth, M. E., Lindsay, R. M. and Yancopoulos, G. D. (1990) 'Neurotrophin-3: a Neurotrophic Factor Related to NGF and BDNF.' *Science*, 247(4949 Pt 1) pp. 1446–1451.
- Malik, S. C., Sozmen, E. G., Baeza-Raja, B., Le Moan, N., Akassoglou, K. and Schachtrup, C. (2021) 'In vivo functions of p75NTR: challenges and opportunities for an emerging therapeutic target.' *Trends in Pharmacological Sciences*, 42(9) pp. 772–788.
- Mansour-Robaey, S., Clarke, D. B., Wang, Y. C., Bray, G. M. and Aguayo, A. J. (1994) 'Effects of ocular injury and administration of brain-derived neurotrophic factor on survival and regrowth of axotomized retinal ganglion cells.' *Proceedings of the National Academy of Sciences*, 91(5) pp. 1632–1636.
- Martin, K. R. G., Quigley, H. A., Zack, D. J., Levkovitch-Verbin, H., Kielczewski, J., Valenta, D., Baumrind, L., Pease, M. E., Klein, R. L. and Hauswirth, W. W. (2003) 'Gene Therapy with Brain-Derived Neurotrophic Factor As a Protection: Retinal Ganglion Cells in a Rat Glaucoma Model.' *Investigative Ophthalmology & Visual Science*, 44(10) p. 4357.
- Martin, R. W., Vaezy, S., Kaczowski, P., Keilman, G., Carter, S., Caps, M., Beach, K., Plett, M. and Crum, L. (1999) 'Hemostasis of punctured vessels using Doppler-guided high-intensity ultrasound.' *Ultrasound in Medicine & Biology*, 25(6) pp. 985–990.
- Masin, L., Claes, M., Bergmans, S., Cools, L., Andries, L., Davis, B. M., Moons, L. and De Groef, L. (2021) 'A novel retinal ganglion cell quantification tool based on deep learning.' *Scientific Reports*, 11(1) p. 702.
- Matthews, V. B., Åström, M.-B., Chan, M. H. S., Bruce, C. R., Krabbe, K. S., Prelovsek, O., Åkerström, T., Yfanti, C., Broholm, C., Mortensen, O. H., Penkowa, M., Hojman, P., Zankari, A., Watt, M. J., Bruunsgaard, H., Pedersen, B. K. and Febbraio, M. A. (2009) 'Brain-derived neurotrophic factor is produced by skeletal muscle cells in response to contraction and enhances fat oxidation via activation of AMP-activated protein kinase.' *Diabetologia*, 52(7) pp. 1409–1418.
- May, A. E., Seizer, P. and Gawaz, M. (2008) 'Platelets: Inflammatory Firebugs of Vascular Walls.' *Arteriosclerosis, Thrombosis, and Vascular Biology*, 28(3).
- McDonald, N., Lapatto, R., Murray-Rust, J., Gunning, J., Wlodawer, A. and Blundell, T. (1991) 'New protein fold revealed by a 2,3-A resolution crystal structure of nerve growth factor.' *Nature*, 354(6352) pp. 411–414.

McMorran, B. J., Marshall, V. M., de Graaf, C., Drysdale, K. E., Shabbar, M., Smyth, G. K., Corbin, J. E., Alexander, W. S. and Foote, S. J. (2009) 'Platelets Kill Intraerythrocytic Malarial Parasites and Mediate Survival to Infection.' *Science*, 323(5915) pp. 797–800.

Mead, B., Ahmed, Z. and Tomarev, S. (2018) 'Mesenchymal Stem Cell-Derived Small Extracellular Vesicles Promote Neuroprotection in a Genetic DBA/2J Mouse Model of Glaucoma.' *Investigative Ophthalmology & Visual Science*, 59(13) p. 5473.

Mead, B., Kerr, A., Nakaya, N. and Tomarev, S. I. (2021) 'miRNA Changes in Retinal Ganglion Cells after Optic Nerve Crush and Glaucomatous Damage.' *Cells*, 10(7) p. 1564.

Mead, B., Thompson, A., Scheven, B. A., Logan, A., Berry, M. and Leadbeater, W. (2014) 'Comparative Evaluation of Methods for Estimating Retinal Ganglion Cell Loss in Retinal Sections and Wholemounts.' Badea, T. C. (ed.) *PLoS ONE*, 9(10) p. e110612.

Meeker, R. and Williams, K. (2014) 'Dynamic nature of the p75 neurotrophin receptor in response to injury and disease.' *J Neuroimmune Pharmacol*, 9(5) pp. 615–628.

Meng, L., Liu, B., Ji, R., Jiang, X., Yan, X. and Xin, Y. (2018) 'Targeting the BDNF/TrkB pathway for the treatment of tumors (Review).' *Oncology Letters*, 17, December, pp. 2031–2039.

Merkouris, S., Barde, Y.-A., Binley, K. E., Allen, N. D., Stepanov, A. V., Wu, N. C., Grande, G., Lin, C.-W., Li, M., Nan, X., Chacon-Fernandez, P., DiStefano, P. S., Lindsay, R. M., Lerner, R. A. and Xie, J. (2018a) 'Fully human agonist antibodies to TrkB using autocrine cell-based selection from a combinatorial antibody library.' *Proceedings of the National Academy of Sciences*, 115(30) pp. E7023–E7032.

Merkouris, S., Barde, Y.-A., Binley, K. E., Allen, N. D., Stepanov, A. V., Wu, N. C., Grande, G., Lin, C.-W., Li, M., Nan, X., Chacon-Fernandez, P., DiStefano, P. S., Lindsay, R. M., Lerner, R. A. and Xie, J. (2018b) 'Fully human agonist antibodies to TrkB using autocrine cell-based selection from a combinatorial antibody library.' *Proceedings of the National Academy of Sciences*, 115(30) pp. E7023–E7032.

Meuchel, L. W., Thompson, M. A., Cassivi, S. D., Pabelick, C. M. and Prakash, Y. S. (2011) 'Neurotrophins induce nitric oxide generation in human pulmonary artery endothelial cells.' *Cardiovascular Research*, 91(4) pp. 668–676.

Mey, J. and Thanos, S. (1993a) 'Intravitreal injections of neurotrophic factors support the survival of axotomized retinal ganglion cells in adult rats in vivo.' *Brain Research*, 602(2) pp. 304–317.

Mey, J. and Thanos, S. (1993b) 'Intravitreal injections of neurotrophic factors support the survival of axotomized retinal ganglion cells in adult rats in vivo.' *Brain Research*, 602(2) pp. 304–317.

Mitragotri, S., Blankschtein, D. and Langer, R. (1995) 'Ultrasound-mediated transdermal protein delivery.' *Science*, 269(5225) pp. 850–853.

-
- Mogi, M., Togari, A., Kondo, T., Mizuno, Y., Komure, O., Kuno, S., Ichinose, H. and Nagatsu, T. (1999) 'Brain-derived growth factor and nerve growth factor concentrations are decreased in the substantia nigra in Parkinson's disease.' *Neuroscience Letters*, 270(1) pp. 45–48.
- Morgan, J. E. (2012) 'Retina ganglion cell degeneration in glaucoma: an opportunity missed? A review: RGC degeneration.' *Clinical & Experimental Ophthalmology*, 40(4) pp. 364–368.
- Morgan, J. E. and Tribble, J. R. (2015) 'Microbead models in glaucoma.' *Experimental Eye Research*, 141, December, pp. 9–14.
- Mori, T., Shimizu, K. and Hayashi, M. (2003) 'Levels of serum brain-derived neurotrophic factor in primates.' *Primates*, 44(2) pp. 167–169.
- Morrison, J. C., Johnson, E. and Cepurna, W. O. (2008) 'Rat models for glaucoma research.' *In Progress in Brain Research*. Elsevier, pp. 285–301.
- Mowla, S. J., Farhadi, H. F., Pareek, S., Atwal, J. K., Morris, S. J., Seidah, N. G. and Murphy, R. A. (2001) 'Biosynthesis and Post-translational Processing of the Precursor to Brain-derived Neurotrophic Factor.' *Journal of Biological Chemistry*, 276(16) pp. 12660–12666.
- Mowla, S. J., Pareek, S., Farhadi, H. F., Petrecca, K., Fawcett, J. P., Seidah, N. G., Morris, S. J., Sossin, W. S. and Murphy, R. A. (1999) 'Differential Sorting of Nerve Growth Factor and Brain-Derived Neurotrophic Factor in Hippocampal Neurons.' *The Journal of Neuroscience*, 19(6) pp. 2069–2080.
- Mukai, R., Park, D. H., Okunuki, Y., Hasegawa, E., Klokman, G., Kim, C. B., Krishnan, A., Gregory-Ksander, M., Husain, D., Miller, J. W. and Connor, K. M. (2019) 'Mouse model of ocular hypertension with retinal ganglion cell degeneration.' Agudo-Barriuso, M. (ed.) *PLOS ONE*, 14(1) p. e0208713.
- Murali, A., Ramlogan-Steel, C. A., Andrzejewski, S., Steel, J. C. and Layton, C. J. (2019a) 'Retinal explant culture: A platform to investigate human neuro-retina.' *Clinical & Experimental Ophthalmology*, 47(2) pp. 274–285.
- Murali, A., Ramlogan-Steel, C. A., Andrzejewski, S., Steel, J. C. and Layton, C. J. (2019b) 'Retinal explant culture: A platform to investigate human neuro-retina.' *Clinical & Experimental Ophthalmology*, 47(2) pp. 274–285.
- Mysona, B. A., Zhao, J. and Bollinger, K. E. (2017) 'Role of BDNF/TrkB pathway in the visual system: therapeutic implications for glaucoma.' *Expert Review of Ophthalmology*, 12(1) pp. 69–81.
- Nadal-Nicolás, F. M., Jiménez-López, M., Salinas-Navarro, M., Sobrado-Calvo, P., Albuquerque-Béjar, J. J., Vidal-Sanz, M. and Agudo-Barriuso, M. (2012) 'Whole Number, Distribution and Co-Expression of Brn3 Transcription Factors in Retinal Ganglion Cells of Adult Albino and Pigmented Rats.' Harvey, A. R. (ed.) *PLoS ONE*, 7(11) p. e49830.

Naegelin, Y., Dingsdale, H., Säuberli, K., Schädelin, S., Kappos, L. and Barde, Y.-A. (2018a) 'Measuring and Validating the Levels of Brain-Derived Neurotrophic Factor in Human Serum.' *eneuro*, 5(2) p. ENEURO.0419-17.2018.

Naegelin, Y., Dingsdale, H., Säuberli, K., Schädelin, S., Kappos, L. and Barde, Y.-A. (2018b) 'Measuring and Validating the Levels of Brain-Derived Neurotrophic Factor in Human Serum.' *eneuro*, 5(2) p. ENEURO.0419-17.2018.

Nagahara, A. H. and Tuszynski, M. H. (2011) 'Potential therapeutic uses of BDNF in neurological and psychiatric disorders.' *Nature Reviews Drug Discovery*, 10(3) pp. 209–219.

Nebie, O., Buée, L., Blum, D. and Burnouf, T. (2022) 'Can the administration of platelet lysates to the brain help treat neurological disorders?' *Cellular and Molecular Life Sciences*, 79(7) p. 379.

O'Brien, W. (1986) 'Biological Effects of Ultrasound: Rationale for the Measurement of Selected Ultrasonic Output Quantities.' *Echocardiography*, 3 pp. 165–179.

Oddone, F., Roberti, G., Micera, A., Busanello, A., Bonini, S., Quaranta, L., Agnifili, L. and Manni, G. (2017) 'Exploring Serum Levels of Brain Derived Neurotrophic Factor and Nerve Growth Factor Across Glaucoma Stages.' Vavvas, D. G. (ed.) *PLOS ONE*, 12(1) p. e0168565.

Osborne, A., Khatib, T. Z., Songra, L., Barber, A. C., Hall, K., Kong, G. Y. X., Widdowson, P. S. and Martin, K. R. (2018) 'Neuroprotection of retinal ganglion cells by a novel gene therapy construct that achieves sustained enhancement of brain-derived neurotrophic factor/tropomyosin-related kinase receptor-B signaling.' *Cell Death & Disease*, 9(10) p. 1007.

Otto, C., Baumann, M., Schreiner, T., Bartsch, G., Borberg, H. and Schwandt, P. (2001) 'Standardized ultrasound as a new method to induce platelet aggregation Evaluation, influence of lipoproteins and of glycoprotein IIb/IIIa antagonist tirofiban.' *European Journal of Ultrasound* p. 10.

Palasz, E., Wysocka, A., Gasiorowska, A., Chalimoniuk, M., Niewiadomski, W. and Niewiadomska, G. (2020) 'BDNF as a Promising Therapeutic Agent in Parkinson's Disease.' *International Journal of Molecular Sciences*, 21(3) p. 1170.

Pardridge, W, Kang, Y, and Buciak, J (1994) 'Transport of human recombinant brain-derived neurotrophic factor (BDNF) through the rat blood brain barrier in vivo using vector-mediated peptide drug delivery.' *Pharmaceutical Research*, 11(5) pp. 738–746.

Park, K. (2016) 'Acoustic Cluster Therapy for better treatment of solid tumors.' *Journal of Controlled Release*, 236, August, p. 117.

Parrilla-Reverter, G., Agudo, M., Sobrado-Calvo, P., Salinas-Navarro, M., Villegas-Pérez, M. P. and Vidal-Sanz, M. (2009) 'Effects of different neurotrophic factors on the survival of retinal ganglion cells after a complete intraorbital nerve crush injury: A quantitative in vivo study.' *Experimental Eye Research*, 89(1) pp. 32–41.

Pattamatta, U., McPherson, Z. and White, A. (2016) 'A mouse retinal explant model for use in studying neuroprotection in glaucoma.' *Experimental Eye Research*, 151, October, pp. 38–44.

Pearson, H. and Thompson, T. (1993) 'Atrophy and degeneration of ganglion cells in central retina following loss of postsynaptic target neurons in the dorsal lateral geniculate nucleus of the adult cat.' *Experimental Neurology*, 119(1) pp. 113–119.

Pease, M. E., McKinnon, S. J., Quigley, H. A., Kerrigan, L. A. and Zack, D. J. (2000) 'Obstructed Axonal Transport of BDNF and Its Receptor TrkB in Experimental Glaucoma,' 41(3) p. 11.

Penzes, P., Johnson, R. C., Sattler, R., Zhang, X., Huganir, R. L., Kambampati, V., Mains, R. E. and Eipper, B. A. (2001) 'The Neuronal Rho-GEF Kalirin-7 Interacts with PDZ Domain-Containing Proteins and Regulates Dendritic Morphogenesis.' *Neuron*, 29(1) pp. 229–242.

Perez, M.-T. R. and Caminos, E. (1995) 'Expression of brain-derived neurotrophic factor and of its functional receptor in neonatal and adult rat retina.' *Neuroscience Letters*, 183(1–2) pp. 96–99.

Perry, V. H. and Cowey, A. (1984) 'Retinal ganglion cells that project to the superior colliculus and pretectum in the macaque monkey.' *Neuroscience*, 12(4) pp. 1125–1137.

Poduslo, J. F. and Curran, G. L. (1996a) 'Permeability at the blood-brain and blood-nerve barriers of the neurotrophic factors: NGF, CNTF, NT-3, BDNF.' *Molecular Brain Research*, 36(2) pp. 280–286.

Poduslo, J. F. and Curran, G. L. (1996b) 'Permeability at the blood-brain and blood-nerve barriers of the neurotrophic factors: NGF, CNTF, NT-3, BDNF.' *Molecular Brain Research*, 36(2) pp. 280–286.

Prigent-Tessier, A., Quirié, A., Maguin-Gaté, K., Szostak, J., Mossiat, C., Nappey, M., Devaux, S., Marie, C. and Demougeot, C. (2013) 'Physical training and hypertension have opposite effects on endothelial brain-derived neurotrophic factor expression.' *Cardiovascular Research*, 100(3) pp. 374–382.

Quigley, H. A. (2011) 'Glaucoma.' *The Lancet*, 377(9774) pp. 1367–1377.

Quigley, H. A., Addicks, E. M., Green, W. R. and Maumenee, A. E. (1981) 'Optic Nerve Damage in Human Glaucoma: II. The Site of Injury and Susceptibility to Damage.' *Arch Ophthalmol*, 99(4) pp. 635–649.

Quigley, H. A., McKinnon, S. J., Zack, D. J., Pease, M. E., Kerrigan, L. A., Kerrigan, D. F. and Mitchell, R. S. (2000) 'Retrograde Axonal Transport of BDNF in Retinal Ganglion Cells Is Blocked by Acute IOP Elevation in Rats,' 41(11) p. 7.

Radka, S. F., Hoist, P. A., Fritsche, M. and Altar, C. A. (1996) 'Presence of brain-derived neurotrophic factor in brain and human and rat but not mouse serum detected by a sensitive and specific immunoassay.' *Brain Research*, 709(1) pp. 122–130.

-
- Rasmussen, P., Brassard, P., Adser, H., Pedersen, M. V., Leick, L., Hart, E., Secher, N. H., Pedersen, B. K. and Pilegaard, H. (2009) 'Evidence for a release of brain-derived neurotrophic factor from the brain during exercise: Brain-derived neurotrophic factor release during exercise.' *Experimental Physiology*, 94(10) pp. 1062–1069.
- Rauskolb, S., Zagrebelsky, M., Drenjak, A., Deogracias, R., Matsumoto, T., Wiese, S., Erne, B., Sendtner, M., Schaeren-Wiemers, N., Korte, M. and Barde, Y.-A. (2010) 'Global Deprivation of Brain-Derived Neurotrophic Factor in the CNS Reveals an Area-Specific Requirement for Dendritic Growth.' *Journal of Neuroscience*, 30(5) pp. 1739–1749.
- Rebsam, A., Bhansali, P. and Mason, C. A. (2012) 'Eye-Specific Projections of Retinogeniculate Axons Are Altered in Albino Mice.' *Journal of Neuroscience*, 32(14) pp. 4821–4826.
- Remtulla, S. and Hallett, P. E. (1985) 'A schematic eye for the mouse, and comparisons with the rat.' *Vision Research*, 25(1) pp. 21–31.
- Ren, R., Li, Y., Liu, Z., Liu, K. and He, S. (2012) 'Long-Term Rescue of Rat Retinal Ganglion Cells and Visual Function by AAV-Mediated BDNF Expression after Acute Elevation of Intraocular Pressure.' *Investigative Ophthalmology & Visual Science*, 53(2) p. 1003.
- Rezola-Pardo, C., Hervás, G., Arrieta, H., Hernández-de Diego, A., Ruiz-Litago, F., Gil, S. M., Rodriguez-Larrad, A. and Irazusta, J. (2020) 'Physical exercise interventions have no effect on serum BDNF concentration in older adults living in long-term nursing homes.' *Experimental Gerontology*, 139, October, p. 111024.
- Rheume, B. A., Jereen, A., Bolisetty, M., Sajid, M. S., Yang, Y., Renna, K., Sun, L., Robson, P. and Trakhtenberg, E. F. (2018a) 'Single cell transcriptome profiling of retinal ganglion cells identifies cellular subtypes.' *Nature Communications*, 9(1) p. 2759.
- Rheume, B. A., Jereen, A., Bolisetty, M., Sajid, M. S., Yang, Y., Renna, K., Sun, L., Robson, P. and Trakhtenberg, E. F. (2018b) 'Single cell transcriptome profiling of retinal ganglion cells identifies cellular subtypes.' *Nature Communications*, 9(1) p. 2759.
- Rho, S., Park, I., Seong, G. J., Lee, N., Lee, C.-K., Hong, S. and Kim, C. Y. (2014) 'Chronic Ocular Hypertensive Rat Model using Microbead Injection: Comparison of Polyurethane, Polymethylmethacrylate, Silica and Polystyrene Microbeads.' *Current Eye Research*, 39(9) pp. 917–927.
- Riesz, P. and Berdahl, D. (1985) 'Free Radical Generation by Ultrasound in Aqueous and Nonaqueous Solutions.' *Environmental Health Perspective*, 64 pp. 233–252.
- Robert D. Rosenfeld, Lisa Zeni, Mitsuru Hani, Jane Talvenheimo, Susan Radka, Larry Bennett, James A. Miller, and Andrew A. Welcher (1995) 'Purification and identification of brain-derived neurotrophic factor from human serum.' *Protein Expr. Purif*, 6(4) pp. 465–471.
- Rodriguez, A. R., de Sevilla Müller, L. P. and Brecha, N. C. (2014) 'The RNA binding protein RBPMS is a selective marker of ganglion cells in the mammalian retina: RBPMS identifies retinal ganglion cells.' *Journal of Comparative Neurology*, 522(6) pp. 1411–1443.

Rodríguez-Tébar, A. and Barde, Y.-A. (1988) 'Binding characteristics of brain-derived neurotrophic factor to its receptors on neurons from the chick embryo.' *The Journal of Neuroscience*, 8(9) pp. 3337–3342.

Rodríguez-Tébar, A., Dechant, G. and Barde, Y.-A. (1991) 'Neurotrophins: structural relatedness and receptor interactions.' *Philosophical Transactions of the Royal Society of London. Series B: Biological Sciences*, 331(1261) pp. 255–258.

Rose, C. R., Blum, R., Pichler, B., Lepier, A., Kafitz, K. W. and Konnerth, A. (2003) 'Truncated TrkB-T1 mediates neurotrophin-evoked calcium signalling in glia cells.' *Nature*, 426(6962) pp. 74–78.

Rosenbaum, S., Tiedemann, A., Sherrington, C., Curtis, J. and Ward, P. (2014) 'Physical activity interventions for people with mental illness: a systematic review and meta-analysis.' *Journal of Clinical Psychiatry*, 75 pp. 964–967.

Rosenthal, A., Goeddel, D., Nguyen, T., Lewis, M., Shih, A., Laramée, G., Nikolics, K. and Winslow, J. (1990) 'Primary structure and biological activity of a novel human neurotrophic factor.' *Neuron*, 4(5) pp. 767–773.

Rowley, J. W., Schwartz, H. and Weyrich, A. S. (2012) 'Platelet mRNA: the meaning behind the message.' *Current Opinion in Hematology*, 19(5) pp. 385–391.

Rudge, J. S., Mather, P. E., Pasnikowski, E. M., Cai, N., Corcoran, T., Acheson, A., Anderson, K., Lindsay, R. M. and Wiegand, S. J. (1998) 'Endogenous BDNF Protein Is Increased in Adult Rat Hippocampus after a Kainic Acid Induced Excitotoxic Insult but Exogenous BDNF Is Not Neuroprotective.' *Experimental Neurology*, 149(2) pp. 398–410.

Ruiz-Ederra, J. and Verkman, A. S. (2006) 'Mouse model of sustained elevation in intraocular pressure produced by episcleral vein occlusion.' *Experimental Eye Research*, 82(5) pp. 879–884.

Russo-Neustadt, A. (1999) 'Exercise, Antidepressant Medications, and Enhanced Brain Derived Neurotrophic Factor Expression.' *Neuropsychopharmacology*, 21(5) pp. 679–682.

S A Neeper, F Gómez-Pinilla, J Choi, and C Cotman (1995) 'Exercise and brain neurotrophins.' *Nature*, (373) January, p. 109.

Samsel, P. A., Kisiswa, L., Erichsen, J. T., Cross, S. D. and Morgan, J. E. (2011a) 'A Novel Method for the Induction of Experimental Glaucoma Using Magnetic Microspheres.' *Investigative Ophthalmology & Visual Science*, 52(3) p. 1671.

Samsel, P. A., Kisiswa, L., Erichsen, J. T., Cross, S. D. and Morgan, J. E. (2011b) 'A Novel Method for the Induction of Experimental Glaucoma Using Magnetic Microspheres.' *Investigative Ophthalmology & Visual Science*, 52(3) p. 1671.

Sánchez-Migallón, M. C., Valiente-Soriano, F. J., Nadal-Nicolás, F. M., Vidal-Sanz, M. and Agudo-Barriuso, M. (2016) 'Apoptotic Retinal Ganglion Cell Death After Optic Nerve

Transection or Crush in Mice: Delayed RGC Loss With BDNF or a Caspase 3 Inhibitor.' *Investigative Ophthalmology & Visual Science*, 57(1) p. 81.

Sánchez-Sánchez, J. and Arévalo, J. (2017) 'A Review on Ubiquitination of Neurotrophin Receptors: Facts and Perspectives.' *International Journal of Molecular Sciences*, 18(3) p. 630.

Sánchez-Vidaña, D. I., Chow, J. K. W., Hu, S. Q., Lau, B. W. M. and Han, Y.-F. (2019) 'Molecular Targets of Bis (7)-Cognitin and Its Relevance in Neurological Disorders: A Systematic Review.' *Frontiers in Neuroscience*, 13, May, p. 445.

Sanes, J. R. and Masland, R. H. (2015) 'The Types of Retinal Ganglion Cells: Current Status and Implications for Neuronal Classification.' *Annual Review of Neuroscience*, 38(1) pp. 221–246.

Sangkuhl, K., Shuldiner, A. R., Klein, T. E. and Altman, R. B. (2011) 'Platelet aggregation pathway.' *Pharmacogenetics and Genomics*, 21(8) pp. 516–521.

Sappington, R. M., Carlson, B. J., Crish, S. D. and Calkins, D. J. (2010) 'The Microbead Occlusion Model: A Paradigm for Induced Ocular Hypertension in Rats and Mice.' *Investigative Ophthalmology & Visual Science*, 51(1) p. 207.

Schechterson, L. C., Sanchez, J. T., Rubel, E. W. and Bothwell, M. (2012) 'TrkB Downregulation Is Required for Dendrite Retraction in Developing Neurons of Chicken Nucleus Magnocellularis.' *Journal of Neuroscience*, 32(40) pp. 14000–14009.

Schnichels, S., Paquet-Durand, F., Löscher, M., Tsai, T., Hurst, J., Joachim, S. C. and Klettner, A. (2021) 'Retina in a dish: Cell cultures, retinal explants and animal models for common diseases of the retina.' *Progress in Retinal and Eye Research*, 81, March, p. 100880.

Scholl, B., Burge, J. and Priebe, N. J. (2013) 'Binocular integration and disparity selectivity in mouse primary visual cortex.' *Journal of Neurophysiology*, 109(12) pp. 3013–3024.

Scholz, M., Buder, T., Seeber, S., Adamek, E., Becker, C.-M. and Lu'tjen-Drecoll, E. (2008) 'Dependency of Intraocular Pressure Elevation and Glaucomatous Changes in DBA/2J and DBA/2J-Rj Mice.' *Investigative Ophthalmology & Visual Science*, 49(2) p. 613.

Schuettauf, F., Stein, T., Choragiewicz, T. J., Rejdak, R., Bolz, S., Zurakowski, D., Varde, M. A., Laties, A. M. and Thaler, S. (2011) 'Caspase inhibitors protect against NMDA-mediated retinal ganglion cell death: Caspase inhibitors in NMDA toxicity.' *Clinical & Experimental Ophthalmology*, 39(6) pp. 545–554.

Seki, M., Tanaka, T., Sakai, Y., Fukuchi, T., Abe, H., Nawa, H. and Takei, N. (2005) 'Müller Cells as a Source of Brain-derived Neurotrophic Factor in the Retina: Noradrenaline Upregulates Brain-derived Neurotrophic Factor Levels in Cultured Rat Müller Cells.' *Neurochemical Research*, 30(9) pp. 1163–1170.

Sendtner, M., Holtmann, B., Kolbeck, R., Thoenen, H. and Barde, Y.-A. (1992) 'Brain-derived neurotrophic factor prevents the death of motoneurons in newborn rats after nerve section.' *Nature*, 360(6406) pp. 757–759.

Serra-Millàs, M. (2016) 'Are the changes in the peripheral brain-derived neurotrophic factor levels due to platelet activation?' *World Journal of Psychiatry*, 6(1) p. 84.

Shareef, S. R., Garcia-Valenzuela, E., Salierno, A., Walsh, J. and Sharma, S. C. (1995) 'Chronic ocular hypertension following episcleral venous occlusion in rats.' *Experimental Eye Research*, 61(3) pp. 379–382.

Shimizu, E., Hashimoto, K., Okamura, N., Koike, K., Komatsu, N., Kumakiri, C., Nakazato, M., Watanabe, H., Shinoda, N., Okada, S. and Iyo, M. (2003a) 'Alterations of serum levels of brain-derived neurotrophic factor (BDNF) in depressed patients with or without antidepressants.' *Biological Psychiatry*, 54(1) pp. 70–75.

Shimizu, E., Hashimoto, K., Okamura, N., Koike, K., Komatsu, N., Kumakiri, C., Nakazato, M., Watanabe, H., Shinoda, N., Okada, S. and Iyo, M. (2003b) 'Alterations of serum levels of brain-derived neurotrophic factor (BDNF) in depressed patients with or without antidepressants.' *Biological Psychiatry*, 54(1) pp. 70–75.

Sholl, D. A. (1953) 'Dendritic organization in the neurons of the visual and motor cortices of the cat,' 87 pp. 387–406.

Shorey, M. L. (1909) 'The effect of the destruction of peripheral areas on the differentiation of the neuroblasts.' *Journal of Experimental Zoology*, 7(1) pp. 25–63.

Shpak, A. A., Guekht, A. B., Druzhkova, T. A., Kozlova, K. I. and Gulyaeva, N. V. (2018) 'Brain-Derived Neurotrophic Factor in Patients with Primary Open-Angle Glaucoma and Age-related Cataract.' *Current Eye Research*, 43(2) pp. 224–231.

Smith, C. W. (2022) 'Release of α -granule contents during platelet activation.' *Platelets*, 33(4) pp. 491–502.

Sommerfeld, M. T., Schweigreiter, R., Barde, Y.-A. and Hoppe, E. (2000a) 'Down-regulation of the Neurotrophin Receptor TrkB following Ligand Binding.' *Journal of Biological Chemistry*, 275(12) pp. 8982–8990.

Sommerfeld, M. T., Schweigreiter, R., Barde, Y.-A. and Hoppe, E. (2000b) 'Down-regulation of the Neurotrophin Receptor TrkB following Ligand Binding: EVIDENCE FOR AN INVOLVEMENT OF THE PROTEASOME AND DIFFERENTIAL REGULATION OF TrkA AND TrkB.' *Journal of Biological Chemistry*, 275(12) pp. 8982–8990.

Sontum, Per Christian and Phoenix Solutions (2019) 'Acoustic Cluster Therapy (ACT) With Chemotherapy in Metastatic Liver Metastases of Gastrointestinal Origin (ACT).' [ClinicalTrials.gov](https://clinicaltrials.gov).

Soya, H., Nakamura, T., Deocaris, C. C., Kimpara, A., Iimura, M., Fujikawa, T., Chang, H., McEwen, B. S. and Nishijima, T. (2007) 'BDNF induction with mild exercise in the rat hippocampus.' *Biochemical and Biophysical Research Communications*, 358(4) pp. 961–967.

Sun, W., Li, N. and He, S. (2002) 'Large-scale morphological survey of mouse retinal ganglion cells.' *The Journal of Comparative Neurology*, 451(2) pp. 115–126.

-
- Suslick, K. S. and Flannigan, D. J. (2008) 'Inside a Collapsing Bubble: Sonoluminescence and the Conditions During Cavitation.' *Annual Review of Physical Chemistry*, 59(1) pp. 659–683.
- Suter, U., Heymach, J. V. and Shooter, E. M. (1991) 'Two conserved domains in the NGF propeptide are necessary and sufficient for the biosynthesis of correctly processed and biologically active NGF.' *The EMBO Journal*, 10(9) pp. 2395–2400.
- Szuhany, K. L., Bugatti, M. and Otto, M. W. (2015) 'A meta-analytic review of the effects of exercise on brain-derived neurotrophic factor.' *Journal of Psychiatric Research*, 60, January, pp. 56–64.
- Tamura, S., Suzuki, H., Hirowatari, Y., Hatase, M., Nagasawa, A., Matsuno, K., Kobayashi, S. and Moriyama, T. (2011) 'Release reaction of brain-derived neurotrophic factor (BDNF) through PAR1 activation and its two distinct pools in human platelets.' *Thrombosis Research*, 128(5) pp. e55–e61.
- Tang, Y.-Q., Yeaman, M. R. and Selsted, M. E. (2002) 'Antimicrobial Peptides from Human Platelets.' *Infection and Immunity*, 70(12) pp. 6524–6533.
- Tang, Z., Zhang, S., Lee, C., Kumar, A., Arjunan, P., Li, Y., Zhang, F. and Li, X. (2011) 'An Optic Nerve Crush Injury Murine Model to Study Retinal Ganglion Cell Survival.' *Journal of Visualized Experiments*, (50) April, p. 2685.
- Tao, X., Finkbeiner, S., Arnold, D. B., Shaywitz, A. J. and Greenberg, M. E. (1998) 'Ca²⁺ Influx Regulates BDNF Transcription by a CREB Family Transcription Factor-Dependent Mechanism.' *Neuron*, 20(4) pp. 709–726.
- Templeton, J. P. and Geisert, E. E. (2012) 'A practical approach to optic nerve crush in the mouse.' *Molecular Vision* p. 6.
- Teng, H. K. (2005) 'ProBDNF Induces Neuronal Apoptosis via Activation of a Receptor Complex of p75NTR and Sortilin.' *Journal of Neuroscience*, 25(22) pp. 5455–5463.
- Tham, Y.-C., Li, X., Wong, T. Y., Quigley, H. A., Aung, T. and Cheng, C.-Y. (2014) 'Global Prevalence of Glaucoma and Projections of Glaucoma Burden through 2040.' *Ophthalmology*, 121(11) pp. 2081–2090.
- Thomas, S. G. (2019) 'The Structure of Resting and Activated Platelets.' *In Platelets*. Elsevier, pp. 47–77.
- Tiedt, R., Schomber, T., Hao-Shen, H. and Skoda, R. C. (2007) 'Pf4-Cre transgenic mice allow the generation of lineage-restricted gene knockouts for studying megakaryocyte and platelet function in vivo.' *Blood*, 109(4) pp. 1503–1506.
- Timmusk, T., Lendahl, U., Funakoshi, H., Arenas, E., Persson, H. and Metsis, M. (1995) 'Identification of brain-derived neurotrophic factor promoter regions mediating tissue-specific, axotomy-, and neuronal activity-induced expression in transgenic mice.' *Journal of Cell Biology*, 128(1) pp. 185–199.

-
- Timmusk, T., Palm, K., Metsis, M., Reintam, T., Paalme, V., Saarma, M. and Persson, H. (1993) 'Multiple promoters direct tissue-specific expression of the rat BDNF gene.' *Neuron*, 10(3) pp. 475–489.
- Toyooka, K., Asama, K., Watanabe, Y., Muratake, T., Takahashi, M., Someya, T. and Nawa, H. (2002) 'Decreased levels of brain-derived neurotrophic factor in serum of chronic schizophrenic patients.' *Psychiatry Research*, 110(3) pp. 249–257.
- Tribble, J. R., Cross, S. D., Samsel, P. A., Sengpiel, F. and Morgan, J. E. (2014) 'A novel system for the classification of diseased retinal ganglion cells.' *Visual Neuroscience*, 31(6) pp. 373–380.
- Tribble, J. R., Otmani, A., Kokkali, E., Lardner, E., Morgan, J. E. and Williams, P. A. (2021a) 'Retinal Ganglion Cell Degeneration in a Rat Magnetic Bead Model of Ocular Hypertensive Glaucoma.' *Translational Vision Science & Technology*, 10(1) p. 21.
- Tribble, J. R., Otmani, A., Kokkali, E., Lardner, E., Morgan, J. E. and Williams, P. A. (2021b) 'Retinal Ganglion Cell Degeneration in a Rat Magnetic Bead Model of Ocular Hypertensive Glaucoma.' *Translational Vision Science & Technology*, 10(1) p. 21.
- Tribble, J. R., Otmani, A., Sun, S., Ellis, S. A., Cimaglia, G., Vohra, R., Jöe, M., Lardner, E., Venkataraman, A. P., Domínguez-Vicent, A., Kokkali, E., Rho, S., Jóhannesson, G., Burgess, R. W., Fuerst, P. G., Brautaset, R., Kolko, M., Morgan, J. E., Crowston, J. G., Votruba, M. and Williams, P. A. (2021) 'Nicotinamide provides neuroprotection in glaucoma by protecting against mitochondrial and metabolic dysfunction.' *Redox Biology*, 43, July, p. 101988.
- Tribble, J. R., Vasalauskaite, A., Redmond, T., Young, R. D., Hassan, S., Fautsch, M. P., Sengpiel, F., Williams, P. A. and Morgan, J. E. (2019) 'Midget retinal ganglion cell dendritic and mitochondrial degeneration is an early feature of human glaucoma.' *Brain Communications*, 1(1) p. fcz035.
- Tribble, J. R., Williams, P. A., Caterson, B., Sengpiel, F. and Morgan, J. E. (2018) 'Digestion of the glycosaminoglycan extracellular matrix by chondroitinase ABC supports retinal ganglion cell dendritic preservation in a rodent model of experimental glaucoma.' *Molecular Brain*, 11(1) p. 69.
- Ueda, J., Sawaguchi, S., Hanyu, T., Yaoeda, K., Fukuchi, T., Abe, H. and Ozawa, H. (1998) 'Experimental glaucoma model in the rat induced by laser trabecular photocoagulation after an intracameral injection of India ink.' *Jpn J Ophthalmol*, 42 pp. 337–344.
- Ulsch, M. H., Wiesmann, C., Simmons, L. C., Henrich, J., Yang, M., Reilly, D., Bass, S. H. and de Vos, A. M. (1999) 'Crystal Structures of the Neurotrophin-binding Domain of TrkA, TrkB and TrkC.' *Journal of Molecular Biology*, 290(1) pp. 149–159.
- Unsain, N., Montroull, L. E. and Mascó, D. H. (2009) 'Brain-derived neurotrophic factor facilitates TrkB down-regulation and neuronal injury after status epilepticus in the rat hippocampus.' *Journal of Neurochemistry*, 111(2) pp. 428–440.

-
- Urcola, J. H., Hernández, M. and Vecino, E. (2006) 'Three experimental glaucoma models in rats: Comparison of the effects of intraocular pressure elevation on retinal ganglion cell size and death.' *Experimental Eye Research*, 83(2) pp. 429–437.
- Uzel, M. M., Elgin, U., Boral, B., Çiçek, M., Şen, E., Şener, B. and Yılmazbaş, P. (2018) 'The effect of trabeculectomy on serum brain-derived neurotrophic factor levels in primary open-angle glaucoma.' *Graefes Archive for Clinical and Experimental Ophthalmology*, 256(6) pp. 1173–1178.
- Vaezy, S., Martin, R., Kaczowski, P., Keilman, G., Goldman, B., Yaziji, H., Carter, S., Caps, M. and Crum, L. (1999) 'Use of high-intensity focused ultrasound to control bleeding.' *Journal of Vascular Surgery*, 29(3) pp. 533–542.
- Vecino, E., García-Grespo, D., García, M., Martinez-Millán, L., Sharma, S. C. and Carrascal, E. (2002) 'Rat retinal ganglion cells co-express brain derived neurotrophic factor (BDNF) and its receptor TrkB.' *Vision Research*, 42(2) pp. 151–157.
- Walsh, J. J. and Tschakovsky, M. E. (2018) 'Exercise and circulating BDNF: Mechanisms of release and implications for the design of exercise interventions.' *Appl Physiol Nutr Metab*, 43(11) pp. 1095–1104.
- Wang, C. S., Kavalali, E. T. and Monteggia, L. M. (2022) 'BDNF signaling in context: From synaptic regulation to psychiatric disorders.' *Cell*, 185(1) pp. 62–76.
- Wang, Y., Zhou, H., Luo, Q. and Cui, S. (2022) 'The effect of physical exercise on circulating brain-derived neurotrophic factor in healthy subjects: A meta-analysis of randomized controlled trials.' *Brain and Behavior*, 12(4).
- Wässle, H., Peichl, L. and Boycott, B. B. (1983) 'A spatial analysis of on- and off-ganglion cells in the cat retina.' *Vision Research*, 23(10) pp. 1151–1160.
- Weber, A. J. and Harman, C. D. (2005) 'Structure–Function Relations of Parasol Cells in the Normal and Glaucomatous Primate Retina.' *Investigative Ophthalmology & Visual Science*, 46(9) p. 3197.
- Weinreb, R. N., Liebmann, J. M., Cioffi, G. A., Goldberg, I., Brandt, J. D., Johnson, C. A., Zangwill, L. M., Schneider, S., Badger, H. and Bejanian, M. (2018) 'Oral Memantine for the Treatment of Glaucoma.' *Ophthalmology*, 125(12) pp. 1874–1885.
- West, A. E., Pruunsild, P. and Timmusk, T. (2014) 'Neurotrophins: Transcription and Translation.' In Lewin, G. R. and Carter, B. D. (eds) *Neurotrophic Factors*. Berlin, Heidelberg: Springer Berlin Heidelberg (Handbook of Experimental Pharmacology), pp. 67–100.
- White, J. G. (2008) 'Electron opaque structures in human platelets: Which are or are not dense bodies?' *Platelets*, 19(6) pp. 455–466.
- Williams, A. R. (1983) 'Interactions of Ultrasound with Platelets and the Blood Coagulation System.' In Millner, R., Rosenfeld, E., and Cobet, U. (eds) *Ultrasound Interactions in Biology and Medicine*. Boston, MA: Springer US, pp. 171–177.

Williams, P. A. (2016) 'Inhibition of the classical pathway of the complement cascade prevents early dendritic and synaptic degeneration in glaucoma' p. 13.

Williams, P. A., Harder, J. M., Foxworth, N. E., Cochran, K. E., Philip, V. M., Porciatti, V., Smithies, O. and John, S. W. M. (2017) 'Vitamin B₃ modulates mitochondrial vulnerability and prevents glaucoma in aged mice.' *Science*, 355(6326) pp. 756–760.

Wong-Riley, M. (2010) 'Energy metabolism of the visual system.' *Eye and Brain*, July, p. 99.

Yan, Q., Elliott, J. and Snider, W. D. (1992) 'Brain-derived neurotrophic factor rescues spinal motor neurons from axotomy-induced cell death.' *Nature*, 360(6406) pp. 753–755.

Yang, X., Chou, T.-H., Ruggeri, M. and Porciatti, V. (2013) 'A New Mouse Model of Inducible, Chronic Retinal Ganglion Cell Dysfunction Not Associated with Cell Death.' *Investigative Ophthalmology & Visual Science*, 54(3) p. 1898.

Yeo, G. S. H., Connie Hung, C.-C., Rochford, J., Keogh, J., Gray, J., Sivaramakrishnan, S., O'Rahilly, S. and Farooqi, I. S. (2004) 'A de novo mutation affecting human TrkB associated with severe obesity and developmental delay.' *Nature Neuroscience*, 7(11) pp. 1187–1189.

Yoshii, A. and Constantine-Paton, M. (2007) 'BDNF induces transport of PSD-95 to dendrites through PI3K-AKT signaling after NMDA receptor activation.' *Nature Neuroscience*, 10(6) pp. 702–711.

Yu, T., Zhang, Z., Zhou, D. and Li, C. (2022) 'Systematic Review and Meta-Analysis on the Rehabilitation Effect of Different Intensity Exercise on the Patients with Cardiovascular Diseases.' Tang, M. (ed.) *Computational and Mathematical Methods in Medicine*, 2022, July, pp. 1–9.

Yun, H., Lathrop, K. L., Yang, E., Sun, M., Kagemann, L., Fu, V., Stolz, D. B., Schuman, J. S. and Du, Y. (2014) 'A Laser-Induced Mouse Model with Long-Term Intraocular Pressure Elevation.' Bui, B. V. (ed.) *PLoS ONE*, 9(9) p. e107446.

Yun, S.-H., Sim, E.-H., Goh, R.-Y., Park, J.-I. and Han, J.-Y. (2016) 'Platelet Activation: The Mechanisms and Potential Biomarkers.' *BioMed Research International*, 2016 pp. 1–5.

Zagrebelsky, M. and Korte, M. (2014) 'Form follows function: BDNF and its involvement in sculpting the function and structure of synapses.' *Neuropharmacology*, 76, January, pp. 628–638.

Zhang, D., Vetrivel, L. and Verkman, A. S. (2002) 'Aquaporin Deletion in Mice Reduces Intraocular Pressure and Aqueous Fluid Production.' *Journal of General Physiology*, 119(6) pp. 561–569.

Zuccato, C., Liber, D., Ramos, C., Tarditi, A., Rigamonti, D., Tartari, M., Valenza, M. and Cattaneo, E. (2005) 'Progressive loss of BDNF in a mouse model of Huntington's disease and rescue by BDNF delivery.' *Pharmacological Research*, 52(2) pp. 133–139.

Appendix

Appendix 1 - List of materials

- A1.1. Reagents and consumables
- A1.2. Antibodies
- A1.3. Solutions
- A1.4. Other consumables
- A1.5. Equipment
- A1.6. Medications

Appendix 2 - Exercise tracker construction

- A2.1. Construction materials
- A2.2. Circuit diagram
- A2.3. Python code
- A2.4. RStudio Script

Appendix 3 - Additional RStudio Scripts

- A3.1. RGC Sholl data collation
- A3.2. RGC Field data collation
- A3.2. RGC count heatmap

Appendix 4 – Rosa26-BDNF-Myc/PF4iCre genotyping PCR records

Appendix 5 – Exercise tracking data

- A5.1. Exercise tracking data – serum BDNF following 7 days of exercise, WT mice
- A5.2. Exercise tracking data – serum BDNF following 7 days of exercise in B Cre+ mice
- A5.3. Exercise tracking data – plasma BDNF following 3 days of exercise, B Cre+ mice

Appendix 1

A1.1. Reagents

Agar	Sigma-Aldrich, A1296-500G
B27	Gibco, 10889-038
Bovine Serum Albumin	Sigma-Aldrich, A7030-500G
Brain-derived neurotrophic factor <i>E. coli</i> recombinant	Regeneron/Amgen partners
Dichloromethane	D7566-500ML, Sigma
Dil Stain (1,1'-Diocadecyl-3,3,3',3'- Tetramethylindocarbocyanine Perchlorate (<i>Dil</i> ; <i>DilC18(3)</i>))	Invitrogen, D282, Thermo Fisher
DiO'; DiOC18(3) (3,3'- Diocadecyloxacarbocyanine Perchlorate)	Invitrogen, D275, Thermo Fisher
Dynabeads M-450 Epoxy	Invitrogen, 14011, Thermo Fisher Scientific
FluorSave Reagent	Millipore, 345789, Sigma-Aldrich
GlutaMAX	Gibco, 35050-61
Hank's Balanced Salt Solution (HBSS)	Gibco, 24020-091, Fisher Scientific
Hoescht 33342	Thermo Scientific, 62249, Thermo Fisher Scientific
Horse Serum	Sigma-Aldrich, H0146-5ML
Methylene chloride	European Pharmacopoeia (EP), M1550000, Sigma-Aldrich
N2	Gibco, 17502-048
Neurobasal-A Medium	Gibco, 10888-022, Fisher Scientific
OCT Embedding Matrix for Frozen Sections	CellPath, KMA-0100-00A, Fisher Scientific
Paraformaldehyde 4%, buffered pH6.9	Sigma-Aldrich, 100496500
PBS pH 7.4 (10X)	Gibco, 70011-044, Fisher Scientific
PCRBIO Rapid Extract PCR Kit	PCR BioSystems, PB10.24-08
PCRBIO Ladder IV. 100Lanes	PCR BioSystems, PB40. 14-01

Penicillin Streptomycin	Gibco, 15140-122, Fisher Scientific
Pierce RIPA Buffer	Thermo Scientific, 89901, Thermo Fisher Scientific
Polyurethane microbeads, 17µm	Sunjin Beauty Ltd
Protein G Sepharose 4 Fast Flow beads	GE Healthcare, GE17-0618-01
Pure & Simple Primers	Sigma-Aldrich, VC00026N
Sucrose	Sigma-Aldrich, S0389-1KG
Triton X-100, SigmaUltra	Sigma-Aldrich, T9284-500ML
Tungsten M-25 Microcarrier, 1.7µm	Bio-Rad, 1652269
Tungsten powder, APS <1 micron, 99.95% (metals basis)	Alfa Aesar, Thermo Fisher Scientific, 44210

A1.2. Antibodies

Anti-TrkB, goat polyclonal	R&D systems, AF1494
Anti-RBPMS, rabbit	Novus, NBP2-20112
Donkey anti-goat IgG (H+L) Cross-Adsorbed Secondary Antibody, Alexa Fluor 594	Invitrogen, A-11058
Goat anti-Rabbit IgG (H+L), Cross-Adsorbed Ready Probes, Secondary Antibody, Alexa Fluor 594	R37117, Thermo Fisher
mAB BDNF-#9 Hybridoma	Developmental Studies Bank, BDNF-#9

A1.3. Solutions

ACD Buffer
85mM Trisodium citrate, 65mM Citric acid, 100mM Glucose, pH 5 in ddH₂O

Phosphate Buffered Saline (PBS) 10%
80g Sodium Chloride (NaCl), 2.0g Potassium Chloride (KCl), 14.4g Sodium phosphate (Na₂HPO₄), 2.4g Potassium phosphate (KH₂PO₄) was dissolved in 800mL ddH₂O. The pH was adjusted to pH 7.4 and the volume adjusted to 1L with the addition of ddH₂O

Tyrodes Buffer
134mM NaCl, 12mM NaHCO₃, 2.9mM KCl, 0.34mM Na₂PO₄, 1mM MgCl₂, 10mM Hepes, 5mM Glucose, pH 7.4 in ddH₂O

TAE Buffer (50x)

Tris 242g, Acetic Acid 57.1mL and EDTA 0.5M pH8 100mL dissolved and made up to 1L with ddH₂O

Retinal Explant Media

For 10 mL

100 µL N-2 supplement (100X), 200 µL B-27 supplement (50X), 100µL Pen/Strep (10000 U/mL), 25 µL GlutaMAX supplement (200 mM), 9.565 mL Neurobasal-A Medium

A1.4. Other Consumables

BD Microlance Stainless Steel Needles. Orange 25G	Fisher Scientific, 12389169
BD Microlance Stainless Steel Needles, Brown 26G	Fisher Scientific, 10703815
Capillary Glass, 1.0mm OD, 0.58mm ID, 7.62c, (3 inches) long	World Precision Instruments, 1B100-3
Eppendorf 1.5mL	
Falcon Cell Culture Inserts, 3.0 µm pore Size, for use with 6 well plate	Falcon, 353092, Fisher Scientific
Falcon tube 50mL	
Falcon tube 15mL	
Millicell, Cell Culture Inserts 0.4µm, 30mm Diameter	Merck Millipore, PICMORG50, Fisher Scientific
MX35 Premier+ Microtome Blades	Thermo Scientific, 3052835
Tefzel Tubing	Bio-Rad, 1652441
TSK Steriject, Invisible Needle	TSK, LDS-02009-100
0.2mL 8-Strip PCR Tubes, Attached Dome Cap Strip	Starlab UK Ltd, I1402-2800
Thermo Scientific BioLite Multidishes and Microwell Plate (6 well)	Fisher Scientific, 11825275
Thermo Scientific Superfrost Plus Adhesion slides J1800AMNZ Pack of 72	Fisher Scientific, 10149870

A1.5. Equipment

Dumont Tweezer, Style N5	Dumont, 0304-N5-PO, Electron Microscopy Sciences
FLUOstar Omega, BMG Labtech Platereader	
Helios Gene gun	Bio-Rad, 1652432
TonoLab rebound tonometer	Icare
Disposable transducer for Icare Tonolab tonometer	Icare, 1736010, Eickemeyer
Microelectrode Beveler	World Precision Instruments, BV-10
Leica CM3050 S Cryostat	Leica
LSM 780 Carl Zeiss Confocal Microscope	Zeiss
McPherson Straight Tying Forceps	Blink Medical, 10-9008
NanoFil Syringe, 100uL	World Precision Instruments, NANOFIL-100
NanoFil needle, 33 G bevelled	World Precision Instruments, NF33BV-2
NanoFil needle, 35 G bevelled	World Precision Instruments, NF35BV-2
1.00mm Glass Pipette Holder for NANOFIL Syringe	World Precision Instruments, NFINHLD-G10
Pierse Notched Forceps	Duckworth & Kent Ltd, 2-100E
Vannas Scissors (straight)	Duckworth & Kent Ltd, 1-110

A1.6. Medications

Atipamezole, Antisedan, 5mg/ml	Orion Pharma
Chloramphenicol 0.5% Minims	Bausch & Lomb, PL03468/0069
Isoflurane 200% Inhalation Vapour, Liquid	Piramal Healthcare UK Ltd
Ketamine, Ketamidol 100mg/ml	Chanelle Pharma,
Medetomidine, Domitor, 1mg/ml	Orion Pharma
Oxybuprocaine Hydrochloride 0.4% Minims	Bausch & Lomb, PL03468/0053

Povidone Iodine 5% Minims

Bausch & Lomb, PL03468/0020

Viscotears Liquid Gel

Bausch & Lomb, PL13757/0020

Appendix 2 – Exercise Tracker

A2.1. Construction Materials

Cage Construction

RB3R Cage

PLUTEO Silent Hamster Running Wheel, 13cm/5.1 Inch

Crestglass 3mm Perspex Clear Acrylic Plastic Sheet (420 x 297mm, A3)

Crestglass 3mm Perspex White Acrylic Plastic Sheet (420 x 297mm, A3)

PVC Equal Corner - CQFD 2002-68540, 1m, 15 x 15mm

M4 x 16mm nut/bolt

M4 x 12mm nut/bolt

M3 x 16mm nut/bolt

Electronic equipment

Tecnoware UPS ERA PLUS 800 Together On - Uninterruptable power supply

Raspberry pi 4 B Model B

Freenove Ultimate Starter Kit for Raspberry pi 4 B 3 B+ (solderless breadboard)

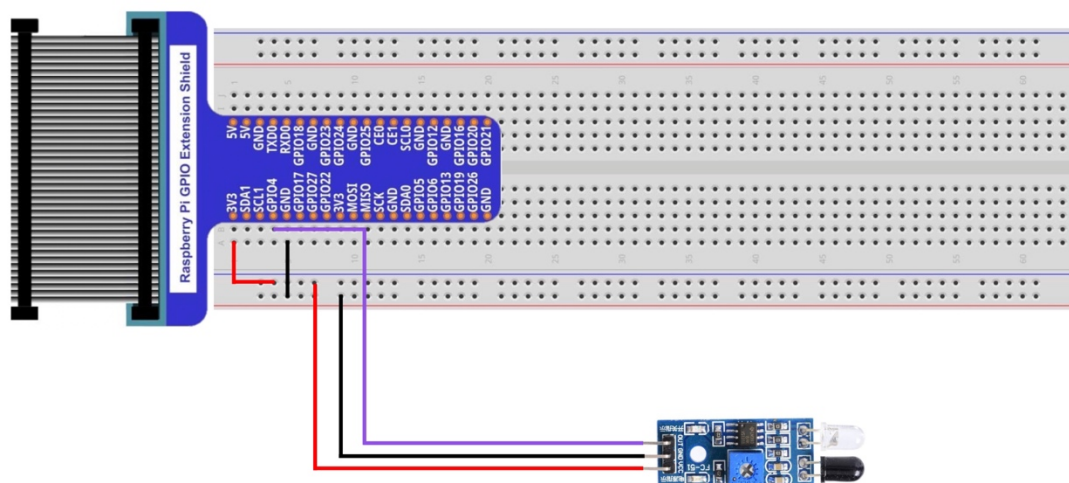
Infrared Obstacle Avoidance Sensor Module, 3 wire, Friendly, Friendly-Obstacle-431S

TRIXES Crab Clamp Mount Stand Desk Wall Panel Holder Clip Professional 1/4" and 3/8" Thread

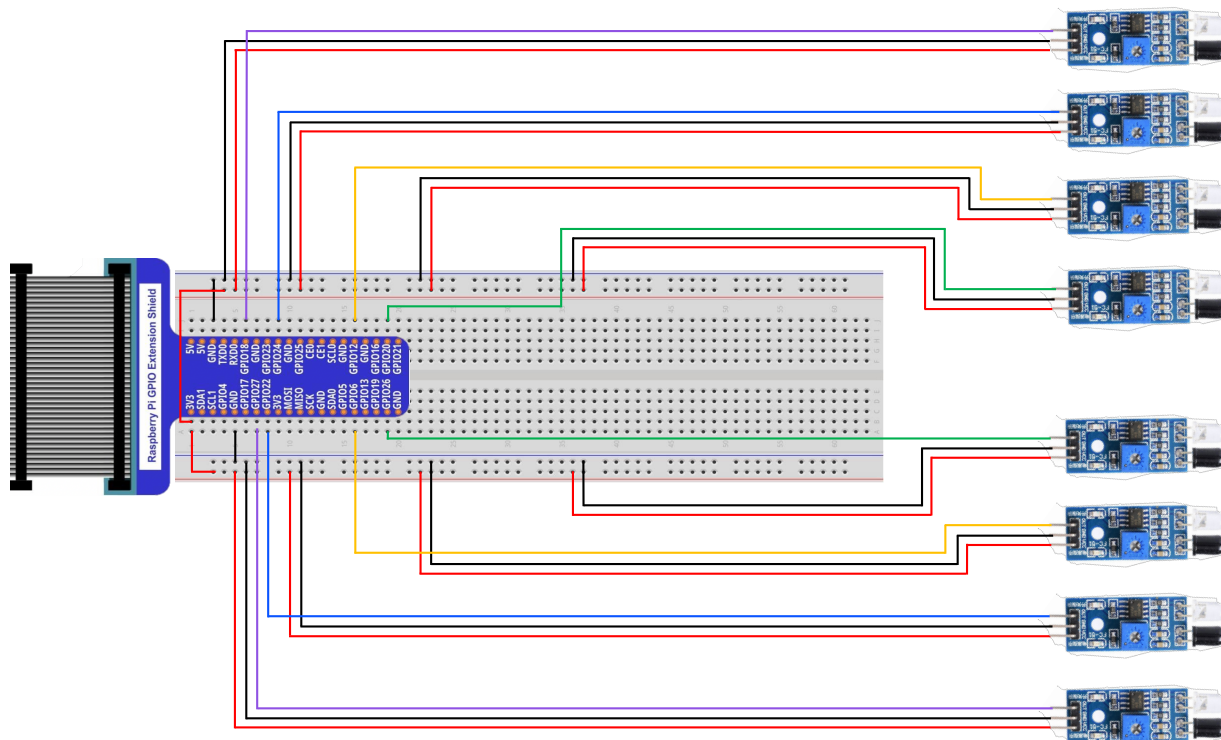
4 Core Alarm Cable, 0.2mm² x 25m, TIME Cables

A2.2. Circuit Diagram

Example of single IR tracker circuit



Full circuit IR tracking apparatus



A2.3. Exercise tracker Python Script

To be run on Raspberry Pi 4B

Script tracks activity from a single cage. The same script is run in parallel amending the GPIO input for additional cages.

```
# Exercise Tracker Cage 1A

### Author: Andrew Want
### Date: December 2021

import RPi.GPIO as GPIO
sensorPin = 11                                # define sensorPin (GPIO 17)

import time
import datetime
import csv

file = open("/home/pi/Exercise_tracker/Results/Cage1A_results.csv",mode="a", encoding="UTF8")

def setup():
    file.write("Time, RPM, Count" + "\n")
    GPIO.setmode(GPIO.BOARD)                  # use PHYSICAL GPIO Numbering
    GPIO.setup(sensorPin, GPIO.IN)            # set sensorPin to INPUT mode
    global totalcount
    revcount = 0                               # revolutions count
    totalcount = 0
    global rev_time
    rev_time = 0                               # revolutions count
    global time_start
    time_start = time.time()
    global rpm
    rpm = 0
    GPIO.remove_event_detect(sensorPin)

def revtime(channel):
    global rev_time, time_start, totalcount
    rev_time = time.time() - time_start
    time_start = time.time()
    totalcount +=1
    now = datetime.datetime.now()
    date_time_string = str(now)
    calculate_rpm()
    print (f'Time: {datetime.datetime.now()},', 'RPM {0}' .format(rpm), 'Count :
%.2f'%(totalcount))
    rowdata2 = (date_time_string, rpm, totalcount)
    rowdatastring = str(rowdata2)
    print (rowdata2)
```

```

        with open("/home/pi/Exercise_tracker/Results/Cage1A_results.csv",mode="a",
encoding="UTF8") as file:
            csv_output = csv.writer(file)
            csv_output.writerow ([date_time_string, rpm, totalcount])
            file.close ()

def calculate_rpm():
    global rev_time, rpm
    if time.time() - time_start > 1.5:
        rpm = 0
    else:
        if rev_time != 0:
            rpm = 60/rev_time

def destroy():
    GPIO.cleanup()                # Release GPIO resource

if __name__ == '__main__':
    # Program entrance
    print ('Program is starting...')
    setup()
    GPIO.add_event_detect(sensorPin, GPIO.RISING, callback=revtime)

    while True:
        time.sleep(0.1)

if KeyboardInterrupt:
    # Press ctrl-c to end program
    file.close ()
    destroy ()

```

A2.4. Exercise Tracker R Script

Written to process exercise tracker data

```

# Exercise tracker data analysis
# Author: Andrew Want

#Instructions
#Step 1
#Manually import the dataset you need to analyse
    # You will need to do one cage at a time and then copy the graphs and numbers etc
    #Use the 'Import Dataset' dropdown menu, click 'From text (base)' and pick the file
    # File type should be .csv

#Step 2
# Rename the data set so the same code can be used each time

```

```

# Write the name of the dataset (e.g. Cage1A_results) after 'new_tracker_data <- '

#Step 3
#Highlight everything and click 'Run" at the top of this window
#This should make a histogram and then give you the count, mean/SD of RPM and the time spent
exercising
#After you have run the full code once, you can highlight single parts if you want to see just
that bit (e.g. scatter plot)

#Step 4
#When you have finished, make sure to clear all the stored info in the environment box
#If you don't it may mess up the results for the next dataset
#Click on the small picture of a broom near the 'Import Dataset' button

#Import the required packages
library(lubridate)
library(ggplot2)
library(data.table)
library(dplyr)
library(tibble)
library(stringr)

#Manually import the dataset (Use the 'Import Dataset' dropdown menu, click 'From text (base)'
and pick the file)

#Rename dataset
#(type the name of the dataset after the arrow, this renames it as 'new_tracker_data')
new_tracker_data <- Cage2A_results

#Adjust time if Raspberry pi not synced properly
new_tracker_data$V1 <- as.POSIXct(new_tracker_data$V1, format="%Y-%m-%d %H:%M:%OS")

# Number of days to be corrected (replace X with number of days to be added)
Time_days <- 81 * 24 * 60 * 60

# Hours to be corrected (replace Y with number of hours to be added)
Time_hours <- 16 * 60 * 60

# Minutes to be corrected (replace Z with number of minutes to be added)
Time_minutes <- 17 * 60

#Total correction in seconds
correction = Time_days + Time_minutes + Time_hours
new_tracker_data$Corrected_time <- as.POSIXct(correction, format="%Y-%m-%d %H:%M:%OS.",
origin=new_tracker_data$V1)

```

```

#Create column showing time interval
new_tracker_data2 <- tibble(new_tracker_data)
new_tracker_data2$Timeinterval <- new_tracker_data2$Corrected_time -
lag(new_tracker_data2$Corrected_time, n=1)

#Remove false positive results (when sensor fires multiple times for single rotation)
#Remove rows if Time interval is > X (was set at 0.275)
new_tracker_data3 <- subset(new_tracker_data2, Timeinterval>0.275)

#Create column showing new time interval
new_tracker_data4 <- tibble(new_tracker_data3)
new_tracker_data4$Newtimeinterval <- new_tracker_data4$Corrected_time -
lag(new_tracker_data4$Corrected_time, n=1)

#Calculate new RPM from corrected time intervals
new_tracker_data4$RPM <- 60 / as.numeric(new_tracker_data4$Newtimeinterval)
#View (new_tracker_data4)

RPMdata <- new_tracker_data4$RPM

mean(RPMdata, na.rm = TRUE)
sd(RPMdata, na.rm = TRUE)

#Calculate exercise time (sum of time intervals where interval is less than 2 seconds)
exercise_time_data <- subset(new_tracker_data4, Timeinterval<2.0)
exercise_time_number <- tibble(exercise_time_data$Newtimeinterval)
exercise_time_na_omit <- na.omit(exercise_time_number)
exercise_time <- sum(exercise_time_na_omit$`exercise_time_data$Newtimeinterval`)

#Plot graphs and show important values

#plot scatter graph
ggplot(new_tracker_data4, aes(x=Corrected_time, y=RPM)) + theme_bw() +
  theme(panel.grid.major = element_blank(),
        panel.grid.minor = element_blank(), text = element_text(size = 12, colour="black"),
        axis.title.x = element_text(margin = margin(t = 10, r = 0, b = 10, l = 0)),
        axis.title.y = element_text(margin = margin(t = 0, r = 15, b = 0, l = 10))) +
  xlab("Time") + scale_x_datetime(labels = function(x) str_wrap(x, width=10), breaks = "24
hours", date_minor_breaks = "12 hours") + ylab("RPM") + ylim(0,300) + #xlim(c(as.POSIXct("2022-
03-22 10:00:00", format = "%Y-%m-%d %H:%M:%S"), as.POSIXct("2022-03-28 12:00:00", format = "%Y-
%m-%d %H:%M:%S"))) +
  geom_point(aes(x=Corrected_time, y=RPM), size = 0.1) #+ geom_line(aes(x=Corrected_time,
y=RPM))

#Plot histogram

```

```
#Histogram of RPM
ggplot(new_tracker_data4, aes(x=RPM)) + geom_histogram(binwidth = 10, colour = "black", fill =
"white") + ylim(0,40000) + xlim(0,200) + ylab("Count") +
  theme(text = element_text(size = 18, colour="black"),
    axis.title.x = element_text(margin = margin(t = 10, r = 0, b = 10, l = 0)),
    axis.title.y = element_text(margin = margin(t = 0, r = 15, b = 0 , l = 10)))

#Show important values - will be displayed in the 'Console' box below
count(new_tracker_data4)
mean(RPMdata, na.rm = TRUE)
sd(RPMdata, na.rm = TRUE)
print(exercise_time)
```

Appendix 3 – Additional RStudio Scripts

A3.1. RGC Sholl Collation

```

####RGC_Sholl_collation
##Author: Andrew Want (edited from script by E. Kokkali)
### Date: July 2021

#load various libraries (not all of these are used here)
library(RColorBrewer)
library(tidyverse)
library(statmod)
library(ggrepel)
library(readxl)
library(mgcv)
library(reshape2)
library(openxlsx)
library(pracma)

#set working directory

#import all xlsx fiels at once

#Sholl
sholl_xlsx_list <- list.files(path = "~/Desktop/Sholltest", pattern = "*.xlsx", full.names = T)
sholl_data <- sapply(sholl_xlsx_list, read_excel, sheet = "Filament No. Sholl Intersec-28",
range = "A2:A48", simplify = T)
filament_length <- sapply(sholl_xlsx_list, read_excel, sheet = "Filament Length (sum)", range
= "A2:A3", simplify = T)
dendrite_level <- sapply(sholl_xlsx_list, read_excel, sheet = "Dendrite Branch Level", range =
"A2:A300", simplify = T)
dendrite_depth <- sapply(sholl_xlsx_list, read_excel, sheet = "Dendrite Branch Depth", range =
"A2:A300", simplify = T)

#make one big dataframe with columns stuck next to each other
sholl_dataframe <- as.data.frame(sholl_data)

#replace all NA values with 0
sholl_dataframe[is.na(sholl_dataframe)] <- 0

# Make Sholl maximum dataframe
#create loop for area under the curve (AUC), capture.output allows to save the output
MaxSholl <- capture.output(for(i in sholl_dataframe){
  print(max(i))
})

MaxSholl <- as.data.frame(MaxSholl)

```

```

#Remove "[1] "
MS <- as.data.frame(sub("[1] ", "", MaxSholl$MaxSholl, fixed = TRUE))
colnames(MS) <- "Max Sholl"

#make a radius vector, which should match exactly in length
Radius <- seq(0, 450, by =10)

#create loop for area under the curve (AUC), capture.output allows to save the output
auc <- capture.output(for(i in sholl_dataframe){
  print(trapz(Radius, i))
})
auc <- as.data.frame(auc)
#Remove "[1] "
AUC <- as.data.frame(sub("[1] ", "", auc$auc, fixed = TRUE))
colnames(AUC) <- "AUC"

#Incorporate radius in the sholl dataframe
sholl_dataframe <- cbind(sholl_dataframe, Radius)

# Make filament length dataframe
filament_length_dataframe <- as.data.frame(filament_length)

#Collect Dendrite branching level data
#make one big dataframe with columns stuck next to each other
dendritelevel_dataframe <- as.data.frame(dendrite_level)

#Collect Dendrite branching depth data
#make one big dataframe with columns stuck next to each other
dendritedepth_dataframe <- as.data.frame(dendrite_depth)

#export sholls and AUC
write.xlsx(sholl_dataframe, "~/Desktop/Sholltest/All_sholls.xlsx")
write.xlsx(AUC, "~/Desktop/Sholltest/All_AUC.xlsx")
write.xlsx(filament_length_dataframe, "~/Desktop/Sholltest/All_filament_length.xlsx")
write.xlsx(MS, "~/Desktop/Sholltest/All_Max_Sholl.xlsx")
write.xlsx(dendritelevel_dataframe, "~/Desktop/Sholltest/All_Dendrite_Level.xlsx")
write.xlsx(dendritedepth_dataframe, "~/Desktop/Sholltest/All_Dendrite_Depth.xlsx")

```

A3.2. RGC Field Area Collation

#Collect Dendrite field area from convex hull xlsx files

Author: Andrew Want

Date: June 2021

#load various libraries (not all of these are used here)

library(RColorBrewer)

library(tidyverse)

library(statmod)

library(ggrepel)

library(readxl)

library(mgcv)

library(reshape2)

library(openxlsx)

library(pracma)

#set working directory

#import all xlsx fiels at once

#Files

area_xlsx_list <- list.files(path = "~/Desktop/Sholltest", pattern = "*.xlsx", full.names = T)

field_area <- sapply(area_xlsx_list, read_excel, sheet = "Area", range = "A2:A3", simplify = T)

Make Field area dataframe

field_area_dataframe <- as.data.frame(field_area)

FA <- as.data.frame(t(field_area_dataframe))

#Remove "[1] "

FA <- as.data.frame(sub("[1] ", "", FA\$V1, fixed = TRUE))

colnames(FA) <- "Field Area"

View(FA)

write to excel file

write.xlsx(FA, "~/Desktop/Sholltest/All_Field_Area.xlsx")

A3.3. RGC Cell Count Heatmap

```
# Circular heatmap
### Author: Andrew Want
### Date: May 2022

#Import library
library(RColorBrewer)
library(tidyverse)
library(statmod)
library(ggrepel)
library(readxl)
library(circlize)
library(ggplot2)
library(reshape)
library(ComplexHeatmap)

#Import data set

heatdata1 <- read_excel("Documents/WCAT/PhD Project/ONC Model/ONC 10 RBPMS/ONC10 RBPMS cell
counts.xlsx",
                        sheet = "WT ONC", range = "B1:D5")

heatdata2 <- read_excel("Documents/WCAT/PhD Project/ONC Model/ONC 10 RBPMS/ONC10 RBPMS cell
counts.xlsx",
                        sheet = "BDNF-PF4 ONC", range = "B1:D5")

heatdata3 <- read_excel("Documents/WCAT/PhD Project/ONC Model/ONC 10 RBPMS/ONC10 RBPMS cell
counts.xlsx",
                        sheet = "WT CTL", range = "B1:D5")

heatdata4 <- read_excel("Documents/WCAT/PhD Project/ONC Model/ONC 10 RBPMS/ONC10 RBPMS cell
counts.xlsx",
                        sheet = "BDNF-PF4 CTL", range = "B1:D5")

#Draw circoheatmaps
col_fun1 = colorRamp2(c(1000, 2000, 3000, 4000), c("white", "lightcoral", "firebrick1",
"firebrick4"))
circos.heatmap(heatdata1, col = col_fun1, track.height = 0.95, cluster=FALSE, na.col =
"lightgrey")
circos.clear()

circos.heatmap(heatdata2, col = col_fun1, track.height = 0.95, cluster=FALSE, na.col =
"lightgrey")
circos.clear()

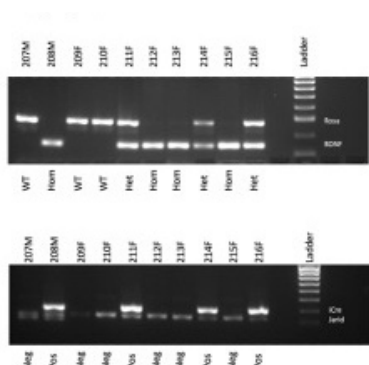
circos.heatmap(heatdata3, col = col_fun1, track.height = 0.95, cluster=FALSE, na.col =
"lightgrey")
```

```
circos.clear()

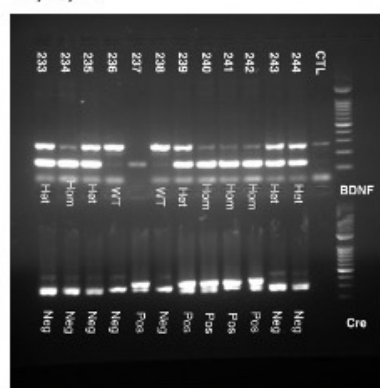
circos.heatmap(heatdata4, col = col_fun1, track.height = 0.95, cluster=FALSE, na.col =
"lightgrey")
circos.clear()
lgd = Legend(col_fun = col_fun1, legend_height = unit(1.5, "inch"))
draw(lgd, x = unit(0.05, "npc"), just = "left")
```

Appendix 4 - PCR Records

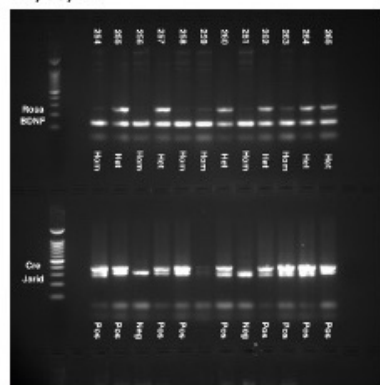
Images from PCR genotyping gels for Rosa26-LSL-Bdnf-myc-IG/Pf4iCre mice



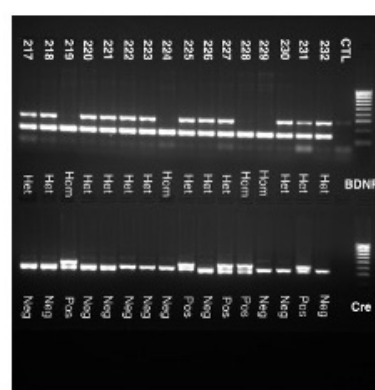
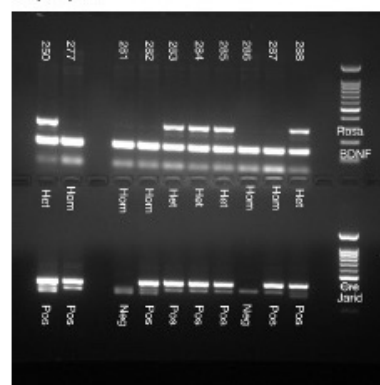
12/03/21



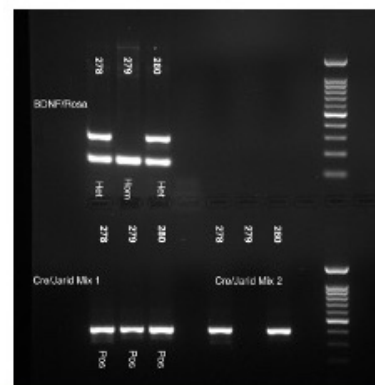
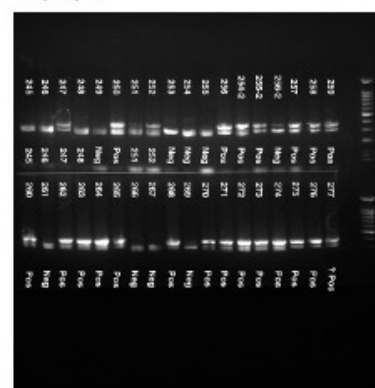
12/03/21



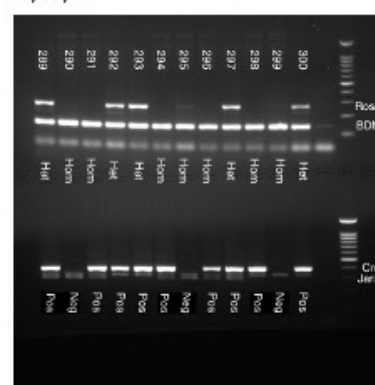
12/09/21



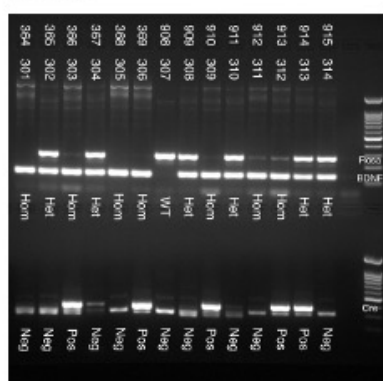
08/06/21



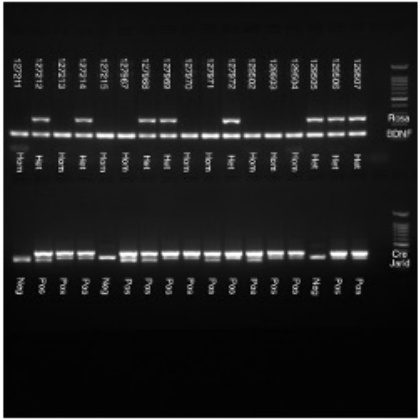
12/09/21



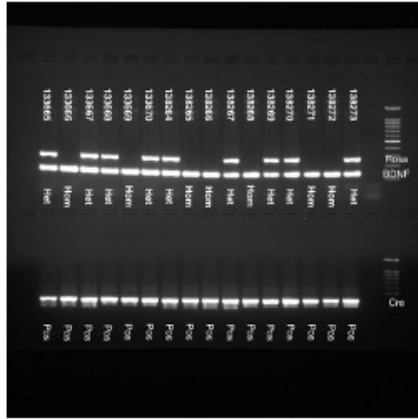
28/09/21



10/05/22



10/08/22



Appendix 5 – Exercise Tracking data

This appendix contains the raw data obtained from the exercise tracking experiments using the customised tracking equipment. In each experiment, a scatter plot and histogram of the tracking data is provided for each individual in the exercise group.

Scatter plot

Points represent individual events, caused by an interruption of the IR sensor when the exercise wheel rotates. The time the event occurred is plotted on the x-axis, and the revolutions per minute (RPM, calculated based on the time interval between events) is plotted on the y-axis. These scatter plots are useful for illustrating the times of peak activity.

Histograms

Histograms show the frequency of events (wheel revolutions) occurring based on their RPM (bin size 10RPM). This plot is a useful representation of the variation in speed between individuals, as well as the total number of revolutions.

Data is included for the following experiments

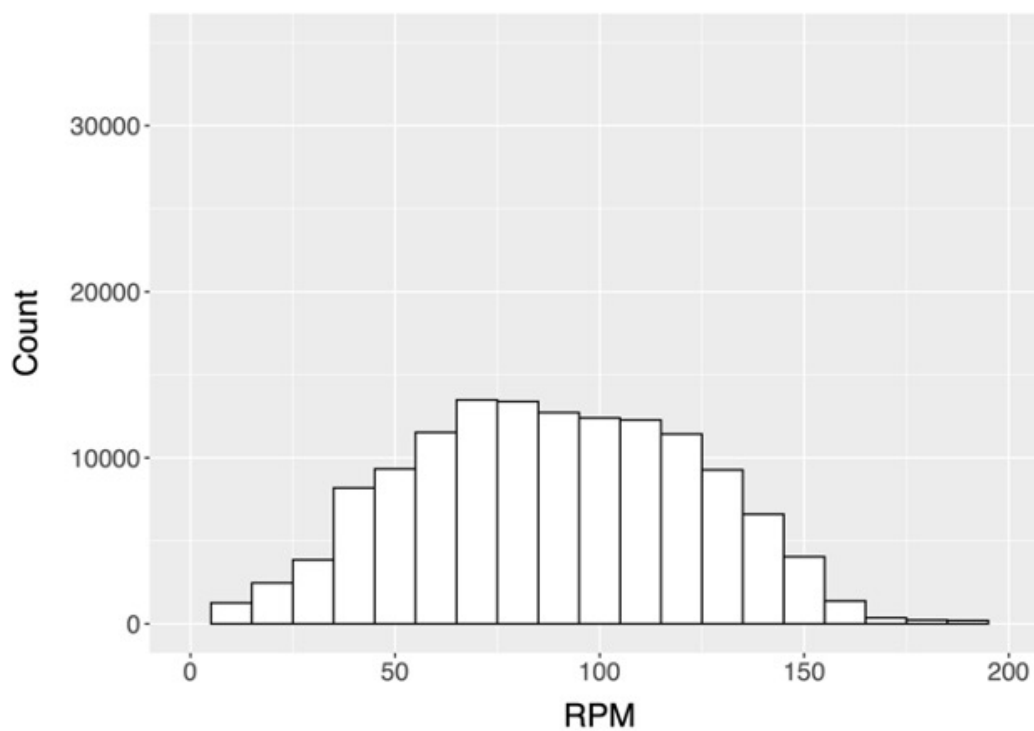
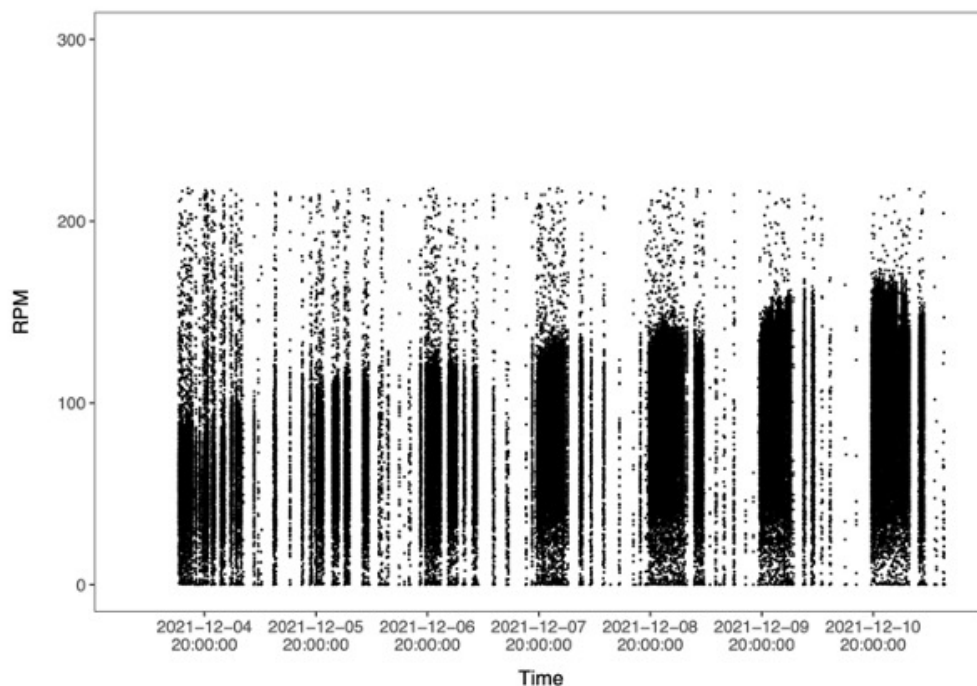
A5.1. Exercise tracking data – serum BDNF following 7 days of exercise, WT mice

A5.2. Exercise tracking data – serum BDNF following 7 days of exercise in B Cre⁺ mice

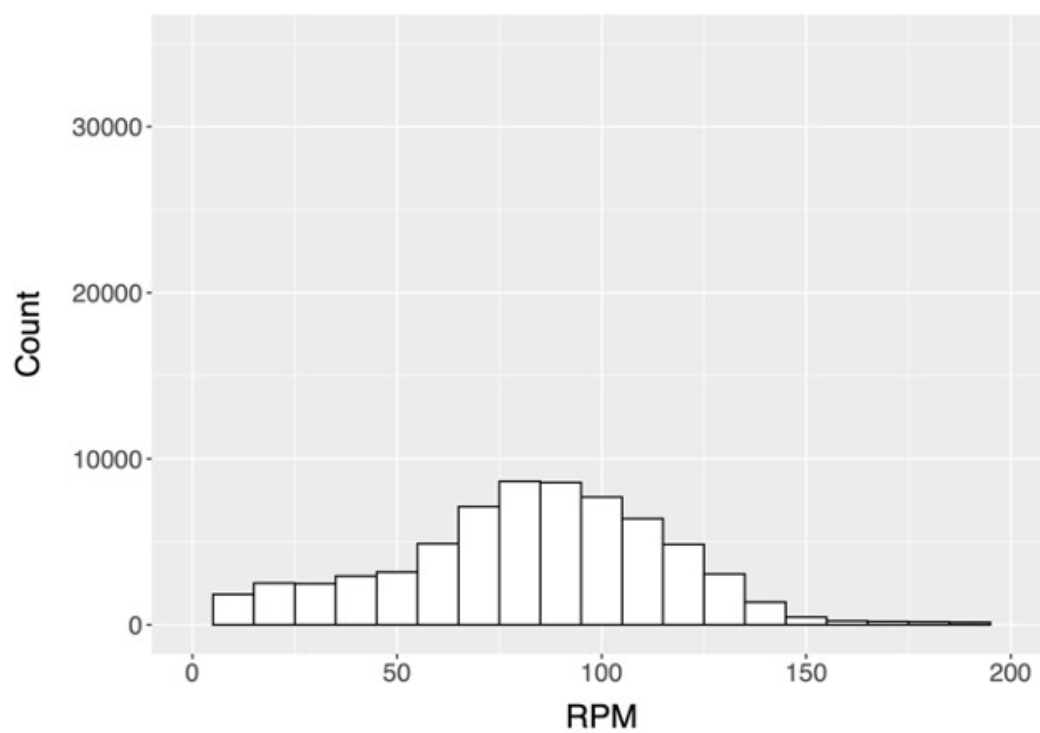
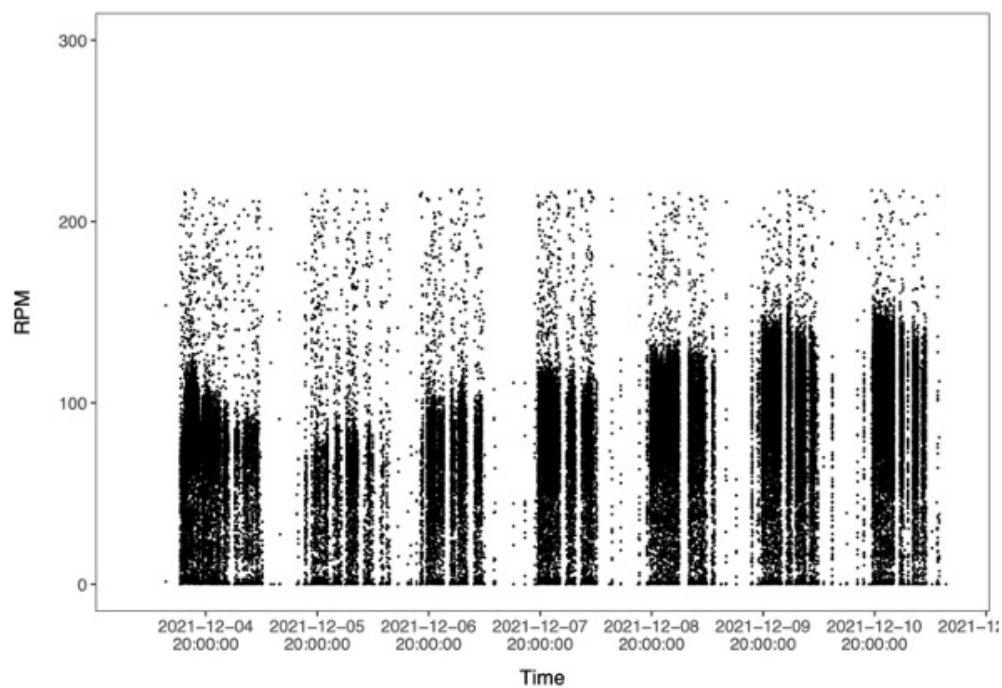
A5.3. Exercise tracking data – plasma BDNF following 3 days of exercise, B Cre⁺ mice

A5.1. Exercise tracking data – serum BDNF following 7 days of exercise, WT mice

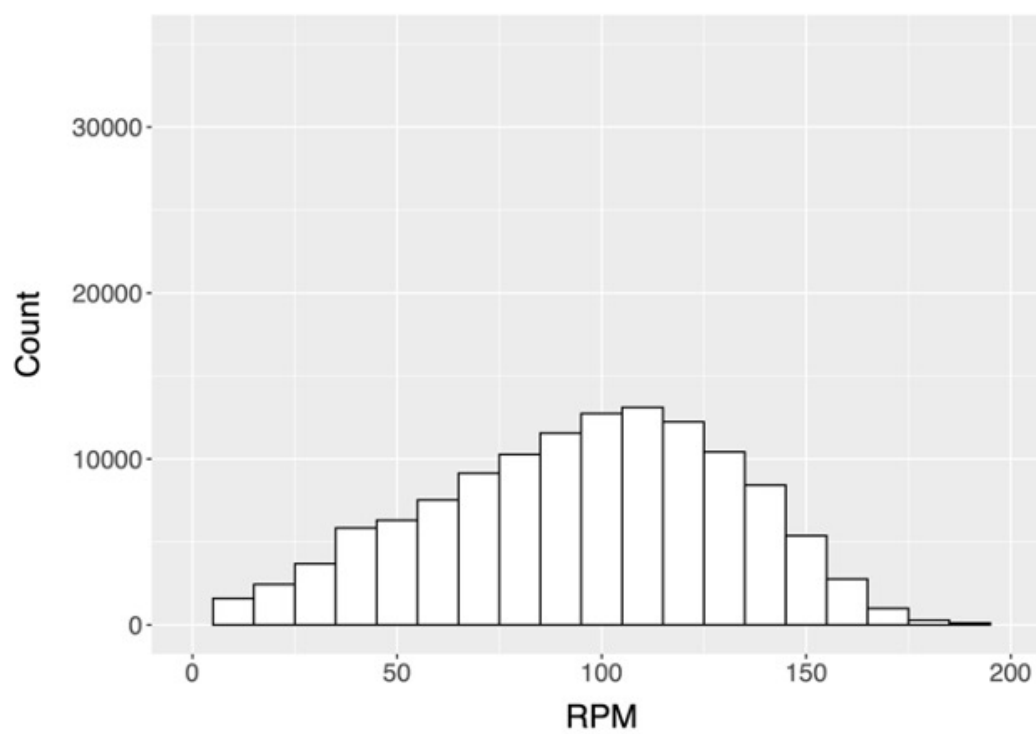
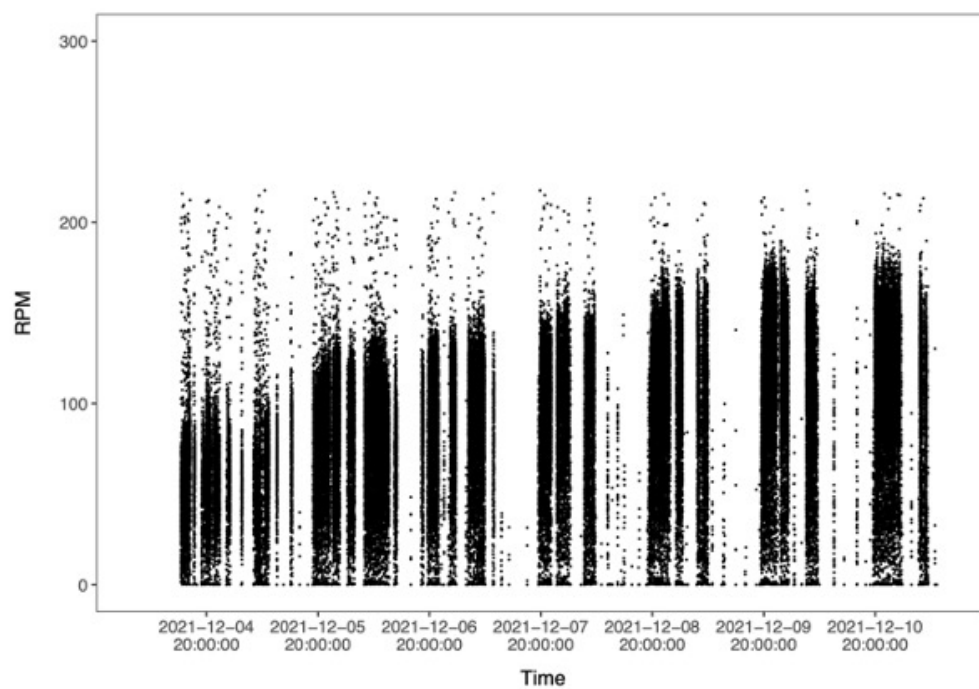
Animal: 112892
Cage: 1A
Sex: Male
Genotype: C57BL/6J



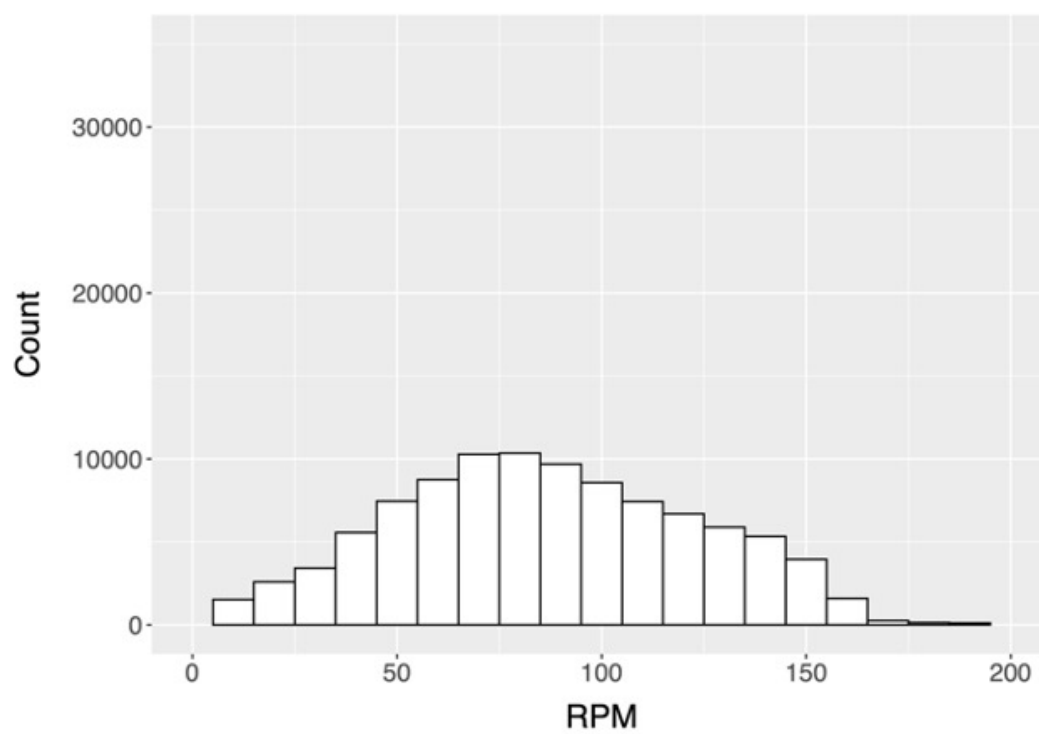
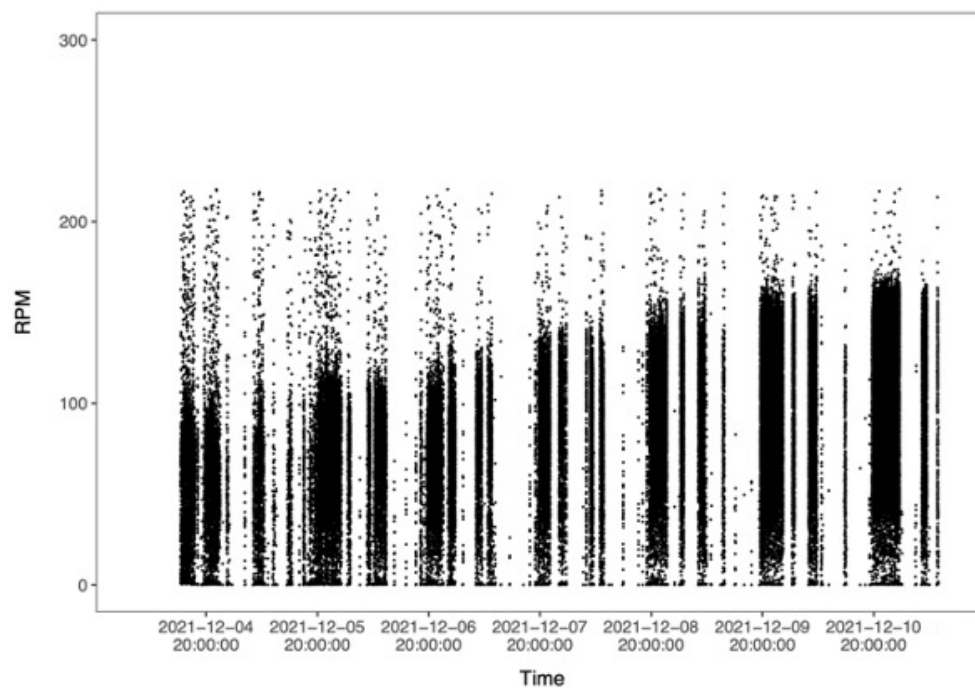
Animal: 112893
Cage: 1B
Sex: Male
Genotype: C57BL/6J



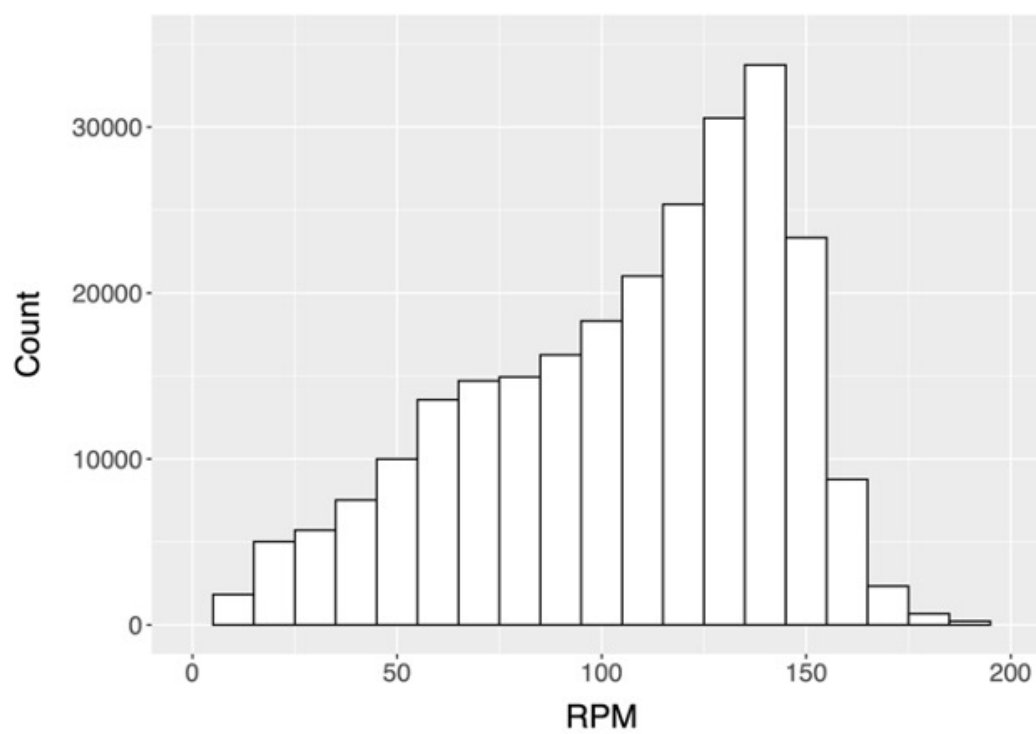
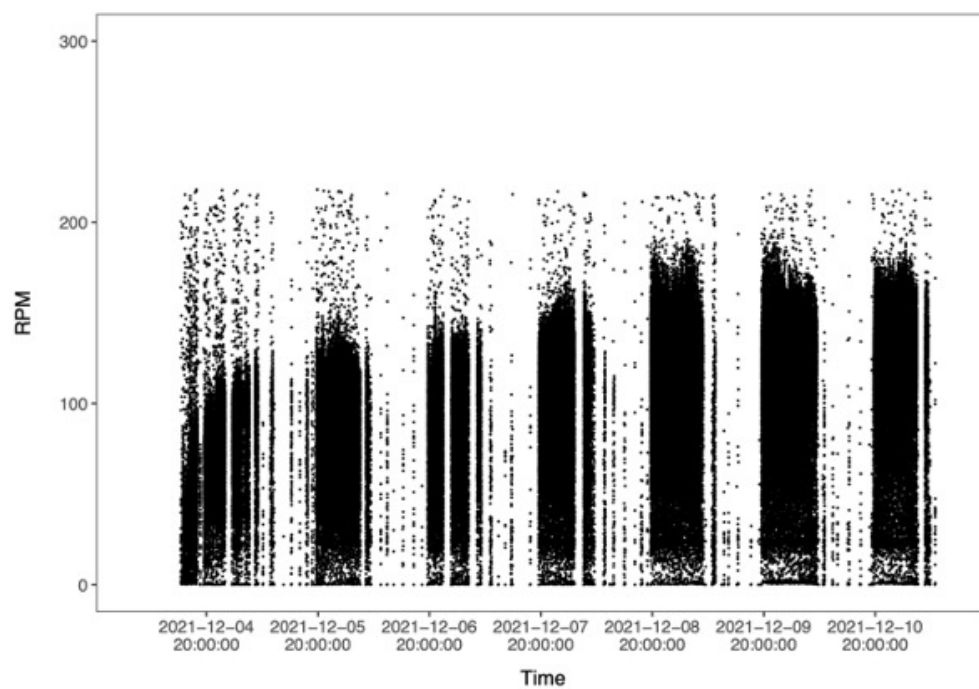
Animal: 112896
Cage: 2A
Sex: Male
Genotype: C57BL/6J



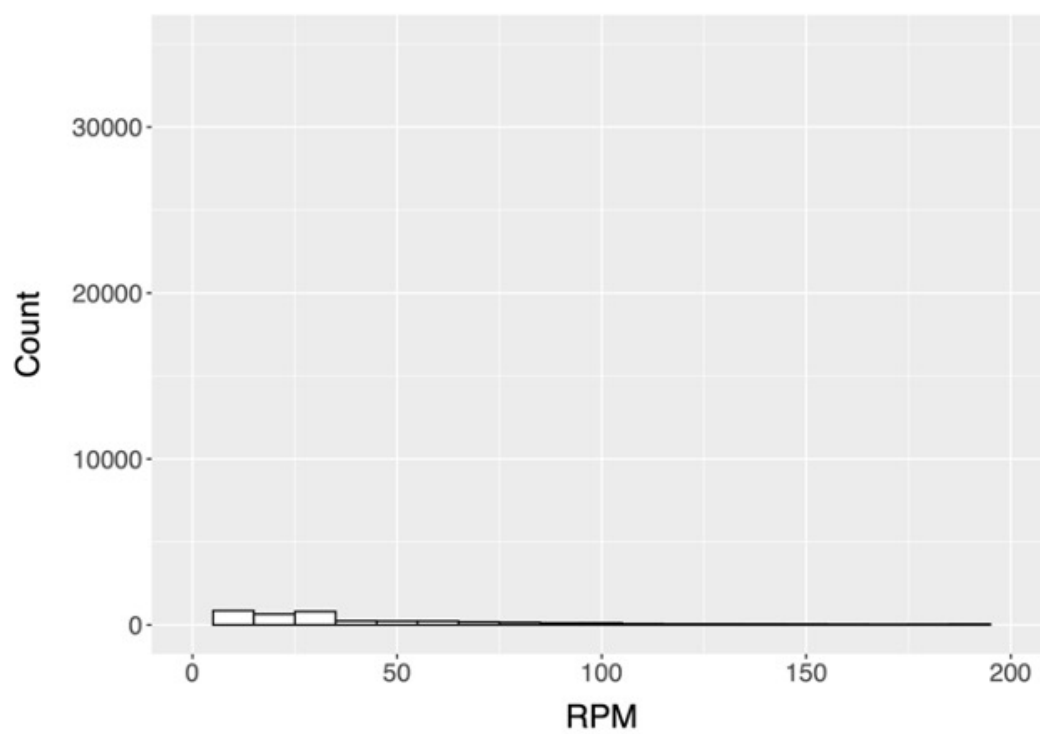
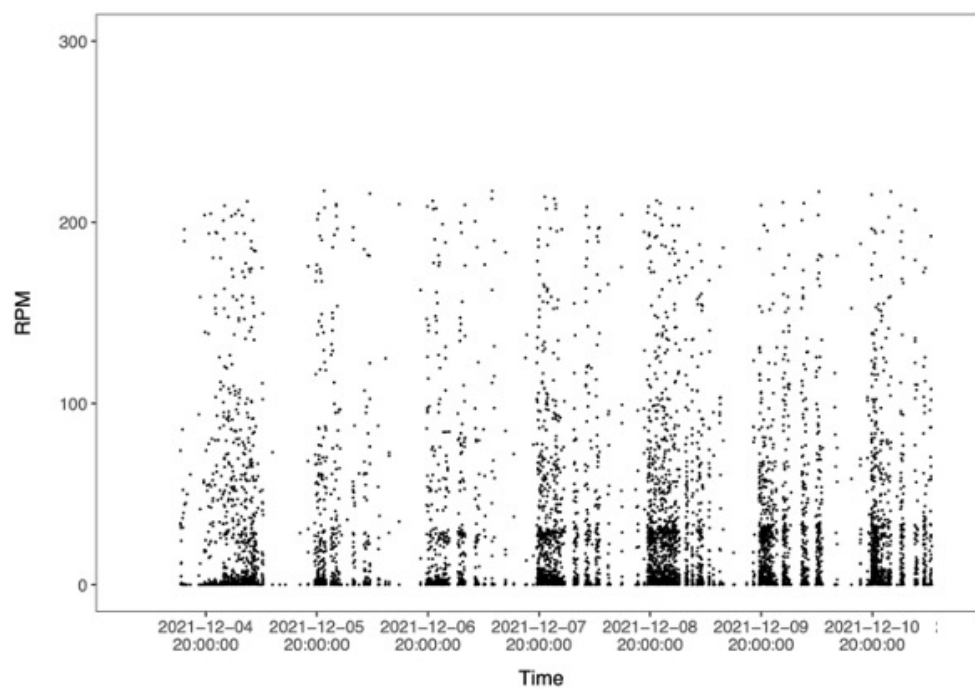
Animal: 112897
Cage: 2B
Sex: Male
Genotype: C57BL/6J



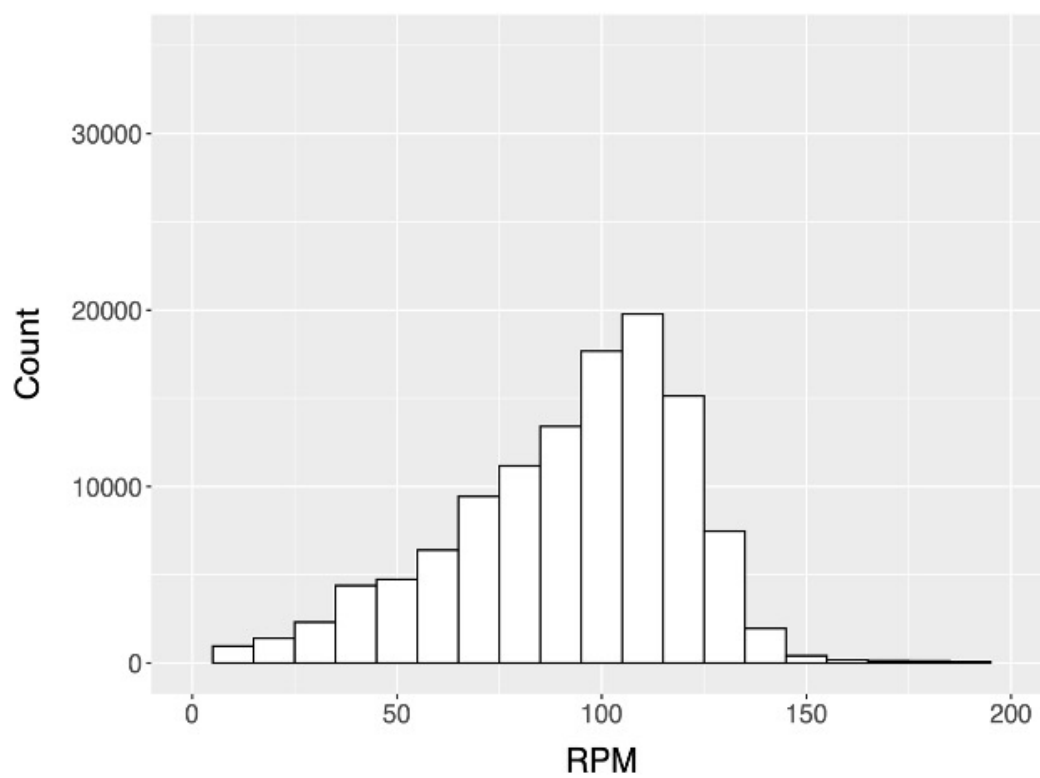
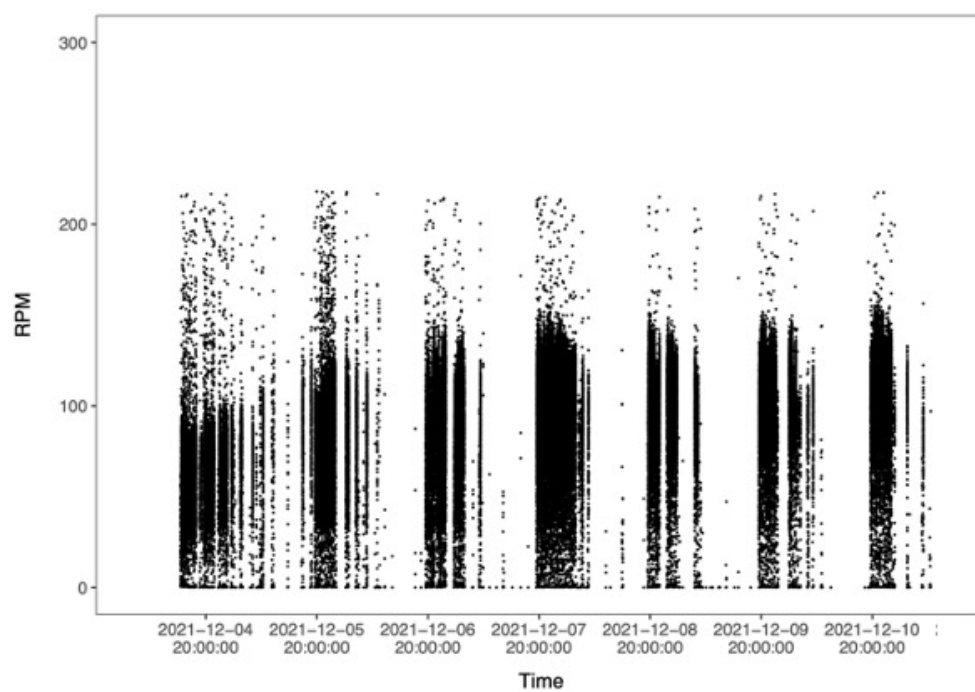
Animal: 112865
Cage: 3A
Sex: Female
Genotype: C57BL/6J



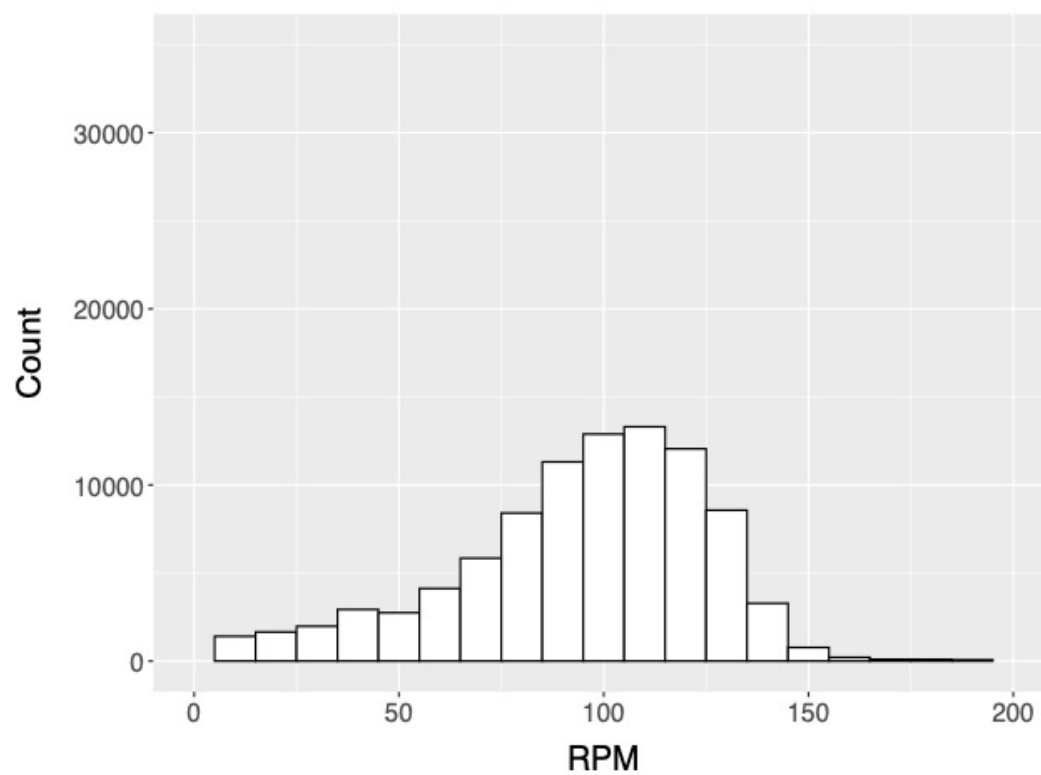
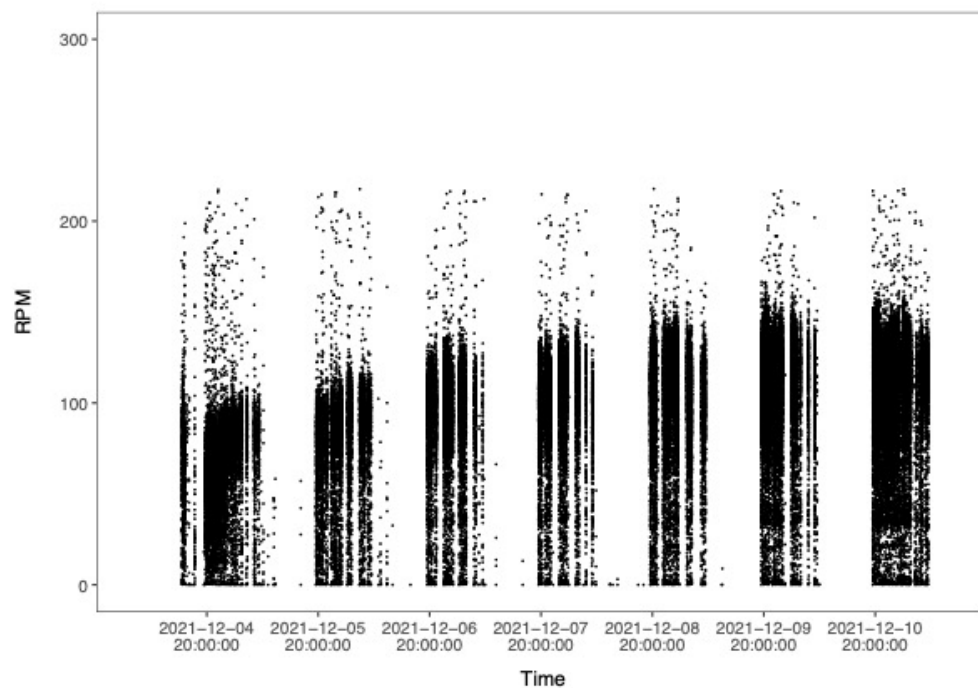
Animal: 112866
Cage: 3B
Sex: Female
Genotype: C57BL/6J



Animal: 112869
Cage: 4A
Sex: Male
Genotype: C57BL/6J

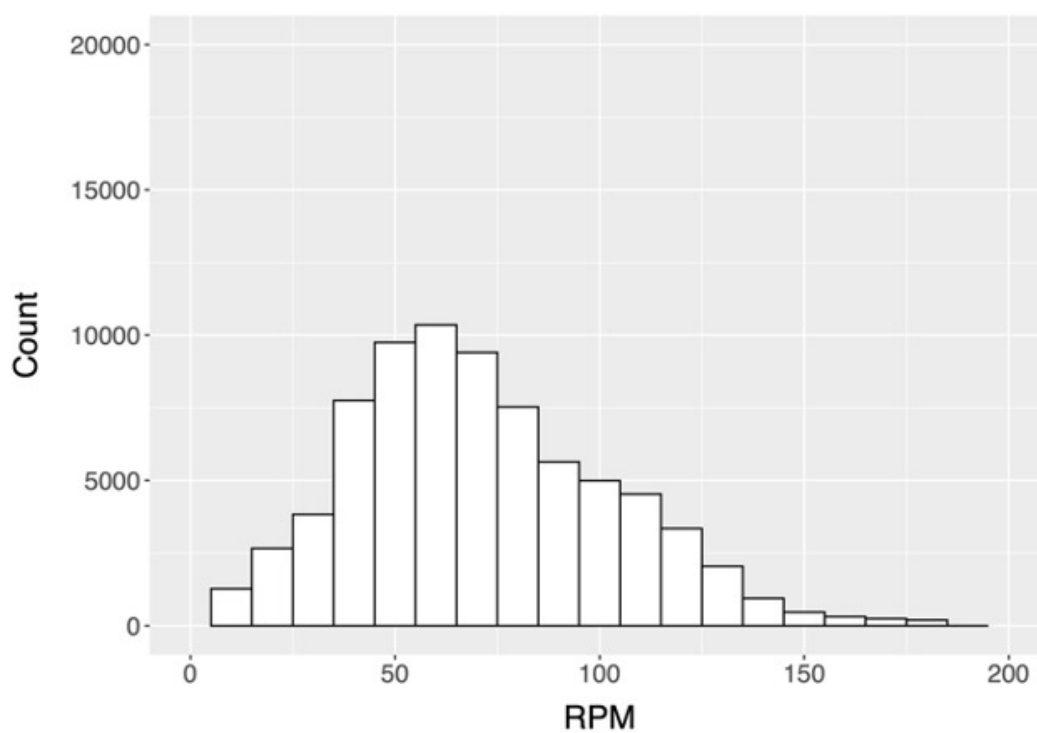
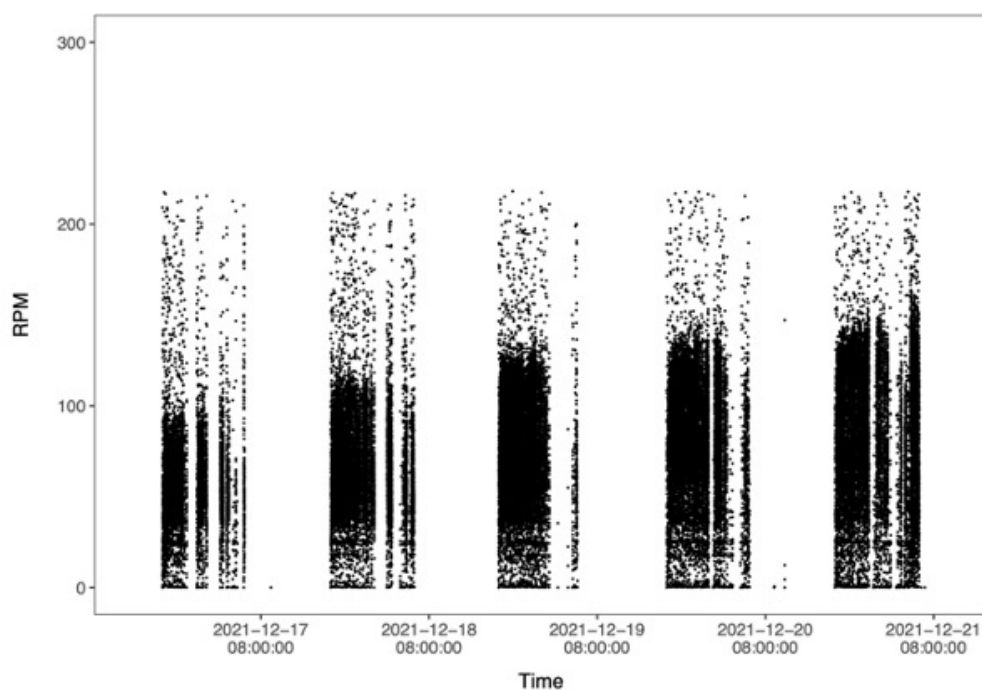


Animal: 112870
Cage: 4B
Sex: Male
Genotype: C57BL/6J

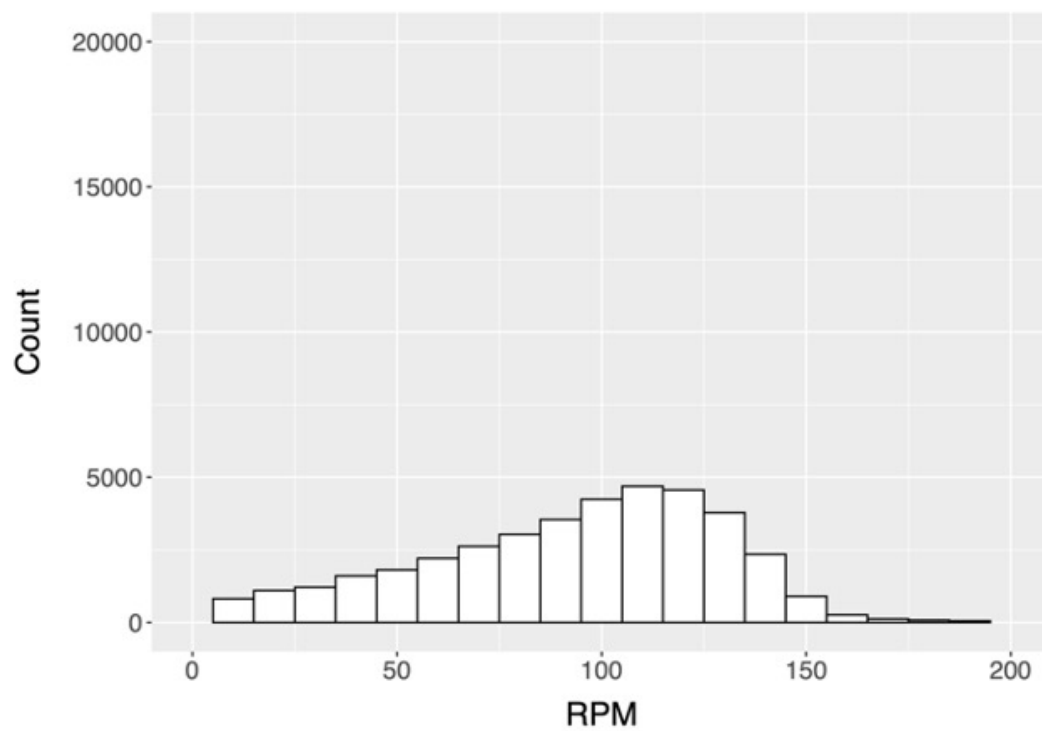
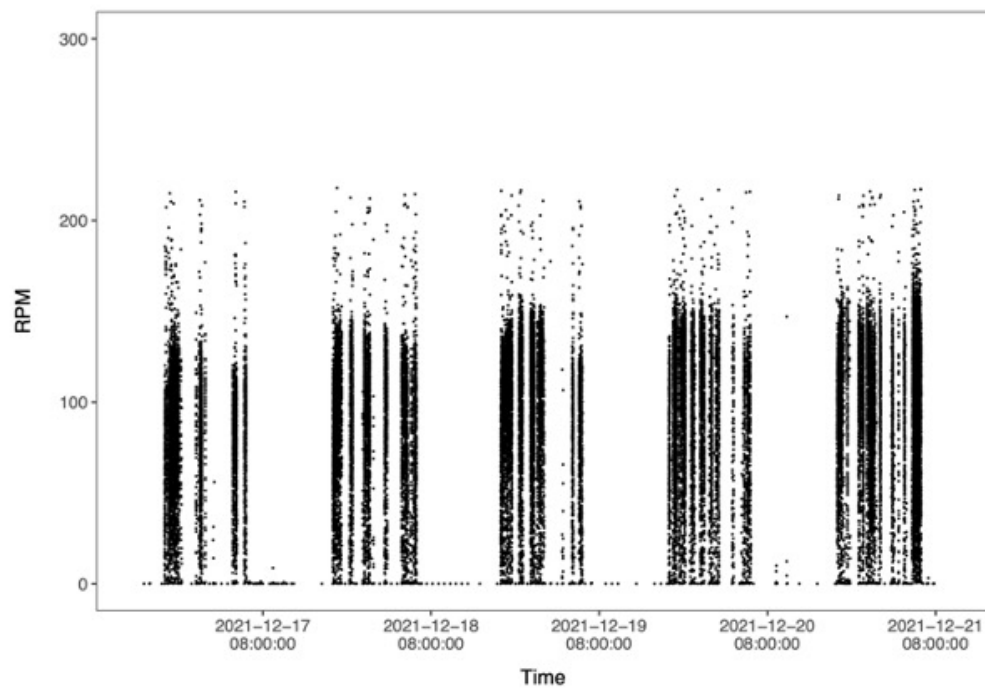


A5.2. Exercise tracking data – serum BDNF following 7 days of exercise in B Cre⁺ mice

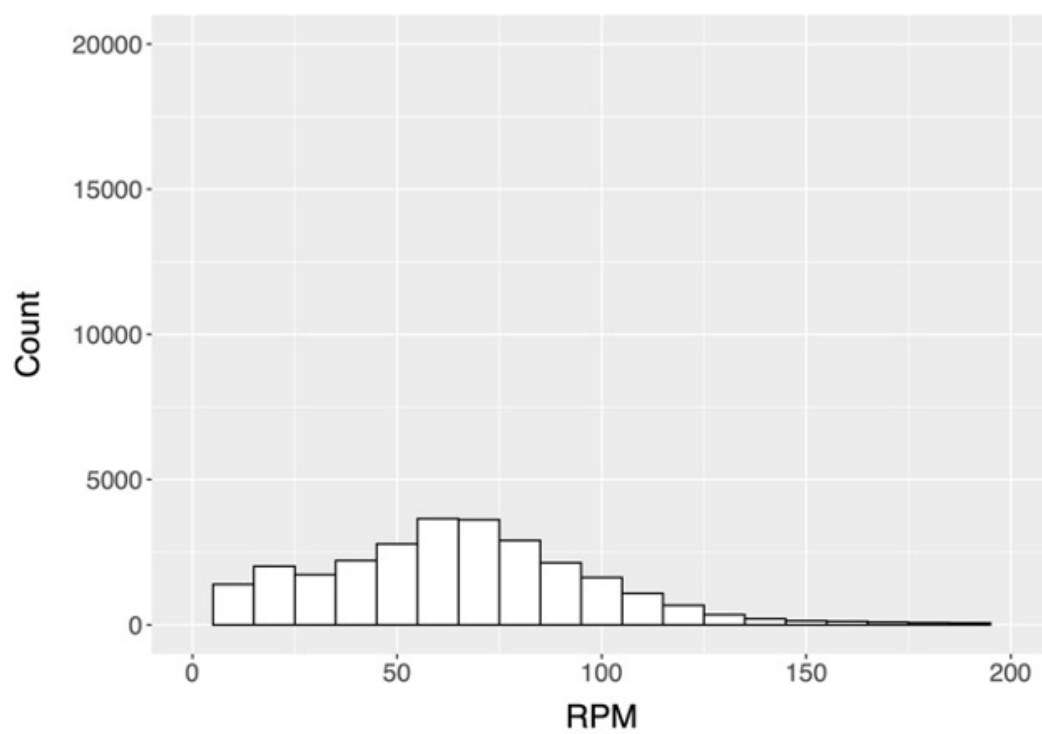
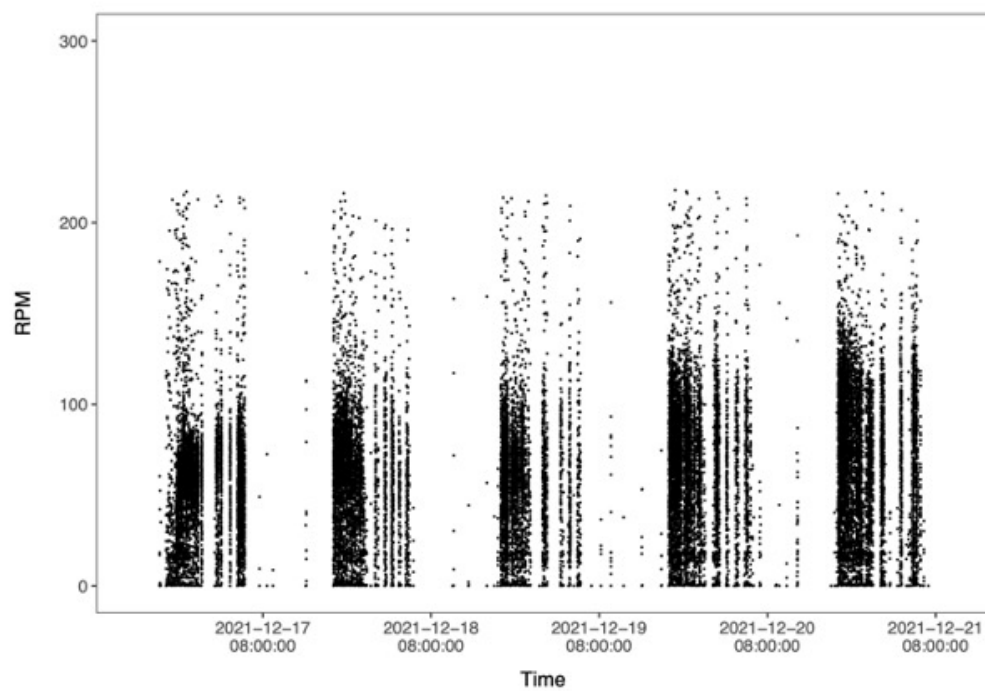
Animal: 112138
Cage: 1A
Sex: Male
Genotype: Het



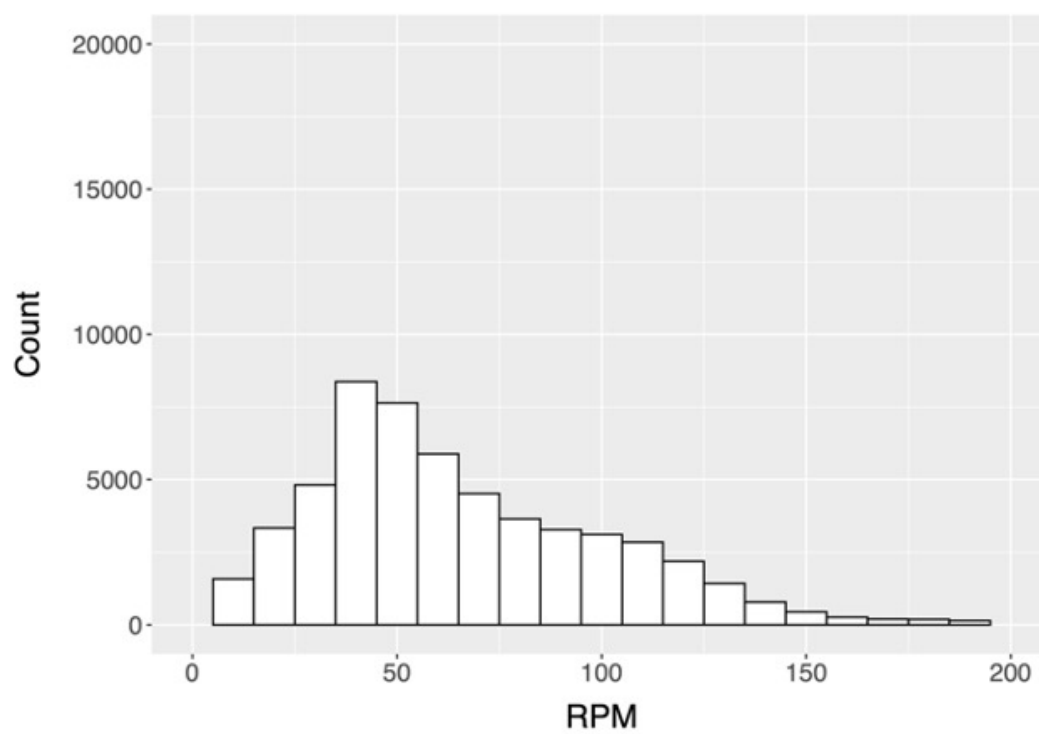
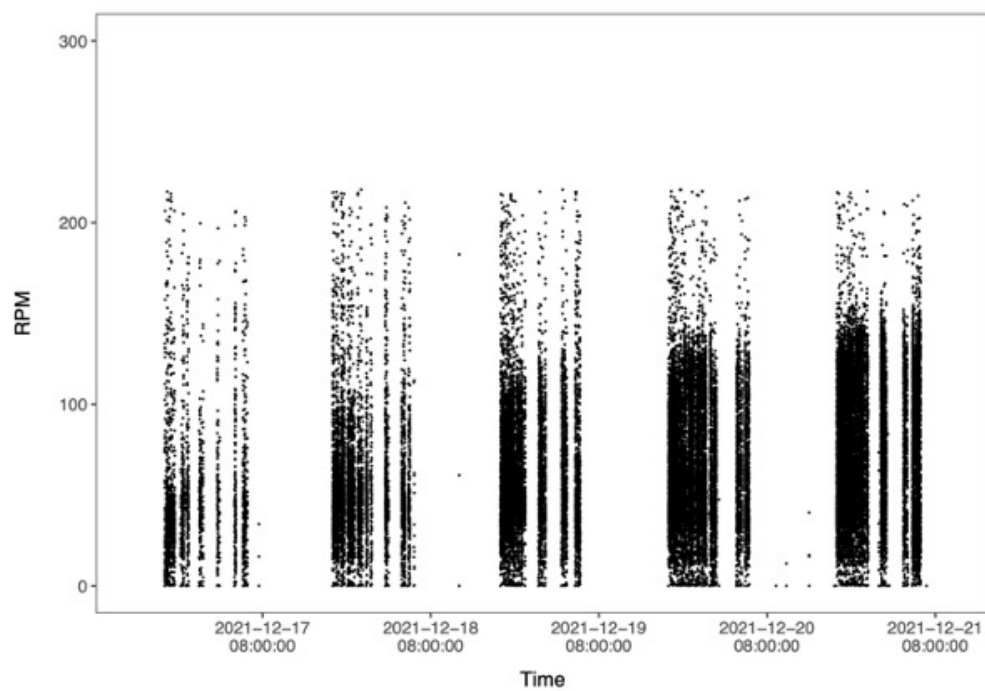
Animal: 112139
Cage: 1B
Sex: Male
Genotype: Het



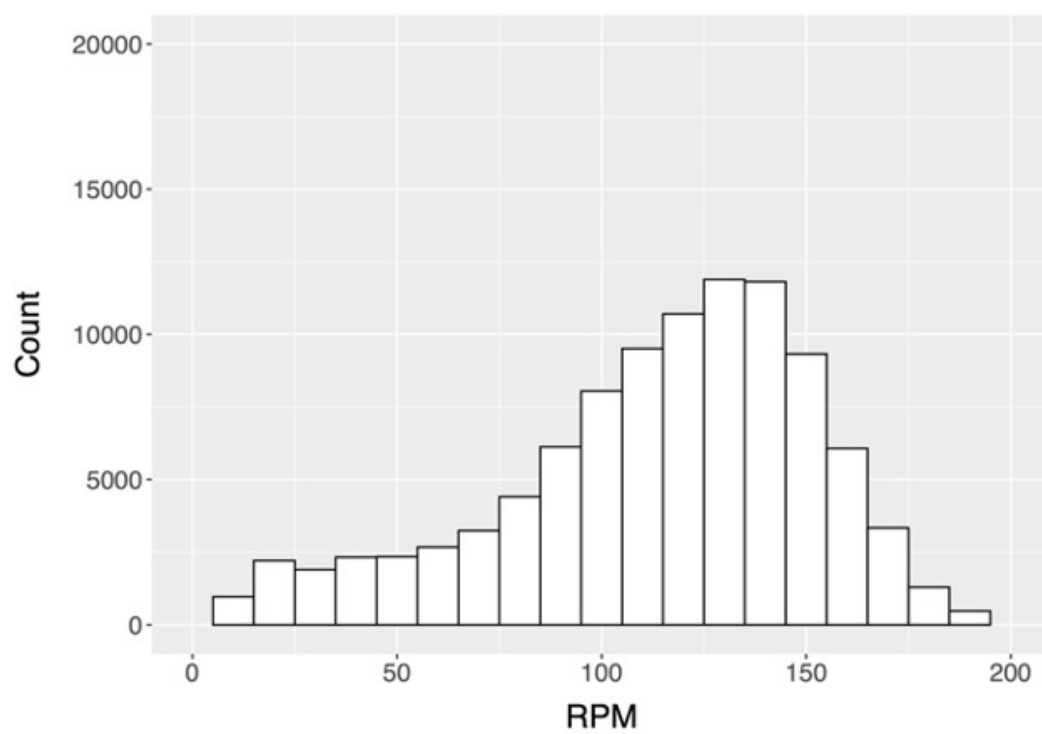
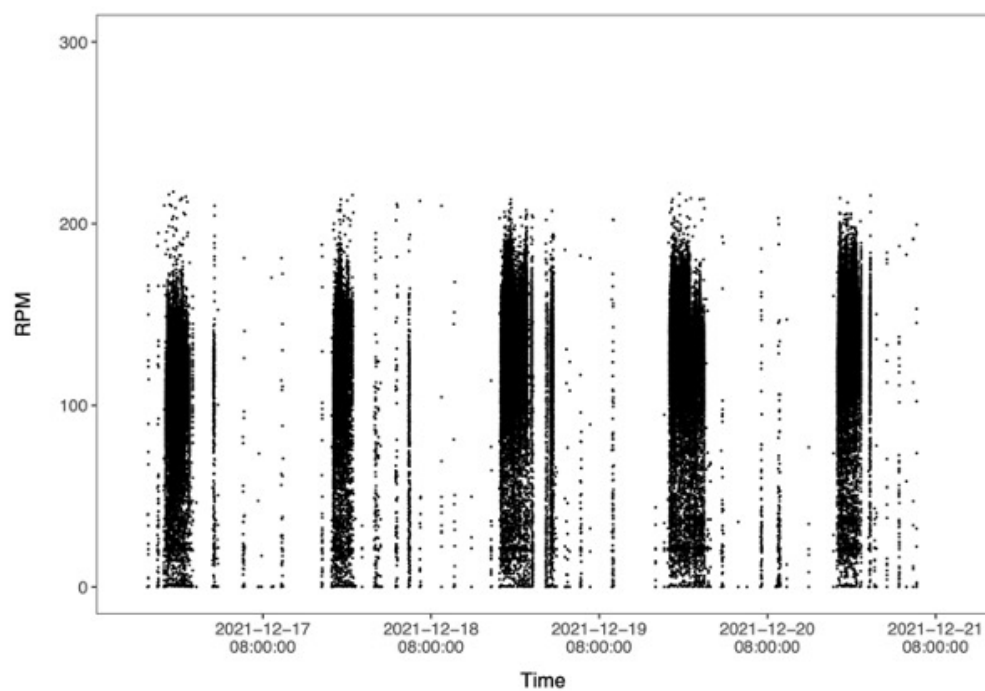
Animal: 108981
Cage: 2A
Sex: Male
Genotype: Hom



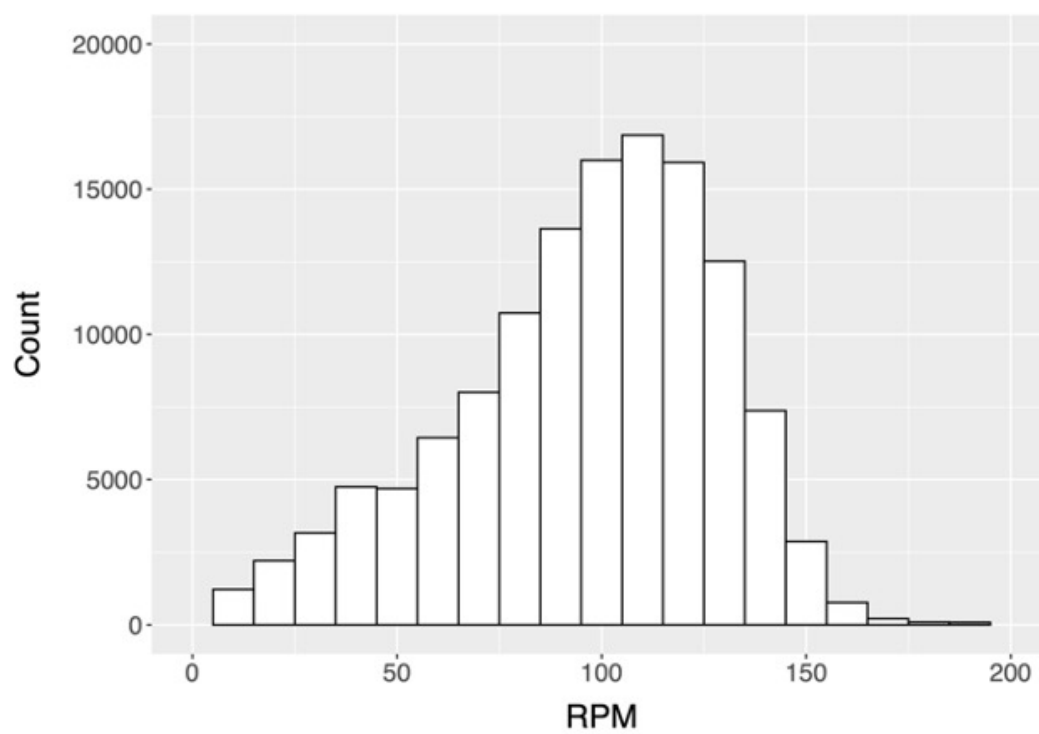
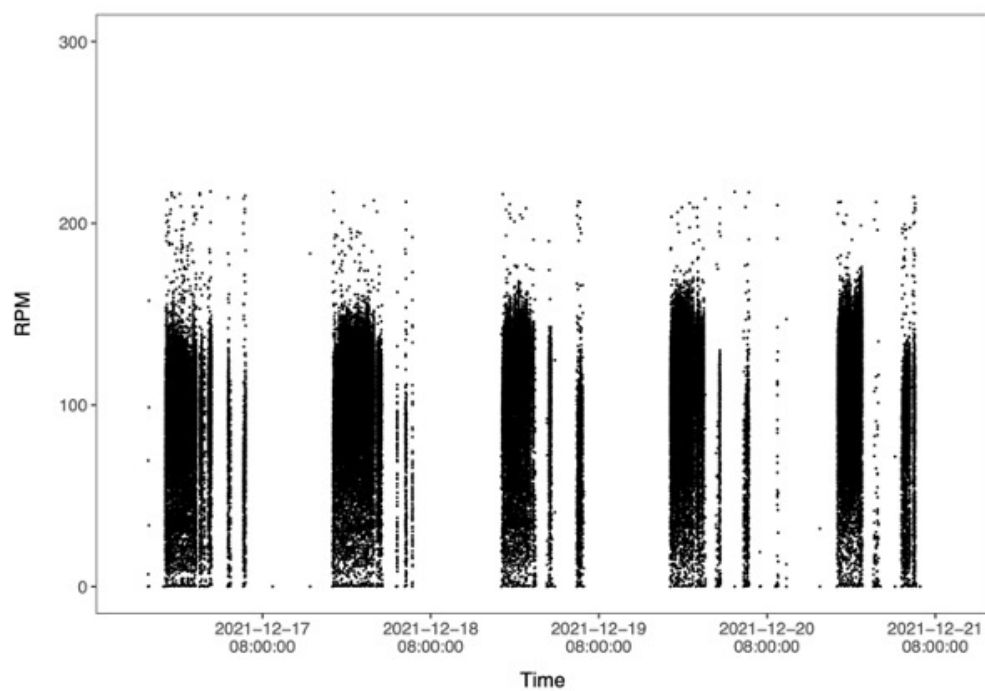
Animal: 108980
Cage: 2B
Sex: Male
Genotype: Hom



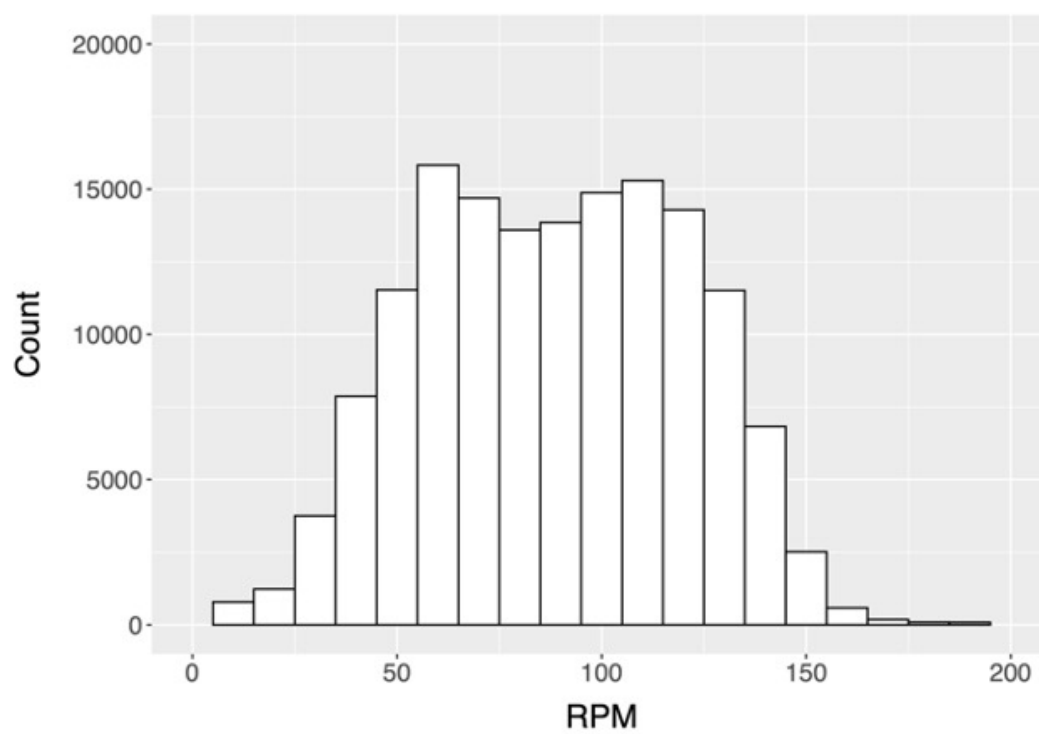
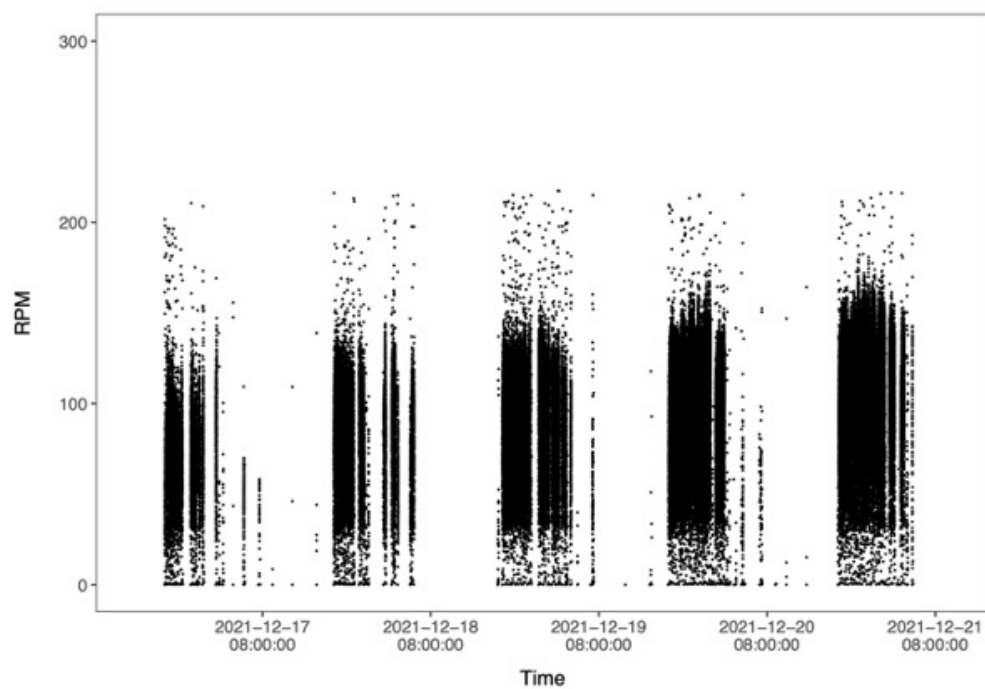
Animal: 108971
Cage: 3A
Sex: Female
Genotype: Hom



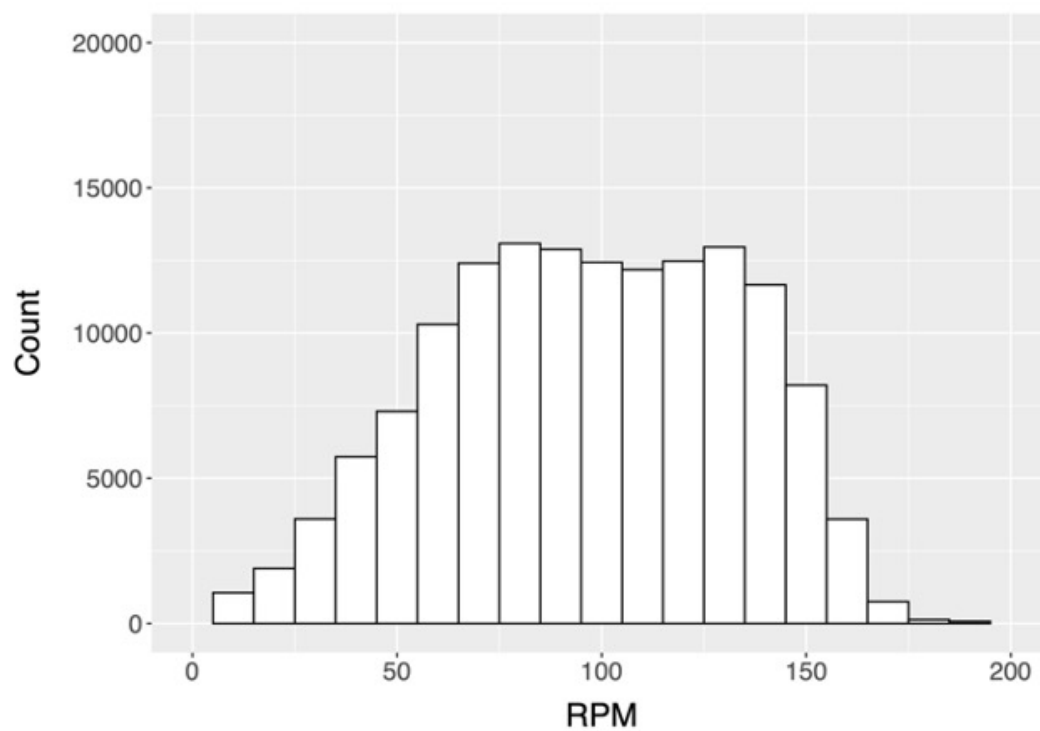
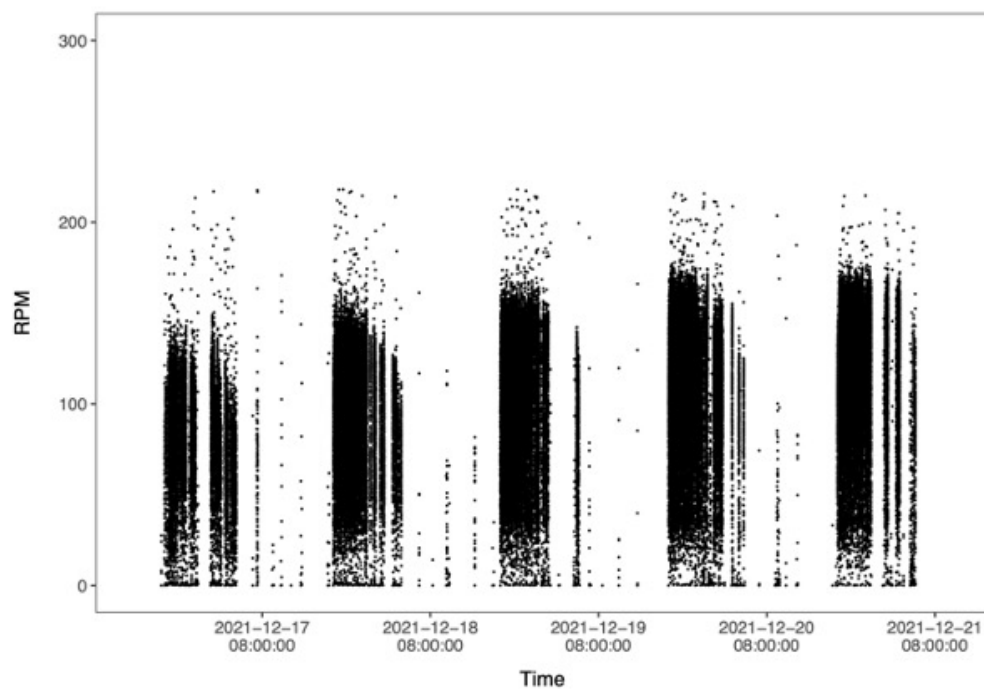
Animal: 112066
Cage: 4B
Sex: Female
Genotype: Hom



Animal: 112064
Cage: 4A
Sex: Female
Genotype: Hom



Animal: 112065
Cage: 4B
Sex: Male
Genotype: Hom



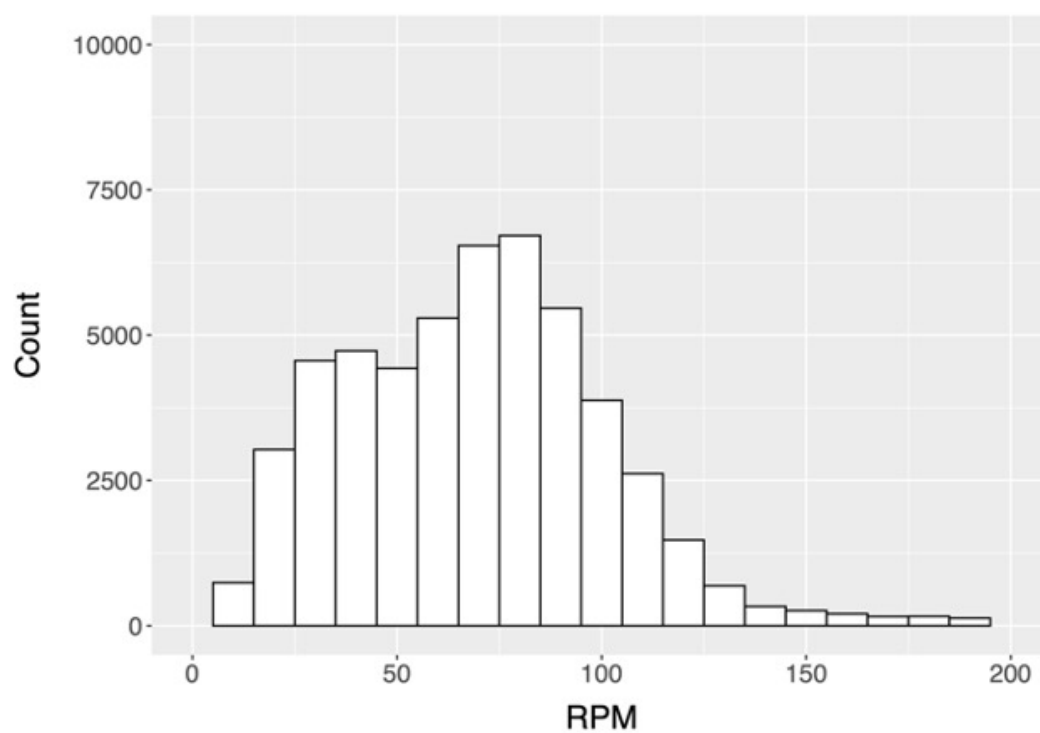
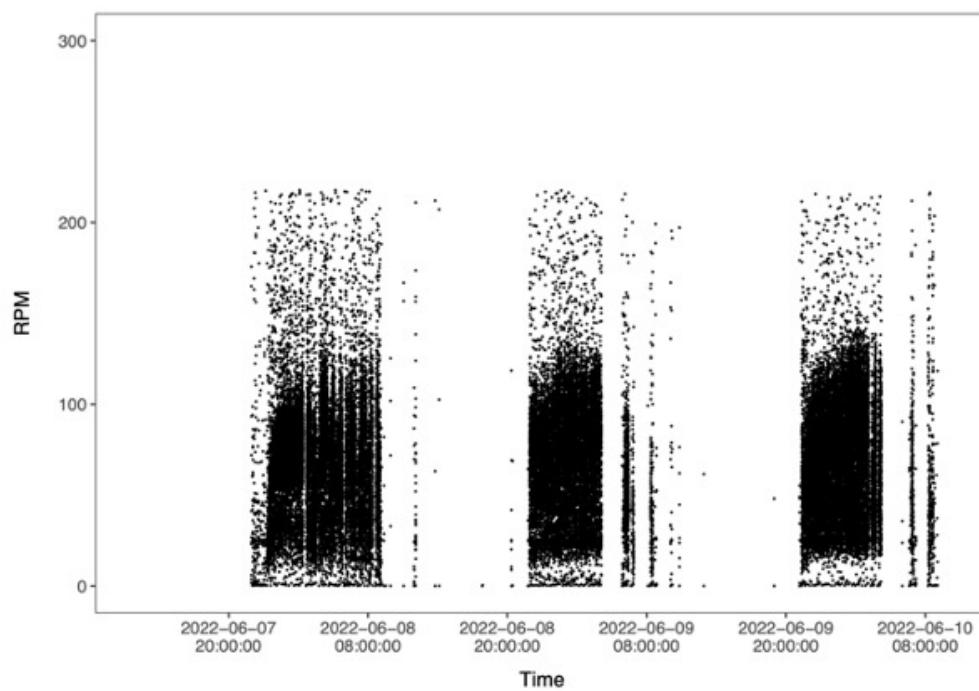
A5.3. Exercise tracking data – plasma BDNF following 3 days of exercise, B Cre⁺ mice

Animal: 127212

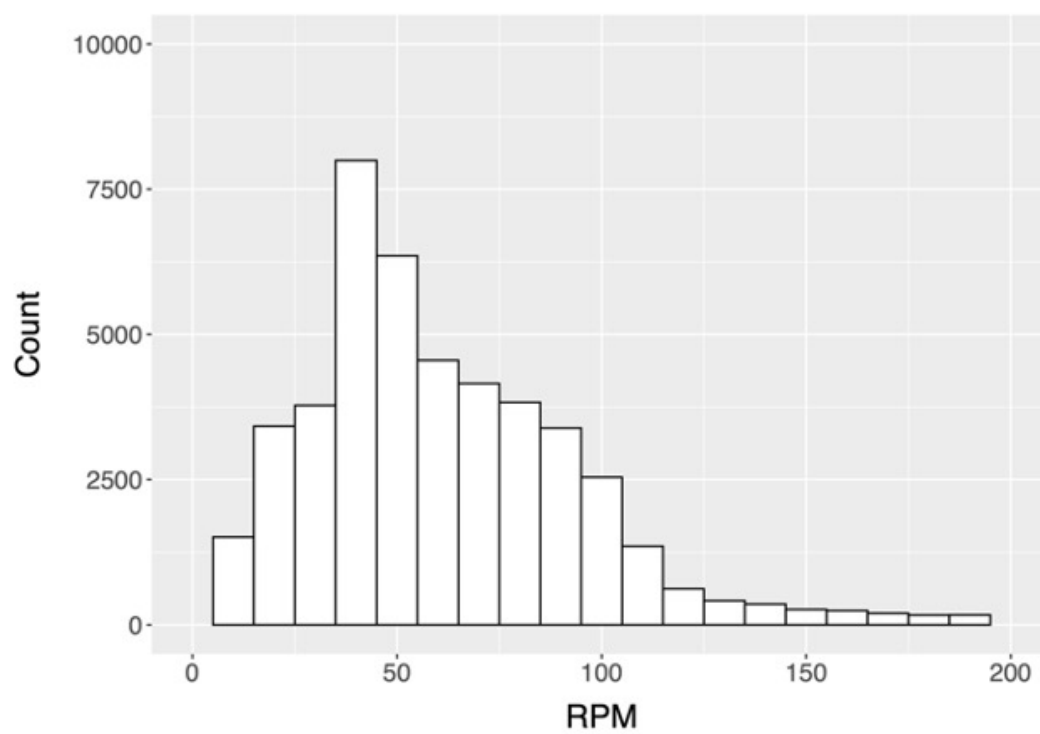
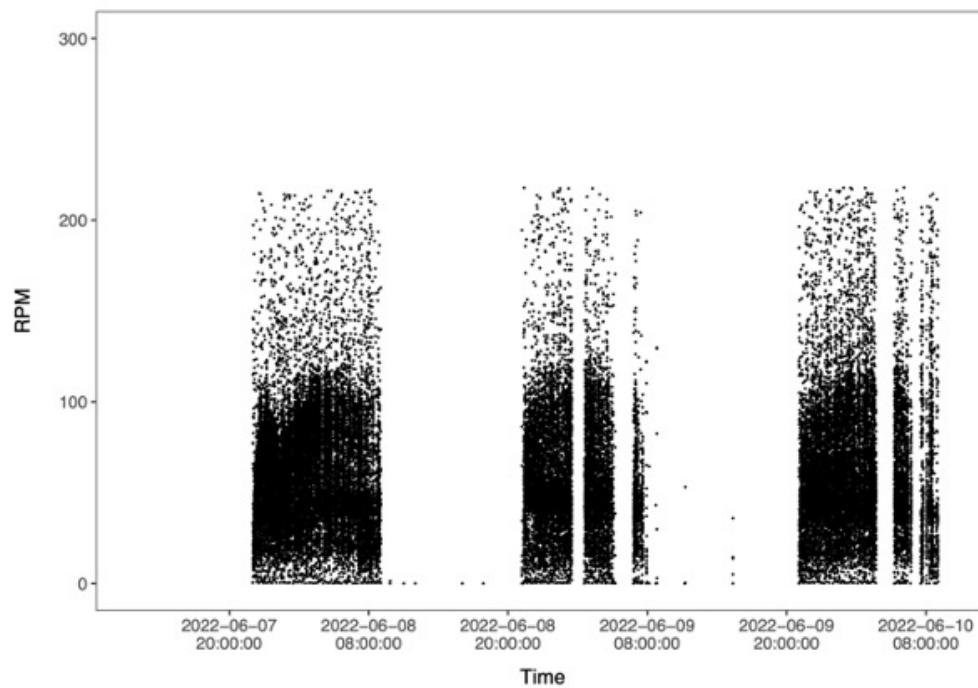
Cage: 1A

Sex: Male

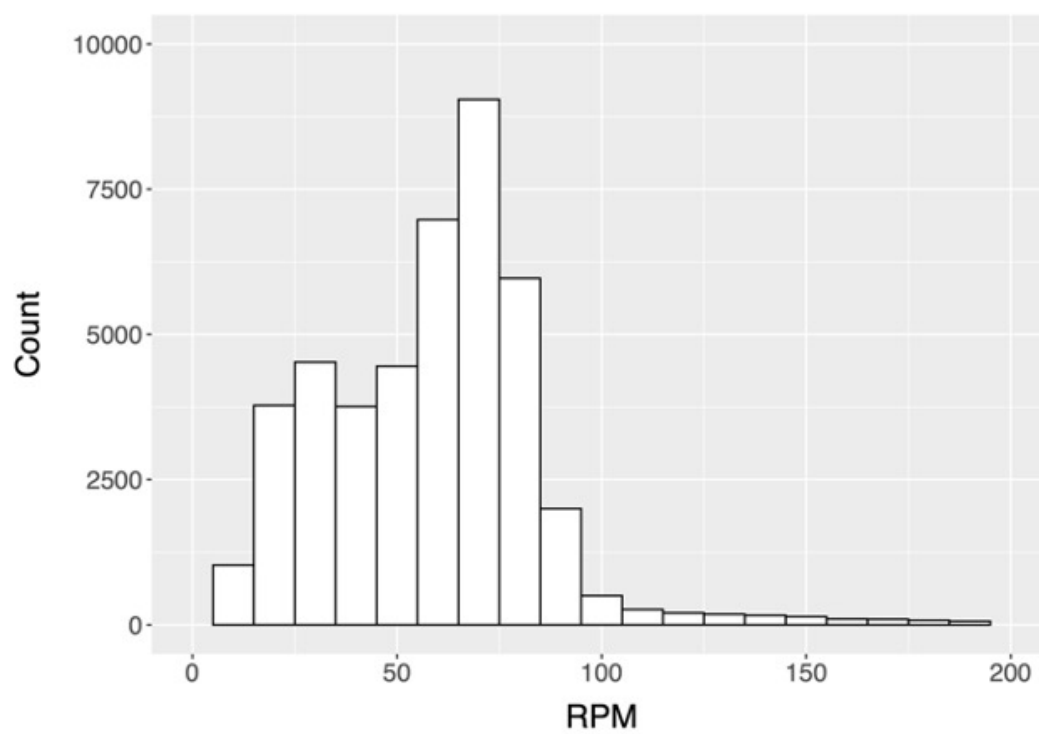
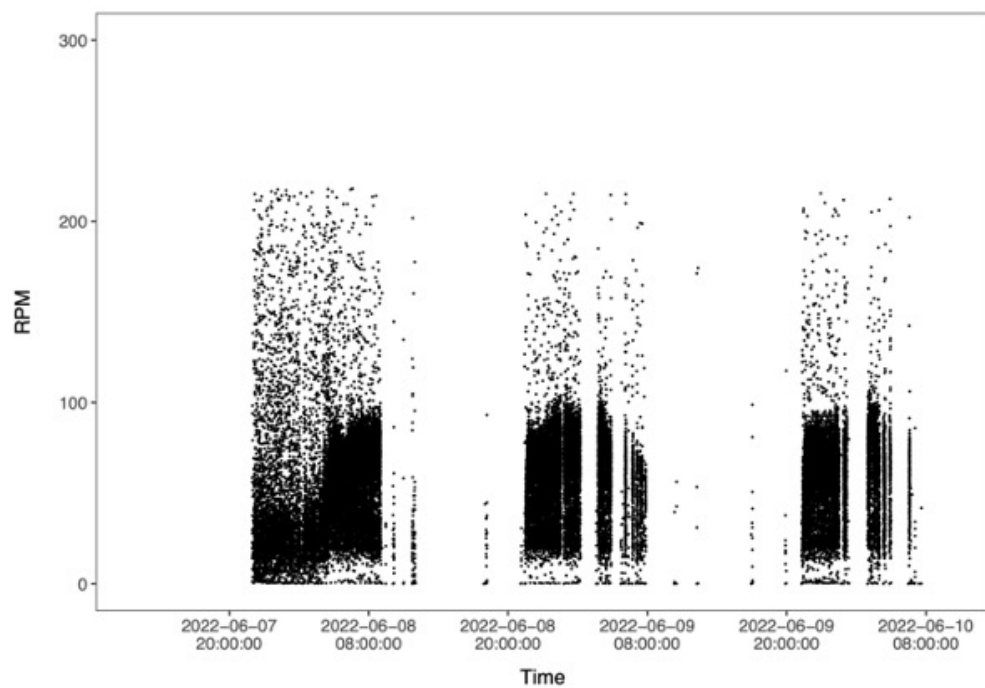
Genotype: Het



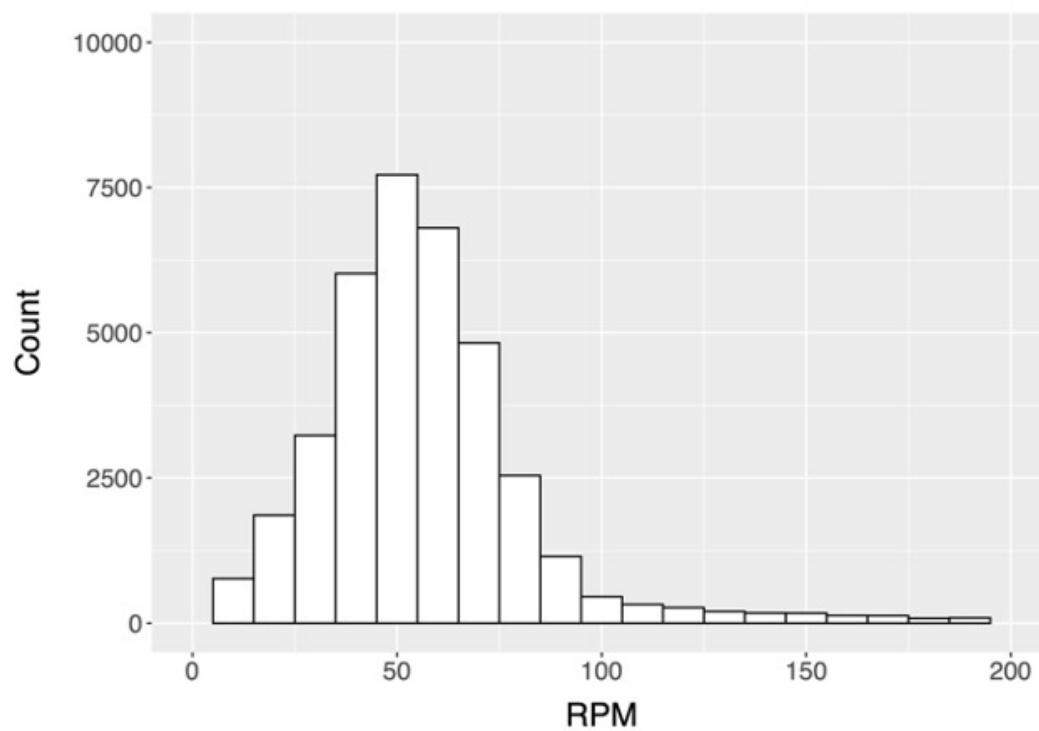
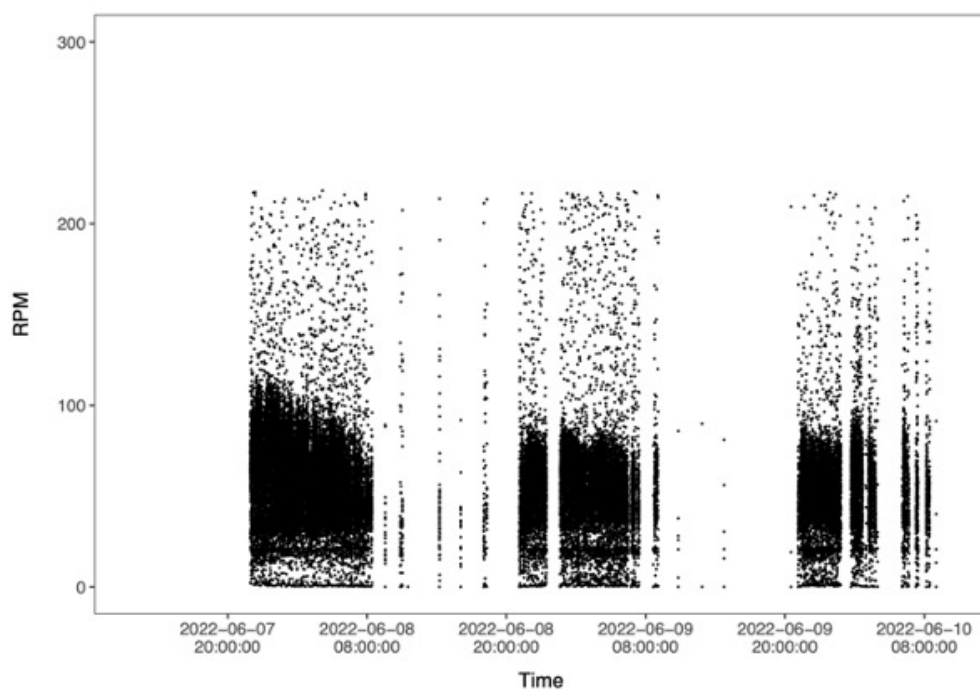
Animal: 127967
Cage: 1B
Sex: Male
Genotype: Hom



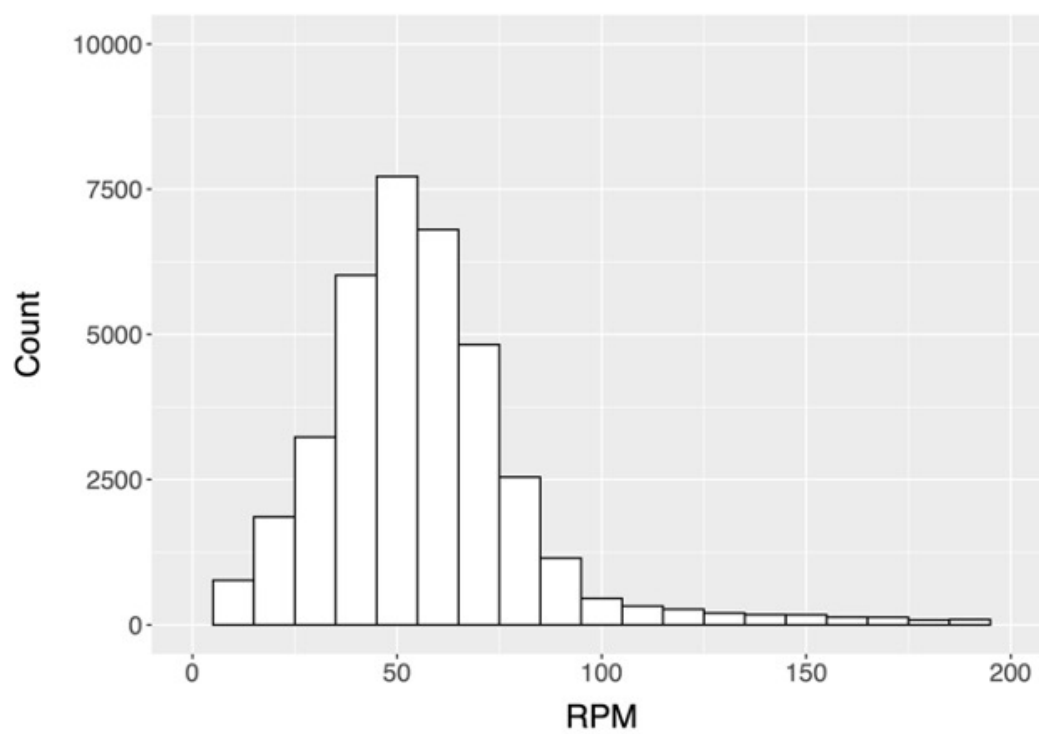
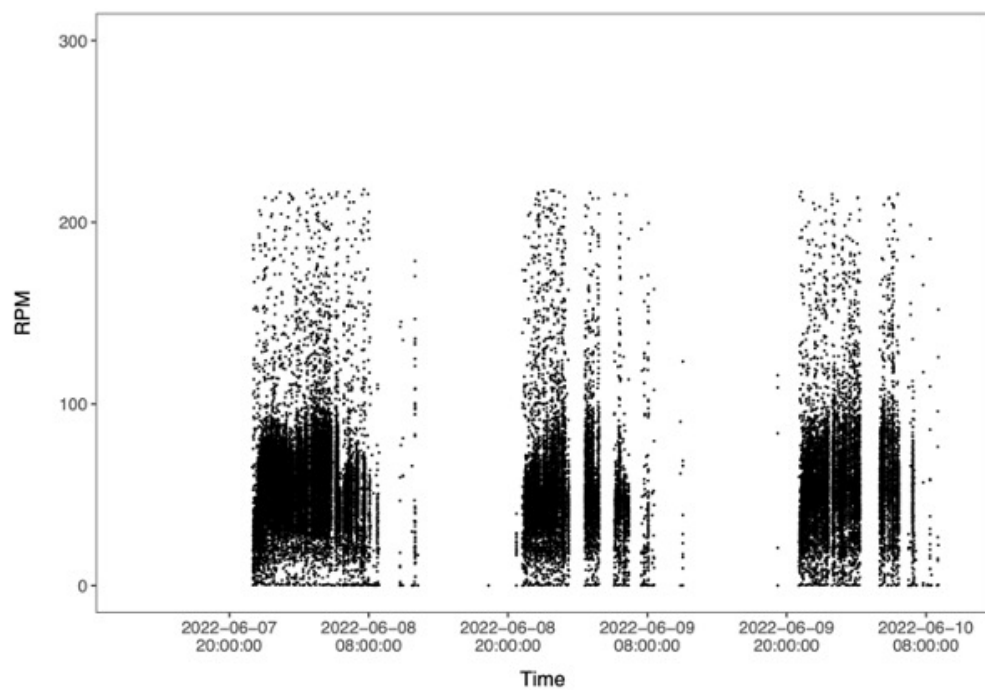
Animal: 127213
Cage: 3A
Sex: Female
Genotype: Hom



Animal: 129507
Cage: 3B
Sex: Female
Genotype: Het



Animal: 127969
Cage: 4A
Sex: Female
Genotype: Het



Animal: 127969
Cage: 4B
Sex: Female
Genotype: Hom

